

Investigating neural differentiation
capacity in Alzheimer's disease iPSC-
derived neural stem cells

Alysha Burrows

PhD 2022

Investigating neural differentiation
capacity in Alzheimer's disease iPSC-
derived neural stem cells

Alysha Burrows

A thesis submitted in fulfilment of the
requirements of the Manchester
Metropolitan University for the degree of
Doctor of Philosophy

Centre for Bioscience
Manchester Metropolitan University

Abstract

Neurodegeneration in Alzheimer's disease (AD) may be exacerbated by dysregulated hippocampal neurogenesis. Neural stem cells (NSC) maintain adult neurogenesis and depletion of the NSC niche has been associated with age-related cognitive decline and dementia. We hypothesise that familial AD (FAD) mutations bias NSC toward premature neural specification, reducing the stem cell niche over time and accelerating disease progression.

Somatic cells derived from patients with FAD (*PSEN1* A246E and *PSEN1* M146L heterozygous mutations) and healthy controls were reprogrammed to generate induced pluripotent stem cells (iPSC). Pluripotency for patient and control iPSC lines was confirmed, then cells were amplified and cryopreserved as stores. iPSC were subjected to neural specification to rosette-forming SOX2+/nestin+ NSCs for comparative evaluations between FAD and age-matched controls. FAD patient and control NSC were passaged under defined steady state culture conditions to assess stem cell maintenance using quantitative molecular markers (SOX2, nestin, NeuN, MAP2 and β III-tubulin). We observed trends towards downregulated expression of the nestin coding gene *NES* ($p=0.051$) and upregulated expression of *MAP2* ($p=0.16$) in *PSEN1* NSC compared with control NSC, indicative of a premature differentiation phenotype induced by presence of the *PSEN1* mutation.

Cell cycle analysis of *PSEN1* NSC showed that compared with controls, a greater number of *PSEN1* NSC were retained in G0/G1 phase of the cell cycle ($p=0.39$), fewer progressed to S-phase ($p=0.11$) and fewer still reached G2 phase ($p=0.23$), suggesting cell cycle progression may be impaired in *PSEN1* NSC. Nuclear DNA fragmentation was increased ($p=0.10$) in FAD NSC compared with controls, indicative of elevated cell death/apoptosis. Flow cytometry-based analysis of live, nestin+ NSC and NPC indicated increased apoptosis ($p=0.14$) in FAD NSC compared with controls, as well as increasing levels of apoptosis ($p=0.33$) in FAD NSC as they specified to neural progenitor cells.

Global RNA sequencing was used to identify transcriptomic changes occurring during both disease and control neural specification. GO analysis of DEGs between *PSEN1* and control NSC at P3 revealed significant upregulation (FDR<0.0000259) of 5 biological processes related to transcription and gene expression as well as significant upregulation (FDR<0.00000725) of 12 molecular functions related to DNA binding and transcription factor activity. These data suggest significant changes in gene expression were occurring in *PSEN1* NSC at P3 compared with control NSC at the same stage in neural specification. The number of DEGs ($p<0.05$) between *PSEN1* and control NSC at P3 was 9.92-fold higher than the number of DEGs between *PSEN1* and control NSC at P2, suggesting transcriptomic differences between *PSEN1* and control NSC become more pronounced as cells specify further down the neural lineage.

Gene ontology (GO) analysis of differentially expressed genes (DEGs) specific to AD neural differentiation revealed significant dysregulation (FDR $p<0.05$) of genes related to neurogenesis, apoptosis, cell cycle, transcriptional control, and cell growth/maintenance as *PSEN1* NSC matured from P2 to P3. The number of DEGs ($p<0.05$) in *PSEN1* neural differentiation was 4.7-fold higher than the number of DEGs seen in control neural differentiation, indicating more transcriptional changes occurred in *PSEN1* NSC than in controls at the same time point in neural specification.

Dysregulation of Notch signalling was specific to *PSEN1* neural differentiation and Notch related DEGs significantly upregulated ($p<0.05$) in *PSEN1* NSC at P3 compared with P2 included *NCOR2*, *JAG2*, *CHAC1* and *RFNG*. qPCR based validation displayed significant upregulation of *RFNG* ($p=0.04$) in *PSEN1* NSC at P3 compared with *PSEN1* NSC at P2, and indicated a trend towards upregulation of *JAG2* expression, correlating with RNA sequencing data. Data generated in this study indicate that presence of the *PSEN1* mutation significantly increases the number of transcriptional changes occurring during neural differentiation. It is plausible that transcriptional changes to Notch signalling cause dysregulated neural specification and increased apoptosis in *PSEN1* NSC, ultimately resulting in depletion of the NSC niche.

Contents:

Table 1. Materials used, origin and catalogue number	61
Table 2. Information available on control and <i>PSEN1</i> lines used.....	67
Table 3. The composition of HESC media	72
Table 4. Primary antibodies and concentration used for immunocytochemistry (ICC).	78
Table 5. Secondary antibodies and concentration used for immunocytochemistry (ICC).	78
Table 6. Forward and reverse primers designed for verification of AD mutations...79	
Table 7. qPCR primers for housekeeping genes.	82
Table 8. qPCR primers used for investigation of AD neurogenesis.	84
Table 9. Example of average Ct values measured using primers designed to detect transcripts generated from the housekeeping gene <i>UBE2D2</i>	86
Table 10. The components of each well of a 96 well PCR plate.	88
Table 11. qPCR cycling parameters	89
Table 12. qPCR melt curve settings.....	89
Table 13. Materials used to perform cell cycle analysis of <i>PSEN1</i> and control NSC..92	
Table 14. Initial panel design for investigating apoptosis and necrosis in AD and control NSC.....	94
Table 15. Final panel design for investigating apoptosis and necrosis in AD and control NSC.	94
Table 16. mRNA denaturation program.....	99
Table 17. mRNA elution 1 program	100
Table 18. Elution-2-frag-prime program	101
Table 19. Synthesise first strand program	101
Table 20. ATAIL70 program.....	103
Table 21. LIG program.....	104
Table 22. mRNA PCR program.....	105
Table 23. DNA standards for JetSeq qPCR	108

Table 24. qPCR reagents per reaction.....	108
Table 25. Primer sequences for JetSeq qPCR.....	109
Table 26. JetSeq qPCR cycling parameters	109
Table 27. Cell densities of NSC for nucleofection with the pmax GFP [™] vector.....	130
Table 28 FITC-A median data acquired from DV Verse flow cytometer displaying unstained and stained values for OCT4 expression.	145
Table 29. Log2(FC) Values for significant DEGs Related to Cell Cycle Regulation ...	222
Table 30. Gene ontology results for biological processes dysregulated between control NSC P3 and <i>PSEN1</i> NSC P3.....	225
Table 31 Molecular functions significantly dysregulated in <i>PSEN1</i> P3 NSC compared with control NSC at P3.	228
Table 32. Index sequences and reads identified per index.....	304
10.2.2.1 Table 33. ASCII character quality score.....	305
Table 34. Example FastQC input parameters.....	307
Table 35. Overrepresented sequences in RNA sequencing data.....	310
Table 36. Example Trimmomatic settings for merged Fastq files.....	311
Table 37. Infer experiment parameters	312
Table 38. Example parameters for alignment to reference genome using HISAT2	313
Table 39. Example filtering parameters post alignment with HISAT2	315
Table 40. Percentage duplication data for all samples post-alignment to Hg38.....	316
Table 41. Feature Counts Input Parameters	320
Table 42. Percentage of reads assigned pre- and post- filtering	323
Table 43. DESeq2 input parameters	324
Table 44. Parameters for generation of volcano plot.....	326
Table 45. Parameters for GO biological process.....	327
Table 46. Parameters for GO molecular function	327
Table 47. Parameters for GO cellular component	328

Figure 1. APP cleavage pathways.....	25
Figure 2. Pathology of Alzheimer’s disease	27
Figure 3. The γ -secretase complex.....	28
Figure 4. Known γ -secretase protein substrates.	29
Figure 5. Genes associated with effect or risk of AD	31
Figure 6. Therapies targeting AD	36
Figure 7. Canonical Notch ligands and their structural domains.....	39
Figure 8. Release of the NICD to initiate Notch signalling pathways.....	40
Figure 10. Canonical (β -Catenin dependent) and non-canonical (β -catenin independent) Wnt signalling pathways.	45
Figure 11. Mechanisms of NSC cell division and factors which may have a role in cell fate determination.....	49
Figure 12. Cortical development in the embryo	50
Figure 13. Normal cortical development and cortical development in disease	52
Figure 14. Location of the hippocampus in the adult human brain	54
Figure 15. Primer efficiency scatter plot.....	87
Figure 16. Gating the population of interest in flow cytometry	96
Figure 17. Gating of cells for analysis of apoptosis in flow cytometry	97
Figure 18. Waddington’s epigenetic landscape modified to show trans-differentiation and de-differentiation by reprogramming.....	119
Figure 19. Derivation of stem cells.....	120
Figure 20. The neurosphere assay compared with in vivo neural differentiation ..	122
Figure 21. Diagram of a neural stem cell rosette.....	123
Figure 22. Schematic outlining model development in chapter 1.....	125
Figure 23. Culture and expansion of axol NSC	127
Figure 24. Nucleofection with the pmax GFP TM vector	129
Figure 25. Nucleofection of control NSC with reprogramming factors	131
Figure 26. iPSC generated from the de-differentiation of control NSC, SHEF3 NSC and nHDF.....	132

Figure 27. Colony formation	134
Figure 28. ICC for pluripotency markers	135
Figure 29. Trilineage differentiation of control iPSC.....	136
Figure 30. De-differentiation of control and AD NSC to iPSC	139
Figure 31. Generation of feeder free iPSC	140
Figure 32. ICC for pluripotency markers in <i>PSEN1</i> iPSC	141
Figure 33. Trilineage differentiation of <i>PSEN1</i> iPSC.....	143
Figure 34. Flow cytometry data displaying OCT4 expression in <i>PSEN1</i> and control iPSC	144
Figure 35. Flow cytometry-based analysis of OCT3/4 expression in control and <i>PSEN1</i> A246E iPSC.	146
Figure 36. Sanger Sequencing of <i>PSEN1</i> A246E iPSC for Mutation Confirmation ...	147
Figure 37. Stages of neural differentiation.	149
Figure 38. Neural rosettes and tubes.....	150
Figure 39. ICC for OCT3/4 expression in SHEF3 NSC and NPC.....	151
Figure 40. ICC for SOX2 expression in SHEF3 NSC and NPC.....	151
Figure 41. ICC for nestin expression in SHEF3 NSC and NPC	152
Figure 42. SHEF3 NPC differentiation	153
Figure 43. Control and AD neural differentiation to NSC and NPC.....	154
Figure 44. Neural differentiation of <i>PSEN1</i> and control iPSC to NSC.....	155
Figure 45. Neural differentiation to NPC	156
Figure 46. ICC for SOX2 and nestin in <i>PSEN1</i> and control NSC	157
Figure 47. Percentage of Cells which stained positive for nestin expression in <i>PSEN1</i> P2 and <i>PSEN1</i> P3 NSC.....	158
Figure 48. Nestin expression in <i>PSEN1</i> and control NPC	159
Figure 49. Staining for mature neural markers.....	160
Figure 50. Generation of neurospheres.....	161
Figure 51. Control neurosphere stained for DAPI (A), SOX2 (B)	162
Figure 52. Categorisation of cytoskeletal molecules	164

Figure 53. Cytoskeletal components in neurons	165
Figure 54. Effects of ageing on the NSC niche	169
Figure 55. Altered neural differentiation in <i>PSEN1</i> A246E NSC.....	176
Figure 56. qPCR based analysis of autophagy in <i>PSEN1</i> NSC.....	178
Figure 57. Expression of markers related to Wnt signalling.....	179
Figure 58. qPCR based analysis of antioxidant-response and inflammation-related gene expression in NSC and neurospheres.....	180
Figure 59. qPCR based analysis of markers of neural differentiation in NSC and neurospheres	181
Figure 60. qPCR based investigation of markers of neural differentiation	183
Figure 61. Forward scatter vs side scatter differences in <i>PSEN1</i> NSC	184
Figure 62. Distribution of control and <i>PSEN1</i> A246E NSC in cell cycle plots	186
Figure 63. Cell cycle analysis of <i>PSEN1</i> A246E and control NSC	189
Figure 64. Overview of library preparation and RNA sequencing	192
Figure 65. Overview of RNA sequencing.....	193
Figure 66. RNA sequencing adapters	194
Figure 67. RNA sequencing workflow	196
Figure 68. Bioanalyzer traces displaying cDNA used for RNA sequencing	198
Figure 69. Number of reads identified per group.....	200
Figure 70. Number of reads assigned to the reference genome post-filtering.....	203
Figure 71. PCA plot displaying variance between RNA seq samples	205
Figure 72. Sample-to-sample distances heatmap.....	206
Figure 73. Dispersion estimates RNA sequencing data	207
Figure 74. p-value histograms for DEGs.....	208
Figure 75. MA-plots for RNA sequencing data.....	210
Figure 76. Number of DEGs per sample group comparison	212
Figure 77. Volcano plots for DEGs.....	213
Figure 78. significantly dysregulated molecular functions in <i>PSEN1</i> neural differentiation.	214

Figure 79. Pathway alterations during control neural differentiation.....	215
Figure 80. Pathway alterations during <i>PSEN1</i> neural differentiation.....	216
Figure 81. Pathway Analysis of DEGs in control Neural Differentiation	217
Figure 82. Pathway analysis of DEGs in <i>PSEN1</i> neural differentiation	218
Figure 83. Biological processes associated with DEGs in control neural differentiation	219
Figure 84. Biological processes associated with DEGs in <i>PSEN1</i> neural differentiation	221
Figure 85. Analysis of DEGs exclusively found in <i>PSEN1</i> neural differentiation	223
Figure 86. DEGs in <i>PSEN1</i> neural differentiation linked with Wnt and Notch signalling	224
Figure 87. Biological processes dysregulated between <i>PSEN1</i> and control NSC at P3	227
Figure 88. Pie graph to represent molecular functions significantly dysregulated in <i>PSEN1</i> NSC at P3 compared with controls	229
Figure 89. Molecular functions dysregulated between <i>PSEN1</i> and control NSC at P3	230
Figure 90. Pathways dysregulated between <i>PSEN1</i> and control NSC at P3	231
Figure 91. Pathway dysregulation between <i>PSEN1</i> and control NSC at P3.....	232
Figure 92. qPCR based interrogation of Wnt signalling in <i>PSEN1</i> neural differentiation	238
Figure 93. qPCR based interrogation of Notch signalling in <i>PSEN1</i> neural differentiation	239
Figure 94. Apoptosis in <i>PSEN1</i> neural differentiation.....	240
Figure 95. Apoptosis in <i>PSEN1</i> NPC compared with controls	241
Figure 96. Full sequence map for pCXWB-EBNA1.....	297
Figure 97. Full sequence map for pCXLE-hSK.....	298
Figure 98. Full sequence map for pCXLE-hUL.	299
Figure 99. Full sequence map for pCXLE-hOCT3/4-shp53-F.	300

Figure 100. Vector map for the pmax GFP™ Vector	301
Figure 101. Bioanalyzer traces displaying cDNA fragment size of samples.....	302
Figure 102. Example of contamination with larger DNA fragments.....	303
Figure 103. Q score of sequencing reads	303
Figure 104. FastQC results for sequencing samples	309
Figure 105. HISAT2 alignment scores.....	315
Figure 106. Deduplication Statistics.....	316
Figure 107. Number of mapped reads per contig.....	318
Figure 108. ChrXY mapped reads	319
Figure 109. Read distributions before and after alignment-based filtering.....	320
Figure 110. FeatureCounts: assignments before and after filtering.....	323
Note: Figures 96-110 can be found in the Appendix.	
Contents:	7
Acknowledgements.....	22
1. Overall Introduction	23
1.1.0 Alzheimer’s Disease	23
1.1.1 Impact of Alzheimer’s disease.....	23
1.1.2 AD Pathophysiology	23
1.1.3 Amyloidogenic and non-amyloidogenic processing of APP.....	24
1.1.4 Aβ and tau in AD	26
1.1.5 The role of γ-secretase.....	27
1.1.6 Risk factors and causes of AD	31
1.1.7 Treatment options for AD	34
1.1.8 Notch and <i>PSEN1</i> in AD	37
1.2.0 Neurogenesis.....	41
1.2.1 Stem cells	41

1.2.2 Symmetric and asymmetric cell division.....	41
1.2.3. Neurogenesis and development.....	49
1.2.4 Adult hippocampal neurogenesis.....	53
1.3 Unifying hypothesis.....	60
1.4 Aims.....	60
2.0 Materials.....	61
2.1 Cell lines used.....	66
2.2 Plasmids used.....	68
3.0 Methods.....	70
3.1 Cell culture methodologies.....	70
3.1.1 Expansion and culture of NSCs purchased from Axol Bioscience.....	70
3.1.2 Mitotic inactivation of MEFs for iPSC culture.....	70
3.1.3 Reprogramming NSCs.....	71
3.1.4 Trilineage differentiation.....	73
3.1.5 Culture and expansion of induced pluripotent stem cells (iPSC) and human embryonic stem cells (hESC).....	73
3.1.6 Feeder free culture and expansion of hESC/iPSC.....	74
3.1.7 Neural differentiation of human ESC and iPSC to NSC and NPC.....	74
3.1.8 Generation of neurospheres.....	75
3.1.9 Terminal differentiation.....	75
3.2 Bacterial work.....	75
3.2.1 Increasing stocks of episomal plasmids for reprogramming.....	75
3.2.2 Bacterial transformation.....	76
3.2.3 Plasmid isolation.....	76

3.3. Immunostaining	77
3.4 Molecular work	79
3.4.1 Isolation of genomic DNA.....	79
3.4.2 DNA sequencing of AD iPSC	79
3.4.3 Isolation of RNA.....	80
3.4.4 Determination of RNA concentration and purity	81
3.4.5 DNase treatment of RNA	81
3.4.6 Generation of first strand cDNA for two-step RT-qPCR.....	81
3.4.7 Selecting primers for qPCR.....	82
3.4.8 Calculating primer efficiency.....	85
3.4.9 qPCR based investigation of transcriptomic differences between control and <i>PSEN1</i> neural cells	87
3.4.10 Delta Delta Ct method to calculate fold change gene expression.....	89
3.4.11 Statistical analysis of results	90
3.5 Flow cytometry	90
3.5.1 Analysis of OCT4 expression in <i>PSEN1</i> and control iPSC using flow cytometry.....	90
3.5.2 Analysis of cell cycle in <i>PSEN1</i> and control NSC using flow cytometry.....	91
3.5.3 Analysis of apoptosis and necrosis in <i>PSEN1</i> and control NSC using flow cytometry.....	92
3.5.4 Panel design for flow cytometry using the MACSQuant® analyzer 10 flow cytometer.....	94
3.5.5 Using the MACSQuant® analyzer 10 flow cytometer	95
3.5.6 Analysis of flow cytometry results	96
3.6 Library preparation for RNA sequencing	97

3.6.1 Isolation of RNA and preparation for RNA seq	97
3.6.2 Analysis of RNA integrity	98
3.6.3 Library preparation using the TruSeq stranded mRNA.....	99
3.6.3.1 Purification of mRNA.....	99
3.6.3.2 Fragmentation of mRNA	100
3.6.3.3 Synthesis of first strand cDNA.....	101
3.6.3.4 Synthesis of second strand cDNA	102
3.6.3.5 Purification of cDNA.....	102
3.6.3.6 Adenylation of 3' ends	103
3.6.3.7 Ligation of adapters	104
3.6.3.8 Clean up of ligated fragments.....	104
3.6.3.9 Enrichment of DNA fragments.....	105
3.6.3.10 Clean-up of amplified DNA	106
3.6.4 Analysis of library quality	106
3.6.5 Library quantification	108
3.6.5.1 Standard curve and analysis of results	109
3.6.6 Normalisation and pooling of libraries for RNA sequencing	110
3.6.7 Cluster generation and RNA sequencing mid output	111
3.7 Processing and quality control of initial RNA sequencing data	111
3.7.1 Merging Read 1 and Read 2 Fastq files.....	111
3.7.2 Assesment of sequence quality	111
3.7.3 Trimming and filtering RNA sequencing data	114
3.7.4 Infer experiment on BAM file	115
3.7.5 Alignment to a reference genome.....	115

3.7.6	Assesment of alignment quality.....	115
3.7.7	Filtering of aligned sequences	116
3.7.8	Generation of read counts	116
3.7.9	Differential gene expression analysis	116
3.7.10	Analysis of RNA sequencing data	117
4.0	Development of a relevant model for investigation of AD.....	118
4.1.0	Introduction	118
4.1.1	Derivation of stem cells.....	118
4.1.2	2D and 3D disease modelling.....	121
4.2	Aims.....	124
4.3.0	Results	125
4.3.1	Culture of Axol AD and control NSC.....	126
4.3.2	De-differentiation of control NSC to generate control iPSC.....	127
4.3.2.1	Optimising nucleofection of NSC	128
4.3.3	De-differentiation of SHEF3 and nHDF lines for comparison of reprogramming efficiency	131
4.3.4	Verification of pluripotency in control iPSC.....	133
4.3.4.1	Alkaline phosphatase staining	133
4.3.4.2	Immunocytochemistry	134
4.3.4.3	Trilineage differentiation of control iPSC.....	135
4.3.5	De-differentiation of <i>PSEN1</i> NSC to produce <i>PSEN1</i> iPSC lines	137
4.3.6	Production of feeder free iPSC.....	140
4.3.7	Assessment of pluripotency in <i>PSEN1</i> iPSC.....	141
4.3.7.1	Immunocytochemistry for pluripotency markers in <i>PSEN1</i> iPSC	141

4.3.7.2 Trilineage differentiation of <i>PSEN1</i> iPSC.....	142
4.3.7.3 Analysis of OCT3/4 expression in <i>PSEN1</i> and control iPSC by flow cytometry	143
4.3.8 Sanger sequencing of iPSC to confirm presence of <i>PSEN1</i> A246E mutation..	147
4.3.9 Generation of models for investigation of AD neurogenesis	147
4.3.9.1 Validation of the neural differentiation protocol using SHEF3 ESC.....	148
4.3.9.2 immunocytochemistry for confirmation of neural phenotype	150
4.3.9.3 Neural differentiation of <i>PSEN1</i> and control iPSC to NSC	153
4.3.9.4 Neural differentiation to NPC	155
4.3.9.5 Validation of <i>PSEN1</i> and control NSC and NPC.....	156
4.3.9.6 Flow cytometry to assess nestin expression in <i>PSEN1</i> and control NSC and NPC	157
4.3.9.7 Generation of neurospheres.....	160
4.3.9.8 Chapter summary.....	162
5.0 Investigation of AD neurogenesis	163
5.1.0 Introduction	163
5.1.1 The cytoskeleton	163
5.1.2 Markers of neural differentiation	165
5.1.3 Self-renewal and differentiation in neural precursors	168
5.1.4 Autophagy, inflammation, and the antioxidant response.....	171
5.2 Aims.....	172
5.3 Results	173
5.3.1 qPCR-based analyses of <i>PSEN1</i> NSC and neurospheres	177
5.3.2 Cell cycle analysis in <i>PSEN1</i> and control NSC.....	183

5.3.3 Chapter summary.....	190
6. RNA sequencing	191
6.1 Introduction	191
6.1.1 Overview of RNA sequencing.....	191
6.1.2 Quality control of RNA seq data	194
6.2 Aims.....	194
6.3 Results	195
6.3.1 Analysis of cDNA fragment sizes post library preparation	197
6.3.2 Processing of RNA sequencing data.....	198
6.3.3 Quality control of RNA sequencing data.....	201
6.3.4 Alignment, generation of read counts and data analysis	202
6.3.5 Analysis of variance in rna sequencing data	203
6.3.6 Analysis of differential gene expression in rna sequencing data	207
6.3.6 Analysis of pathways and molecular functions altered in <i>PSEN1</i> and control neural differentiation	214
6.3.7 Analysis of pathways and molecular functions altered between <i>PSEN1</i> and control NSC at P3	224
6.3.8 Chapter summary.....	232
7.0 Interrogation of RNA sequencing results.....	236
7.1 Introduction	236
7.2 Aims.....	236
7.3 Results	237
7.3.1 Wnt and Notch signalling in <i>PSEN1</i> neural differentiation.....	237
7.3.2 Apoptosis in <i>PSEN1</i> neural differentiation.....	240

7.3.3 Chapter summary.....	243
8.0 Discussion.....	244
8.1 Adult hippocampal neurogenesis	244
8.2 Dysregulated neural differentiation in AD NSC/NPC	245
8.3 Altered Cell Signalling in AD NSC/ NPC	247
8.4 Dysregulated Cell Cycle Progression and Apoptosis in AD NSC and NPC	249
8.5 Comparison of <i>PSEN1</i> and control Neural Differentiation	252
8.6 Comparison of <i>PSEN1</i> and control NSC at P3	257
8.7 Limitations and further study	259
8.8 Conclusion and Impact.....	260
9.0 Bibliography	263
10.0 Apendices	263
10.1 Appendix 1	297
10.1.1 Plasmid maps for plasmids used in iPSC reprogramming.....	297
10.2 Appendix 3: RNA sequencing data analysis	301
10.2.1 Bioanalyser traces of cDNA fragments post library preparation.....	301
10.2.2 Initial quality data for sequencing reads.....	303
10.2.3 Quality control of RNA sequencing data.....	307
10.2.4 Trimming and filtering of sequencing data.....	311
10.2.5 Determination of strandedness	312
10.2.6 Alignment to reference genome.....	313
10.2.7 HISAT2 alignment scores.....	315
10.2.8 Filtering and QC of alignment	315
10.2.8.1 Picard: MarkDuplicates	316

10.2.8.2 Samtools idxsats.....	317
10.2.8.3 RSeQC.....	320
10.2.9 Feature counts	320
10.2.10 Percentage of reads assigned to the reference genome.....	323
10.2.11 DeSeq2	324
10.2.12 Volcano plot	326
10.2.13 GeneOntology, Panther classification system	327

Acknowledgements

I would like to thank my director of studies Prof. Tristan McKay for his kindness, support, and guidance throughout my time at MMU.

I would like to thank all previous and present members of team McKay for their knowledge, their technical expertise and for their friendship: Lorna FitzPatrick, Christopher Thornton, Rhys Smith, Oriana Mandolfo, Marta Guevara, Louise Bullen, Stuart Fielding and Aseel Sharaireh.

I would also like to express my gratitude to everyone at MMU who has offered their help over the years, especially Dr Stephen White whose support and knowledge has been invaluable in my new position as a KTP associate with MMU and InstilBio, and Liam Hanson who provided support and guidance that was vital to the success of my RNA sequencing library preparation. It has been a pleasure to work in such a supportive and collaborative research environment.

Finally, I would like to thank my friends and family for their love and support. Special thanks to Toby, Fran, Mia, Kerin, Mum, Dad, Grandma, Grandad, and my brothers. Hopefully you all enjoy reading this!

1. Overall Introduction

1.1.0 Alzheimer's Disease

1.1.1 Impact of Alzheimer's disease

Dementia is a term which encompasses a range of disorders with characteristic features of declining cognition, function, and behaviour. Alzheimer's disease (AD) is a progressive neurodegenerative disease and is the most common form of dementia among aged people, accounting for 60-80% of cases (Aghaizu *et al.*, 2020; Hampel *et al.*, 2018; Wang *et al.*, 2017). AD is a chronic illness, with an average clinical duration of 8-10 years. In people over 65 years of age, AD has a prevalence of 10-30%. It is estimated that globally, more than 50 million people are affected by dementia; this number is expected to increase significantly with increasing life span in populations across the world and is predicted to reach over 250 million by 2050. In England and Wales alone, the number of patients with dementia is expected to reach 1.2 million by the year 2040 (Vaz and Silvestre., 2020; Hampel *et al.*, 2018; Masters *et al.*, 2015).

1.1.2 AD Pathophysiology

AD pathophysiology includes neuroinflammation, synapse loss, aberrant processing of amyloid precursor protein (APP) and breakdown of the blood brain barrier. In patients with AD, there is also a significant reduction in brain volume compared with healthy patients (Mattson *et al.*, 2004). This loss of brain volume results from the degeneration of synapses and the death of neurons, primarily seen in the hippocampus (Cheignon *et al.*, 2017). AD has been shown to present with loss of neural stem cells (NSC) in the hippocampus (Nicaise *et al.*, 2020, Moreno-Jiménez *et al.*, 2019), which may lead to impaired regenerative repair, culminating in accelerated disease progression. Patients initially present with mild cognitive impairment (MCI) which may have developed over decades before becoming detectable (Lazarov and Hollands., 2017). AD presents with early onset (EOAD), or sporadic with disease presenting later in life. Sporadic AD, also termed late onset AD

(LOAD) presents in patients over 65 years of age and comprises over 95% of AD cases. Early onset AD (EOAD) presents in patients under 65 years of age, with a mean age of onset of 45 years of age. EOAD accounts for 5-10% of all AD cases and 10-15% of EOAD cases show mutations in genes *PSEN1*, *PSEN2* and *APP* which are involved in the processing of APP. Mutations in *PSEN1*, *PSEN2* and *APP* have a familial pattern of inheritance and are described as familial AD (FAD) mutations (Ayodele *et al.*, 2021; Masters *et al.*, 2015). Disease manifestation varies largely between LOAD patients and between patients with different FAD mutations, however, in all subtypes, histopathological analysis of post-mortem tissue indicates the presence of abnormal protein aggregates. These protein aggregates consist of amyloid beta (A β) plaques and tau neurofibrillary tangles (NFT) and have been proposed to be the causative agents of AD progression (Hardy and Higgins., 1992).

1.1.3 Amyloidogenic and non-amyloidogenic processing of APP

The single-pass membrane protein APP which is primarily produced by neurons, is expressed in the synapses of neurons and has a role in neuronal growth, synaptic formation, and repair, as well as in iron export and anterograde neuronal transport. In mammals, APP is part of a family of similar proteins, which includes the amyloid precursor-like proteins APLP1 and APLP2. In the brain, APP is expressed at high levels, and is metabolised rapidly via the action of the proteases α -secretase, β -secretase, and γ -secretase. APLP1 and APLP2 function in a similar way to APP but metabolism of these proteins does not result in the generation of insoluble A β (Turner *et al.*, 2003; O'Brien and Wong., 2011). The amyloid cascade hypothesis formulated by Hardy and Higgins., (1992) described how APP processing can generate insoluble A β proteins, this theory proposed that the generation and accumulation of A β initiates disease progression in AD leading to the formation of senile plaques and NFT. The inter- and intraneuronal presence of A β plaques and NFT was proposed to cause neurotoxicity, culminating in neuronal cell death and neurodegeneration (Hardy and Higgins., 1992; Armstrong., 2011). In the amyloid cascade hypothesis, APP can be cleaved via two pathways -one of which results in the generation of insoluble A β , the

other results in the generation of soluble peptides. In non-amyloidogenic processing, cleavage of APP is mediated by membrane bound α -secretase, generating CTF α which is an α -C terminal fragment and sAPP α which is an N-terminal fragment, CTF α then undergoes cleavage by γ -secretase, generating the APP intracellular domain (AICD) and P3 (Figure 1.). In amyloidogenic processing of APP, membrane bound β -secretase (BACE1) cleaves APP into C-terminal fragments β (CTF β or C99) and N-terminal soluble APP β (sAPP β), after which CTF β undergoes cleavage by γ -secretase to generate AICD and the insoluble protein A β . Insoluble A β is secreted into the extracellular space, where it accumulates and aggregates to form A β senile plaques (Chen *et al.*, 2017) (Figure 1.).

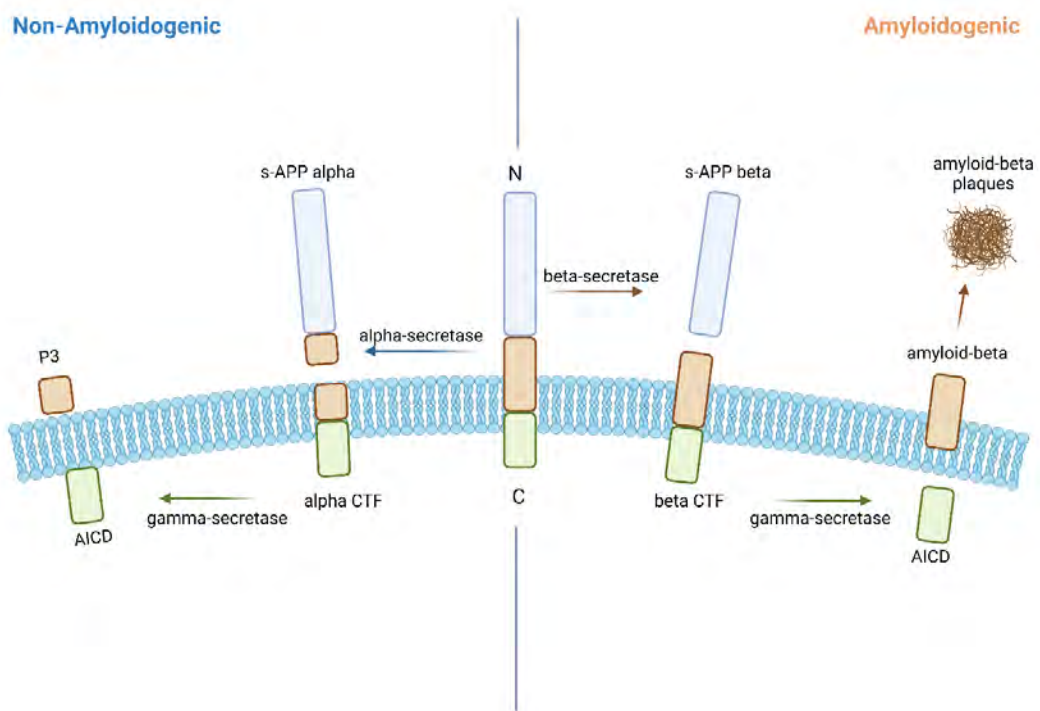


Figure 1. APP cleavage pathways

The amyloid precursor protein (APP) may be cleaved by both amyloidogenic and non-amyloidogenic pathways. During non-amyloidogenic processing, APP is cleaved by α -secretase and γ -secretase to generate soluble proteins (CTF α , sAPP α , AICD and P3). During amyloidogenic processing, APP is cleaved by β -secretase and γ -secretase to generate the insoluble protein A β . Accumulation of A β occurs within the neurons of patients with Alzheimer's disease. Diagram constructed using Biorender, based on the schematic by Thordardottir *et al.*, (2017) and work by Chen *et al.*, (2017).

1.1.4 A β and tau in AD

There are two major isoforms of A β , which can be produced from proteolytic cleavage of A β , the A β_{40} isoform which is 40 residues long and the A β_{42} isoform, which is 42 residues long (Gu and Guo., 2013). A β_{40} and A β_{42} monomers can assemble into oligomers, fibrils and protofibrils. Oligomers of A β are soluble and can diffuse into synaptic clefts, here they can interfere with synaptic signalling. A β oligomers can polymerise into amyloid fibrils which are insoluble and can assemble into plaques (Tiwari *et al.*, 2019; Chen *et al.*, 2017). When A β_{42} isoforms self-assemble into aggregates, the surface of the fibril formed can catalyse secondary nucleation, leading to the formation of oligomers which are neurotoxic (Lattanzi *et al.*, 2021). Amyloid plaques are mostly composed of A β_{42} which may result from increased efficiency of A β_{42} isoforms to be incorporated into A β_{42} fibrils, whereas in cerebrospinal fluid taken from patients with AD, the concentration of A β_{40} is much higher than that of A β_{42} (Gu and Guo., 2013). Both LOAD and FAD subtypes display accumulation of the 42 amino acid peptide amyloid beta (A β_{42}) and hyperphosphorylation of tau protein to form NFT (Baldacci *et al.*, 2017). Tau is the major microtubule associated protein (MAP) found in neurons. In the absence of neurological disease, MAP promote assembly of tubulin into cytoskeletal microtubules and help to stabilise their structure, in this way MAP regulate microtubule networks in neuronal axons and dendrites (Dehmelt and Halpain, 2005). In AD, the polymerisation of A β into insoluble fibrils leads to p38 MAP Kinase activation and hyperphosphorylation of tau proteins, hyperphosphorylation leads to detachment of tau from microtubules, leading to an increase in the formation of filamentous inclusions such as NFT, these accumulate within neurons and can lead to loss of normal neuronal function (Figure 2) (Tiwari *et al.*, 2019; Ittner *et al.*, 2008; Sun *et al.*, 2003). NFT have also been identified in >20 distinct neurodegenerative diseases, in which tau mutations lead to neuronal dysfunction and disease progression, these are termed tauopathies. There are six isoforms of the Tau protein in the human brain, which are encoded by the *MAPT* gene found on chromosome 17

(Iqbal *et al.*, 2010). Mutations in the *MAPT* gene are not linked with AD and dysregulate production of tau isoforms, leading to altered assembly of microtubules. Autosomal dominant mutations in the *MAPT* gene have been shown to cause NFT and result in frontotemporal dementia with parkinsonism. Many tauopathies occur without the presence of amyloid beta plaques, suggesting a role for NFT in AD aetiology, without the contribution of A β (Naseri *et al.*, 2019; Ricciarelli and Fedele., 2017).

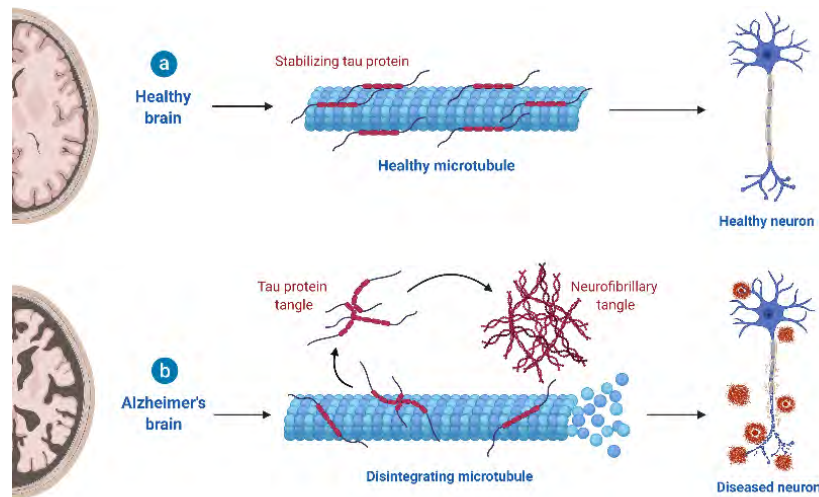


Figure 2. Pathology of Alzheimer's disease

Cartoon representation of a healthy brain and an AD brain displaying Tau pathology. In the healthy brain, tau protein acts to stabilise microtubules. Patients with AD often display reduced brain volume and the intraneural accumulation of tau NFT, which results in the destabilisation of microtubules and contribute to disease pathology. Figure created in Biorender.com.

1.1.5 The role of γ -secretase

Γ -secretase is an intramembrane protease which cleaves a range of type-1 transmembrane proteins including APP (Watanabe and Shenb., 2017). Four integral membrane proteins combine to form the γ -secretase proteasomal complex, these are presenilin 1, presenilin 2 (also termed presenilin enhancer 2 -PEN-2), nicastrin (NCT) and anterior pharynx defective-1 (APH1) (Figure 3. The γ -secretase complex). The transmembrane protein presenilin 1 is the catalytic component of γ -secretase and

presenilin 2 promotes presenilin endoproteolysis. Nicastrin plays a role in substrate selection and is a single span membrane protein. APH-1 has an important role in the trafficking, stabilisation, and assembly of the γ -secretase complex. Interactions between the transmembrane domains of nicastrin and Aph-1 mediate formation of a sub-complex between the two components, which then associates with presenilin. Presenilin initiates the process of auto-endoproteolysis, forming heterodimers NTF and CTF- these heterodimers make up the proteasomal aspects of presenilin and thus of γ -secretase (Beel and Sanders., 2008).

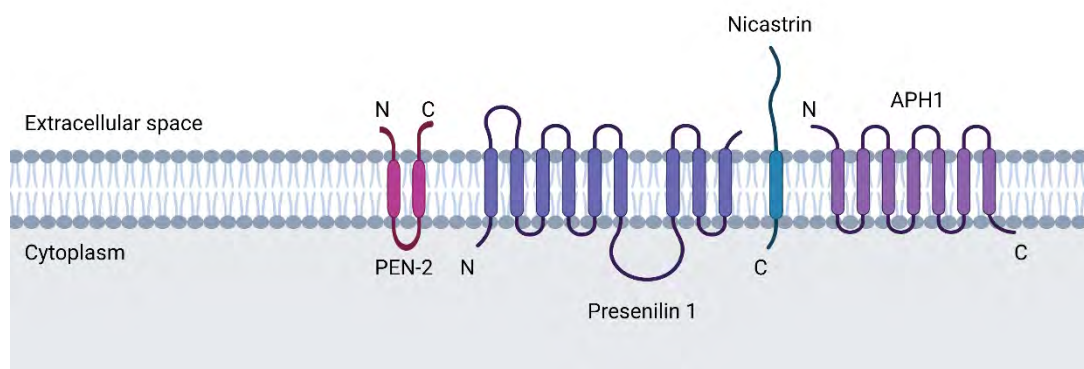


Figure 3. The γ -secretase complex

The γ -secretase proteasomal complex consists of Nicastrin (NCT), anterior pharynx defective-1 (APH1), Presenilin 2 (PEN-2) and Presenilin 1. Presenilin-1 is the catalytic subunit of γ -secretase, it has 8 transmembrane domains and a cytoplasmic loop which is found between the 6th and 7th transmembrane domains (Kabir *et al.*, 2020). Figure created in Biorender.com.

One of the primary roles of γ -secretase is to carry out hydrolysis within the cell membrane. In recent years, over 149 substrates of γ -secretase have been identified, 55 of which are displayed in Figure 4. Identification of γ -secretase substrates has led to improved understanding of the roles of γ -secretase in signal transduction, protein degradation, tissue homeostasis and embryonic development. Most substrates of γ -secretase have a long extracellular domain and ectodomain shedding is required before cleavage by γ -secretase. However, short substrates such as the B cell maturation antigen are also cleaved by γ -secretase. Recently identified substrates of

γ -secretase include CHL1, *TREM2* and TNFR1 (Beel and Sanders., 2008; Güner and Lichtenthaler., 2020).

Protein	10	20	30	Sheddase(s)	Sheddase Regulation	Reference
Alcadein α	H P F A V V P S T A T V V I V V C V S T L V F V M I I G V E			ND	ND	[101]
Alcadein γ	Q H S - - S Y V P S L A T V V I I I S Y C M L V F V V A M G V Y			ND	ND	[101]
AFLP1	A G T G W S R E A M S C E L I M G R G G S L I T V I S M I L T E			B1	N-glycosylation	[102, 103]
AFLP2	R E D F S L S S A L E T G L L V I A V A T R T V I S I S M L E			BL, A10, A17	ND	[98, 102-104]
ApoER2	- - - - - M G S T V I T A A V I G I I V P I V V I A I L C M S G Y L I			ND	apoE, recitin, $\alpha 2$ -macroglobulin	[105, 106]
APP	A E D V S N K K A I I G L M V G O V V I A T V I V I I L V M L			BL, A9, 10, 17	E-spondin	[107-109]
CD43	R N P - D E N S R G M L P V A V L V A L L A V I V L V A L L L L			ND	ND	[110]
CD44	P I R - T P Q I P E W L T I L A S L L A I A I L A V C I A V			A10, A17, M	hyaluronan, monoclonal	[111-117]
CSF1R	A H T - H P P D E F L F L P V V V A C M S I M A L L L L L L L L L Y K Y			A17	N-glycosylation	[118-120]
CXCL16	P T A - - R T S A T M P V I C L I A I E L I T A A L S Y V I			A10	lipopolysaccharide, IFN γ	[121-125]
CX3CL1	- - - - - A Q A A T R R Q A V G L L A F L G L L F C L G V A M F T Y Q S L			A10, A17	ND	[122-125]
DCC	V T P - Q K N S N L I V I V V T V G V I T V L V V T V A V L C T R R S S A Q Q R			ND	ND	[126]
Delta1	S Q G - - - G P F P W V A V C A G V V I V L L L L L G C A A V V V C V R L			A9, A10, A12, A17	Notch	[127-131]
E-cadherin	V E A - G L Q I P A I I G I L G I I L A L L I L L L L L L L L - - - R R R A V V K E N			A10	ionomycin, mechanical scraping	[132-134]
EphrinB1	E F N - - - S K V A L P A A V G A G V E I L L I I L L L L L K L R			ND	ND	[135]
EphrinB2	- - - - - G S E V A L P A G L A S G C I I I I I I L V V L L L K Y R			ND	LipB2	[136]
EphB2	S I K - - E K L P L L I V G S S A A G L V E L L A V Y V I A I V - - C N R			A10	EphrinB2	[137]
ErbB4	L P Q - - H A R T P L T A A G V P G I F I L V I V G L T F A Y Y V R R K S I K K K			A17	heregulin/NRG1	[138-142]
GHR	E A C E E D I O P W F L I I I F G I F G V A M L F V V I F S - - K Q Q			A17	dimertization inhibits cleavage	[143-145]
HLA-A2	S S Q - - P T V P T V G T I A G I V L F G A V I T G A V V A A M W R R N S S D R K			A10	ND	[146]
IGF1R	T G Y - - E N F I B L I E A I P V A V F L I V G G E V T M L Y V F H R K R N S R I L			ND	ND	[147]
IFN α 2	S F S - - - A E S A K I G G I T I V F L A T V T S T I V I L - - K W I G Y F C L			ND	IFN α 2, IFN β	[148]
IL1R2	K E A - - - S S T I S M G T M A P I S L A F L V G G I W M - - - H R			A17, A8	ND	[123, 149]
IR	D V P - - - S N I A K L I G P I T I F E I S V Y I G S Y I F L R K R O P D G P			ND	ND	[150]
Irf6	- - - - - P V D S M L K D M A T I I S T E L L G W V A I T I T V P L S M H Q Q			ND	ND	[151]
Jagged2	V T G - - S S T G I L P V P I C G A F S V L A C V V I C V W W T R K R K E R E			A17	Notch	[130, 151]
L1	P P A - G F A T E G W I G F V S A I I L L L L V L I L C F I - - K R S			A10, A17	NMDA agonist	[152]
LRP	V F S - Q Q P G H I A S T I L P L L L L L L L V L V A G V F W Y K R R V G G A K			B1, M	O-glycosylation	[106, 153-155]
LRP1B	D H I - - - S T R S I A T I V P E I V L I T I T I V I G L V L C R K R			ND	ND	[156]
LRP2	K G I - - S P G T A V A V L I T I L L V V I G A L A T A G E - F H Y R			ND	Vitamin-D binding protein	[157]
LRP6	T E E P A P Q A T N - - - T V G S V I G V I V T I V S G T V Y F I C Q R M L C P R			ND	Wnt3a	[158]
N-cadherin	H A - - - I E A I T A T L C G I A L L F L V M E F V W M - - M K R			A10	ionomycin, NMDA agonist	[159, 160]
Nectin1 α	R A G - - - P P T A I I L G V A G S I L L V L I V V G G L V A L R R R			ND	ND	[161]
Notch1	V E P - P P P A Q I H L - M Y V A A A F V L L F F V G G V L L S R K R R Q H G			A10, A17	Delta, Jagged	[162-165]
Notch2	L E S - P R N A Q L I Y L A V A V Y I L F I L L G Y I M - - - A K			ND	Delta, Jagged	[166, 167]
Notch3	E A P - E Q S V - P L I P L V A G A V F L L I F I L G V M V - - A R			ND	ND	[167]
Notch4	P P A N Q L P W P T L C S P V Y G V L L L A I G A L V L Q I L - - - - R R R R R			ND	ND	[167]
NRAD	E P P - G A S S - N I I P V Y C A L L A T V I L G L L A V A F K C W R S H K Q R Q			ND	N-glycosylation	[168]
p75-NTR	V T R - G T T D - N I I P V Y S I L A A V V G L V A Y I A F K R W N S C K Q -			A17	neurotrophins; NGF; BDNF	[169-173]
PKHD1	V T R K E K S T I T L A A S S S V A S W L A L S C L V C W L - - - - R E S K S			ND	A23187	[174, 175]
Pcdh α 4	- - - - - D A A L V D V N V Y I I A T C A V S S L V I T E L L Y T A L			A10	homophilic heteromers	[176]
Pcdh γ -C3	- - - - - Q K K N I T E Y L L S L L L V S M G V M T Y E G M I T F K V Y K W K Q			A10	homophilic association	[176, 177]
PTP α	K Q T - - D R V V K I A G I S A G I I V F I L L I L V V I I V - - K K S			A10	LAKK X α -CO $_2$ H	[178]
PTP-Lar	- - - - - K Q T D H T V K A G V I A G I L L F V I I F L G V V L M K K R			ND	LAKK X α -CO $_2$ H	[178]
PTP-LAR	A Q Q - Q E E P E M L W - V T G P V I A V I L I I L V I A I L L F K R K O			A17	A23187	[179-181]
SorCS1b	V D L T P T H S G - - - - - S A M I M L S V V F V G L A V E V I Y K F K			A17	ND	[182, 183]
SorLA	- - - - - A A R S T D V A A V V V P I L F L I I S T G V G F A I L Y T K H R R L Q			A17	head-activator	[182-185]
Sortilin	E K Q N S K S N S V P I I A I V G L M L V T V V A G V I T V - - - K K Y			A17	ND	[182, 183]
Syndecan3	K S I - L E R K E M I V A V I V G G V G A F F A T L V T L I V R M K K D E G			ND	ND	[186]
Tyrosinase	- - - - - E Q A S R I V S W L I G R A M V G A V I T L L R G L V S L L C			ND	ND	[187]
TYRP1	- S R - E F S V P E L I A I A M G A L L V A L I P G T A S Y L I R A R			ND	ND	[187]
TYRP2	E T P - - - G W P T T L L V V M G I L V A L V G L F V L A F I - - - Q Y R			ND	ND	[187]
VEGF-R1	T S D - - K S N L E L I T L T C T C V A A T I F W L L L I L F I - - R K M			ND	VEGF	[188]
VGSC β 2	P E R - - D S T V A V I G A S V G T L A V V I L V L M V Y - - - K C V			B1	ND	[189, 190]
VLDLR	S V P P K G T S A - - - - A W A I L P L L L L Y M A A V G G Y L M W R N W Q H K N M			ND	apoE, recitin, $\alpha 2$ -macroglobulin	[105]

Figure 4. Known γ -secretase protein substrates.

Sequences and properties of 55 known γ -secretase protein substrates. (Beel and Sanders., 2008).

The role of γ -secretase in cleavage of APP is well identified due to its relevance to AD. In LOAD, it is hypothesised that efficiency of APP metabolism declines with age, leading to increase the generation of A β plaques, which become neurotoxic as concentrations increase (Paroni *et al.*, 2019). Mutations in genes *APP*, *PSEN1* and *PSEN2* all result in altered proteolytic cleavage of APP, leading to an increase in the

production of the longer, self-aggregating isoform A β ₄₂ and a reduction in the generation of the shorter isoform A β ₄₀ (Ricciarelli and Fedele., 2017). Many FAD mutations have been shown to cause a partial loss of function in the γ -secretase complex (Steiner *et al.*, 1999; Shen *et al.*, 2007; De Strooper *et al.*, 2007). APP mutations can reduce the efficiency of APP cleavage by γ -secretase, suggesting that these mutations result in impaired recognition of APP by γ -secretase. One hypothesis proposes that APP mutations cause tilting of the APP transmembrane domain helix, thus changing the substrate site that is presented to γ -secretase for cleavage (Götz *et al.*, 2019; Xu *et al.*, 2016). As presenilin 1 makes up the catalytic subunit of γ -secretase, mutations in *PSEN1* can affect the ability of γ -secretase to cleave its substrates and thus, can affect downstream signalling pathways of γ -secretase substrates. Various hypotheses have been presented to explain how *PSEN1* mutations lead to disease pathology. One hypothesis in line with the amyloid cascade hypothesis, is that *PSEN1* mutations lead to increased APP processing and increased generation of A β ₄₂, this is backed up by data generated from mouse models and transfected cells which showed that *PSEN1* mutations increased plasma levels of A β ₄₂ (Borchelt *et al.*, 1996; Scheuner *et al.*, 1996; Duff *et al.*, 1996; Hardy and Selkoe 2002). In recent years, research has focused on the relative ratios of A β ₄₀ to A β ₄₂ and indicates that levels of A β ₄₂ increase relative to levels of A β ₄₀ in most cases of FAD (Selkoe and Hardy., 2016). The presenilin hypothesis proposes that *PSEN1* mutations can lead to loss of function of presenilin, leading to AD disease progression (Heilig *et al.*, 2010, 2013), in mouse models, severe mutations in *PSEN1* have also been shown to completely inhibit γ -secretase function and the generation of A β (Xia *et al.* 2015, 2016). Presenilin 1 plays a role in learning and memory formation. Presenilin 1 is also required for macroautophagy, a process which uses lysosomes for degradation of waste materials, and which is necessary for neuronal survival. Importantly, normal function of presenilin is vital for neural survival during the process of ageing (Kabir *et al.*, 2020).

1.1.6 Risk factors and causes of AD

Although FAD and LOAD subtypes present with a similar lack of intraneuronal clearance of A β and NFTs, they differ in disease aetiology and progression. Sporadic or LOAD presents in patients aged 65 and over with no clear disease causing mutation, whereas FAD mutations have a clear genetic origin and a severe disease phenotype, with symptoms progressing more rapidly than in patients with sporadic AD. FAD is caused by mutations in genes *PSEN1*, *PSEN2* and *APP* (Figure 5). Some allelic variants such as *APOE4* are associated with LOAD but have varying risk levels based on whether they present as a heterozygous or homozygous mutation (Figure 5) (Uddin *et al.*, 2021).

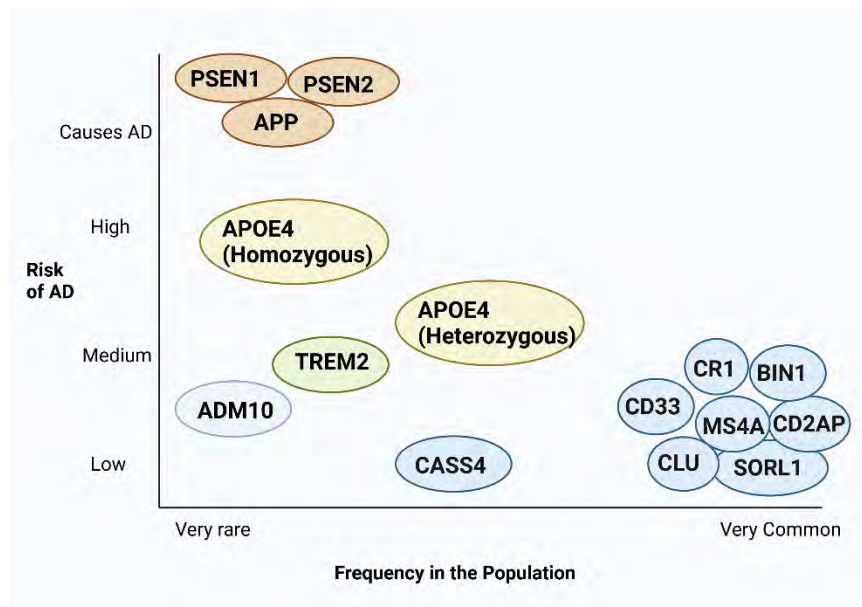


Figure 5. Genes associated with effect or risk of AD

Mutations in genes *PSEN1*, *PSEN2* and *APP* cause AD. Some allelic variants such as *APOE4* are associated with late onset AD. Next generation sequencing of early onset AD patients has identified several genes associated with development of disease including *NOTCH3*, *SORL1* and *TYROBP*. Figure based on work by Uddin *et al.*, (2021).

Patients with LOAD present with an increase in the production of the longer, self-aggregating isoform A β 42 and a reduction in the generation of the shorter isoform A β 40 (Ricciarelli and Fedele., 2017). According to the amyloid cascade hypothesis,

altered cleavage of APP which may result from age related impairments in APP metabolism leads to the intracellular accumulation of aggregated $A\beta_{42}$ and generation of NFT which leads to defective neural signalling and neural decline in LOAD (Wang *et al.*, 2017). Presence of the *APOE4* allele is a strong genetic risk factor for the development of LOAD, and large-scale genome-wide association studies (GWAS) and GWAS meta-analyses have indicated that the *APOE2* allele is a protective factor in reducing risk of developing LOAD. The *APOE* gene codes for the protein Apolipoprotein E (APOE), which has been shown to mediate a range of processes including cholesterol transport, clearance of $A\beta$, regulation of neurite outgrowth, synapse formation, synaptic plasticity, and destabilisation of microtubules (Hunsberger *et al.*, 2019). Mouse models which express human *APOE* alleles have been used to investigate disease by modulating APOE levels, enhancing APOE lipidation and blocking interactions with $A\beta$ (Serrano-Pozo *et al.*, 2021). APOE is expressed by astrocytes and microglia in the healthy brain, and most brain APOE is lipidated by ATP-binding cassettes A1 (ABCA1) and G1 (ABCG1). Receptors such as low-density lipoprotein receptor related protein 1 (LRP1) are expressed on astrocytes and neurons and enable internalisation of lipidated APOE (Serrano-Pozo *et al.*, 2021). In brains with AD, $A\beta$ plaques, NFT and cerebral arteries afflicted with amyloid, and tau all cause microglia and astrocytes to react. This leads to altered lipid metabolism and altered transcription of *APOE* in microglia and astrocytes.

FAD mutations in *APP*, *PSEN1* and *PSEN2* result in altered proteolytic cleavage of APP, generally leading to increased levels of the $A\beta_{42}$ isoform compared with the $A\beta_{40}$ isoform (Buckles *et al.*, 2021, Watanabe and Shen., 2017). The gene *PSEN1* is located on the long arm of chromosome 14 at position 24.2 (14q24.2), it contains 12 exons and codes for the transmembrane protein, Presenilin 1, which forms the catalytic subunit of the γ -secretase complex (Cacquevel *et al.*, 2012). The human *PSEN2* gene is located on the long arm of chromosome 1 at position 42.13 (1q42.13), it consists of 12 exons and encodes the protein presenilin 2, which is another subunit of γ -secretase (Cai *et al.*, 2015). Presenilin's 1 and 2 are membrane spanning proteins

which contain nine transmembrane domains and a hydrophilic intracellular loop region (Donoviel *et al.*, 1999; Wakabayashi and De Strooper, 2008). Presenilin's 1 and 2 combine with NCT and APH-1 to form the γ -secretase complex that catalyses the cleavage of various membrane proteins, including APP and Notch.

Heterozygous mutations in *PSEN1* cause FAD (Arber *et al.*, 2021) and *PSEN1* mutations resulting in loss of function are the most common cause of familial, early onset AD (Chong *et al.*, 2018). Generally, patients with a FAD linked mutation in *PSEN1* also carry a functional copy of *PSEN1*, this may offer compensation for the loss of activity in the allele with the *PSEN1* mutation (Veugelen *et al.*, 2016). There have been more than 200 dominantly inherited *PSEN1* mutations reported, most of which are missense mutations (Watanabea and Shen., 2017). *PSEN1* mutations range in disease onset and clinical pathology and are named by the amino acid changes they cause. The *PSEN1* A246E mutation is a point, missense mutation occurring on exon 7 of chromosome 14 in which an adenine replaces cytosine at position Chr14:73659540, this base change results in a codon shift from GCG to GAG, resulting in alanine being switched out for glutamic acid at amino acid position 246. The *PSEN1* A246E mutation is a coding mutation with autosomal-dominant inheritance. Patients with this mutation present with significant neural loss, neurofibrillary plaques and tangles and clinical features such as intellectual dysfunction (Gliebus *et al.*, 2009). In cells and rodent models, this mutation is associated with an increase in the A β 42/A β 40 ratio (Borchelt *et al.*, 1996), however Sun *et al.*, (2017) reported a decrease in the production of both A β 42 and A β 40 isoforms in both cell lines and in transgenic animals. The *PSEN1* A246E mutation also increases the intracellular concentration of APP β -C-terminal fragments (β -CTFs) leading to endosomal disruption (Kwart *et al.*, 2019). The *PSEN1* M146L mutation is a point, missense mutation occurring on exon 5 of chromosome 14 in which a cytosine base replaces an adenine at position Chr14:73640371, this base change results in a codon shift from ATG to CTG, resulting in Methionine being switched out for Leucine at amino acid position 246 (Kowalska *et al.*, 2004). The *PSEN1* M146L mutation is a coding mutation

with autosomal-dominant inheritance. Patients with the *PSEN1* M146L mutation present with mixed neuropathology including plaques, NFT and pick bodies and often present with psychotic-like symptoms. In terms of altered *PSEN1* and γ -secretase function, the *PSEN1* M146L mutation results in close contact between *PSEN1* and the APP transmembrane helix (Zhou *et al.*, 2019). All *PSEN1* mutations appear to alter binding of substrate to the *PSEN1* active site region, in the case of APP binding, this results in mispositioning of the APP C99 cleavage domain, likely leading to the altered A β 42/A β 40 ratio seen in patients with *PSEN1* mutations (Fukumori and Steiner, 2016; Trambauer *et al.*, 2020). Alterations to the γ -secretase complex caused by mutations in *PSEN1* may also alter γ -secretase cleavage of its other substrates, this may contribute to the diversity in disease presentation and cell behaviour seen as a result of different *PSEN1* mutations. (Arber *et al.*, 2021). Next generation sequencing of early onset AD patients has also identified several genes associated with development of disease including *NOTCH3*, *SORL1* and *TYROBP* (Figure 5) (Uddin *et al.*, 2021). Disease mechanisms require further characterisation for all subtypes of AD (Vaz and Silvestre., 2020), thus, investigation of FAD mutations which have a clear genetic origin could be beneficial to improving understanding for all subtypes of AD.

1.1.7 Treatment options for AD

Drugs which have been approved for treatment of AD include 4 acetylcholinesterase (AChE) inhibitors (AChEi), Tacrine, Donepezil, Rivastigmine and Galantamine. Acetylcholine (ACh) is a key neurotransmitter for neural cell communication, and AChEi act by inhibiting the action of acetylcholinesterase and increasing concentration of ACh, thus, improving neural communication and reducing some symptoms of AD (Čolović *et al.*, 2013). Galantamine is a reversible and selective AChEi, Donepezil is a reversible, non-competitive inhibitor of AChEi and Rivastigmine inhibits both AChE and butyrylcholinesterase. Treatment with Tacrine results in hepatotoxicity so is no longer used as a therapeutic agent. The other approved drug for treatment of AD is Memantine which is a N-methyl-D-aspartate (NMDA) receptor antagonist. Excitatory glutamatergic neurotransmission occurs via NMDA receptors,

although this activity is necessary for neural survival and synaptic plasticity, too much NMDAR activity can result in cell death due to excitotoxicity (Rothman and Olney 1986). Cell survival and neuronal plasticity can be increased by activation of synaptic NMDARs, however, when extrasynaptic NMDARs are activated, this results in an increase in cell death which may contribute to AD pathology. Memantine regulates glutamate activity in the brain by selectively blocking extrasynaptic NMDARs (Wang and Reddy., 2017). Memantine was approved by the FDA in 2004 and is the most recently approved AD treatment (Vaz and Silvestre., 2020; Maia and Sousa., 2019; Cummings *et al.*, 2014). These current therapeutic options provide benefits in symptom management but do not prevent brain atrophy, neuronal loss, and progressive deterioration of cognition. (Vaz and Silvestre., 2020). Therapeutic approaches to target amyloid beta in AD have not thus far been proven effective in clinical trials -when tested in late-stage clinical trials, the majority of candidate drugs which target A β did not display clinical efficacy (Foroutan *et al.*, 2019). Therapies targeting Tau pathology have produced positive outcomes in preclinical studies and are currently being assessed in clinical trials (Congdon and Sigurdsson, 2018). TauRx therapeutics is one company that has passed through phase 3 trials with the drug hydromethylthionine mesylate (HMTM), an inhibitor of Tau aggregation. The study thus far has shown significant reductions in disease progression, measured in terms of cognitive function and brain atrophy (Wischik et al., 2022). The TauRx studies were carried out on patients with LOAD and are yet to be carried out on patients with FAD mutations. Therapies which were in clinical trials for treatment of AD in 2018 are shown in Figure 6. The majority of therapies currently in development for treatment of AD focus on modulating the activity of the proteases β and γ -secretase (Figure 6).

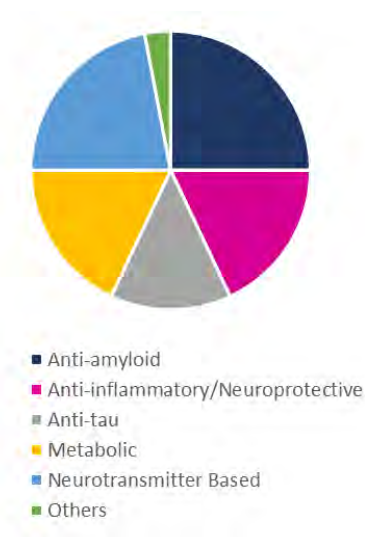


Figure 6. Therapies targeting AD

Therapies targeting AD in clinical trials in 2018. The majority (25%) of AD treatments focused on therapies to reduce amyloid- β , these included small molecules and immunotherapy. Of the remaining clinical trials taking place at the time of reporting, 22% of trials were using neurotransmitter-based therapies, 18% of therapies focused on anti-inflammatory and neuroprotective targets, 18% of agents focused metabolic targets and only 14% were using anti-tau agents (Figure based on work by Maia and Sousa., 2019; Cummings *et al.*, 2018).

β -secretase-1 (BACE1) inhibitors decrease levels of BACE1 reducing APP cleavage by amyloidogenic pathways and the generation of insoluble A β . In clinical trials, treatment with BACE inhibitors has not provided a positive effect on AD symptoms and has, in several cases led to worse cognition (Egan *et al.*, 2019; Henley *et al.*, 2019; Wessels *et al.*, 2020), adverse events and hippocampal atrophy (Egan *et al.*, 2018; Egan *et al.*, 2019; Wessels *et al.*, 2019; Sur *et al.*, 2020). This is likely due to the effect of BACE inhibition on other substrates of β -secretase which have a role in neural function such as seizure-related gene 6 (*SEZ6*) family proteins (Nash *et al.*, 2021). Γ -secretase therapeutic targets focus on inhibiting action of γ -secretase to reduce the formation of A β peptides. Semagacestat and Avagacestat are γ -secretase inhibitors which have been tested in clinical trials for treatment of AD. Avagacestat was tolerated at lower doses in clinical trials (25 mg and 50 mg daily), less so at higher doses (100 mg and 125 mg), resulting in adverse effects which were predominantly

gastrointestinal and dermatologic, but also included reversible glycosuria and nonmelanoma skin cancer (Coric *et al.*, 2012). Treatment with higher doses of Avagacestat resulted in trends of cognitive worsening in patients (Coric *et al.*, 2012). These negative effects of γ -secretase inhibition may be a result of a lack of γ -secretase function in other signalling pathways. One example of affected γ -secretase function is in Notch signalling, NICD is released after ϵ -cleavage and translocates to the nucleus to regulate processes such as cell division (Maia and Sousa., 2019).

AChEi may reduce AD symptoms, but do not prevent disease progression. Treatments focussed on modulating β and γ -secretase function are at significant risk of generating off target effects. Tau targeting therapeutics offer great hope for reduction of atrophy and cognitive decline in LOAD upon disease onset but may not tackle other disease symptoms in FAD patients. The lack of therapeutic options currently available to patients with FAD encouraged the exploration of alternative hypotheses for disease progression in this project, with the hope of identifying different targets for preventing disease progression.

1.1.8 Notch and *PSEN1* in AD

A Notch-related hypothesis was proposed by Ethell (2010) to explain the aetiology behind how FAD mutations, particularly *PSEN* mutations, lead to the pathology seen in AD. APP is expressed in all cells of the body, but is predominantly expressed in metabolically demanding tissues such as the brain and skeletal muscle, which have developed vascular networks. AD patients present with dense vascular networks interspersed with A β plaques in brain regions which are affected with AD pathology (Iadecola, 2004, Finch, 2005, Meyer *et al.*, 2008). Ethell (2010) proposed that A β production from metabolism of APP acts as a biomarker to signal that increased vascular perfusion is required in metabolically demanding areas. The γ -secretase substrate Notch plays a role in angiogenesis and in endothelial cell specification (Phng and Gerhardt 2009). Inhibitors of γ -secretase increase the production of endothelial tip cells, leading to branching of blood vessels and the generation of

vascular networks which are dense, with poor perfusion (Suchting *et al.*, 2007). APP and Notch can act as competitors for γ -secretase binding, Ethell (2010) hypothesised that Notch activation by γ -secretase is inhibited by increased APP and A β , leading to an increase in high density vascular networks and unstable dendritic spines, which cause early cognitive impairments (Ethel 2010).

Γ -secretase and presenilin-1 substrates have a range of functions in both developing and adult tissues, Notch proteins 1-4 are substrates of the γ -secretase complex. After ligands Jagged and delta like-1 (DLL) bind to the Notch receptor, the Notch protein is cleaved by α -secretase and γ -secretase to release the Notch intracellular domain (NICD) which translocates to the nucleus for activation of Notch target genes (Wolfe., 2020; Medoro *et al.*, 2018; Haapasalo and Kovacs., 2011). Mutations in *PSEN1* which impair γ -secretase function may reduce activation of Notch by γ -secretase and alter neurogenesis. FAD mutations have been shown to lead to a decrease in Notch cleavage by γ -secretase. Song *et al.*, (1999) demonstrated that release of the NICD was reduced in *PSEN1* deficient cells but increased when *PSEN1* function was restored (Chávez-Gutiérrez *et al.*, 2012, Song *et al.*, 1999).

Notch genes encode a family of transmembrane receptors in mammalian cells (Hu *et al.*, 2020), there are four Notch receptors: Notch 1, Notch2, Notch 3 and Notch 4. Notch signalling pathways are highly conserved and play a role in the regulation of cell proliferation, differentiation, and apoptosis in all animals. Notch signalling is also associated with tissue growth, cancer, cell death and tumour suppression (D'Souza *et al.*, 2010). Canonical Notch ligands are integral cell surface proteins, so activation of Notch signalling pathways is dependent on direct cell-to-cell interactions (D'Souza *et al.*, 2010). Most Notch signalling in mammals is induced by a family of ligands which have a Delta, Serrate, and Lag2 (DSL) domain, thus are referred to as DSL ligands. The DSL ligands are classed as Delta-like (DLL1, DLL3 and DLL4) or Serrate (Jagged) like (Jagged1 and Jagged2) (Figure 7.)(D'Souza *et al.*, 2010, Kopan and Ilagan, 2009). Jagged ligands are transmembrane proteins and have large extracellular

domains consisting of epidermal growth factor (EGF) -like repeats, (Bray., 2006) (Figure 7.).

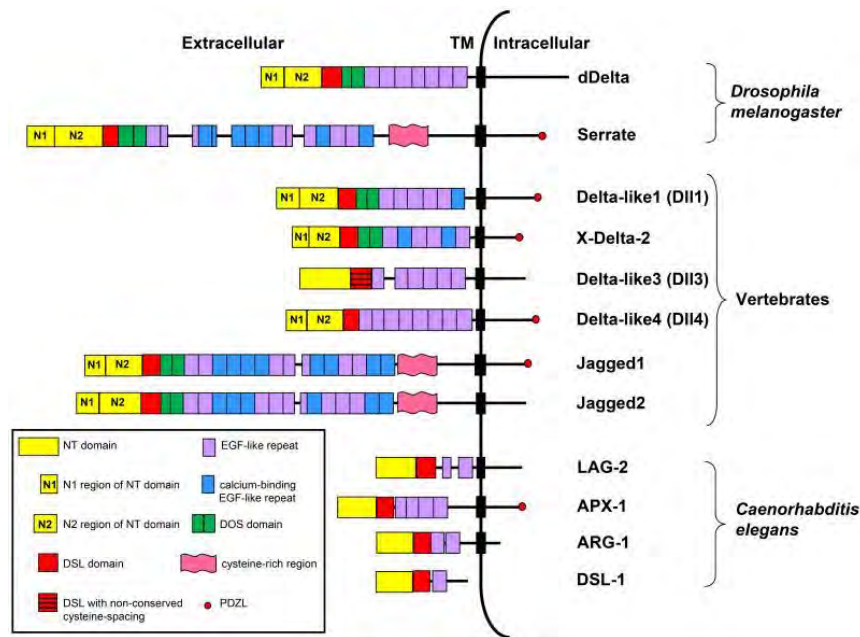


Figure 7. Canonical Notch ligands and their structural domains

Most Notch signalling in mammals is induced by a family of ligands which have a Delta, Serrate, and Lag2 (DSL) domain, thus are referred to as DSL ligands. The DSL ligands are classed as Delta-like (DLL1, DLL3 and DLL4) or Serrate (Jagged) like (Jagged1 and Jagged2) Jagged ligands are transmembrane proteins and have large extracellular domains consisting of epidermal growth factor (EGF) -like repeats, (D'Souza *et al.*, 2010; Kopan and Ilagan, 2009 ; Bray., 2006).

Notch signalling relies on intercellular signalling interactions; cells with DSL ligands on their cell surface interact with cells displaying Notch receptors on their surface. Notch receptors have an extracellular domain, an intracellular domain, and a transmembrane component. Binding of a ligand to the Notch receptor initiates proteolytic cleavage of the Notch extracellular domain, which is mediated by ADAM-family metalloproteases (S2 cleavage), after which, cleavage by the γ -secretase complex releases the notch intracellular domain (NICD) for translocation to the nucleus. In the nucleus, NICD displaces a repression complex and forms a complex with the DNA binding protein (CSL), its coactivator Mastermind and the protein p300, which functions as a histone acetylase. This protein complex can then upregulate

transcription of Notch target genes such as *MYC*, *p21* and the gene *CCND3* which encodes the cell cycle regulatory protein Cyclin D3 (Bray., 2006).

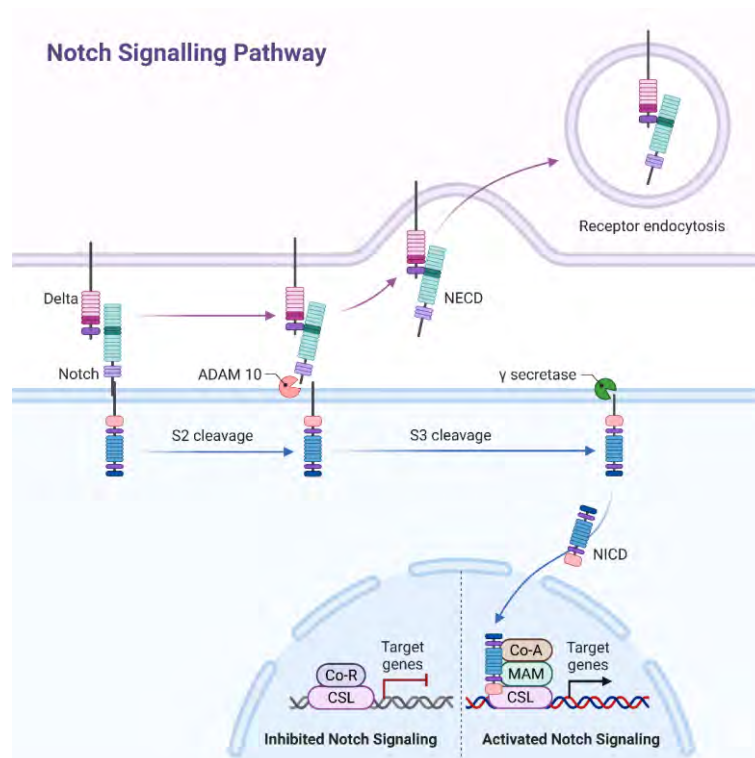


Figure 8. Release of the NICD to initiate Notch signalling pathways

Binding of a ligand to the Notch receptor initiates S2 and S3 cleavage, releasing the NICD to translocate to the nucleus and upregulate transcription of Notch target genes (Bray., 2006).

Notch proteins have roles in cell fate determination and in maintenance of stem cells (Castilla-Ortega *et al.*, 2011, Song *et al.*, 1999). A reduction in functional γ -secretase may lead to a reduction in Notch activation, and a downregulation in transcription of Notch target genes, altering processes such as cell division, self-renewal, and differentiation.

1.2.0 Neurogenesis

1.2.1 Stem cells

Stem cells are immature cells that are unspecialised and have the capacity to self-renew without differentiating down a specific lineage. Stem cells can be categorised by their level of stemness; - totipotent stem cells can differentiate into all possible cell types including cells which give rise to the placenta, pluripotent stem cells can differentiate into cells of all three germ layers- endoderm, ectoderm and mesoderm, multipotent stem cells can differentiate into more specialised cells of one particular lineage and unipotent stem cells are capable of differentiation into only a single cell type. Pluripotent stem cells were originally derived from the inner cell mass of mammalian blastocyst and are termed embryonic stem cells. Multipotent stem cells are cells which have begun the process of specialisation and are capable of differentiating into more specialised cells of one particular lineage, they can be found in specialised niches in adult mammals where they remain as reserves for tissue repair and regeneration (Ottoboni *et al.*, 2020). Examples of multipotent stem cells include adult haemopoietic stem cells and neural stem cells. Many adult tissues maintain reserves of multipotent stem cells which have roles in tissue development and repair and in maintaining homeostasis, they are able to fulfil these roles due to their ability to produce new-born differentiated progeny but must balance the need for differentiated cells with maintenance of the stem cell niche (Chen *et al.*, 2016).

1.2.2 Symmetric and asymmetric cell division

The balance between proliferation and differentiation is regulated by switching between different methods of cellular division. Symmetric cell division results in the generation of two identical daughter cells and can be carried out by cells for self-renewal or for the generation of two differentiating daughter cells. Asymmetric cell division results in the generation of one differentiating cell and one daughter cell which is identical to the parent. Both intracellular and extracellular mechanisms guide cell fate to regulate asymmetric cell division (Chen *et al.*, 2016, Venkei and

Yamashita., 2018). Extrinsic factors in the stem cell niche can guide cells to undergo asymmetric cellular division, the stem cell resulting from asymmetric cell division will remain in the stem cell niche and the differentiated daughter cell will move out of the niche to acquire its fate (**Error! Reference source not found. A**). Intrinsic factors which determine cell fate may be distributed unevenly in dividing stem cells, leading to maturation of only one daughter cell (**Error! Reference source not found. B**). Asymmetric stem cell division may result from a combination of both intrinsic and extrinsic factors (**Error! Reference source not found. C**)– initial intrinsic or extrinsic factors which are reinforced by the other (Chen *et al.*, 2016).

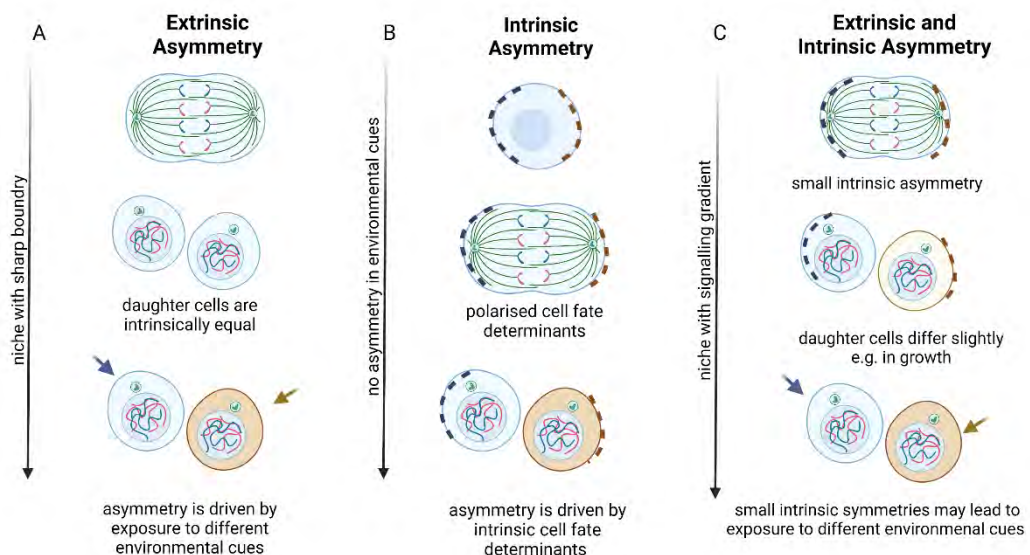


Figure 9. Mechanisms of asymmetric cell division

Asymmetric cell division can be driven by extrinsic and intrinsic factors. Figure is based on work by Chen *et al.*, (2016) and was created in BioRender.com.

One intrinsic mechanism which plays a role in determination of cell fate is the distribution of molecular components between daughter cells, which is often carried out via regulation of the mitotic spindle and results in asymmetric cell division. Extrinsic signals can regulate the frequency of cell divisions (Smith *et al.*, 2017).

Signalling molecules which govern tissue development are termed morphogens and act alongside positional cues to guide cell fate. Planar cell polarity (PCP) is a highly conserved polarity axis which is necessary for normal development to occur. To establish PCP in tissues, gradients of gene expression and gradients of Wnt ligands are required to direct enrichment of PCP proteins, these proteins assemble into complexes at opposing ends of cells. Planar tissue patterning can be regulated by degradation of PCP components, endosomal trafficking, and endocytosis. Polarisation is propagated throughout tissues to generate a polarity axis, which can direct cellular rearrangements and the localisation of subcellular structures, leading to the tissue-wide changes seen in development (Butler and Wallingford., 2017). During cortical neurogenesis, non-canonical Wnt signalling, and PCP have been shown to regulate asymmetric cell division and determination of cell fate via regulation of spindle size. Wnt signalling plays a crucial role in both the development of the central nervous system and in regulation of the adult central nervous system. During mammalian development, Wnt signalling pathways regulate proliferation, asymmetric cell division and cell-fate specification, with an important role in CNS tissue patterning. Wnt signalling is necessary for development of the hippocampus, during which, Wnt3a acts via canonical Wnt signalling pathways to regulate NPC proliferation and differentiation (Aghaizu *et al.*, 2020; Yoshinaga *et al.*, 2010; Hirabayashi *et al.*, 2005; Zechner *et al.*, 2003; Lee *et al.*, 2002; Galceran *et al.*, 2000). In hippocampal development, Wnt5a regulates axonal differentiation and Wnt7b regulates dendritic differentiation via non-canonical Wnt/PCP signalling (Viale *et al.*, 2019; Slater *et al.*, 2013; Zhang *et al.*, 2007; Ohno, 2007; Rosso *et al.*, 2005).

In the mature brain Wnt plays a role tissue homeostasis and modulates the function and integrity of the blood brain barrier (Rapp *et al.*, 2017, Aghaizu *et al.*, 2020). Wnt signalling also modulates synapse number and function as well as microglial biology and is a major regulator of cellular proliferation and differentiation (Palomer *et al.*, 2019). In satellite stem cells of muscle fibres undergoing regeneration, noncanonical Wnt7A/ VANGL2 signalling regulates asymmetric cell division and determination of

cell fate via spindle pole orientation. Wnt/ VANGL2 signalling also regulates the size of the mitotic spindle to guide glial cell fate during cortical neurogenesis. Symmetric cell division can be enhanced by sonic hedgehog signalling (SHH), in cerebellar progenitor cells and cortical stem cells, interactions between SHH, Wnt and Notch signalling pathways guide cell fate determination (Smith *et al.*, 2017).

Wnt ligands are growth stimulatory proteins that have a palmitoleic acid attached to facilitate binding. Wnt ligands bind to a cell surface heterodimeric receptor complex which is composed of Frizzled and single-pass transmembrane co-receptors Ror1, Ror2, LRP5, LRP6 or Ryk proteins (Fradkin *et al.*, 2009, Schulte and Bryja., 2007). In mammals, there are 19 known Wnt ligands and 10 identified Frizzled (FZD) receptors (Ring *et al.*, 2014, Nile *et al.*, 2017). There are two subcategories of Wnt signalling, canonical (β -catenin dependent) and non-canonical (β -catenin independent). Non-canonical pathways can also be described as the PCP and Wnt/Ca²⁺ pathways. In canonical Wnt signalling, β -catenin levels are regulated by degradation: the absence of Wnt ligand leads to binding of β -catenin with the proteins adenomatous polyposis coli (APC), axis inhibition protein (AXIN), Dishevelled (DVL), β -TrCP and glycogen synthase kinase 3-beta (GSK-3 β) to form the β -catenin destruction complex. Binding with the destruction complex leads to phosphorylation of β -catenin at serine and threonine sites which signals the E3 ubiquitin ligase β -TrCP to ubiquitinate the β -catenin and target it for proteasomal degradation (Figure 9.). Thus, in canonical Wnt signalling, the absence of Wnt ligand leads to lower levels of intracellular β -catenin.

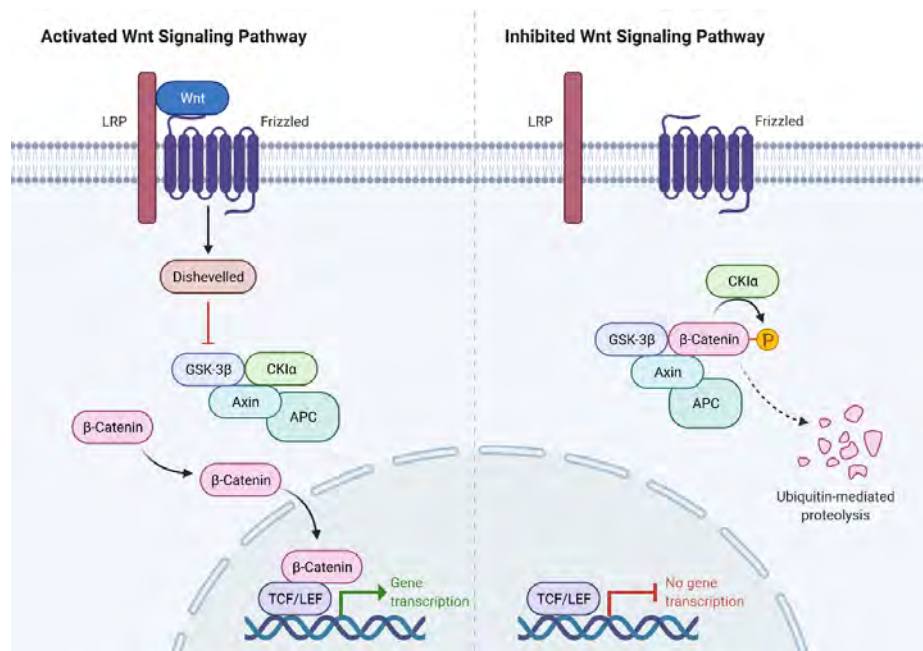


Figure 9. Canonical (β -Catenin dependent) and non-canonical (β -catenin independent) Wnt signalling pathways.

Figure created using Biorender.com.

In canonical Wnt signalling, the binding of Wnt ligand with a FZD receptor induces formation of a receptor complex which is formed of Wnt, FZD, DVL, lipoprotein receptor-related protein (LRP) and AXIN. Phosphorylation of LRP induces translocation of the receptor complex to the region of the membrane where Frizzled and LRP receptors are located. Upon binding with LRP, DVL in the receptor complex becomes phosphorylated, this leads to inhibition of GSK-3 β , preventing it from phosphorylating β -catenin and preventing β -TrCP from becoming part of the destruction complex, thus preventing ubiquitination and degradation of β -catenin. The subsequent intracellular accumulation of β -catenin leads to an increase in the amount of β -catenin that translocates to the nucleus and forms a complex with T-cell factor (TCF)/Lymphoid enhancer-binding factor (LEF) transcription factors (Rapp *et al.*, 2017). TCF/LEF transcription factors mediate Wnt signalling via the induction of Wnt target genes such as those encoding c-Myc and cyclin. In the absence of Wnt ligand, TCF is inhibited via binding with Groucho, however in the presence of Wnt

ligand, when cellular β -catenin levels are high, translocation of β -catenin to the nucleus dislodges Groucho and enables binding of TCF/LEF with β -catenin and transcription of Wnt target genes (Rapp *et al.*, 2017). In canonical Wnt signalling, absence of Wnt ligand leads to degradation of β -catenin and presence of Wnt ligand leads to nuclear translocation of β -catenin and upregulated transcription of Wnt target genes. Wnt ligand binding to cell surface receptors initiates intracellular signalling pathways which regulate processes such as the cell cycle, cellular migration, cell polarity, cell growth and proliferation. Dysregulation of Wnt signalling is associated with the development of cancers (Clevers and Nusse., 2012), for example, mutations in APC can lead to increased intracellular levels of β -catenin in the absence of Wnt ligand binding. APC mutations causing loss of function can prevent the destruction complex from ubiquitinating β -catenin, preventing its degradation by the proteasome and leading to upregulated transcription of Wnt related genes in the absence of Wnt signalling. High expression of FZD receptors on the cell surface can also contribute to overactive Wnt signalling and is associated with subsets of gastric, ovarian, colorectal, and pancreatic tumours (Nile *et al.*, 2017).

Downregulated Wnt signalling can induce synaptic dysfunction, leading to neurodegeneration. Folke *et al.*, (2018) showed reduced expression of Wnt ligands Wnt2B, Wnt6 and Wnt7a and frizzled receptors FZD2 and FZD3 in the human brain with age, which presented alongside enhanced expression of the secreted frizzled-related protein 1 (SFRP1). SFRP1 sequesters ligands of Wnt in the extracellular space so upregulation of SFRP1 may reduce Wnt signalling (Folke *et al.*, 2018; Palomer *et al.*, 2019). Hofmann *et al.*, (2014) reported downregulation of Wnt ligands Wnt2, Wnt4, Wnt9a and transcription factors TCF3 and *LEF1* with age in the rodent brain. Downregulated expression of *AXIN2*, *DVL2* and nuclear β -catenin was shown by Orellana *et al.*, (2015) in the hippocampus of aged rats. Interestingly, downregulated expression of Wnt3 and Wnt3a was also found in the dentate gyrus (DG) of the hippocampus in rodents aged from 1-22 months. In these rodents, downregulation

of Wnt3 signalling during ageing correlated with impaired adult neurogenesis (Hofmann *et al.*, 2014; Orellana *et al.*, 2015; Okamoto *et al.*, 2011).

Wnt signalling has also been shown to be dysregulated in some Alzheimer's mutations. Features of AD pathophysiology associated with abnormal Wnt signalling include neuroinflammation, synapse loss, tau pathology, aberrant amyloid precursor processing and blood brain barrier breakdown (Aghaizu *et al.*, 2020). In cells which had a lack of functional presenilin, inhibition of GSK3 activity via sequestration of GSK3 within multivesicular endosomes (MVE) led to sustained canonical Wnt signalling, increased Wnt responsiveness and MVE expansion, this enhanced activity of Wnt was dependent on the functional endosomal sorting complex required for transport (ESCRT). In MVEs, the ESCRT is required to form intraluminal vesicles. Canonical Wnt signalling may be enhanced by the accumulation of late endosomal structures, which leads to upregulated Wnt signalling via increased sequestration of the Wnt receptor/GSK3 and a decrease in GSK3 cytosolic activity (Dobrowolski *et al.*, 2012).

In FAD causing APP mutations, which result in a locus duplication, APP binds with β -catenin, preventing translocation to the nucleus and reducing canonical Wnt signalling (Zhang *et al.*, 2018; Rovelet-Lecrux *et al.*, 2006). FAD causing *PSEN1* mutations appear to negatively regulate canonical Wnt signalling. Interactions between β -catenin and *PSEN1* generally lead to stabilisation of β -catenin, however, in HEK containing a *PSEN1* mutation, β -catenin was less stable and less capable of nuclear translocation to initiate gene transcription of Wnt signalling pathways. Interestingly, in the brains of transgenic mice, *PSEN1* mutations which led to destabilisation of β -catenin resulted in increased degradation of β -catenin and an increase in neuronal apoptosis (Zhang *et al.*, 1998).

In opposing research carried out in neuronal (PC-12) and fibroblast cell lines, *PSEN1* mutations led to increased levels of β -catenin. These differing results may be a result

of transient differences in Wnt signalling, different cell types and altered Notch signalling (Kang *et al.*, 1999; Teo *et al.*, 2005; Aghaizu *et al.*, 2020).

Wnt and Notch signalling pathways are both active during tissue development and homeostasis, however, they often guide cell fate in opposing directions. As cell specification is controlled by both Notch and Wnt signalling, signalling occurs through these pathways as either Wnt-on/Notch-off or Notch-on/Wnt-off. In skin and mammary glands, stem cell self-renewal is promoted by Wnt signalling, this signalling is inhibited by Notch to enable cell specification to a more differentiated phenotype (Zhu *et al.*, 1999). Wnt signalling is dependent of the ability of β -catenin to translocate to the nucleus to interact with TCF/LEF and induce transcription of Wnt target genes. Membrane restricted Notch and the NICD can inhibit Wnt/ β -catenin signalling to allow for cell fate determination. Membrane-restricted Notch can prevent nuclear translocation of β -catenin by sequestering it to the membrane. The NICD can form a complex with β -catenin to prevent its interaction with TCF/LEF, this complex is stabilised by the nuclear restricted DNA binding protein RBPj. These mechanisms enable regulation of Wnt signalling by Notch for control of cellular proliferation and differentiation (Acar *et al.*, 2021; Reya *et al.*, 2005; Logan *et al.*, 2004).

When NSC in the niche divide via symmetric cell division to produce two stem cells, the stem cell pool expands, when NSC divide by asymmetric cell division to produce one stem cell and one more differentiated cell, the size of the stem cell pool remains the same, when NSC undergo symmetric cell division to produce two differentiated daughter cells, the stem cell niche is depleted (Figure 10. A). Shifting between asymmetric and symmetric cell divisions occurs in individual groups of cells but can also occur at once in the whole population (Silva-Vargas., *et al.*, 2018). Symmetric cell division is the principal mode of cell division in adult ventricular-subventricular zone (V-SVZ) neural stem cells (NSCs). NSC in the brains of mice are retained in the walls of the lateral ventricles (V-SVZ) well into adulthood, this allows for the generation of new neurons throughout life (Obernier *et al.*, 2018). The majority of V-SVZ NSCs

studied by Obernier *et al.*, (2018) were undergoing symmetric cell division, of which 20-30% were doing so for self-renewal and could remain in the stem cell niche for months before differentiating. The remaining 70-80% of NSCs were dividing symmetrically to generate two more differentiated progeny, which led to an eventual reduction in the NSC niche. Intrinsic and extrinsic factors both play a role in regulation of stem cell division and in determination of cell fate, the mechanisms of stem cell division during different states such as in ageing and disease are yet to be fully understood (Figure 10. B).

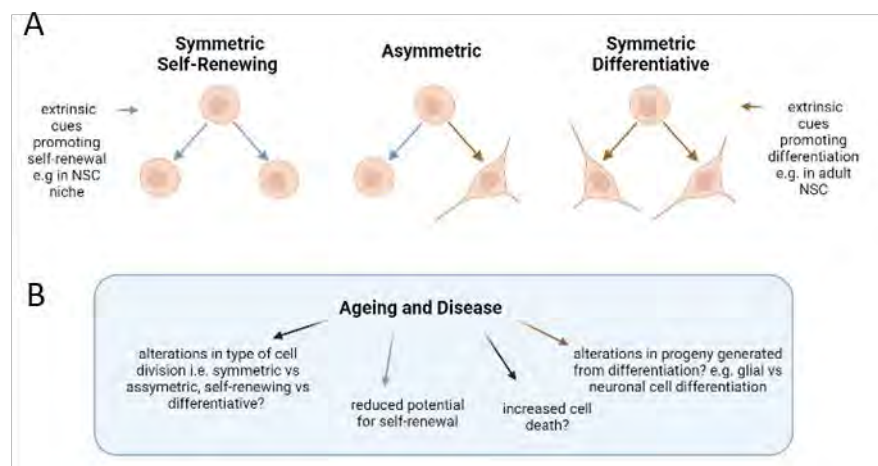


Figure 10. Mechanisms of NSC cell division and factors which may have a role in cell fate determination.

Figure is based on work by Silva-Vargas *et al.*, (2018) and was created in BioRender.com.

1.2.3. Neurogenesis and development

Neurogenesis is the generation of new neurons from early neural stem and progenitor cells. Regulation of neurogenesis is fundamental during development when intrinsic and extrinsic signals dictate the proliferation and differentiation of neural progenitors and the migration of more mature neural cells. During cortical development in the embryo, apical precursor cells in the ventricular zone (VZ) receive signals to either divide or remain in quiescence. Glial cells in the VZ act as a scaffold

to aid migration of neurons up towards the mature layer of the cortex -the cortical plate. The subventricular zone (SVZ) which is in between the VZ, and cortical plate contains neural precursors which can migrate up to the cortical plate (Figure 11 A). At day 10.5 in embryonic development, increased levels of VANGL2 in apical precursor cells undergoing cell division produces mitotic spindles of equal size, leading to symmetric cell division and generating two apical precursor cells. Decreasing expression of VANGL2 at day 14.5 of embryonic development leads to asymmetry of spindle size and increased asymmetric cell division generating a mature neuron and a precursor cell (Smith *et al.*, 2017) (Figure 11 B).

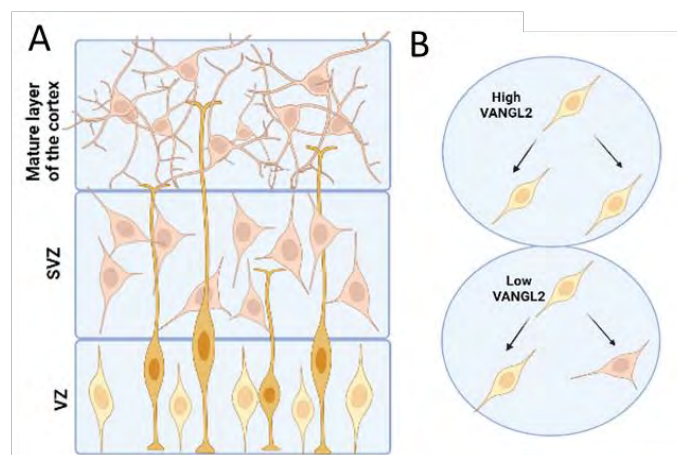


Figure 11. Cortical development in the embryo

Representation of a section through a neonatal cortex. The mature layer of the cortex, the subventricular zone (SVZ) and the ventricular zone (VZ) are labelled. The VZ contains apical precursor cells, which divide or remain quiescent and glial cells, which act as a scaffold for migrating neurons. The SVZ contains precursor cells, and the cortical plate contains mature neural cells. Expression of VANGL2 in the VZ regulates the switch between symmetric and asymmetric cell division. Figure is based on work by Smith *et al.*, (2017) and was created using BioRender.com.

Alterations in neurogenesis during cortical development can lead to disorders termed malformations of cortical development (MCDs) symptoms of which include intellectual disability and drug-resistant epilepsy. Radial glia are specialised progenitor cells which have long radial processes that enable them to guide new neurons in radial migration from the ventricular zone to the mantle regions during

the expansion of the neural tube. Radial glia use symmetrical division to generate more neural progenitor cells, and asymmetrical cell division to generate post-mitotic neurons (Figure 12. A). Alterations in the timing of the switch from symmetric to asymmetric cell division can cause abnormal proliferation of neural progenitors (Figure 12.B). During cell division, molecular components are split between daughter cells, this is often carried out through regulation of the mitotic spindle (Smith *et al.*, 2018). Defects in progenitor proliferation can also be caused by problems with mitotic spindle orientation. These defects in progenitor proliferation can lead to increased or decreased production of neurons causing disorders such as megalencephaly or microcephaly. Neural proliferation and migration can be impaired by alterations in radial glia scaffolding, leading to neurons accumulating in the VZ (Figure 12.C). Disruption of the basal membrane can increase neuronal migration so that they accumulate on the pial surface (Figure 12.D). Intrinsic cellular defects such as impaired ability of neurons to migrate to the CP can lead to delayed neuronal migration (Figure 12.E). Defects can occur later in development with impaired synaptogenesis, neurite extension and impaired connectivity with target cells (Figure 12.F) (Guarnieri *et al.*, (2018).

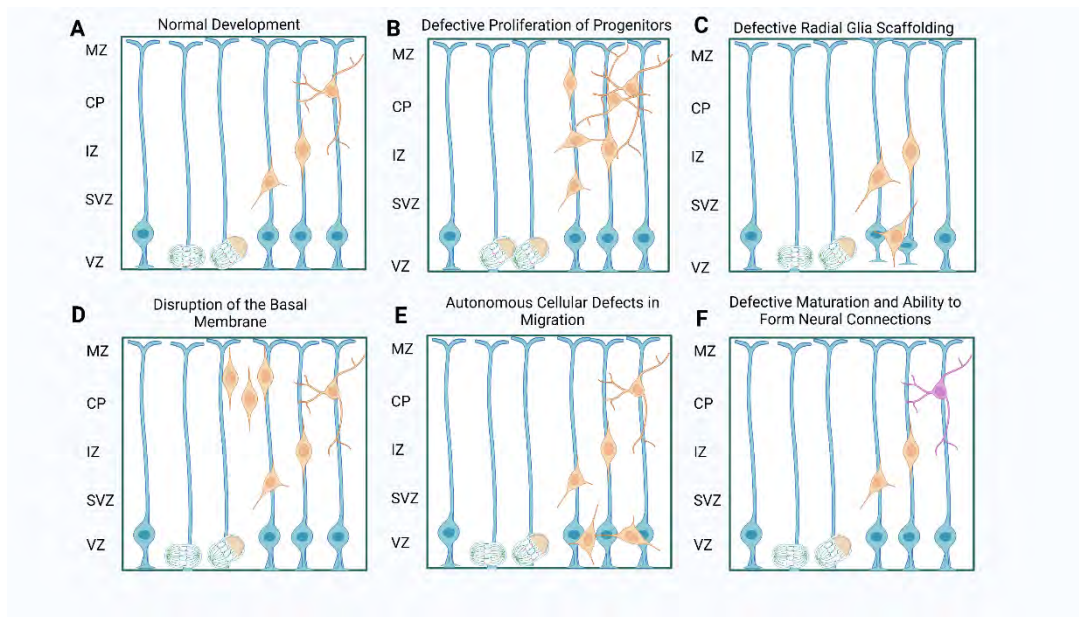


Figure 12. Normal cortical development and cortical development in disease

Brain regions are shown on the y-axis, Marginal zone (MZ), Cortical Plate (CP), Intermediate zone (IZ), subventricular zone (SVZ), Ventricular zone (VZ). A. Radial glia are shown in white and undergo symmetrical division to generate more neural progenitor cells, they also undergo asymmetrical cell division to generate post-mitotic neurons. B. Dysregulated timing of the switch from symmetric to asymmetric cell division can cause abnormal proliferation of neural progenitors, defects in progenitor proliferation can also be caused by problems with mitotic spindle orientation. These defects in progenitor proliferation can lead to increased or decreased production of neurons which can cause megalencephaly or microcephaly. C., Neural proliferation, and migration can be impaired by alterations in radial glia scaffolding, this can lead to neurons accumulating in the VZ. D. Disruption of the basal membrane can increase neuronal migration so that they accumulate on the pial surface. E. Intrinsic cellular defects such as impaired ability of neurons to migrate to the CP can lead to delayed neuronal migration. F. Defects can occur later in development with impaired synaptogenesis, neurite extension and impaired connectivity with target cells (Guarnieri et al.,2018).

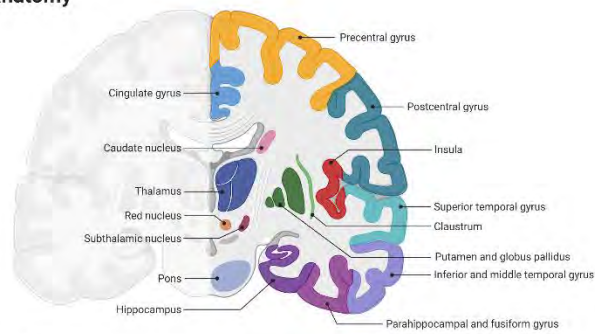
Microtubules are key components of the cytoskeleton, interactions of actin filament and microtubules determine the movement and organisation of dendritic and axonal growth cones (Dent *et al.*, 2003, 2011). During embryonic development, the microtubule cytoskeleton plays an important role for neurons facilitating cell division, migration, synapse formation, intracellular trafficking, and signal transduction (Lasser *et al.*, 2018). The DCX protein binds with microtubules to

increase stability and alter the cytoskeleton, a process which enables neuronal migration in the developing brain (Slepek *et al.*, 2012).

1.2.4 Adult hippocampal neurogenesis

The hippocampus has a key role in short- and long-term processing of declarative memory (memory of facts, data, events) and thus is important for learning and memory formation (Castilla-Ortega *et al.*, 2011). The presence or absence of hippocampal neurogenesis in the adult human brain remains a heavily debated topic (Sorrells *et al.*, 2018, 2021, Moreno-Jiménez *et al.*, 2021). However, in recent years, strong evidence has emerged to support the persistence of adult hippocampal neurogenesis (AHN) in humans, specifically in the sub granular zone (SVZ) and the DG of the hippocampus (Figure 13.) (Boldrini *et al.*, 2018; Moreno-Jiménez *et al.*, 2019, 2021; Tobin *et al.*, 2019). The generation of new neurons and glia in the adult hippocampus during AHN is thought to play a role in the generation and maintenance of hippocampal memories. Adult NSC in the mammalian SVZ retain the capacity to self-renew, proliferate, and differentiate into a range of cell types (Gil-Perotín *et al.*, 2013; Alvarez-Buylla and García-Verdugo, 2002; Kempermann, 2002). Throughout life, neurons are added to the granular cell layer of the DG (Deng *et al.*, 2010; Lazarov and Hollands., 2017) and in AHN, new neurons generated within the SVZ of the DG can be recruited for hippocampal-dependent learning (Ladrón de Guevara-Miranda *et al.*, 2018). Adult and embryonic neurogenesis both originate with NSC, the fate of which is regulated by their local niche (Engler *et al.*, 2018).

Coronal Neuroanatomy



The Limbic System

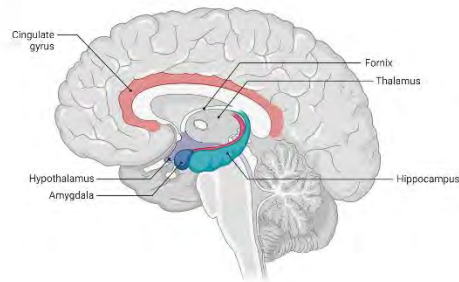


Figure 13. Location of the hippocampus in the adult human brain

Figure 10 displays the location of the Hippocampus and was created using BioRender.com.

Neurodegenerative disorders commonly present with chronic inflammation and a decline in the generation of functional neurons (Vivar, 2015; François *et al.*, 2013). In mammals, hippocampal neurogenesis declines with age, and this decline is even more significant in AD (Vivar, 2015; Moreno-Jiménez *et al.*, 2019). Defective neurogenesis occurring in the subgranular zone (SGZ) of the hippocampal DG has been linked with memory loss and cognitive decline (Zaletel *et al.*, 2018). Upregulation of AHN has the potential to rescue cognitive impairments resulting from age and AD and may be a therapeutic target for disease (Lazarov and Hollands., 2016).

Various markers have been used to identify the presence or absence of neural stem and progenitor cells in the human adult hippocampus, these markers include doublecortin (DCX), a MAP expressed by NPC and immature neurons, prospero homeobox 1 (Prox1) a transcription factor that is highly expressed in dentate granule

cells of the DG (Karalay *et al.*, 2007; Kempermann *et al.*, 2004; Lavado and Oliver., 2007) and polysialic acid–neural cell adhesion molecule (PSA-NCAM), a marker of immature neurons which are developing and migrating, also used to identify synaptogenesis. PSA-NCAM expression is retained by cells in the adult brain in regions in which cells have the potential for functional and morphological changes (Quartu *et al.*, 2008). In 2019, Moreno-Jiménez *et al.*, obtained healthy brain tissue from human participants aged 43-89 and identified thousands of DCX positive immature neurons in the DG of the hippocampus. A subset DCX+ cells expressed immature neural markers PSA-NCAM and calretinin (CR), Prox1 expression was also found in 91% of DCX+ cells which suggested these cells had acquired a dentate granule cell (DGC) fate. CR is a calcium binding protein which is expressed in a range of neuronal subtypes, it has a role in intrinsic neuronal excitability and in induction of long-term potentiation (Camp and Wijesinghe., 2009). PSA-NCAM and CR are transiently expressed by immature neurons (Moreno-Jiménez *et al.*, 2019). In the study carried out by Moreno-Jiménez *et al.*, (2019), neural markers β III-tubulin, neuronal nuclei (NeuN) and tau were also found in 40-60% of DCX+ cells and markers of a more mature neural cell type such as Calbindin (CB) were found in approximately 40% of DCX+ cells. NeuN is a marker which is exclusively found in the nuclei of post-mitotic neurons (Duan *et al.*, 2015), β III-tubulin is a cytoskeletal protein which is expressed in the brain at relatively high levels and is expressed most highly during development (Katsetos *et al.*, 2003) and CB is a calcium binding protein that has a vital role in neuronal plasticity and function. Cells expressing CB can be found in the DG and CA1 of the hippocampus (Alkadhi., 2019; Westerink *et al.*, 2012; Abraham *et al.*, 2009; Sloviter *et al.*, 1989. Moreno-Jiménez *et al.*, (2019) found that in healthy brain tissue, expression of DCX declined as age increased from 40-90 years, indicating a decline in AHN with age; they also reported a reported significant decline in the number of DCX+ immature neurons in patients with AD compared with age-matched controls, suggesting much greater decline in AHN occurs in patients with AD, which may result from accelerated depletion of the neural stem cell niche. Interestingly, a

decline in the number of DCX+ immature neurons was seen in patients that were not yet suffering from severe cognitive decline, indicating that mechanisms causing loss of immature neurons begin to occur prior to the onset of severe symptoms of AD. Moreno-Jiménez *et al.*, (2019) also analysed the expression of markers related to distinct stages in AHN in AD samples and detected reduced expression of PSA-NCAM, Prox1, NeuN, β III-tubulin and CB as disease progressed from Braak stage III onwards, indicating impaired maturation of DCX+ cells in AD. Tissue samples acquired for histopathological analysis of AHN were obtained and processed within 38hrs post-mortem and were sectioned rapidly on ice before fixation using 4% PFA. Many previous studies investigating AHN in humans have been unsuccessful in detecting immature neural cell types in the adult hippocampus. One possible reason for the detection of immature neural cell types under these conditions is the rapid tissue processing and the absence of freezing, paraffin inclusion or mechanical alteration of tissue (Moreno-Jiménez *et al.*, 2019).

In 2020, Scopa *et al.*, reported a significant decline in the proliferation of adult neural stem cells derived from the SVZ of Tg2576 transgenic mice aged 1.5 months. Tg2576 transgenic mice are an animal model of AD which overexpress an isoform of human APP which contains a Lys670 \rightarrow Asn, Met671 \rightarrow Leu mutation. Tg2576 mice display increased accumulation of A β , an increase in the ratio of A β ₄₂ to A β ₄₀, the presence of amyloid plaques and cognitive memory deficits (Hsiao *et al.*, 1996). At 1.5 months, Tg2576 mice do not display A β accumulation nor symptoms of neurodegeneration, however cells derived from these mice did display reduced olfactory bulb neurogenesis and a reduction in their ability to differentiate into mature neurons. This impaired neuronal maturation was proposed to be a result of tau-mediated and microtubule hyperstabilization (Scopa *et al.*, 2020).

Vacuolar sorting protein 35 (VPS35) is a component of retromer and a deficiency of VPS35 has been linked with increased susceptibility to AD. Deficiency in VPS35 has also been reported to lead to increased microglial activation and reduced adult hippocampal neurogenesis (Appel *et al.*, 2018). This indicates that microglial

activation and reduced adult hippocampal neurogenesis may increase susceptibility to AD. In *PSEN1* NSCs, a decline in functional presenilin 1 results in suppression of autophagy, along with reduced autophagosome formation and transcription factor EB (TFEB) expression, this occurs in part via inhibition of γ -secretase-independent ERK/cAMP response element-binding protein (CREB) signalling and activation of glycogen synthase kinase 3 beta (GSK3 β) (Chong *et al.*, 2018).

In histopathological examination, post-mortem tissue samples from patients with FAD displayed a trend towards a reduction in new-born neurons, indicative of altered neurogenesis and premature ageing, they also displayed a trend towards increased neurogenesis in patients who had a longer disease duration (Arber *et al.*, 2021).

Arber *et al.*, (2021) generated a 3D cerebral organoid and used cortical differentiation to produce immature and mature neural cells for modelling of neurogenesis. In 2D and 3D models of *PSEN1* cortical differentiation, *PSEN1* NSC were more predisposed to undergo premature neurogenesis when compared with controls. Neural cultures containing the *PSEN1* mutation showed an increase in post mitotic neurons and a reduction in progenitor cells (Arber *et al.*, 2021). The *PSEN1* mutations analysed affect a domain of *PSEN1* which enables docking of extracellular substrates (Somavarapu and Kepp, 2016; Takagi-Niidome *et al.*, 2015), these mutations may reduce activity of γ -secretase. Inhibition of γ -secretase using DATPT in neural precursor cells has been shown to result in cell cycle exit and terminal differentiation to mature neurons (Borghese *et al.*, 2010; Main *et al.*, 2013; Woo *et al.*, 2009). The rate of neurogenesis is not significantly affected by inhibition of β -secretase with the inhibitor LY2886721, indicating the importance of γ -secretase in neural development (Arber *et al.*, 2021).

Dysregulation of neural precursor cell self-renewal and differentiation is a recurring theme in cell and rodent models of AD (Appel *et al.*, 2018; Scopa *et al.*, 2020). AD subtypes differ in aetiology but commonly present with impaired neurogenesis resulting from either an increase or decrease in neural differentiation -in either case,

impaired differentiation of neural precursors results in a loss of functional mature neurons. Premature neural differentiation in particular, may be a trait that occurs more commonly in neural cells containing *PSEN1* mutations, these *PSEN1* specific effects may be due to the role of *PSEN1* in activation of Notch signalling. FAD mutations have been shown to reduce Notch signalling by reducing γ -secretase mediated Notch cleavage (Chávez-Gutiérrez *et al.*, 2012; Song *et al.*, 1999) and mutations in *PSEN1* may drive premature neurogenesis in humans via reduced Notch signalling (Arber *et al.*, 2021). Analysis of gene expression data by Arber *et al.*, (2021) from the BrainSpan reference atlas indicated differences in spatiotemporal expression of β and γ -secretase subunits during human development, with enrichment of *PSEN1* and *APH1A* in cells which were capable of self-renewal, and enrichment of *PSEN2* and *APH1A* in neurons that had undergone terminal differentiation, this data indicates that *PSEN1* gene expression plays a vital role in early neural cell specification, and the reduced enrichment of *PSEN1* seen by Arber *et al.*, (2021) in mature neurons indicates that loss of canonical *PSEN1* signalling in immature neurons may lead to their specification. Notch ligands and receptors were shown to be enriched in the VZ and SVZ of the cortex during development, indicating that Notch signalling was highest in neurogenic regions. NSC generally displayed enrichment of Notch and γ -secretase, whereas neurons displayed enhanced expression of APP and β -secretase (Arber *et al.*, 2021), this research indicates that Notch and γ -secretase play important roles during neural stem cell specification, and that alterations in Notch signalling and in γ -secretase function may lead to abnormal neural specification and thus, abnormal AHN.

Yang *et al.*, (2017) also showed premature neural differentiation in neural precursor cells derived from patients with *PSEN1* mutations S169del and A246E, along with premature differentiation, neural precursors also displayed increased levels of A β , phosphorylated tau, and apoptosis when compared with controls (Yang *et al.*, 2017).

PSEN1 mutations may alter proliferation and differentiation of neural progenitor cells via impaired abnormal Notch and Wnt signalling, leading to an altered balance

between symmetric and asymmetric cell division. Effects of Notch and γ -secretase inhibition on the cell cycle were seen by Borghese *et al.*, (2010) who found that inhibiting γ -secretase activity in NSC using N-[N-(3,5-difluorophenacetyl)-L-alanyl]-S-phenylglycine t-butyl ester (DAPT), resulted in delayed transition from G1 to S phase and led to premature neural differentiation both in vitro and in vivo models (Borghese *et al.*, 2010).

Regulation of Notch signalling is critical during development. Notch signalling determines the timing and duration of neural progenitor proliferation and differentiation and thus plays a pivotal role in brain development (Hansen *et al.*, 2010). Notch signalling has also been shown to regulate neural rosette polarity, cell polarity in basal and apical cells is necessary for stem cell maintenance and for neural tube closure. Inhibition of Notch signalling resulted in a loss of neural rosettes and premature neural differentiation (Main *et al.*, 2013). Radial glia are specialised progenitor cells which have long radial processes that enable them to guide new neurons in radial migration from the ventricular zone to the mantle regions during the expansion of the neural tube. Notch signalling is vital for the proliferation of radial glia stem cells and is one factor in determining neuronal number in the mammalian cortex (Fiddes *et al.*, 2018). There are three human specific *NOTCH2*-derived genes (*NOTCH2NLA*, *NOTCH2NLB* and *NOTCH2NLC*) which are highly expressed in human cortical neural progenitor cells and may be candidates for 1q21.1 distal duplication/deletion syndromes. These three paralogs of human specific *NOTCH2NL* are expressed highly in radial glia (Fiddes *et al.*, 2018). Duplications of notch related genes lead to conditions such as macrocephaly and deletions lead to conditions such as microcephaly. Data published by Fiddes *et al.*, (2018) suggests that the emergence of *NOTCH2NL* genes in humans may have led to the larger and more complex neocortex seen in humans when compared with other primates (Fiddes *et al.*, 2018). This data indicates that enhanced Notch signalling prolongs cortical neurogenesis and may delay differentiation of neural progenitors. Despite significant differences in adult and embryonic neurogenesis, Notch signalling, and inhibitor of DNA-binding

(ID) factors are vital to both processes (Boareto *et al.*, 2017). Alterations to the γ -secretase complex caused by mutations in *PSEN1* may also alter γ -secretase cleavage of its other substrates, this may contribute to the diversity in disease presentation and cell behaviour seen as a result of different *PSEN1* mutations (Arber *et al.*, 2021).

It is not yet clear how significant human adult neurogenesis is in the context of health and disease, but significant alterations in adult neurogenesis have been reported in both human and animal models of AD (Arber *et al.*, 2021; Moreno-Jiménez *et al.*, 2019; Sung *et al.*, 2020; Teixeira *et al.*, 2018). Premature AHN in AD may result in depletion of NSC reserves, resulting in reduced capacity for regenerative repair and accelerated cognitive decline. Notch and Wnt signalling are possible mechanisms to investigate for modulation of AHN and reduction of disease progression in AD.

1.3 Unifying hypothesis

FAD mutations in *PSEN1* lead to dysregulation of neural cell specification *in vitro*, leading to depletion of neural stem cell reserves.

1.4 Aims

1. To generate an *in vitro* model of human adult neurogenesis which would be used to investigate neural cell specification in FAD compared with controls.
2. To use qPCR and flow cytometry to investigate key pathways governing cell specification in AD and control NSC.
3. To use RNA sequencing to identify the most significant changes in the AD transcriptome during neural differentiation.
4. To validate RNA sequencing results using qPCR and flow cytometry.

2.0 Materials

Materials were sourced as highlighted in table 1.

Table 1. Materials used, origin and catalogue number

Material	Origin	Catalogue Number
Dulbecco's Modified Eagles Medium (DMEM)	Gibco	BE12-614F
Foetal bovine serum (FBS)	Fisher Scientific UK	11550356
Dimethyl Sulfoxide DMSO	Fisher Scientific UK	BP231-100
Penicillin/Streptomycin (P/S) antibiotics (100x)	Lonza	DE17-603E
Plasmocin (50mg)	Invitrogen	ant-mpp
L-Glutamine	Lonza	17-605E
Human Embryonic Kidney cell line (HEK293T)	ATCC	CRL-3216
Trypsin/EDTA	Lonza	CC-5012
Plasmid pCMVR8.74	Addgene	22036
Plasmid pMD2.G	Addgene	12259
Stbl3™ Chemically Competent E. coli	Thermo Fisher	C737303
Plasmid Mini Kit	QIAGEN	27104

DMEM/F12 (1:1)	Gibco, Life Technologies	31331093
Non-essential amino acids	Life Technologies	1140050
B27 (50x)	Life Technologies	12587010
N2 (100x)	Life Technologies	17502048
bFGF (100µg/mL)	R&D systems	233-FB-025
Heparin (2mg/mL)	Sigma	H3149
Knockout Serum Replacement	Gibco, Life Technologies	10828-028
2-mercaptoethanol (BME)	Sigma-Aldrich	60-24-2
ROCK Inhibitor (Y-27632)	Sigma-Aldrich	Y0503-1mg
Mitomycin C	Calbiochem	475820
Matrigel® Matrix	Corning®	11573560
Gelatin from porcine skin	Sigma	G1890
TrypLE™	Gibco™	12604013
mTeSR™1 Basal Medium	Stem Cell Technologies	05851

mTeSR™1 5x Supplement	Stem Cell Technologies	05852
Human iPSC-Derived Neural Stem Cells - Alzheimer's Disease Patient (APOE4 HOM)	Axol Bioscience	Ax0111
Human iPSC-Derived Neural Stem Cells - Alzheimer's Disease Patient (<i>PSEN1</i> L286V)	Axol Bioscience	Ax0112
Human iPSC-Derived Neural Stem Cells - Alzheimer's Disease Patient (<i>PSEN1</i> M146L)	Axol Bioscience	Ax0113
Human iPSC-Derived Neural Stem Cells - Alzheimer's Disease Patient (<i>PSEN1</i> A246E)	Axol Bioscience	Ax0114
Human iPSC-Derived Neural Stem Cells - Alzheimer's Disease Patient (<i>PSEN2</i> N141I)	Axol Bioscience	Ax0115
Human iPSC-Derived Neural Stem Cells (Healthy Female donor)	Axol Bioscience	Ax0019
Neural Plating XF Medium	Axol Bioscience	Ax0033
NucBlue	Invitrogen™	R37606
ISOLATE II Genomic DNA Kit	Bioline	BIO-52065

Human Dermal Fibroblast Nucleofector™ Kit	Lonza	VVPD-1001
Nucleofector™ 2b Device	Lonza	AAB-1001
pCXLE-hOCT3/4-shp53-F	Addgene	27077
pCXLE-hSK	Addgene	27078
pCXLE-hUL	Addgene	27080
pCXWB-EBNA1	Addgene	37624
Plasmid Midi Kit	QIAGEN	12162
pLV-TetO-hNGN2-eGFP-Puro	Addgene	79823
Anti-hSOX2 primary antibody	R&D Systems	AF2018
Anti-hOCT3/4 primary antibody	R&D Systems	AF1759
Anti-Tra-1-18 primary antibody	R&D Systems	MAB8495
SQSTM1/p62 primary antibody	Abcam	Ab56416
Anti-LC3 primary antibody	NanoTools	0231-100/LC35F10
Anti-LAMP1 primary antibody	Abcam	ab24170
Anti-alpha-SMA primary antibody	Abcam	ab5694
Anti-SOX17 primary antibody	R&D Systems	AF1924
Anti- Beta-III tubulin primary antibody	Abcam	ab18207

Goat Anti-Rabbit IgG H&L (Alexa Fluor® 488)	Alexa Fluor®	ab150077
Goat Anti-Mouse IgG H&L (Alexa Fluor® 488)	Alexa Fluor®	ab150113
Goat Anti-Mouse IgG H&L (Alexa Fluor® 568)	Alexa Fluor®	(ab175473)
Donkey Anti-Goat IgG H&L (Alexa Fluor® 568)	Alexa Fluor®	ab175474
The Human Dermal Fibroblast (HDF) Nucleofector™ Kit	Lonza	VPD-1001
RNeasy Mini Kit	Qiagen	74104
QIAshredder columns	Qiagen	79656
RQ1 Rnase- Free Dnase	Promega	M6101
M-MLV enzyme and 5X reaction buffer	Promega	M5313
dNTPs (10mM each)	Thermo Scientific™	10610851
RNasin® Ribonuclease Inhibitor	Promega	N2111
Random Primers	Invitrogen™	48190011
SensiFAST™ SYBR® No-ROX Kit	Meridian Bioscience (Bioline)	BIO-98020
RNA 6000 Nano Kit	Agilent	5067-1511

Fixation buffer (4% PFA)	BioLegend	420801
Bovine Serum Albumin (BSA)	Sigma- Aldrich	B6917
eBioscience™ Fixable Viability Dye eFluor™ 780	Invitrogen	65-0865-14
Apotracker Green	BioLegend	427402
Dulbecco's Phosphate Buffered Saline DPBS (1X),9.5 mM PO4 without Calcium or Magnesium, 1 L	Lonza	BE17-512Q
eBioscience™ Propidium Iodide	Invitrogen	BMS500PI
Nestin Monoclonal Antibody (10C2)	Thermo Fisher	MA1-110
Goat Anti-Mouse IgG H&L (Alexa Fluor® 405)	Abcam	ab175660

2.1 Cell lines used

MEF feeder cells were purchased from Cambridge Bioscience (CBA-310).

Shf3 Human Embryonic stem cells (hESCs) were procured from the UK stem cell bank (SCSC10-48).

control neonatal dermal fibroblasts (nhDF) were purchased from Fisher Scientific (C0045C) and PromoCell (CAT NO).

HEK293T cells were acquired from Dr Steve Howe – institute of child health, UCL.

PSEN1 A246E, *PSEN1* M146L and control NSC were purchased from Axol Bioscience (Ax0114, Ax0113 and Ax0019, respectively), NSC purchased from Axol Bioscience were all purchased as iPSC derived neural stem cells which were generated from patient fibroblasts.

PSEN2 N141I (Ax0115) and *APOE4* HOM NSC (Ax0111) had been purchased prior to initiation of this project from Axol Bioscience (Ax0115) by a student in the McKay lab group. Stores of these NSC were low as they had previously been passaged a number of times and reprogramming of *PSEN2* N141I mutation containing NSC was not successful. Reprogramming of *APOE4* HOM NSC (Ax0111) was successful in that iPSC colonies were generated, (Figure 29) but these did not survive multiple passages. For this reason, experiments to compare AD lines with controls were carried out using the Axol Bioscience lines Ax0113, Ax0114 and Ax0119 (Table 1, Table 2).

Table 2. Information available on control and *PSEN1* lines used.

Identifier	Control	<i>PSEN1</i> A246E	<i>PSEN1</i> M146L
Product name	ax0019	ax0114	ax0113
Gender	Female	Female	Male
Age of donor (years)	64	31	53
Disease information	Healthy	clinically affected with AD	
Age of onset of AD	N/A	45	

APOE genotype	E3/E3	E3/E4	E2/E3
Karyotype	Normal		
Ethnicity		Caucasian	Caucasian
Reprogramming method	Episomal vector	Episomal vector	Episomal vector
HLA Serotype		A2 A24, B18(Bw6) B44(Bw4), Cw2 Cw12	A1 A3, B35(Bw6) B47(Bw4), Cw4 Cw6

Control ax0019 NSC purchased from AxolBioscience were de-differentiated to produce iPSC and used as controls for comparison of *PSEN1* lines purchased from the same company. *PSEN1* A246E NSC purchased from AxolBioscience were de-differentiated to produce iPSC and were used throughout this project for investigation of neural differentiation in neural cells containing the *PSEN1* A246E mutation. *PSEN1* M146L NSC purchased from Axol Bioscience were de-differentiated to produce iPSC and were used during the initial stages of this project for investigation of neural differentiation in neural cells containing the *PSEN1* M146L mutation. iPSC generated from *PSEN1* A246E were able to be expanded to a greater degree than iPSC generated from *PSEN1* M146L, this is not likely due to genotypic differences between the two but was the main reason that the project later progressed to focus on comparing controls against the *PSEN1* A246E line only.

2.2 Plasmids used

pCXLE-hOCT3/4-shp53-F was a gift from Shinya Yamanaka (Addgene plasmid # 27077; <http://n2t.net/addgene:27077> ; RRID:Addgene_27077)

pCXWB-EBNA1 was a gift from Shinya Yamanaka (Addgene plasmid # 37624 ; <http://n2t.net/addgene:37624> ; RRID:Addgene_37624)

pCXLE-hUL was a gift from Shinya Yamanaka (Addgene plasmid # 27080 ;
<http://n2t.net/addgene:27080> ; RRID:Addgene_27080)

pCXLE-hSK was a gift from Shinya Yamanaka (Addgene plasmid # 27078 ;
<http://n2t.net/addgene:27078> ; RRID:Addgene_27078)

3.0 Methods

3.1 Cell culture methodologies

Cell culture methodologies were used to culture somatic cells, generate, and propagate iPSC and to specify these to neural stem and progenitor cells for use in downstream experiments to model and investigate FAD neural specification. GM work was carried out according to the appropriate SOPs, COSHH and risk assessments.

3.1.1 Expansion and culture of NSCs purchased from Axol Bioscience

AD and control NSCs were purchased from Axol Bioscience and were expanded to generate small stores of NSC before being de-differentiated to iPSC. The lines expanded were ax0019, ax0114 and ax0113 (Table 2).

AD and control NSC lines were revived into Neural Plating XF Medium onto plates pre-coated with Matrigel. The following day, Neural Plating XF medium was replaced with neural expansion medium (NEM) composed of DMEM/F12 (1:1) supplemented with NEAA (1x), N2 (1x), B27 (1x), Pen/Strep (1x), Plasmocin (100ng/mL), bFGF (20ng/mL) and Heparin (2µg/mL). Throughout NSC culture and expansion, NEM was replaced every 2-3 days. When NSCs reached confluency, they were passaged using TrypLE™ and plated in NEM + RI onto Matrigel® coated plates. All cells were incubated at 37°C and 5% CO₂.

3.1.2 Mitotic inactivation of MEFs for iPSC culture

Inactivated mouse embryonic fibroblasts (iMEFs) can be used as a feeder layer to maintain stem cell pluripotency and to promote colony expansion, they are inactivated using Mitomycin C.

Prior to plating MEFs, tissue culture flasks were coated with 0.1% Gelatin (0.1% Gelatin in ddH₂O) for a minimum of 20 minutes at room temperature. Gelatin was removed before cells were plated and cultured in complete DMEM (DMEM

(4500mg/L glucose), 10% FBS (v/v), L-Glutamine (4mM), supplemented with 1x (v/v) non-essential amino acids and with (1x) Penicillin/Streptomycin) which was replaced on alternate days.

When MEFs reached 85-90% confluency, 150 μ L/cm² of TrypLE was used to enzymatically disrupt the cells which were centrifuged at 258 x g for 5 minutes and then resuspended in the volume of complete DMEM required to passage them in the ratio 1:4 onto Gelatin coated flasks.

When MEFs reached 85-90% confluency at passage 4 (P4), they were mitotically inactivated to generate iMEFs. Mitotic inactivation of MEFs was achieved by incubation in complete DMEM with Mitomycin C (0.1 μ g/ μ L) for 3 hours at 37°C. After mitotic inactivation was complete, the now inactivated MEFs (iMEFs) were washed three times in 10mL of Dulbecco's Phosphate Buffered Saline (DPBS) and then were enzymatically disassociated from the flask using TrypLE.

iMEFs were centrifuged and resuspended in freezing media (FBS supplemented with 10% Dimethyl Sulfoxide (DMSO)) at a density of \sim 5 x 10⁶ cells/mL. iMEFs were stored at -80°C and defrosted when required for use in culturing induced pluripotent stem cells (iPSC). For use as a feeder layer in culture of iPSCs, iMEFs were seeded at a density of 5 x 10⁴ cells/cm² onto cell culture flasks/ plates which had been coated in 0.1% Gelatin.

3.1.3 Reprogramming NSCs

NSC purchased from Axol Bioscience and expanded (3.1.1) were de-differentiated to generate larger stores of control iPSC and iPSC containing the *PSEN1* A246E and *PSEN1* M146L mutations. NSC were nucleofected with reprogramming factors and shortly after, plated onto iMEFs (3.1.2) for de-differentiation to iPSC, during which they were cultured in human embryonic stem cell (HESC) media.

HESC Media was made up of DMEM F12 supplemented with components required for expansion of ESC and iPSC (Table 3).

Table 3. The composition of HESC media

Component	Percentage (%)
DMEM F12	77.88
FBS	20
BME	0.02
P/S	1
Plasmocin	0.1
NEAA	1

An EBNA based system was used for cellular reprogramming of somatic cells to iPSC. This EBNA based system consisted of the episomal plasmids pCXLE-hSK (Addgene ID 27078), pCXLE-hUL (Addgene ID 27080), pCXLE-hOCTshp53 (Addgene ID 27077) which enable integration-free, episomal expression of human pluripotency factors OCT3/4, SOX2, KLF4, L-MYC and LIN28. Alongside plasmids used for expression of pluripotency factors, the plasmid pCXLE-EBNA1 (Addgene ID 37624) was used to enhance transfection efficiency and expression of pluripotency factors. NSCs were plated into a T25 pre-coated with Matrigel and were expanded until they reached 90% confluency. NSCs were then enzymatically disrupted using TrypLE™, resuspended in DPBS, then centrifuged at 146 x g. Media was aspirated off and pellet was resuspended in 100µl of electroporation buffer (from a Nucleofector™ Kit) supplemented with 2µg of each episomal plasmid; pCXLE-hSK (Addgene ID 27078), pCXLE-hUL (Addgene ID 27080), pCXLE-hOCTshp53 (Addgene ID 27077), pCXLE-EBNA1 (Addgene ID 37624) (the EBNA based system). The cells, electroporation buffer and plasmids were transferred to an electroporation cuvette and electroporated using programme A-033 on the Nucleofector™ 2b Device. Nucleofected cells were then transferred into 2ml NEM + RI in one well of a 6 well

plate pre-coated with Matrigel. NEM was replaced every 2 days until day 8 when 3×10^4 nucleofected cells were plated onto one well of a 6 well plate pre-seeded with iMEFs. Media was changed to HESC + FGF 1 day after plating to MEFs and was replaced every 2 days. HESC was composed of DMEM/F12, supplemented with 10% knockout serum (KSR), 1% non-essential amino acids (NEAA), 0.2% mercaptoethanol, 1% P/S, 0.1% Plasmocin. 2-3 weeks after plating to MEFs, colonies were picked using a p200/p1000 sterile pipette and plated onto new iMEFs, this was repeated each time iPSC reached confluency.

3.1.4 Trilineage differentiation

iPSC pluripotency was confirmed by differentiation to all three germ layers, to carry out trilineage differentiation, iPSC on feeder cells were disrupted using a p200 or p1000 pipette and plated onto one well of a 6-well plate pre-coated with Matrigel in mTeSR™1 media. When feeder free iPSC reached 70% confluency, they were enzymatically disrupted using TrypLE™, centrifuged at 146 x g for 8 minutes and plated in suspension onto plates with no charge in HESC and RI. After eight days of culture in HESC, cells were plated onto Nucleon™ Delta positively charged plates, cultured in DMEM, supplemented with 10% FBS, 100x Penicillin/Streptomycin antibiotics and 4mM L-Glutamine, herein after referred to as complete DMEM (cDMEM). Cells from each of the three germ layers were formed after 6-8 days and immunostaining was used to assess differentiation; SOX17 was used as marker of endoderm, α -SMA as a marker of mesoderm and β -III tubulin was used to stain for cells of ectoderm lineage.

3.1.5 Culture and expansion of induced pluripotent stem cells (iPSC) and human embryonic stem cells (hESC)

For continued culture and expansion, iPSC and hESC, can be cultured on feeders (for example iMEFs) or can be cultured without feeders (feeder free). For reprogramming and the initial few weeks after generation of iPSC, iPSC were cultured on iMEFs to

allow for stabilisation and expansion of colonies before transfer to feeder free culture.

iMEFs were seeded on Nucleon™ Delta plates pre-coated with Gelatin. After a minimum of 5 hours post plating iMEFs, iPSC lines were plated onto the iMEFs and cultured in HESC + FGF2. Throughout iPSC culture and expansion, media was replaced every 2 days. When iPSC reached confluency, they were disrupted using a p200 sterile pipette tip, plated onto new iMEFs and cultured in HESC + FGF2. Cells were incubated at 37°C and 5% CO₂.

3.1.6 Feeder free culture and expansion of hESC/iPSC

After stabilisation and expansion of iPSC and hESC colonies on iMEFs, iPSC/hESC were transferred to feeder free culture. Stem cells were picked and plated onto Matrigel® Matrix in mTeSR medium, composed of mTeSR™1 Basal medium and mTeSR™1 5x Supplement. When iPSC/hESC cultured feeder free required passaging, they were enzymatically disrupted using TrypLE™ and plated onto Matrigel coated plates in mTeSR medium with 0.1% rock inhibitor (RI). The following day medium was replaced with fresh mTeSR.

3.1.7 Neural differentiation of human ESC and iPSC to NSC and NPC

iPSC were cultured feeder free on Matrigel coated plates, then enzymatically disrupted and plated into neural induction medium (NIM), composed of DMEM/F12 (1:1) supplemented with NEAA (1x), N2(1x), Pen/Strep (1x), Plasmocin (100ng/mL), bFGF (20ng/mL) and Heparin (2µg/mL). iPSC in NIM were then plated at a density of 1×10^4 into a Nunc 96 V bottom well plate. Neuroepithelial clusters formed in suspension and media was replaced every day for 5 days. On day 6, aggregates were re-plated to Matrigel® coated 6-well cell culture plates to allow neural rosette formation (2-3 days). Rosette clusters formed (NSCs) and were picked using a p200/p1000 pipette tip for continued culture. To generate NPC, rosette clusters were resuspended in Neural expansion media (NEM) composed of DMEM/F12 (1:1)

supplemented with NEAA (1x), N2(1x), B27 (1x), Pen/Strep (1x), Plasmocin (100ng/mL), bFGF (20ng/mL) and Heparin (2µg/mL) and plated onto Matrigel® coated cell culture plates. NPCs were then expanded as a monolayer culture on Matrigel® coated plates.

3.1.8 Generation of neurospheres

iPSC cultured feeder free on Matrigel® coated plates were enzymatically disrupted and plated into neural induction medium (NIM) composed of DMEM/F12 (1:1) supplemented with NEAA (1x), N2(1x), Pen/Strep (1x), Plasmocin (100ng/mL), bFGF (20ng/mL) and Heparin (2µg/mL). iPSC in NIM were then plated at a density of 1×10^4 into a Nunc 96 V bottom well plate. Neuroepithelial clusters formed in suspension and media was replaced every day for 5 days, from then on.

3.1.9 Terminal differentiation

NPC generated from the neural differentiation protocol detailed in **3.1.7** were cultured in NEM composed of DMEM/F12 (1:1) supplemented with NEAA (1x), N2(1x), B27 (1x), Pen/Strep (1x), Plasmocin (100ng/mL), bFGF (20ng/mL) and Heparin (2µg/mL) and plated onto Matrigel® coated plates at low density to encourage neural differentiation.

3.2 Bacterial work

3.2.1 Increasing stocks of episomal plasmids for reprogramming

Stocks of the EBNA based episomal plasmids used for reprogramming pCXLE-hSK (Addgene ID 27078), pCXLE-hUL (Addgene ID 27080), pCXLE-hOCTshp53 (Addgene ID 27077) were maintained using Stbl3™ Chemically Competent E. coli bacteria. The Stbl3™ chemically competent cells were transformed with plasmid, expanded and then plasmid DNA was isolated using the Plasmid Midi kit by Qiagen.

3.2.2 Bacterial transformation

S.O.C medium was warmed to room temperature and selective plates were warmed to 37°C in an incubator for 30 minutes. One vial of One Shot™ Stbl3™ chemically competent cells was thawed on ice for each transformation. 100ng of plasmid DNA was added into one vial of comp cells and mixed gently, the mixture was incubated on ice for 30 minutes to enable DNA entry into cells. The cells were then heated to 42°C for 45 seconds (heat shock) to close the pores of the membrane with the DNA insert inside, after which the cells were placed on ice for 2 minutes. 250 µL of S.O.C medium was added to each vial and the vials were shaken horizontally at 37°C for 1 hour at 225 rpm in a shaking incubator. 25-100 µl from each transformation were streaked on a pre-warmed selective plate and incubated overnight at 37°C. Colonies were selected and isolated using the Plasmid Midi Kit by Qiagen.

3.2.3 Plasmid isolation

The Plasmid Midi kit by Qiagen was used to isolate plasmid DNA from transformed bacterial cells. After transformed Stbl3™ chemically competent cells were streaked on selective plates and incubated overnight at 37°C, a single colony was picked and used to inoculate 2-5mL of LB medium containing a selective antibiotic. The colony in LB medium was incubated for approximately 8 hours at 37°C with vigorous shaking (approximately 300 rpm). The starter culture was diluted 1/500 to 1/1000 into selective LB medium depending on whether the plasmid was high or low copy and was grown for 12-16 hours at 37°C with vigorous shaking (approximately 300 rpm).

Bacterial cells were then harvested by centrifugation at 6000 x g for 15 minutes at 4°C. Bacterial pellets were resuspended in 4ml of Buffer P1, buffer P2 was then added, mixed thoroughly, and incubated at room temperature for 5 minutes. To precipitate DNA, 4ml of Buffer P3 (chilled) was added, mixed and the resulting solution was incubated on ice for 15 minutes. The solution was centrifuged at $\geq 20,000$ x g for 30 min at 4°C and the supernatant containing plasmid DNA was promptly removed. A QIAGEN-tip 100 was equilibrated by applying 4 ml of Buffer

QBT and allowing the column to empty by gravity flow. The supernatant from step 8 was applied to the QIAGEN-tip which was allowed to enter the resin by gravity flow. The QIAGEN-tip was washed with 2 x 10 ml Buffer QC. DNA was eluted with 5 ml of Buffer QF and was then precipitated by adding 3.5 ml of room-temperature isopropanol to the eluted DNA. The solution was mixed and centrifuged immediately at $\geq 15,000 \times g$ for 30 minutes at 4°C and supernatant was carefully decanted. The DNA pellet was washed with 2 ml of room temperature 70% ethanol and centrifuged at $\geq 15,000 \times g$ for 10 min. The supernatant was then carefully decanted without disturbing the pellet. The pellet was air-dried for 5–10 min, and the DNA was then redissolved in a suitable volume of buffer (TE buffer, pH 8.0, or 10 mM Tris-Cl, pH 8.5). DNA yield was determined using spectrophotometry.

3.3. Immunostaining

Immunostaining was used to validate the pluripotency of iPSC produced. Unless otherwise specified, steps were carried out at room temperature.

Cells were washed with PBS and fixed in 4% paraformaldehyde for 10 minutes. Cells were then permeabilised with 0.3% Triton X-100 in PBS for 10 minutes. Permeabilization was not carried out when staining for cell surface proteins. Cells were washed again with PBS and then blocked in blocking buffer for 60 minutes. Blocking buffer consisted of 2% BSA and 0.1% Tween 20 in PBS. Cells were then incubated in blocking buffer with primary antibodies at 4°C overnight. After incubation with primary antibodies, cells were washed with PBS and incubated in blocking buffer with the appropriate Alexa Fluor conjugated secondary antibodies for 1 hour in the dark at room temperature. Fluorescence was detected using fluorescence microscopy (Leica live cell imaging microscope). Primary and secondary antibodies and concentrations used are displayed in tables 3 and 4.

Table 4. Primary antibodies and concentration used for immunocytochemistry (ICC).

Primary antibodies	Concentration
Anti-hSOX2 primary antibody	2µg/ml
Anti-hOCT3/4 primary antibody	1µg/ml
Anti-Tra-1-18 primary antibody	2.5µg/ml
SQSTM1/p62 primary antibody	1µg/ml
Anti-LC3 primary antibody	2µg/ml
Anti-LAMP1 primary antibody	2.5µg/ml
Anti-alpha-SMA primary antibody	1µg/ml
Anti-SOX17 primary antibody	1µg/ml
Anti- Beta-III tubulin primary antibody	1µg/ml

Table 5. Secondary antibodies and concentration used for immunocytochemistry (ICC).

Secondary antibodies	Concentration
Goat Anti-Rabbit IgG H&L (Alexa Fluor® 488)	4µg/ml
Goat Anti-Mouse IgG H&L (Alexa Fluor® 488)	4µg/ml
Goat Anti-Mouse IgG H&L (Alexa Fluor® 568)	4µg/ml
Donkey Anti-Goat IgG H&L (Alexa Fluor® 568)	4µg/ml

3.4 Molecular work

All plastics and nuclease free water were subjected to UVC-light prior to use in molecular work to reduce the risk of DNA contamination in samples.

3.4.1 Isolation of genomic DNA

The ISOLATE II Genomic DNA Kit is a column-based method which was used for isolation of genomic DNA from control and AD iPSC lines. iPSC were expanded on a feeder layer of inactivated mouse embryonic fibroblasts (iMEFs) until they reached 80-90% confluency. Colonies were then picked using a p200/p1000 pipette tip and re-suspended in lysis buffer GL. Proteinase K solution and lysis buffer G3 were added, and the sample was incubated at 70°C. 96-100% ethanol was added to adjust DNA binding conditions and the sample was vortexed. DNA was bound to the silica membrane of a spin column and washed using wash buffers GW1 and GW2. The silica membrane was then dried, and DNA was eluted using elution buffer pre-heated to 70°C. DNA samples were checked for quality based on their 260/280 ratio being around 1.8 (samples were discarded if their 260/280 ration was not between 1.7-2.0).

3.4.2 DNA sequencing of AD iPSC

Forward and reverse primers were designed specific to the site of each mutation and were used to sequence these genomic regions for verification of AD iPSC.

Table 6. Forward and reverse primers designed for verification of AD mutations.

Mutation/Allelic Variation	<i>PSEN1</i> A246E	<i>PSEN1</i> M146L
Forward Primer	TGGAATTTTGGTGTGG TGGG	GGAGGTGGTAATGTGGTT GGT
Reverse Primer	CAGTGGGGCATTCTG TGAC	ATGCTCACCTTATAGCACCT GT

--	--	--

3.4.3 Isolation of RNA

The RNeasy® Mini Kit is a column-based method that was used to isolate RNA from control and *PSEN1* NSC and neurospheres for transcriptome-based investigation of neural differentiation in disease. P2 and P3 NSC were expanded on Matrigel® Matrix coated plates until they reached 80-90% confluence. Approximately 1×10^6 NSC were enzymatically dissociated from the plates using TrypLE™ and centrifuged at 258 x g for 5 minutes. Supernatant was removed and the cell pellet was resuspended in DPBS. Cells were centrifuged again at 258 x g for 5 minutes to form a pellet. Supernatant was removed and cells were resuspended in 350µl of Buffer RLT. Cells in RLT were transferred to a Qiagen QIAshredder column for homogenisation (cells were passed through the column using centrifugation at maximum speed for 2 minutes). Post homogenisation, 350µl of 70% ETOH was added to the flow-through to aid precipitation of RNA. 700µl of sample was then transferred to a RNeasy Mini spin column placed in a 2ml collection tube and centrifuged at ≥ 8000 x g for 15 seconds to bind total RNA -flow through was discarded. Total RNA bound to the spin column membrane was washed using 700µl of buffer RW1 (centrifuged at ≥ 8000 x g for 15 seconds), 500µl of buffer RPE (centrifuged at ≥ 8000 x g for 15 seconds) and then 500µl of buffer RPE (centrifuged at ≥ 8000 x g for 2 minutes). After washes with buffers RW1 and RPE, the RNeasy spin column was then placed in a new 2ml collection tube and centrifuged at full speed for 1 minute to dry the membrane. RNA was eluted into a new 1.5ml collection tube using 30µl of RNase-free water pipetted directly into the centre of the spin column (centrifuged at ≥ 8000 x g for 1 minute). All RNA samples were stored at -80°C.

3.4.4 Determination of RNA concentration and purity

A NanoDrop™ One/OneC Microvolume UV-Vis Spectrophotometer was used after each RNA isolation to determine concentration and sample purity. All RNA samples used had a 260/230 ratio in the range 2.0-2.2 and a 260/280 ratio in the range 1.9-2.2.

3.4.5 DNase treatment of RNA

The RQ1 RNase-Free DNase is a DNase I (endonuclease) that was used to degrade both double-stranded and single-stranded DNA in all RNA samples prior to RT-PCR. DNase digestion was carried out to prevent genomic contamination in RNA samples prior to generation of cDNA.

1µg of each RNA sample (1-8µl) was treated with 1µl (1 unit/µg of RNA) of RQ1 RNase-Free DNase and 1µl of RQ1 DNase buffer (total solution was made up to 10µl using nuclease free water). Post incubation of RNA with DNase at 37°C for 30 minutes, 1µl of RQ1 DNase Stop Solution was added and the mixture was heated to 65°C for 10 minutes to terminate the reaction.

3.4.6 Generation of first strand cDNA for two-step RT-qPCR

Post treatment with DNase, RNA was reverse transcribed to generate complementary DNA (cDNA) for investigation using quantitative polymerase chain reaction (qPCR). Each RNA sample was separated into two: A and B. A underwent reverse transcription using the enzyme M-MLV reverse transcriptase (RT) and B was maintained as a no-RT control.

For first-strand cDNA synthesis, 1µg of total RNA was added to 0.5µg of random primers and made up to 15µl with nuclease free water. To break up the secondary structure within the template strand, samples were heated to 70°C for 5 minutes, then cooled immediately on ice to prevent reformation of the secondary structure. In this order, the following components were added to the reaction: 5µl of M-MLV 5X reaction buffer, 5µl of dNTPs (10mM), 0.6µl of Recombinant RNasin®

Ribonuclease Inhibitor (25 units), 1µl of M-MLV reverse transcriptase (200 units) and nuclease free water, which was used to make the solution up to 25µl. Samples were incubated for 1 hour at 37°C to allow for first-strand cDNA synthesis to take place and then stored at -20°C. Second strand cDNA synthesis for each sample took place using forward PCR primers during the first amplification cycle of PCR.

3.4.7 Selecting primers for qPCR

Primer sequences were taken from peer reviewed publications and tested for efficiency. Primers sets used for qPCRs were between 90-110% efficient.

Multiple housekeeping genes (Table 7.) were selected based on the stability of those genes in AD. Penna *et al.*, (2011) evaluated common housekeeping genes used for normalisation during qPCR using human post-mortem brain samples from AD patients and controls. Genes *CYC1* (Cytochrome c1) and *EIF4A2* (eukaryotic translation initiation factor 4a2) were found to be the most stable between AD and control samples. In a later assessment of brain reference genes for RT-PCR studies in human neurodegenerative studies, *UBE2D2* and *RPL13* were reported to be the most stable reference genes in both the cerebellum and prefrontal cortex (Rydbirk *et al.*, 2016).

Table 7. qPCR primers for housekeeping genes.

Gene	Forward Primer Sequence 5-3'	Reverse Primer Sequence 5-3'
<i>UBE2D2</i>	TGCCTGAGATTGCTCGGATCT	TCGCATACTTCTGAGTCCATTCC
<i>RPL13</i>	CCTGGAGGAGAAGAGGAAAGAGA	TTGAGGACCTCTGTGTATTTGTCAA
<i>EIF4A2</i>	AATCCGGTCAGGGTCAAGTC	GCCACACCTTTCCTCCCAA
<i>CYC1</i>	GAGGTGGAGGTTCAAGACGG	TAGCTCGCACGATGTAGCTG

qPCR primers (

Table 8) used for investigation of neural differentiation capacity in *PSEN1*, and control neural cells were selected to investigate a range of different pathways. Genes *AXN2*, *LEF1*, *B-catenin* and *GSK3B* are associated with canonical Wnt signalling (Rapp *et al.*, 2017) (1.2.2). Using qPCR, expression of these genes was compared in *PSEN1* and control NSC and neurospheres to investigate alterations to Wnt signalling in AD (Figure 56). Genes *Notch1* and *Jagged1* are associated with Notch signalling (Wolfe., 2020; Medoro *et al.*, 2018; Haapasalo and Kovacs., 2011) (1.1.8) and their expression was compared in *PSEN1* and control NSC and neurospheres to investigate Notch signalling in AD. Genes *CSNK1G2*, *CDH20*, *ACTG2* and *FZD9* are associated with Wnt signalling pathways (Rapp *et al.*, 2017) (1.2.2) and were shown to be significantly dysregulated ($p < 0.05$) in RNA sequencing data as *PSEN1* NSC matured from P2 to P3. qPCR was used to validate the changes seen in RNA sequencing data (Figure 91). Genes *JAG2*, *HEY1*, *RFNG* were significantly dysregulated during *PSEN1* neural differentiation ($p < 0.05$) in RNA sequencing data and are associated with Notch signalling pathways (Wolfe., 2020; Medoro *et al.*, 2018; Haapasalo and Kovacs., 2011) (1.1.8). qPCR was used to validate the changes seen in RNA sequencing data (Figure 92). Genes *LC3*, *MTOR*, *Beclin1* are associated with autophagy (Tooze and Yoshimori, 2010; Kiriyaama and Nochi, 2015) (5.1.4), thus their expression was measured in *PSEN1* and control NSC and neurospheres to investigate regulation of autophagy in AD. *NQO1*, *NRF2*, *STAT3*, *NFKB1* are genes associated with the antioxidant response and inflammation (Liu *et al.*, 2016) (5.1.4). Their expression was analysed in *PSEN1* and control NSC to investigate inflammation and antioxidant response pathways in AD (Figure 57). Genes *SOX2* and *NES* are expressed by immature neural cells. Expression of *SOX2* and *NES* declines as NSC specify to neurons at which point *MAP2* expression is upregulated (FitzPatrick *et al.*, 2017). Expression of *SOX2*, *Nestin* and *MAP2* was compared between *PSEN1* and control NSC to determine whether the rate of neural specification was altered in AD NSC (Figure 58).

Table 8. qPCR primers used for investigation of AD neurogenesis.

Gene	Forward Primer Sequence 5-3'	Reverse Primer Sequence 5-3'
<i>AXIN2</i>	TACACTCCTTATTGGGCGATCA	TTGGCTACTCGTAAAGTTTTTGGT
<i>LEF1</i>	TGCCAAATATGAATAACGACCCA	GAGAAAAGTGCTCGTCACTGT
<i>B-catenin</i>	CATCTACACAGTTTGATGCTGCT	GCAGTTTTGTCAGTTCAGGGA
<i>GSK3B</i>	AGACGCTCCCTGTGATTTATGT	CCGATGGCAGATTCCAAAGG
<i>Notch1</i>	CAATGTGGATGCCGCAGTTGTG	CAGCACCTTGGCGGTCTCGTA
<i>Jagged1</i>	CGGGATTTGGTTAATGGTTATC	ATAGTCACTGGCACGGTTGTAGCA C
<i>LC3</i>	GAGAAGCAGCTTCTGTTCTGG	GTGTCCGTTACCAACAGGAAG
<i>NRF2</i>	CAGCGACGGAAAGAGTATGA	TGGGCAACCTGGGAGTAG
<i>Keap1</i>	GGCTGTCCTCAATCGTCTCC	TCTGTTTCCACATCGTAGCG
<i>MAP2</i>	CTCAGCACCGCTAACAGAGG	CATTGGCGCTTCGGACAAG
<i>SOX2</i>	GACCAGCTCGCAGACCTACAT	TGGAGTGGGAGGAAGAGGTA
<i>NES</i> (Nestin)	GGCAGCGTTGGAACAGAG	CATCTTGAGGTCGCCAGCT
<i>Beclin1</i>	ACCGTGTCACCATCCAGGAA	GAAGCTGTTGGCACTTTCTGT
<i>NFKB1</i>	TGCCAACAGATGGCCATAC	TGTTCTTTTCACTAGAGGCACCA
<i>STAT3</i>	CATATGCGGCCAGCAAAGAA	ATACCTGCTCTGAAGAACT
<i>NRF2</i>	CAACTACTCCCAGGTTGCC	AGT GAC TGA AAC GTA GCC GAA
<i>NQO1</i>	GGGCAAGTCCATCCCAACTG	GCAAGTCAGGGAAGCCTGGA

<i>MTOR</i>	GGGTCAGAGAGTGGCCTTCAA	ATGCTGTCCCTGGTCCTTATG
<i>Notch1</i>	CAATGTGGATGCCGCAGTTGTG	CAGCACCTTGGCGGTCTCGTA
<i>FZD9</i>	TGCTCACCTTCTTGCTGGAG	GCCAGCGAGTAGACGTTGTA
<i>CSNK1G</i> 2	AAGGAGCGGTACCAGAAGATCG	GAAGAGCTTCCGCAGGTAGTCA
<i>CDH20</i>	GGGACCGACCCTTTGTATGTC	CGATGGTAAACACGATGCCAG
<i>ACTG2</i>	GCGTGTAGCACCTGAAGAG	GAATGGCGACGTACATGGCA
<i>NCOR2</i>	AAGCAGCGAGCGGCTGCCAT	TGCTGAGGGGCGTCGCTCTC
<i>RFNG</i>	TGCTGCTGCGTACCTGGATCTC	ACAGCAGAGCAATTGGTGTTGA
<i>HEY1</i>	GCTGGTACCCAGTGCTTTTGTGAG	TGCAGGATCTCGGCTTTTTCT
<i>JAG2</i>	AGCCATGCCTTAACGCTTTT	CACACACTGGTACCCGTTCA
<i>CHAC1</i>	GGTGACGCTCCTTGAAGATCAT	TCAGTGGTTGGTCAGGAGCAT
<i>NCOR2</i>	GGGTAAATATGACCAGTGGGAAGA G	TGGCATTGAGAGGGTTAAAAGC

3.4.8 Calculating primer efficiency

To determine primer efficiency before use in qPCRs, a standard curve was performed for every new primer set. cDNA samples used for primer efficiency tests were generated from RNA taken from NSCs or NPCs to ensure primers were performing between 90-110% efficiency when using RNA from relevant cell types. The standard curve was performed using serial dilutions of cDNA sample containing a minimum of five points. All cDNA samples investigated using qPCR were diluted 1:10 so to ensure efficiency at this dilution, this point was included in all primer efficiency tests. For the majority of primer efficiency tests, cDNA was diluted 1:10, 1:50, 1:100, 1:200, 1:300,

1:400 and each cDNA dilution was measured in triplicate. To calculate % primer efficiency, average cycle threshold (Ct) values were calculated from the triplicate measures and plotted against the log of each sample dilution as a scatter plot.

Table 9. Example of average Ct values measured using primers designed to detect transcripts generated from the housekeeping gene *UBE2D2*.

Average Ct values	Dilution	Sample Quantity	Log (Sample Quantity)
22.51	1:10	0.1	-1.00
25.84	1:100	0.01	-2.00
26.64	1:200	0.005	-2.30
27.89	1:400	0.0025	-2.60
28.84	1:800	0.00125	-2.90

Sample quantity was calculated based on cDNA dilution. Log (sample quantity) was plotted against Average Ct values on a scatter plot, a trendline was added and was used to find the equation of the line ($y = m x + c$) where m is the slope and c is the y -intercept.

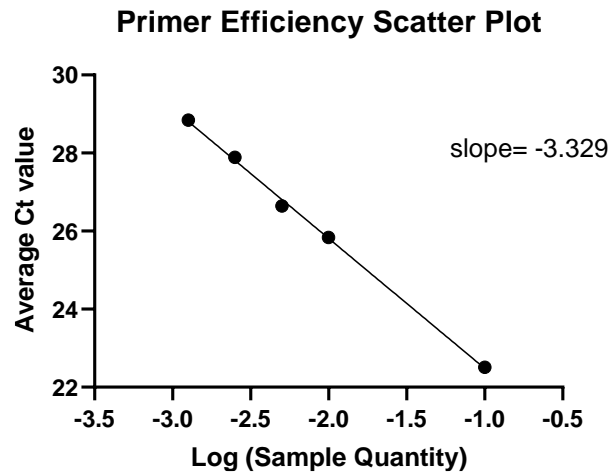


Figure 14. Primer efficiency scatter plot

Average Ct values measured for dilutions of cDNA were plotted against Log (Sample Quantity) to produce a trendline and generate the slope value from the equation $y = m x + c$ (where m is the slope and c the y-intercept).

The slope value was then inputted into the following equation to calculate primer efficiency: $\text{Primer Efficiency (\%)} = (10^{(-1/\text{slope value})} - 1) * 100$

Primer sets which did not fall within 90-110% efficiency at the desired conditions were discarded.

3.4.9 qPCR based investigation of transcriptomic differences between control and *PSEN1* neural cells

Transcriptomic changes in control and AD neural lines were investigated using quantitative polymerase chain reaction (qPCR). qPCR analysis was carried out using the SensiFAST™ SYBR® No-ROX Kit alongside the CFX Connect Real-Time PCR Detection System by Bio-Rad (used as per the manufacturer's instructions).

A master mix was made up for each experiment based on how many wells were required, there was a separate master mix made up for each primer set used. The master mix included forward and reverse primers, SensiFAST™ SYBR® No-ROX and

nuclease free water. 9µl of the master mix was pipetted into each well of a 96 well PCR plate, then 1µl of the required cDNA (diluted 1:10) was added to each well. The composition of each well of a 96 well PCR plate was the same when run on the CFX Connect Real-Time PCR Detection System by Bio-Rad (Table 10. The components of each well of a 96 well PCR plate.). No RT controls were used for every DNA sample to ensure no amplification of undesired products and no template controls (NTCs) were run in triplicate for each primer set (taken from every master mix) to ensure no contaminating DNA was present in the master mix. If contamination was found to be present in the NTC wells, results were discarded, and the experiment repeated. All qPCRs were carried out using the same cycling parameters (Table 11. qPCR cycling parameters) with the same melt curve settings (Table 12. qPCR melt curve settings).

Table 10. The components of each well of a 96 well PCR plate.

Per well (total 10µl)	Volume (µl)
cDNA	1
Forward primer (10µM)	0.3
Reverse primer (10µM)	0.3
SensiFAST™ SYBR® No-ROX	5
Nuclease free water	3.4

All qPCRs were carried out using the following cycling parameters on the CFX Connect Real-Time PCR Detection System by Bio-Rad.

Table 11. qPCR cycling parameters

qPCR Cycling Parameters	Step	Temperature (°C)	Time	Cycles
	Hot start	95	10 minutes	1
	Denaturation	95	15 seconds	39
	Annealing/ Extension	60	1 minute	

Table 12. qPCR melt curve settings

Melt Curve	Temperature (°C)	Time
From 65°C to 95°C in increments of 0.5°C	95	10 seconds
	65	5 seconds
Increment	0.5	

3.4.10 Delta Delta Ct method to calculate fold change gene expression

The Delta-Delta Ct method published by Livak and Schmittgen (2001) was used to calculate fold change gene expression between samples. This method allowed for analysis of *PSEN1* NSC gene expression relative to controls. To begin the Delta-Delta Ct Method, Ct values for technical replicates were averaged, then to calculate delta Ct for the averaged Ct values, the following formula was used:

Delta Ct = Average Ct (gene of interest) – Average Ct (housekeeping gene).

The biological replicates of the control group were averaged to create a 'control Average' and this control Average was used as a calibrator. As all results were calibrated using the control Average, results are presented relative to the control Average Ct values. To calculate Delta-Delta Ct the following formula was used:

$$\text{Delta Delta Ct} = \text{Delta Ct (Sample)} - \text{Delta Ct (control Average)}$$

After calculation of Delta-Delta Ct, fold gene expression values were calculated, using the following formula:

$$\text{Fold gene expression} = 2^{-(\text{Delta Delta Ct})}$$

3.4.11 Statistical analysis of results

All statistical analyses of results were carried out using GraphPad Prism 9.2.0.

Normality tests were used to determine whether data was normally distributed. For parametric data, unpaired students t-tests were used to calculate p-values and determine significance.

For qPCR results, $2^{-\text{Delta-Delta Ct}}$ values were used for statistical analysis.

3.5 Flow cytometry

3.5.1 Analysis of OCT4 expression in *PSEN1* and control iPSC using flow cytometry

Flow cytometry was used to further validate the pluripotency of *PSEN1* and control iPSC. All centrifugation steps took place at 300 x g for 3 minutes. Wash steps involved centrifugation, aspiration of supernatant and re-suspension of the cell pellet in 5ml PBS, before a second centrifugation and re-suspension of the cell pellet in the appropriate solution.

iPSC were picked using a p200 sterile pipette tip and centrifuged. Cell supernatant was removed, and cells were re-suspended in 2ml PBS. For fixation, cells were vortexed whilst 2ml 70% ice cold ethanol was added dropwise, cells were then

incubated on ice for 30 minutes. Post-fixation, cells were washed then re-suspended in 400µl of blocking buffer for 1 hour at room temperature. Blocking buffer consisted of 2% BSA and 0.1% Tween 20 in PBS. After blocking, cells were centrifuged, supernatant was discarded and cells were re-suspended in blocking buffer with 0.5% Anti-hOCT3/4 primary antibody, they were then incubated at 4°C for 17 hours. After incubation with primary antibody, cells were washed and then incubated with the appropriate Alexa Fluor conjugated secondary antibody in the dark for 1 hour at room temperature. Cells were then centrifuged; supernatant was discarded, and cells were re-suspended in BD™ FACSFlow™ Sheath Fluid. Samples were then analysed using the BD FACSVerser™ Flow Cytometer.

3.5.2 Analysis of cell cycle in *PSEN1* and control NSC using flow

cytometry

Propidium iodide (PI) staining was used to investigate cell cycle progression in *PSEN1* and control NSC. Cell cycle analysis was performed to investigate possible reasons for premature neural differentiation in *PSEN1* NSC. Unless specified, all centrifugation steps took place at 300 x g for 5 minutes. Wash steps involved centrifugation, aspiration of supernatant and re-suspension of the cell pellet in 5ml DPBS, before a second centrifugation and re-suspension of the cell pellet in the appropriate solution. DPBS used was azide and protein free. Cells were fixed, washed, stained, and centrifuged in 15ml falcon tubes.

Approximately 1×10^6 NSC harvested per sample at passage 2 (P2) and at passage 3 (P3) from disease and controls. NSC were enzymatically dissociated from the plates using TrypLE™ and centrifuged. Cell supernatant was aspirated off and the cell pellet was re-suspended in 2ml PBS. For fixation, cells were vortexed whilst 2ml of 70% ice cold ethanol was added dropwise, cells were then incubated on ice for 30 minutes. Fixation with 70% ethanol also acts to permeabilise the cells which is necessary here as PI is a nuclear stain. Post-fixation, cells were washed and re-suspended in 0.5ml of PBS. They were then stored for up to 3 weeks at 4°C to enable collection of all

samples at the correct stages for investigation and to allow for simultaneous measurement of all samples. Once all samples had been collected, cells were washed and re-suspended in 200µl of 2% BSA in DPBS (cell staining buffer). To ensure the removal of RNA, 10µl of RNase A was added to each sample, resulting in a final concentration of 0.5ug/ml per sample. After the addition of RNase A, for each sample, 10µl of PI (supplied at 0.02mg/ml) was added to 200µl of cells in cell staining buffer for nuclear staining. Samples were immediately incubated at 37°C for 30 minutes. Post incubation with PI and RNase A, 200µl of each sample was transferred into a flow tube and analysed using the MACSQuant® Analyzer 10 Flow Cytometer.

3.5.3 Analysis of apoptosis and necrosis in *PSEN1* and control NSC using flow cytometry

Apoptosis and Necrosis were investigated in *PSEN1* and control NSC and NPC. Unless specified, all centrifugation steps took place at 300 x g for 5 minutes. Wash steps involved centrifugation, aspiration of supernatant and re-suspension of the cell pellet in 5ml DPBS, before a second centrifugation and re-suspension of the cell pellet in the appropriate solution. DPBS used was azide and protein free. Cells were fixed, washed, stained, and centrifuged in 15ml falcon tubes.

Table 13. Materials used to perform cell cycle analysis of *PSEN1* and control NSC.

Materials	Concentration for use
Bovine Serum Albumin (BSA)	2% in PBS to make cell staining buffer.
Dulbecco's Phosphate Buffered Saline (DPBS) (1X), 9.5 mM PO4 without Calcium or Magnesium, 1 L	As provided.
70% Ethanol	Made up to 70% in water.

eBioscience™ Viability Dye eFluor™ 780	Fixable	1:1000
Apotracker Green		Diluted 1:10 and then 5:100
Nestin Antibody	Monoclonal	1:100
Fixation Buffer (4% PFA)		As provided
Goat (Alexa Fluor® 405)	Anti-Mouse IgG	1:2000

Approximately 1×10^6 NSC were harvested per sample at passage 2 (P2) and at passage 3 (P3) from disease and controls. NSC were enzymatically dissociated from the plates using TrypLE™ and centrifuged. Cell supernatant was aspirated off and the cell pellet was re-suspended in 1ml of PBS, to which $1\mu\text{l}$ of eBioscience™ Fixable Viability Dye eFluor™ 780 was added. Cells were vortexed immediately and then incubated at 5°C in the dark for 30 minutes. After incubation, cells were washed and re-suspended in $100\mu\text{l}$ of cell staining buffer. Separately, Apotracker was diluted 1:10 in cell staining buffer and then $5\mu\text{l}$ of the diluted Apotracker was added to the cells in $100\mu\text{l}$ of cell staining buffer. Cells were incubated with Apotracker for 20 minutes in the dark, then washed. For fixation, cells were resuspended in 0.5ml of fixation buffer and were incubated in the dark at room temperature for 15-20 minutes. Post-fixation, cells were washed and re-suspended in 0.5ml of PBS. They were then stored for up to 2 weeks at 4°C to enable collection of all samples at the correct stages for investigation and to allow for simultaneous measurement of all samples. Once all samples had been collected, cells were washed and re-suspended in $100\mu\text{l}$ of cell staining buffer and incubated for 40 minutes to block. After blocking, $1\mu\text{l}$ of nestin Monoclonal Antibody (MA1-110) was added to each sample containing $100\mu\text{l}$ of cell staining buffer. Cells were incubated with the nestin primary antibody for 1 hour and then washed. Cells were then incubated with the secondary antibody Alexa Fluor 405 Goat Anti-Mouse IgG (diluted 1:2000) for 40 minutes in the dark at room

temperature. Each sample was washed and re-suspended in 200µl of cell staining buffer, which was transferred into a flow tube and analysed using the MACSQuant® Analyzer 10 Flow Cytometer.

3.5.4 Panel design for flow cytometry using the MACSQuant® analyzer 10 flow cytometer

The initial panel designed to carry out analysis of apoptosis and necrosis in AD neural cells involved the use of the secondary antibody Alexa Fluor 647. When the experiment was carried out on control NSC at P2 and P3 using this panel, there was bleed through of the Alexa Fluor Secondary antibody into other channels, meaning that results were unreliable. For this reason, the experiment was carried out from then on using the secondary antibody Alexa Fluor 405, as the use of this secondary did not result in crossover of wavelengths.

Table 14. Initial panel design for investigating apoptosis and necrosis in AD and control NSC.

Laser/Exc Filter	Em Filter	Marker	Colour/Form at	Host/Target	Isotype	Company
640	667/30	nestin	Alexa Fluor 647	Mouse anti-Human	IgG1	Thermofisher
488	615/20	PI	PI	All Species	N/A	Thermofisher
640	785/62	eFluor 780 Fix Viability	eFluor 780 Fix Viability	All Species	N/A	Thermofisher
488	525/50	Apotracker	FITC	All Species	N/A	BioLegend

Table 15. Final panel design for investigating apoptosis and necrosis in AD and control NSC.

Laser/Excitation Filter	Em Filter	Marker	Colour/Form	Host/Target	Isotype	Company
402	421	Nestin	Alexa Fluor 405	Mouse anti-Human	IgG	ThermoFisher
488	615/20	PI	PI	All Species	N/A	ThermoFisher
640	785/62	eFluor 780 Fix Viability	eFluor 780 Fix Viability	All Species	N/A	ThermoFisher
488	525/50	Apotracker	FITC	All Species	N/A	BioLegend

3.5.5 Using the MACSQuant® analyzer 10 flow cytometer

Before running AD and control NSC samples on the MACSQuant® Analyzer 10 Flow Cytometer, experimental settings were adjusted using single stain controls and Fluorescence⁻¹ controls to ensure stains did not bleed through to other channels.

To identify the population of interest, and exclude cellular debris, Forward Scatter (FSC) which is a measure of cell size was plotted against Side Scatter (SSC) which is a measure of cell granularity or complexity. Once identified, the cell population of interest was gated, and these cells were then taken forward to be gated to exclude doublets. For doublet exclusion, SSC-Area was plotted against SSC-Height and cells which did not follow a linear distribution were excluded. Cells which did follow a linear distribution were gated as the single cell population of interest.

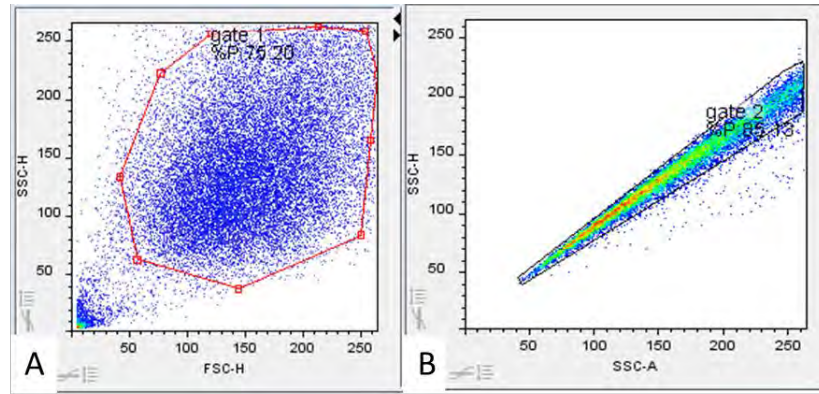


Figure 15. Gating the population of interest in flow cytometry

Initial gating of the population of interest was carried out by plotting FSC-H against SSC-H (A) and then doublets were gated out by plotting SSC-H against SSC-A. Figure 23. Was generated using FlowLogic to enable this gating to be displayed.

Once settings had been adjusted using FMOs, single stains and unstained samples and the population of interest had been gated for, measurements for the protein of interest were taken.

3.5.6 Analysis of flow cytometry results

The program FlowLogic was used to analyse flow cytometry results due to ease of use. For analysis of Apoptosis and Necrosis in NSC and NPC, the population of interest was gated (Figure 15. A) and doublets excluded (Figure 15.B). After this,

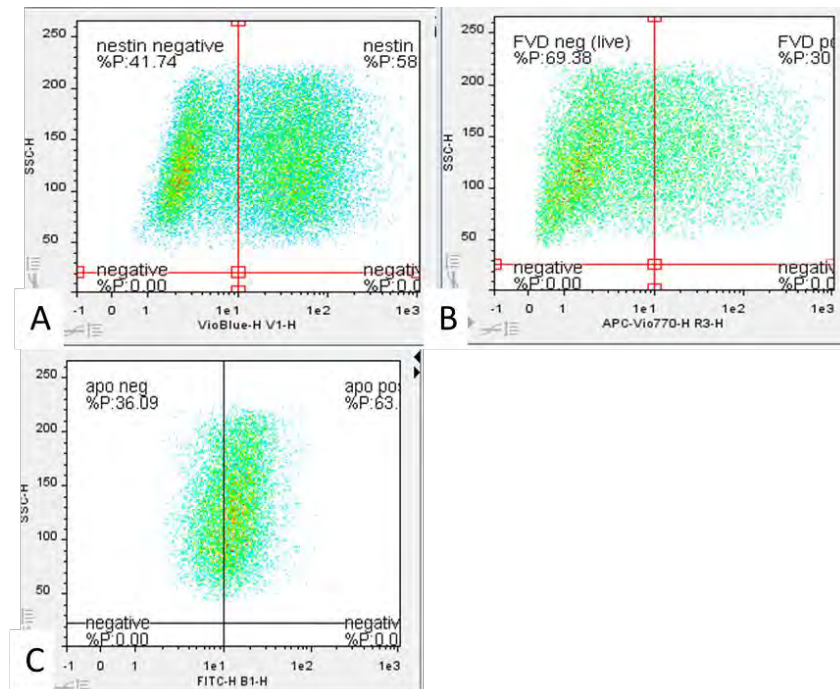


Figure 16. Gating of cells for analysis of apoptosis in flow cytometry

Gating of cells for analysis of apoptosis was carried out by first gating to identify nestin positive cells, SSC-H was plotted against VioBlue-H. Only nestin positive cells were taken forward for investigation of apoptosis and necrosis (A). Looking at only nestin positive cells, cells which were negative for FVD were identified (B). Cells which were positive for FVD were dead so only FVD negative, live cells were selected to be carried forward to the next stages of the experiment. Nestin positive, live cells were then investigated to determine the % of the population which were positive for aptotracker (C).

3.6 Library preparation for RNA sequencing

3.6.1 Isolation of RNA and preparation for RNA seq

RNA extraction was carried out using the Qiagen RNeasy mini kit as described in section 3.4.3. A NanoDrop™ One/OneC Microvolume UV-Vis Spectrophotometer was used after each RNA isolation to determine concentration and sample purity (3.3.4). A Qubit fluorometer was used to quantify RNA samples prior to library preparation and the RQ1 RNase-Free DNase was used to degrade both double-stranded and

single-stranded DNA in all RNA samples to prevent genomic contamination in RNA samples (3.3.5).

3.6.2 Analysis of RNA integrity

The Agilent RNA 6000 Nano Kit was used along with the 2100 Bioanalyzer system by Agilent to determine the integrity of RNA samples. The chip priming station and bioanalyzer were set up ready for use and the RNA ladder was prepared ahead of time by heat denaturing for 2 minutes at 70°C and followed by cooling on ice. Prior to taking any measurements on the Agilent 2100 Bioanalyzer system, electrodes were decontaminated to avoid decomposition of the RNA sample. To do this, wells of the electrode cleaner were filled slowly with 350µl of RNaseZAP. The electrode cleaner was placed in the Agilent 2100 Bioanalyzer, and the lid closed for one minute. The electrode cleaner was removed, and the process repeated with another electrode cleaner. Water on the electrodes was evaporated before carrying out analysis of RNA samples. To prepare the gel for running RNA samples, reagents were equilibrated at room temperature for 30 minutes and then 550µl of Agilent RNA 6000 Nano gel matrix was added into the top receptacle of a spin filter. The spin filter was placed into a microcentrifuge and spun for 10 minutes at 1500 g. After filtering, 65 µl of gel was aliquoted into 0.5 ml RNase- free microfuge tubes. Aliquots were stored at 4 °C and used within one month of preparation. Before preparation of the gel-dye mix, reagents were allowed to equilibrate to room temperature for 30 minutes. RNA 6000 Nano dye concentrate was vortexed for 10 seconds and then spun down, then 1µl was added to 65 µl of filtered gel. The tube containing filtered gel and 1µl of RNA 6000 Nano dye was vortexed to mix the gel and dye, after which the gel-dye mix was centrifuged for 10 minutes at 13000 g. The gel-dye mix was stored at 4°C in the dark for a maximum of one day.

For running samples on the Agilent 2100 Bioanalyzer, the gel-dye mix was equilibrated to room temperature for 30 minutes and then 9µl of the mix was pipetted into the chip, into the bottom of the well-marked G. The syringe was used

to disperse the gel-dye mix throughout the chip and then 9µl of gel-dye mix was added to two more wells. After loading of the gel-dye mix, 5µl of the RNA 6000 Nano Marker was added to each sample well and the ladder well. 1µl of RNA ladder was pipetted into the ladder well and 1µl of each sample was pipetted into each sample well. After addition of the RNA 6000 Nano Marker, the RNA ladder, and all samples, the chip was vortexed for 60 seconds at 2400 rpm and then inserted into the Agilent 2100 Bioanalyzer to start the chip run and to generate results. Successful ladder runs produced one marker peak, five ladder peaks, with correct peak size assignments and good resolution of all peaks. Features of a successful total RNA run included one marker peak and two ribosomal peaks. Values were calculated for RNA concentration, the ribosomal ratio, and the RNA Integrity Number (RIN).

3.6.3 Library preparation using the TruSeq stranded mRNA

The Illumina TruSeq Stranded Total RNA protocol was used for generation of a cDNA library for RNA Sequencing. 500ng of total RNA was inputted per sample. The first step in library preparation was purification and fragmentation of mRNA.

3.6.3.1 Purification of mRNA

Total RNA was diluted in nuclease-free ultrapure water to a final volume of 50µl in each well of a 96-well PCR plate. RNA purification beads (RPB) were vortexed and 50µl of this solution was added to each sample to bind mRNA in the total RNA sample, the solution of beads and RNA was mixed six times. The plate was then placed on a thermal cycler and the mRNA Denaturation program was run (Table 16. mRNA denaturation program).

Table 16. mRNA denaturation program

Temperature (°C)	Time (Minutes)
Preheat lid to 100°C	Throughout
65	5
4	Hold

After running the mRNA Denaturation program, the 96 well plate containing RPB, and diluted RNA was incubated on the bench for five minutes and then centrifuged for one minute at 280 x g. The plate was then placed on a magnetic stand for five minutes to enable the magnetic RPB to move towards one side of the well. Once the RPB in each well had moved towards the closest magnet, the remaining supernatant could be aspirated from each well. The magnetic stand was removed and 200µl of bead washing buffer (BWB) was added to each well, the solution was mixed six times to wash the RPB and bound mRNA. After washing, the plate was placed on a magnetic stand and left for five minutes for the magnetic beads to move towards the closest magnet, which resulted in a clear liquid. At this point, all supernatant was discarded from each well, the magnetic stand was removed and 50 µl of elution buffer (ELB) was added to each well and mixed six times. The plate was centrifuged at 280 g for one minute and then incubated by running the mRNA Elution 1 program on the thermal cycler (Table 17).

Table 17. mRNA elution 1 program

Temperature (°C)	Time (Minutes)
Preheat lid to 100°C	Throughout
80	2
25	Hold

3.6.3.2 Fragmentation of mRNA

After running the mRNA Elution 1 program on the thermal cycler, 50µl of bead binding buffer (BBB) was added to each well and mixed thoroughly. The plate was placed on the thermal cycler and the mRNA denaturation program was run again after which the plate was incubated at room temperature for 5 minutes. After the samples had equilibrated to room temperature, the plate was placed on a magnetic plate and given five minutes for the liquid to clear. All supernatant was discarded from each well and the magnetic plate was removed. 200µl of BWB was added to

each well and pipetted up and down six times. The 96 well sample plate was then placed on a magnetic stand, the solution was allowed to clear, and supernatant was removed. At this point, 19.5µl of Fragment, Prime, Finish Mix (FPF) was added to each well and mixed thoroughly before the plate was centrifuged at 280 x g for one minute. After centrifugation, the plate was transferred to the thermal cycler and the Elution-2 – Frag – Prime program was run (Table 18) after which the plate was centrifuged again at 280 x g for one minute.

Table 18. Elution-2-frag-prime program

Temperature (°C)	Time (Minutes)
Preheat lid to 100°C	Throughout
94	8
4	Hold

3.6.3.3 Synthesis of first strand cDNA

The previous step produced cleaved RNA fragments primed with random hexamers. In this step, these RNA fragments were reverse transcribed to produce first strand cDNA. Actinomycin D was added to the First Strand Synthesis Act D Mix (FSA) to improve strand specificity via the prevention of DNA dependent synthesis meanwhile still allowing RNA- dependent synthesis.

Table 19. Synthesise first strand program

Temperature (°C)	Time (Minutes)
Preheat lid to 100°C	Throughout
25	10
42	15
70	15
4	Hold

After the fragmentation stages described in section **3.6.3.2**, the 96-well plate now containing purified and fragmented mRNA was placed on a magnetic stand and allowed to clear. 17µl of supernatant was transferred from each sample to a fresh 96 well-plate. FSA and SuperScript II (SS II) were mixed in the ration 1:9 and then 8µl of this mixture was added to each sample in the fresh 96-well plate. The FSA-SS II mixture was pipetted six times to mix it in with the purified, fragmented RNA samples and then the 96-well plate was centrifuged at 280 x g for one minute. At this point, the plate containing mRNA samples and FSA-SS II was run on the thermal cycler using the Synthesise First Strand Program (Table 19. Synthesise first strand program).

3.6.3.4 Synthesis of second strand cDNA

After synthesis of first strand cDNA, the RNA template was removed, and a replacement second strand of cDNA was synthesised. During generation of the second strand of cDNA, dUTP is incorporated in place of dTTP to generate ds cDNA. Incorporating dUTP leads to the second strand being quenched during amplification.

The end repair control (CTE) was diluted 1:50 in resuspension buffer and then 5µl of this was added to each sample containing well. 20µl of second strand marking master mix (SMM) was added to each well and mixed thoroughly before the plate was centrifuged at 280 x g for one minute. The plate was then placed on the thermal cycler and incubated for one hour at 16°C.

3.6.3.5 Purification of cDNA

After synthesis of the second strand of cDNA, 90µl of AMPure XP beads were added to each well of the 96-well plate containing cDNA samples. Each well was mixed thoroughly and then the plate was incubated for 15 minutes at room temperature. After incubation, the plate was centrifuged at 280 x g for one minute and then placed on a magnetic stand until the liquid cleared. After the liquid was clear, 135µl of supernatant was removed from each well. Each well was washed twice by adding 200µl of fresh 90% EtOH, incubating on a magnetic stand for 30 seconds and then

removing all supernatant from each well. After two wash steps in 90% ETOH, the beads were air-dried on the magnetic stand for 15 minutes, at which point the magnetic stand was removed and 17.5µl of RSB was added to each well and mixed thoroughly. Samples in RSB were incubated at room temperature for two minutes, after which they were centrifuged and placed on a magnetic stand until the liquid cleared. When all magnetic beads had collected by their closest magnet on the plate, 15µl of supernatant was taken from each sample and transferred to a fresh 96-well plate.

3.6.3.6 Adenylation of 3' ends

An adenine nucleotide was added to the 3' end of each blunt fragment to prevent ligation to one another. A corresponding Thymine nucleotide was added on the 3' end of the adapter to provide a complementary overhang for ligation of adapter to fragment.

The A-Tailing control (CTA) was diluted 1:100 in RSB and then 2.5µl of diluted CTA was added to each sample containing well in the fresh 96-well plate. After addition of CTA to each well, 12.5µl of A-Tailing Mix (ATL) was added to each well and mixed thoroughly. The plate was then centrifuged and incubated using the ATAIL70 program on the thermal cycler (Table 20. ATAIL70 program) after which it was centrifuged for one minute at 280 x g.

Table 20. ATAIL70 program

Temperature (°C)	Time (Minutes)
Preheat lid to 100°C	Throughout
37	30
70	5
4	Hold

3.6.3.7 Ligation of adapters

The ligation of indexing adapters to the ends of double stranded fragments of cDNA prepares them for hybridisation to a flow cell. The ligation control (CTL) was diluted 1:100 in RSB, after which 2.5µl of diluted CTL, 2.5µl of ligation mix (LIG) and 2.5µl of RNA adapters were added to each well containing sample. The mixture was pipetted thoroughly, and the 96-well plate was centrifuged at 280 x g for one minute. At this point, the plate was placed on the thermal cycler and the LIG program was run (Table 21. LIG program). After samples were ligated with adaptors, 5µl of Stop ligation buffer (STL) was added to each well and mixed thoroughly, then the plate was centrifuged.

Table 21. LIG program

Temperature (°C)	Time (Minutes)
Preheat lid to 100°C	Throughout
30	10
4	Hold

3.6.3.8 Clean up of ligated fragments

After ligation of adapters to fragments, AMPure XP beads were used for clean-up of ligated fragments. To initiate the clean-up, 42µl of AMPure XP beads were added to each well containing sample, the AMPure XP beads were allowed to incubate for 15 minutes to enable binding to the cDNA sample, after which the plate was centrifuged at 280 x g for one minute. The 96-well plate containing samples was then placed onto a magnetic stand and liquid was allowed to clear. The supernatant was discarded from each well and two wash steps were performed on the bead bound DNA. Each wash step involved the addition of 200µl of fresh ETOH to each well, without removal of the plate from the magnetic stand, the sample was allowed to incubate in the fresh ETOH for 30 seconds, after which all supernatant was removed from each well. This wash step was repeated once more for each sample after which samples were left to air-dry on the magnetic stand for 15 minutes. After samples had air-dried to ensure

no carry-over of ETOH, the magnetic stand was removed and 52.5µl of RSB was added to each well and mixed thoroughly. The samples were incubated for 2 minutes at room temperature in RSB and then the plate was centrifuged for 1 minute at 280 x g. After centrifugation, the plate was placed on the magnetic stand until liquid cleared, at which point 50µl of supernatant was transferred from each sample to a fresh 96-well PCR plate. In the fresh PCR plate, the clean-up procedure described (adding AMPure XP beads, removing supernatant, washing with ETOH, air-drying, and then resuspending samples in resuspension buffer) was repeated but with 50µl of AMPure XP beads being added in the first step instead of 42µl and later, 22.5µl of RSB being added for resuspension of samples instead of the original 52.5µl. After the final resuspension of samples in 22.5µl of RSB, 20µl of supernatant (containing sample) was transferred to a fresh 96-well PCR plate.

3.6.3.9 Enrichment of DNA fragments

After clean-up of ligated fragments, DNA fragments which have adapters ligated to both ends were selectively enriched using PCR. The purpose of this was to amplify the quantity of DNA in the library. For selective enrichment of ligated fragments, PCR was performed using the PCR Primer Cocktail (PPC) which selectively anneals to the ends of adapters.

To begin this process, the PCR plate containing DNA samples ligated to adapters was placed on ice. 5µl of PPC was added to each well and then 25µl of PCR master mix (PMM) was added to each well, after which the mixture was mixed thoroughly. The plate was centrifuged and then placed on the thermal cycler to run the mRNA PCR program (Table 22).

Table 22. mRNA PCR program

Temperature (°C)	Time
Preheat lid to 100°C	Throughout

98	30 Seconds	15 Cycles
98	10 Seconds	
60	30 Seconds	
72	30 Seconds	
72	5 minutes	
4	Hold	

3.6.3.10 Clean-up of amplified DNA

After enrichment using the mRNA PCR program, the PCR plate was centrifuged. To begin the clean-up of amplified DNA, 50µl of AMPure XP beads were added to each well, the mixture pipetted up and down 10 times, then incubated at room temperature for 15 minutes. The plate was centrifuged and placed on a magnetic stand until the liquid cleared, at which point all supernatant was removed from each well. A wash step was carried out as follows: 200µl of fresh ETOH was added to each well, the plate was incubated on the magnetic stand for 30 seconds and then all supernatant was removed from each well. The wash step was repeated and then samples were air-dried on the magnetic stand for 15 minutes. After air-drying, the plate was removed from the magnetic stand and 32.5µl of RSB was added to each well and mixed thoroughly. Samples were incubated in RSB for 2 minutes at room temperature and then centrifuged, after which they were placed on a magnetic stand until the liquid cleared, at which point, 30µl of supernatant was transferred from each sample to a fresh PCR plate. Samples at this point were ready for running on the Illumina NextSeq and were stored at -25°C.

3.6.4 Analysis of library quality

Upon completion of Library Preparation, the 2100 Bioanalyzer system by Agilent was used to check library quality, which involved checking the fragment sizes within the sample as well as sample purity. Sample fragment sizes were expected to fall within the range of 200-500bp with the majority of fragment sizes being around 260 bp in

size. The DNA 1000 kit by Agilent was used to analyse sample quality post library preparation.

The Bioanalyzer and Chip priming station were set up as recommended and the gel-dye mix was prepared. To prepare the gel-dye mix, the DNA dye concentrate, and DNA gel matrix were allowed to equilibrate to room temperature. The DNA dye-concentrate was vortexed and then centrifuged, after which, 25 μ l of Dye concentrate was added to a vial of DNA gel matrix. The mixture was vortexed to ensure complete mixing of the gel and dye, then the gel-dye mix was transferred to the top receptacle of a spin filter, the spin filter was centrifuged at room temperature at 2240 x g and then discarded. The gel-dye mix was stored at 4°C in the dark until 30 minutes before use when it was equilibrated for 30 minutes at room temperature. To begin analysis of samples using the DNA 1000 kit, 9 μ l of the gel-dye mix was added to the well-marked G and a syringe used to disperse the mix to the rest of the wells of the chip, after which 9 μ l of gel-dye mix was added to the remaining wells marked G. 5 μ l of DNA marker was pipetted into the well-marked with a ladder symbol and into the 12 sample wells. 1 μ l of ladder was added into the ladder well and 1 μ l of each undiluted sample was added to each sample well. If any wells remained without sample, 1 μ l of deionised water was added to the well. After ladder, DNA marker and all samples had been loaded to the chip, the chip was placed on an IKA vortex mixer and vortexed for 60 seconds at 2400 rpm. After vortexing the chip was inserted onto the Bioanalyzer to read results. Successful running of the chip resulted in the visualisation of both lower and upper markers in each sample. Features of a successful ladder run involved 13 peaks for the DNA 1000 ladder and all peaks well resolved with a flat baseline. Features of a successful DNA 1000 sample run included all sample peaks appearing between the lower and upper marker peaks, a flat baseline, baseline readings of at least 5 fluorescent units, marker readings at least 3 fluorescence units higher than baseline readings and both marker peaks well resolved from sample peaks.

3.6.5 Library quantification

JetSeq qPCR was used for quantification of DNA libraries prior to RNA Sequencing. JetSeq qPCR enables quantification of only adapter-ligated library molecules, allowing for optimal flow cell loading to maximise quality and yield of data. The JetSeq qPCR kit contains a series of 6 pre-diluted DNA standards ranging from 10pM to 100aM for standard curve development (Table 23. DNA standards for JetSeq qPCR). The DNA standards consist of a 342bp linear fragment of DNA flanked by stabilising DNA.

Table 23. DNA standards for JetSeq qPCR

DNA standards (342 bp fragments)	Concentration
1	10 pM
2	1 pM
3	100 fM
4	10 fM
5	1 fM
6	100 aM

NTCs were included in this assay to detect for contamination during reaction set-up. NTC reactions gave Ct values at least 3.5 cycles later than the average Ct value for standard 6. Every sample in the library was diluted 1:10,000 using the JetSeq Dilution Buffer. Additional dilutions of 1:100,000 and 1:1,000,000 were utilised for each sample to ensure at least one dilution fell within the dynamic range of the standard curve generated. A qPCR master mix was prepared to give a total volume of 20µl per reaction (Table 24. qPCR).

Table 24. qPCR reagents per reaction

Reagent	Volume (µl)
---------	-------------

2x JetSeq Library Quantification Lo-ROX Mix	10
Primer Mix	5
Diluted library or DNA standard (1-6)	5
Total volume per reaction	20

Table 25. Primer sequences for JetSeq qPCR

Forward	5'-AAT GAT ACG GCG ACC ACC GA-3'
Reverse	5'-CAA GCA GAA GAC GGC ATA CGA-3'

Every sample in the library was run in triplicate at each dilution. Samples were run on a thermal cycler using the parameters displayed below (Table 26).

Table 26. JetSeq qPCR cycling parameters

Cycles	Temperature (°C)	Time	Stage
1	95	2 minutes	Activation of DNA polymerase
35	95	5 seconds	Denaturation
	60	45 seconds	Annealing/Extension
Melt Curve -Acquiring in Green			

3.6.5.1 Standard curve and analysis of results

For analysis of JetSeq qPCR results, a standard curve was generated. Concentration values of the different standard dilutions were correlated against their Ct values (averaged from three technical repeats). Log concentration was plotted against

average Ct value for each standard and the standard curve generated was used to calculate reaction efficiency.

$$\text{Efficiency (\%)} = (10^{-1/a} - 1) \times 100$$

Where a is the slope value of the standard curve. The reaction efficiency fell between 90-110%

Library concentration was calculated using the standard curve generated from the standards. The following equation was used to quantify RNA sequencing libraries:

$$\text{Library Concentration (pM)} = 10^{((Ct-b)/a)} \times (342/\text{average fragment length}) \times \text{dilution factor}$$

Where a = the standard curve slope and b = the y-intercept

A Qubit fluorometer was also used to confirm the quantities measured using JetSeq qPCR.

3.6.6 Normalisation and pooling of libraries for RNA sequencing

DNA templates were prepared for cluster generation. Indexed DNA libraries prepared and stored in the 96-well plate at -25 were thawed on ice and normalised directly before sequencing. Libraries were stored as individual samples up until this point to minimise index hopping. DNA libraries were normalised to 10nM and then pooled together. To begin normalisation of libraries, 10µl of each indexed DNA sample was transferred to a fresh PCR plate. The library concentration was normalised via addition of 10mM of Tris-HCl at pH 8.5 with 0.1% Tween 20, which was made up to 10nM. The sample was mixed thoroughly with Tris-HCl and 0.1% Tween 20 and then the plate was centrifuged at 280 x g for 1 minute. To pool libraries, 10µl of each normalised library was transferred to a single well of a fresh PCR plate. The pooled libraries were pipetted 10 times to mix the library and then the plate was centrifuged at 280 x g for 1 minute.

3.6.7 Cluster generation and RNA sequencing mid output

After pooling of the library, libraries were denatured and diluted to 1.3ml at a concentration of 1.8pM. The sequencing experiment was set up on the BaseSpace sequencing software hub, the flow cell was prepared, and libraries were loaded onto the reagent cartridge. 1.3ml of prepared 1.8pM library was pipetted into reservoir #10. After loading of samples, the flow cell was run on the Illumina NextSeq 500 RNA Sequencing System for cluster generation and sequencing of reads. Clusters are generated when single DNA molecules bind to the surface of the flow cell, these are then amplified to form clusters. Imaging of clusters takes place using two-channel sequencing chemistry and filter combinations that are specific to each of the chain terminators which are fluorescently labelled. Each tile of the flow cell is imaged individually, and imaging of each tile is carried out for each sequencing round. Post image analysis, the BaseSpace software performed base calling, filtering, and quality scoring of the overall sequencing run. For generation of RNA sequencing data, a paired-end run was carried out to a length of 2 x 76 bp.

3.7 Processing and quality control of initial RNA sequencing data

3.7.1 Merging Read 1 and Read 2 Fastq files

For each sample run, there were four sets of Fastq results generated, these four results were for Lane 1, Lane 2, Lane 3, and Lane 4. For each lane, there were two Fastq files generated: read 1- the forward read and read 2 -the reverse read.

Fastq files were merged using the tool Concatenate Data Sets through Galaxy. Read 1 samples for lanes 1, 2, 3, 4 were merged in that order and read 2 samples for lanes 1, 2, 3, 4 were merged in that order using concatenate data sets tail to head (galaxy version 1.0) to produce a merged R1 and merged R2 file for each sample.

3.7.2 Assessment of sequence quality

Sequencing problems often occur in RNA sequencing data, and include low sequencing quality of raw reads, contamination from other species, residual

degradation and varied read coverage. Sequence quality was assessed using the tools FastQC and MultiQC, accessed via the Galaxy website. Each sample file contains the 75bp of sequenced read, a sequence ID, and a quality score. The quality score or Q score is represented as an ASCII character to save data (10.2.2.1 Table 33. ASCII character quality score). Tools like FastQC and MultiQC are able to interpret the ASCII symbols to present a quality score for the calling of each base. FastQC and MultiQC assessed the quality of base calling, so assessed the probability that an incorrect base had been called.

Equation to calculate Phred quality score:

Phred quality score $Q = -10 \cdot \log_{10}(p)$

$Q = -10 \cdot \log_{10}(0.0001)$

$Q = 40$

A Q score of 40 means that there is a 1:10,000 chance the reading is incorrect. This gives a probability value (p) of 0.0001.

Through the galaxy website, FastQC was used to check the quality of base calling-probability of incorrect base being called. The QC results for all merged R1/R2 files were combined using MultiQC. Both Fast QC and MultiQC provide the following modules: Per Base Sequence Quality, Per Base Sequence Content, Adapter Content, Overrepresented Sequences, Per Sequence Quality Scores, Sequence Length Distribution, Sequence Duplication Levels, Per Sequence GC Content, Per Base N Content and Per Tile Sequence Quality. The modules displayed by FastQC and MultiQC provide information on the quality of reads and give information on trimming and filtering required to ensure that analysis is carried out using only high quality sequencing data. FastQC incorporates the Picard-tools libraries for SAM/BAM processing. The contaminants file parameter was borrowed from the independently developed FastQC wrapper contributed to the Galaxy Community Tool Shed by J. Johnson. Adaption to version 0.11.2 by T. McGowan.

Short read data was inputted to FastQC with no contaminant list used, samples were analysed both with and without a list of all Illumina adaptor sequences. No submodule and limit specifying file was used and grouping of bases for reads >50bp was enabled. There was no lower limit set on the length of the sequence to be shown in the report. The Kmer test was disabled. Samples were analysed to determine their per base sequencing quality. Per base sequence quality displays the average quality score (taken across all reads in that sample) for every position in the read (total 75 bp). Bases with a Q score of higher than 28 were considered to be good quality, meaning that there is a very good chance that bases in that position have been called correctly and a very low chance that the reading is incorrect. Bases with a Q score of lower than 20 are considered to be poor quality, as the probability of incorrect base calling is higher. Samples were analysed to determine their overall per base sequence content. This module displays the percentage of each nucleotide base at every position in the read. Due to the high volume of fragments sequenced per sample, equal representation of each base is expected at each position in the read. Samples were analysed for adaptor content. This module gives information on the percentage of adaptor sequence that is found in the sample. If the percentage of adaptor was high in a sample, specific adaptor sequences were filtered out. All samples were analysed for the presence of overrepresented sequences. A sequence is considered overrepresented if it accounts for >0.1% of reads. This module can be triggered when used to analyse small RNA libraries where sequences are not subjected to random fragmentation, and the same sequence may naturally be present in a significant proportion of the library. Overrepresented sequences were removed from samples. Samples were analysed for their per sequence quality scores. This module looks at the quality score distribution across all samples and gives an average quality per read. All samples were analysed for their sequence length distribution. This module gives information on the distribution of sequence lengths over all sequences. Sequence lengths that were too long were trimmed and sequence

lengths that are too short were filtered out. Samples were analysed for their levels of sequence duplication; this module displays the percent of sequences that would remain if duplicated samples were removed. De-duplication of sequences can be used to remove technical duplication, but would also remove biological duplication, when working with RNA sequencing data, removing biological duplication would mean enriched genes would be missed. For this reason, samples were not de-duplicated. All samples were analysed for their per sequence GC content. A normal random library roughly displays normal distribution of GC content where central peak corresponds to the overall GC content of the underlying genome. GC content is calculated from observed data and used to build a reference distribution, spikes outward from the bell curve indicate contamination. Samples were analysed for their per base N content. An N is subbed in when a base call cannot be made with confidence. All samples were analysed for their per tile sequence quality. Warm colours indicate a tile had a worse qualities than other tiles for that base. Causes of poor tile sequence quality include bubbles or debris in the flow cell lane, widespread poor tile quality is indicative of an overloaded flow cell.

3.7.3 Trimming and filtering RNA sequencing data

The Trimmomatic Galaxy tool was developed within the Bioinformatics Core Facility at the University of Manchester, with contributions from Peter van Heusden, Marius van den Beek, Jelle Scholtalbers, Charles Girardot, and Matthias Bernt. It runs the Trimmomatic program which has been developed within Bjorn Usadel's group at RWTH Aachen university (Bolger *et al.*, 2014).

Trimmomatic was used to remove poor quality reads, poor quality sequences and contaminants from RNA sequencing data samples. The RNA sequencing experiment generated paired end reads. The merged read 1 files were inputted with their matching merged read 2 files and an initial ILLUMINACLIP step was performed. Custom adaptor sequences were provided in fasta format. For quality-based trimming, the Trimmomatic operation performed was SLIDINGWINDOW 4:20. The

operation MINLEN ensured filtering out of all sequences with a length lower than 25 bp (Appendix 3. Table 36. Example Trimmomatic settings for merged Fastq files).

3.7.4 Infer experiment on BAM file

The Infer Experiment tool (Wang *et al.*, 2012) was used to determine whether paired end data is forward or reverse stranded (Appendix 3. Table 37. Infer experiment parameters).

3.7.5 Alignment to a reference genome

Hierarchical indexing for spliced alignment of transcripts (HISAT) is a highly efficient system for aligning RNA sequencing reads to a reference genome (Kim *et al.*, 2015, Musich *et al.*, 2021). Post trimming and filtering, HISAT2 was used to align merged Read 1 and merged Read 2 files to the reference genome Hg38 (Appendix 3. Table 38. Example parameters for alignment to reference genome using HISAT2). Sequences aligned to Hg38 using HISAT2 were analysed for % alignment and alignment quality.

3.7.6 Assessment of alignment quality

The tool HISAT2 was used to analyse % alignment of samples to the reference genome (Figure 104). BAM/SAM mapping stats and SAMtools flagstat were tools used to check the mapping statistics of reads, giving data on alignment such as total reads, unique mapped reads, splice mapped reads, reads mapped in a proper pair, and QC failed reads. The tool Picard: MarkDuplicates, was used to determine % duplication in samples (Appendix 3. Figure 105). The tool SAMtools idxstats was used to determine the number of mapped reads per chromosome (Appendix 3. Figure 106). Figure 106. Number of mapped reads per contig and to check the number of reads which mapped to X and Y chromosomes (Appendix 3. Figure 107). The tool MultiQC was used to combine all alignment data for each sample for visualisation. The tool RSeQC was used to look at Gene Body Coverage to determine whether read coverage is uniform along transcripts, RSeQC was also used to investigate PKM Saturation to check read distribution between different genomic features (Appendix 3. Figure 108).

Percentage reads assigned to the reference genome was analysed (Figure 109). Alignment quality was assessed before and after filtering using each of the tools described.

3.7.7 Filtering of aligned sequences

Post alignment of sequences to the reference genome Hg38, aligned BAM files were filtered to leave only reads which are paired, mapped in a proper pair, and have mapping quality above 20 on the Phred scale. The tool used was Filter BAM datasets on a variety of attributes (Galaxy Version 2.4.1), (Barnett *et al.*, 2011), (Appendix 3. Table 39). Filtering of reads aligned to Hg38 removed data such as reads mapping to the Y-chromosome and improved quality of data, without greatly reducing number of reads. Therefore, all aligned BAM files were filtered for quality of alignment.

3.7.8 Generation of read counts

After aligning genes to the reference genome (Hg38) and quality based filtering, the number of reads mapping to each gene were counted. The tool FeatureCounts uses BAM files as input and outputs the number of reads (counts) associated with (mapping to) each feature of interest (genes, exons, transcripts etc.) (Liao *et al.*, 2014). FeatureCounts was used (Galaxy Version 2.0.1+galaxy2) to generate read counts for all samples (Appendix 3. Table 41).

3.7.9 Differential gene expression analysis

DESeq2 uses the read counts files from the feature counts results and determines differentially expressed features from the count tables. DESeq2 (Galaxy Version 2.11.40.7+galaxy1) was used to identify differentially expressed genes (DEGs) between disease and control samples (Appendix 3. Table 43) Disease/ control and passage number (2 or 3) were specified as the two different factor levels. Multiple count tables were needed to determine differentially expressed genes between samples. DESeq2 applies normalisation for sequencing depth and library composition. Gene length normalization does not need to be accounted for because

counts are compared between sample groups for the same gene. DESeq2 can estimate biological variance using replicates for each condition and can estimate significance of expression differences between any two conditions (Love et al. 2014). DESeq2 performs QC on results and filters out genes which have little or no chance of being detected as differentially expressed, this increases the power to detect DEGs. Genes which are filtered out include: genes which have no counts in any sample, genes with low mean normalised counts and genes which have an extreme outlier. DESeq2 performs independent filtering, using the mean of normalised counts as the statistic to filter by. To determine the gene-wise dispersion, DESeq2 uses a measure of dispersion (α) related to the mean (μ) and variance of the data: $\text{Var} = \mu + \alpha * \mu^2$. Dispersion plots display the spread or variability in the RNA sequencing data set. Genes which have moderate to high count value will have a square root of dispersion that is equal to the coefficient of variation, meaning that a dispersion value of 0.01 for a set of biological replicates is equivalent to 10% variation around the expected mean. Post initial analysis and QC of DESeq2 results, DESeq2 data was filtered for significance ($p < 0.05$) and for fold change > 1 .

3.7.10 Analysis of RNA sequencing data

The tool Volcano Plot was used (Galaxy Version 0.0.5) to create a volcano plot displaying Differential gene expression values which were up and downregulated between samples (Appendix 3. Table 44). For pathway analysis, significant ($p < 0.05$) DEGs were isolated and analysed using the tools Gene Ontology/Panther and Reactome (Appendix 3. Table 45 Table 45. Parameters for GO). For all results, the False discovery rate (FDR) was calculated to reduce the possibility of a type 1 error and reduce the number of false positive results. FDR p-value is indicated for all results. For significance, an FDR cut off of $p < 0.05$ was employed.

4.0 Development of a relevant model for investigation of AD

4.1.0 Introduction

4.1.1 Derivation of stem cells

Human embryonic stem cell (ESC) lines are obtained from human in vitro fertilisation (IVF) embryos that cannot be used for infertility treatment. These cells are established and expanded in vitro for use in research or as a cell source for regenerative medicine (Figure 17) (Damdimopoulou *et al.*, 2016). During both embryonic development and in vitro differentiation, pluripotent stem cells are capable of differentiating down different somatic lineages, progressing through a progenitor state to mature and specify. Somatic cells are also capable of undergoing trans-differentiation to become another differentiated state and de-differentiation via reprogramming to revert back to a pluripotent state (Figure 17.) (Ohnuki and Takahashi., 2015).

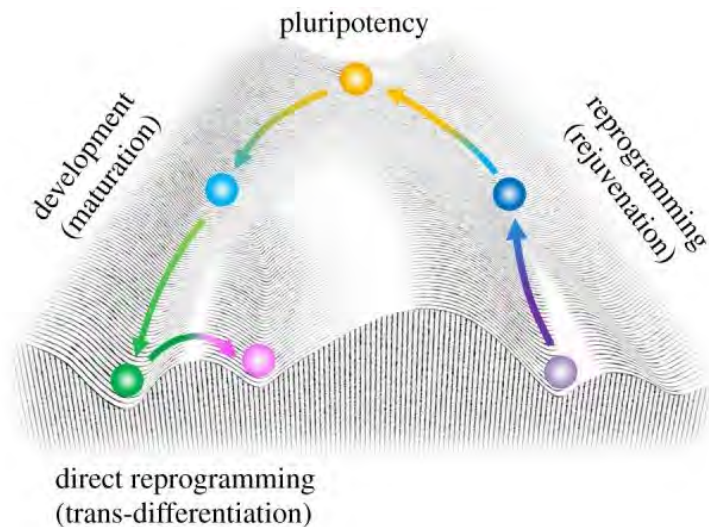


Figure 17. Waddington's epigenetic landscape modified to show trans-differentiation and de-differentiation by reprogramming.

Pluripotent stem cells (yellow) are capable of differentiating down somatic lineages (green) which are capable of becoming another differentiated state (pink) via trans-differentiation. The purple circle displays somatic cells undergoing reprogramming to become a pluripotent stem cell (Ohnuki and Takahashi., 2015, Waddington., 1958).

Induced pluripotent stem cells (iPSC) are a cell type which are phenotypically identical to ESC. Based on techniques pioneered by Takahashi *et al.*, (2007), iPSC reprogramming involves transduction of somatic cells with pluripotency factors such as OCT3/4, SOX2, KLF4, C/L-Myc and LIN28 to induce de-differentiation into pluripotent stem cells capable of near unlimited cellular division and differentiation potential (Figure 18). Reprogramming plasmids used in this project were selected based on work carried out by Takahashi and Yamanaka (2006) and Takahashi *et al.*, (2007), in which 24 pluripotency factors- factors expressed by stem cells- were selected and collectively overexpressed in mouse embryonic fibroblasts (MEFs). Expression of these factors in somatic cells resulted in the generation of iPSC colonies. After the generation of iPSC colonies using all 24 factors, individual factors were withdrawn to determine those which were necessary for iPSC colony formation. Their data indicated that OCT3/4, KLF4, SOX2, and C-Myc were critical for generation of iPSC colonies from MEFs (Takahashi and Yamanaka., 2006).

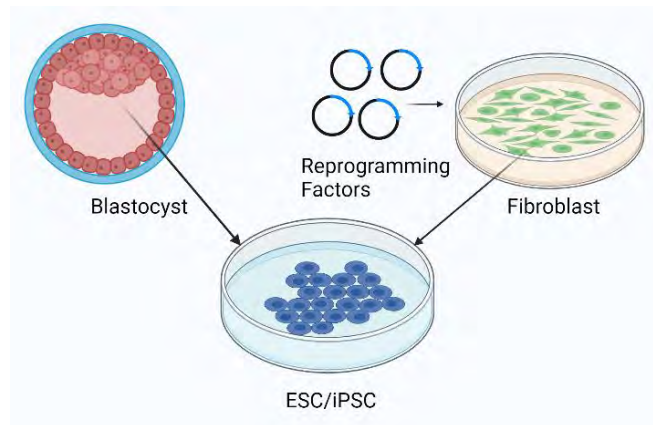


Figure 18. Derivation of stem cells

ESC can be derived from the blastula and cultured *in vitro*. iPSC can be generated via addition of reprogramming factors to an adult somatic cell (Chen *et al.*, 2017).

During this project, patient somatic cells containing mutations in *PSEN1* and patient somatic cells containing the APOE4 allelic variant were reprogrammed to iPSC for patient specific disease modelling of AD. The purpose of generating iPSC for disease modelling was to create a cell based model of neurogenesis, to model AHN in AD (1.4 Aims). For reprogramming of patient and AD somatic cells, and EBNA based integration-free (episomal) system was used. Somatic cells were nucleofected with a combination of four plasmids: pCXWB-EBNA1, pCXLE-hSK, pCXLE-hUL and pCXLE-hOCT3/4-shp53-F (Okita *et al.*, 2011). Cells were nucleofected with plasmid pCXWB-EBNA1 (Figure 95.) for episomal expression of EBNA1, which enhances transfection efficiency and expression of episomal plasmids. Cells were nucleofected with the plasmid pCXLE-hUL (Figure 97.) for episomal expression of human L-MYC and LIN28. Cells were nucleofected with the plasmid construct pCXLE-hSK (Figure 96.) for episomal expression of human SOX2 and KLF4. The plasmid pCXLE-hOCT3/4-shp53-F (Figure 98.) was included in the EBNA based episomal system for expression of human OCT3/4 and shRNA against p53. control and AD iPSC produced were

expanded to generate stocks of iPSC containing mutations in *PSEN1*, stocks of iPSC containing the APOE4 variant and stocks of control iPSC.

4.1.2 2D and 3D disease modelling

2D and 3D cell culture models aim to mimic the molecular mechanisms which represent human physiology *in vivo* (Zbinden *et al.*, 2022). Cell models allow for investigation of human disease at the molecular level. Re-capitulation of adult neurogenesis *in vitro* enables the study of transcriptomic, proteomic and metabolomic changes which occur specific to disease neurogenesis and enables the identification of individual pathways and disease processes which may be causing disease. During this project, iPSC generated from AD patients and controls were differentiated to generate control and AD patient derived early neural cells for 2D modelling of AD neurogenesis. 3D cell culture systems are more capable of recapitulating cellular diversity seen in complex tissues (Costamagna *et al.*, 2019), therefore iPSC from AD and controls were also differentiated to neurospheres for investigation of AD neurogenesis in a 3D culture system. Neurospheres are multicellular organoids. Progression of NSC to mature neurons via progenitors has been demonstrated *in vivo*, however neurospheres *in vitro* contain a heterogenous cell population which don't differentiate simultaneously through the different states of maturity (Figure 19.) (Gil-Perotín *et al.*, 2013).

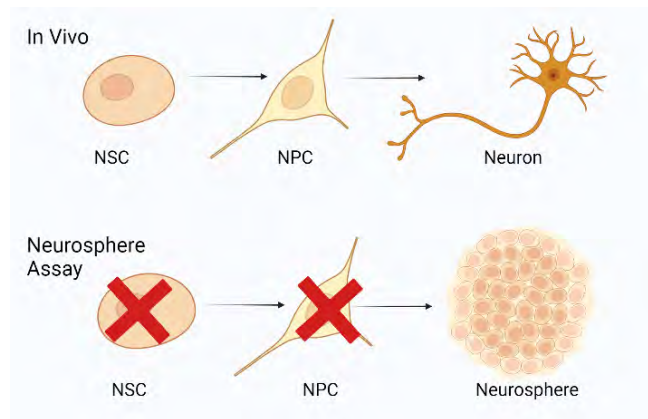


Figure 19. The neurosphere assay compared with in vivo neural differentiation

Neurospheres contain a heterogeneous cell population which don't differentiate simultaneously through progenitor states as NSC in 2D culture do (Gil-Perotín *et al.*, 2013).

2D cell culture enables visualisation of NSC maturation through progenitor cell states to become mature neurons. FitzPatrick *et al.*, (2018) developed a protocol for stepwise differentiation of human ESC to mature neurons which allows for visualisation of neural cell types at defined stages. Cells during the initial stages of neural differentiation were characterised as neuroepithelial cells (NEC), these were differentiated to rosette forming progenitor neural cells (NRPC), which were differentiated further to migratory neural progenitor cells (NPC) and then to mature neurons. Using transcriptomic analysis, FitzPatrick *et al.*, (2018) determined characteristic features of neural cells at the distinct stages in the neural differentiation protocol. Transcriptomic profiles of cells at the NEC and NRPC stages were the most similar and were more similar to ESC than NPC. Pluripotency markers OCT4 and Nanog declined from ESC to NRPC stages and were not detected in NPC. Expression of SOX2 and LIN28 is associated with maintenance of pluripotency in NSC and was high in NEC and NRPC but was not detected in NPC. Expression of nestin and PAX6 was highest at the NRPC stage and remained during the NPC stage. Markers of Vimentin and CDH2 were also high at the NPC stage (FitzPatrick *et al.*, 2018).

The stepwise differentiation protocol developed by FitzPatrick *et al.*, (2018) was used during this project to generate neural rosette forming neural stem cells and neural

progenitor cells for interrogation of neural differentiation in *PSEN1* mutation containing cells compared with controls. The generation of neural rosettes and tubes, confirmed by SOX2+/nestin+ dual staining (Figure 39, Figure 40, Figure 45), confirmed the presence of immature NSC which could be further differentiated and compared between disease and controls to investigate AHN in AD.

NRPC were termed NSC for all future references. The immature NSC (Figure 20.) at the centre of the rosette are pluripotent stem cells which have been activated by neural-specific growth factors, cytokines, and transcription factors to begin to specialise down a neural lineage, these immature NSC are highly proliferative and can be picked and passaged to generate more NSC. Surrounding the immature NSC, are more mature NSC, which are proliferative and divide both for self-renewal and for generation of more differentiated progeny but have less proliferative potential than the immature NSC at the centre of the rosette. As NSC mature and differentiate to NPC, they begin to migrate away and can be found on the outskirts of the neural rosette, NPC have less proliferative potential than NSC. NSC are passaged by picking the proliferative NSC within the rosette and re-plating them on Matrigel® coated plates.

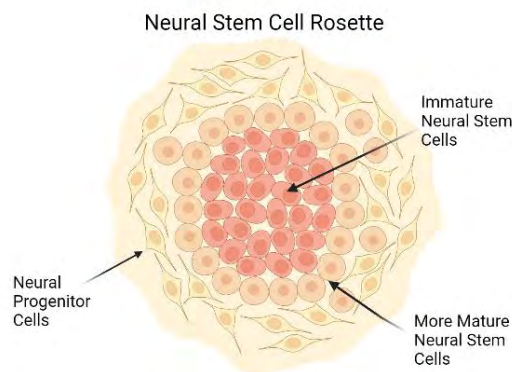


Figure 20. Diagram of a neural stem cell rosette.

Neural stem cell rosettes are composed of immature NSC in the centre with maturing NSC surrounding and NPCs on the outskirts which begin to migrate away from the rosette.

4.2 Aims

The aim of the work carried out in this chapter was to generate stores of iPSC from controls and from AD patients and to use these to generate 2D and 3D neural cell models for the purpose of interrogating mechanisms specific to AD, in particular mechanisms occurring in AD which may be causing abnormal AHN in disease. NSC have a limited number of passages before they become mitotically inactive, whereas iPSC self-renew indefinitely. The generation of stores of iPSC allowed for large-scale production of neural stem and progenitor cells and enabled the performance of experiments which required a large number of cells as their starting material. The number of NSC which could be expanded from the cells purchased was not high enough to carry out the required experiments. Another reason for the generation of control and disease iPSC from the neural cells purchased was because the NSC purchased were not as immature as required for this project -the NSC purchased were unable to generate neural rosettes and tubes and were not highly proliferative. This project aimed to investigate neural stem cells from disease and control lines as they underwent the process of neural specification. De-differentiation of the neural cells to iPSC enabled the investigation of disease and control cells throughout the whole process of neural specification and allowed for AD and control NSC to be compared at the earliest stages in neural differentiation. AD and control neural cells were transduced with an EBNA based cassette to induce reprogramming to iPSC, they were then characterised as iPSC and differentiated to NSC and NPC, at which stage they were further characterised as either NSC or NPC.

The primary objectives of this chapter were:

- Reprogramming of AD and control somatic cells to generate stable iPSC with and without mutations for *PSEN1* and *APOE4*.
- Characterisation of AD and control iPSC using immunocytochemistry to detect markers of stemness, comparison of pluripotency in AD and control iPSC.

- Differentiation of AD and control iPSC to 2D and 3D neural cell models for investigation of disease.
- Validation of NSC and NPC phenotypes in the cell models generated using immunocytochemistry and flow cytometry.

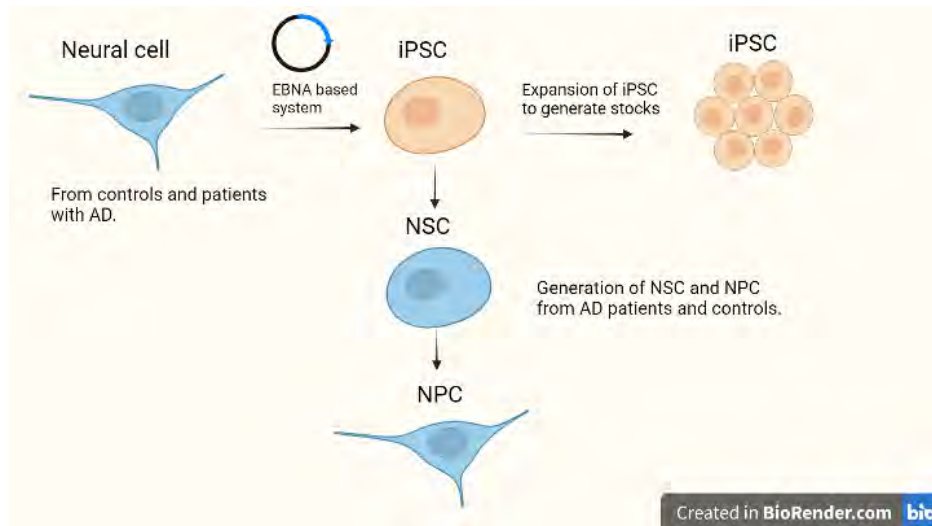


Figure 21. Schematic outlining model development in chapter 1

Schematic displaying the aims of chapter 1 in which control and AD neural cells purchased from Axol Bioscience were to be reprogrammed to iPSC using an EBNA based system and differentiated to NSC and NPC (Created in Biorender.com).

4.3.0 Results

In this chapter, iPSC were generated from controls and from patients with FAD *PSEN1* mutation. control and *PSEN1* iPSC generated were assessed to confirm expression of pluripotency markers and to validate their capacity for differentiation to all three germ layers. control and *PSEN1* iPSC were then differentiated to NSC and NPC to model and interrogate AD neurogenesis. NSC and NPC generated were assessed qualitatively and quantitatively for expression of immature neural markers SOX2 and nestin.

4.3.1 Culture of Axol AD and control NSC

The aim of chapter 1 was to generate 2D and 3D neural cell models for the purpose of interrogating mechanisms specific to AD neurogenesis. To achieve the aims and objectives stated, NSC were purchased from AxolBioscience, these included control NSC, NSC containing mutations in *PSEN1* (*PSEN1* A246E, *PSEN1* M146L) and NSC containing two copies of the APOE4 allele. The NSC purchased were cultured and expanded but were not able to generate neural rosettes and tubes, NSC also have a very limited number of passages before they become mitotically inactive, and the number of NSC that could be expanded from the cells purchased was not high enough to carry out the experiments required to investigate the process of neural differentiation in AD. iPSC can self-renew almost continuously, so generating AD and control iPSC meant that large stocks of control and AD iPSC could be generated and stored to be later differentiated back down the neural lineage for investigation of AD neurogenesis.

AD and control NSC lines purchased from AxolBioscience were revived into Neural Plating XF Medium onto plates pre-coated with Matrigel, which was replaced the following day with NEM. AD and control NSC were cultured and expanded in NEM. control and AD NSC purchased from Axol Bioscience were limited in their capacity to proliferate and did not organise into neural rosettes and tubes, as should be seen during early stages of neural differentiation. These NSC were phenotypically more similar to early stage neurally committed NPC (Figure 22.). For accurate comparison of neural differentiation capacity, *PSEN1* and control lines were required to be compared at the same stages of neural differentiation, thus both control and disease lines were reprogrammed to iPSC and then differentiated simultaneously to NSC and NPC. Simultaneous neural differentiation of *PSEN1* and controls enabled both lines to always be maintained under the same conditions and to be measured at the same stages in their differentiation.

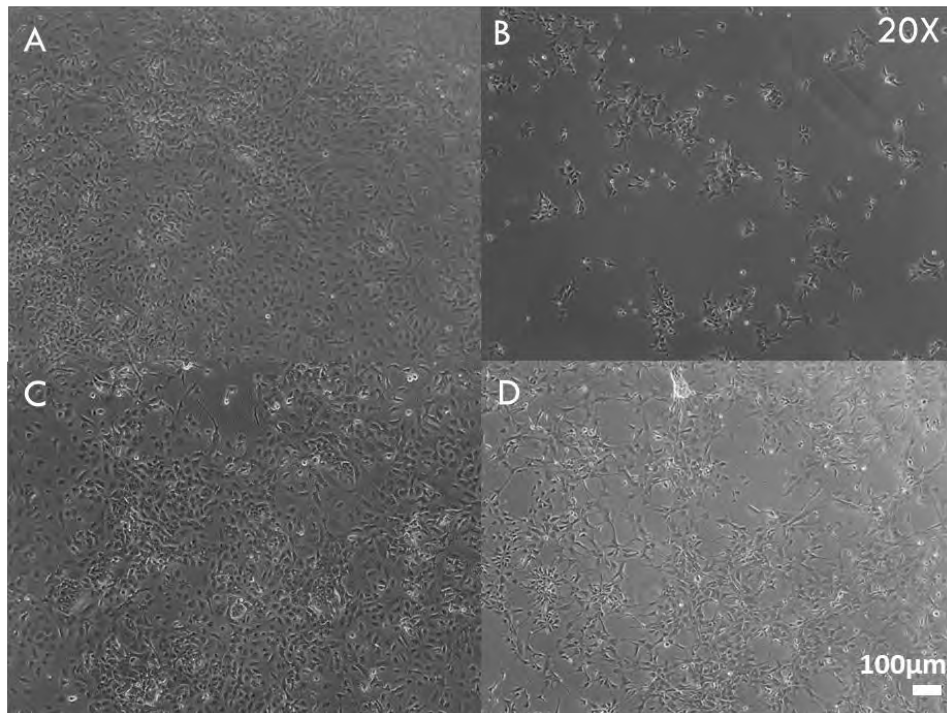


Figure 22. Culture and expansion of axol NSC

Late passage AD and control NSC purchased from AxolBioscience were cultured and expanded in NEM. AD and control NSC did not organise into neural rosettes and tubes as should be seen during early stages of neural differentiation and were phenotypically more similar to early stage NPC. A.) control NSC. B.) *PSEN1* M146L NSC. C.) APOE4 (HOM) NSC. D.) *PSEN1* A246E NSC.

4.3.2 De-differentiation of control NSC to generate control iPSC

To induce de-differentiation, somatic cells were transiently transfected with plasmids that contain genes for expression of pluripotency factors usually expressed by stem cells. The McKay lab uses a combination of four plasmids: pCXWB-EBNA1, pCXLE-hSK, pCXLE-hUL and pCXLE-hOCT3/4-shp53-F which utilise episomal integration to temporarily express pluripotency factors and induce de-differentiation of somatic cells. Nucleofection of NSC with these pluripotency factors had never before been achieved in this lab so optimisation of the nucleofection process in NSC (Figure 23.) was necessary before initiation of reprogramming procedures in AD samples.

4.3.2.1 Optimising nucleofection of NSC

control NSCs obtained from Axol Bioscience (Figure 22.) were first nucleofected with the pmax GFP™ Vector (Figure 99.) for constitutive expression of green fluorescent protein (GFP) for optimisation of nucleofection efficiency and toxicity. The pmax GFP™ Vector has a human CMV promoter, this is a strong promoter and enables high-level constitutive expression of GFP. The pmax GFP™ Vector also has a gene which enables resistance to kanamycin.

Nucleofection of NSC with the pmax GFP™ Vector was carried out using the Human Dermal Fibroblast (HDF) Nucleofector™ Kit from Lonza along with the programme P-022 on the Amaxa Nucleofector. The Human Dermal Fibroblast (HDF) Nucleofector™ Kit had been previously purchased by the lab for reprogramming HDF so nucleofection with this kit and programme was attempted in NSC to reduce experimental costs. 48 hours later, transfected NSC were visualised using the Leica Live Cell Imaging System (Figure 23.). Transfection with the pmax GFP™ Vector resulted in approximately 80% of the population being transfected. Transfection was considered to be successful in NSC which were expressing GFP and NSC not seen to be expressing GFP were considered to be untransfected.

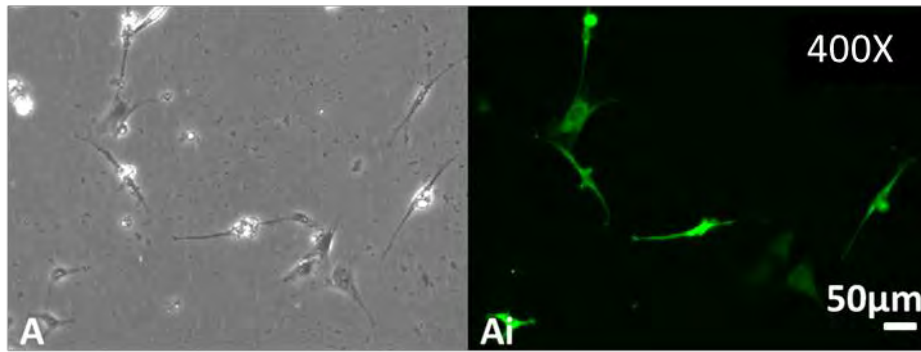


Figure 23. Nucleofection with the pmax GFP™ vector

control NSCs 3 days after nucleofection with The pmax GFP™ Vector. Nucleofection with the GFP plasmid was used to confirm that nucleofection of NSCs was possible using the Human Dermal Fibroblast (HDF) Nucleofector™ Kit from Lonza along with the programme P-022 on the Amaxa Nucleofector. GFP expression is constitutive, meaning cells not expressing GFP have not been nucleofected with the plasmid. Ai.) Phase-contrast image displaying control NSC after nucleofection with GFP plasmid. Aii.) Corresponding GFP image. Images were taken at 400X magnification using Leica Live Cell Imaging System. Scale bar 50µm.

Following transfection of the GFP plasmid, varying cell densities of control NSC ranging from 45×10^4 to 240×10^4 were nucleofected with reprogramming factors OCT3/4, SOX2, L-MYC, LIN28 and KLF4 (using an EBNA based system and short hairpin p53 to transiently knockdown p53 expression). The EBNA based system does not integrate into cellular DNA, but instead binds episomally for transient expression of pluripotency factors. The use of genome integrating viral vectors could influence gene expression of transfected cells. Nucleofection of NSC led to cytotoxicity resulting in low confluencies 6 days post nucleofection, despite cells being plated at a density of approximately 80% confluency. Lower starting cell densities resulted in lower chance of cell-survival post nucleofection, however, using starting cell densities higher than recommended as part of the Amaxa nucleofector protocol resulted in lower percentage confluency 6 days post nucleofection (Table 27. Cell densities of NSC for nucleofection with the pmax GFP™ vector).

Table 27. Cell densities of NSC for nucleofection with the pmax GFP™ vector

Nucleofection	Starting Cell Density of NSC	% Confluency 6 Days Post Nucleofection
1	45 x 10 ⁴ cells	1-5
2	120 x 10 ⁴ cells	5-10
3	240 x 10 ⁴ cells	10-20
4	280 x 10 ⁴ cells	0-5

Optimal cell density for nucleofection of NSCs was determined to be 240 x 10⁴ cells, as this starting cell density resulted in the greatest number of surviving cells after nucleofection. The starting cell density of 45 x 10⁴ cells was recommended by Amaxa, but after nucleofection, a very low number of NSC survived. As successful reprogramming was achieved using a starting NSC density of 280 x 10⁴ cells, further reprogramming experiments were carried out using that same cell density. A large number of cells were lost after each nucleofection due to the cytotoxicity resulting from the harshness of electroporation on the relatively delicate NSC (Figure 24.). The programme A-033 on the Amaxa Nucleofector was selected for use in nucleofecting NSC as it resulted in increased cell survival when compared with the programme P-022.

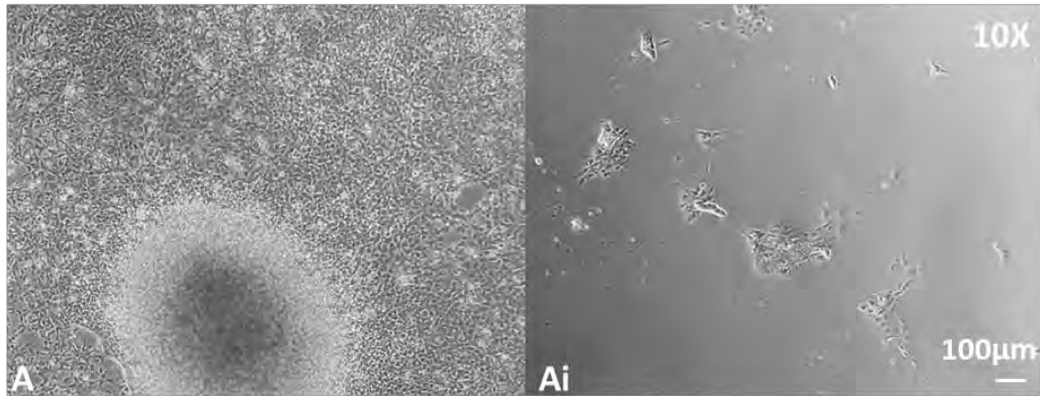


Figure 24. Nucleofection of control NSC with reprogramming factors

Nucleofection of control NSC with reprogramming factors resulted in a massive loss of cells, this cytotoxicity was the result of transducing cells with the relatively high concentration of DNA required for reprogramming. A.) control NSC (at a cell density of 240×10^4 cells) before nucleofection. Ai.) control NSC 6 days after nucleofection with reprogramming factors. All images were taken at 10X magnification using an EVOS® Digital Microscope.

4.3.3 De-differentiation of SHEF3 and nHDF lines for comparison of reprogramming efficiency

After optimisation of reprogramming efficiency, control NSC were de-differentiated to generate large, well characterised cell banks of iPSC. iPSC were generated from control NSC with the aim of carrying out multiple neural differentiation experiments to compare the process of AD and control neural specification. For de-differentiation, control neural cells were transduced with an EBNA based cassette containing a combination of four plasmids: pCXWB-EBNA1, pCXLE-hSK, pCXLE-hUL and pCXLE-hOCT3/4-shp53-F which are able to induce de-differentiation in somatic cells for generation of iPSC.

control iPSC were analysed to confirm expression of pluripotency markers OCT3/4, SOX2, and most importantly, to confirm expression of Tra-181, a pluripotency marker that is not expressed as part of the EBNA-based construct used for reprogramming. The colony forming ability of control iPSC was analysed and compared with that of

other iPSC (Figure 25.) to confirm that control iPSC were an appropriate comparison to be used for future investigation of AD neurogenesis.

De-differentiation of neural cells to iPSC enabled investigation of disease and control cells throughout the process of neural specification and allowed for AD and control NSC to be compared at the earliest stages in neural differentiation. Two different cell lines were reprogrammed alongside control NSC to compare reprogramming efficiency. SHEF3 ESC derived NSCs (SHEF3 NSC) generated during optimisation of neural differentiation were reprogrammed alongside control NSC, as were neonatal human dermal fibroblasts (nHDF) which are commonly used in the McKay lab for iPSC reprogramming. SHEF3 NSC and nHDF were successfully de-differentiated to iPSC alongside control NSC (Figure 25.).

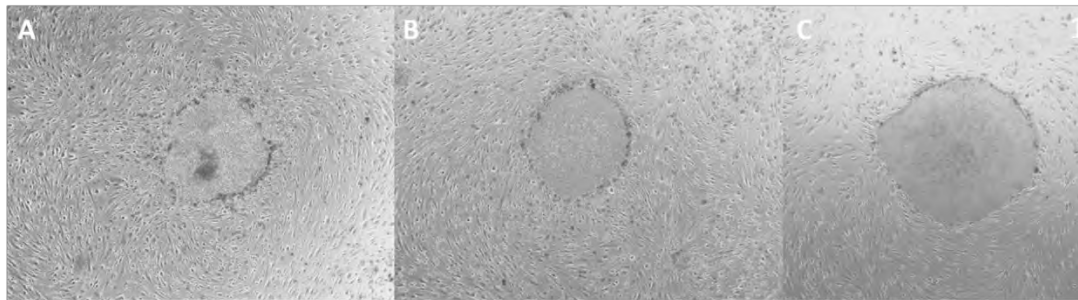


Figure 25. iPSC generated from the de-differentiation of control NSC, SHEF3 NSC and nHDF.

Circular colonies of iPSC generated from the de-differentiation of control NSC, SHEF3 NSC and nHDF. A.) control iPSC. B.) SHEF3 iPSC. C.) nHDF iPSC. iPSC were cultured on a feeder layer of mouse embryonic fibroblasts (MEFs). All images were taken at 10X magnification using an EVOS® Digital Microscope.

4.3.4 Verification of pluripotency in control iPSC

4.3.4.1 Alkaline phosphatase staining

Alkaline Phosphatase Staining was used to compare colony formation in control iPSC with SHEF3 iPSC and nHDF iPSC. An equal number (three) of primary colonies from each reprogramming experiment were plated and allowed to develop for two weeks. Alkaline phosphatase is a membrane bound enzyme which is highly expressed in stem cells and although not a bona fide marker of pluripotency, it is widely used to evaluate de-differentiation to pluripotent stem cells (Štefková *et al.*, 2015). Colonies indicative of pluripotent stem cells stained positive for alkaline phosphatase and were counted; three colonies generated from control NSC produced 52 secondary colonies, three colonies from SHEF3 NSC produced 49 secondary colonies and three primary colonies produced from nHDF produced 44 secondary colonies (Figure 26.). There was a trend towards smaller colonies being produced by control iPSC than by SHEF3 and nHDF iPSC, but the number of colonies detected by positive alkaline phosphatase staining did not differ significantly between the three reprogramming experiments, therefore these results indicate that colony forming ability of control iPSC did not differ significantly to that of SHEF3 iPSC and nHDF iPSC.

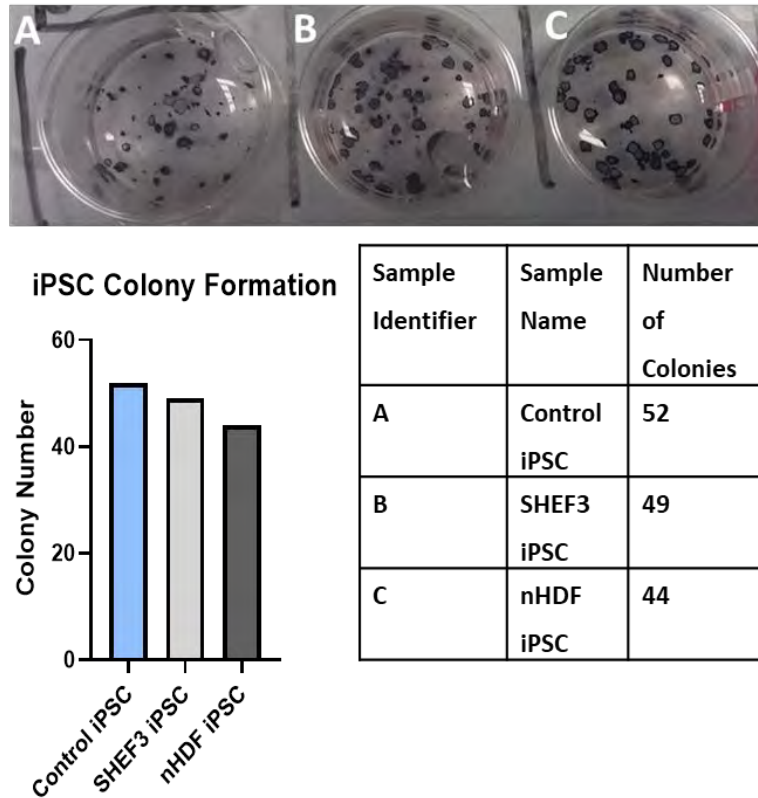


Figure 26. Colony formation

Alkaline phosphatase (AP) staining of colonies. A.) control iPSC. B.) SHEF3 iPSC. C.) nHDF iPSC. AP staining was carried out to ensure that a relatively similar number of colonies were produced from nucleofection of each different cell line with reprogramming factors. The number of secondary colonies derived from three primary iPSC colonies after three weeks of culture was compared between control, SHEF3 and nHDF iPSC. There was no significant difference in the number of secondary colonies between control, SHEF3 and nHDF iPSC (n=1).

4.3.4.2 Immunocytochemistry

iPSC generated from control NSC were further investigated for validation of pluripotency before they could be used as a control to investigate AD neural differentiation. SOX2 and OCT3/4 are markers that are highly expressed in pluripotent stem cells and not expressed in differentiated cells, pluripotent stem cells also have high levels of the antigen Tra-181 (Sokolov *et al.*, 2010). iPSC colonies generated from control NSC stained positively for pluripotency markers SOX2, OCT3/4 and Tra-1-81 (Figure 40.) which indicated that control iPSC were pluripotent

stem cells. control iPSC did not differ significantly from SHEF3 iPSC or nHDF iPSC in staining for pluripotency markers, thus supporting the use of control iPSC as a viable control to be used in investigation of *PSEN1* neural differentiation capacity.

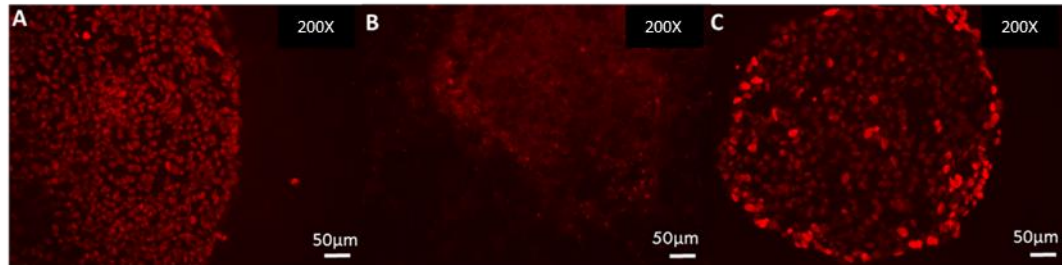


Figure 27. ICC for pluripotency markers

Control iPSC generated from de-differentiation of Axol control NSC stained positive for markers of pluripotency; A.) SOX2, B.) Tra-1-81 and C.) OCT4. All images were taken at 200X magnification using Leica Live Cell Imaging System. Scale bar 50µm.

4.3.4.3 Trilineage differentiation of control iPSC

Trilineage differentiation was used to further validate control iPSC as pluripotent stem cells. control iPSC were cultured in pro-differentiation medium without being directed to differentiate down a particular lineage, they were then stained for markers of all three germ layers: β -III tubulin (ectoderm), SOX17 (endoderm) and α -SMA (mesoderm). Cells derived from control iPSC stained positive for markers of all three germ layers. The ability of control iPSC to differentiate into cells of all three germ layers indicates that they are pluripotent, as only pluripotent (and totipotent) stem cells are capable of differentiation down ectoderm, endoderm, and mesoderm lineages.

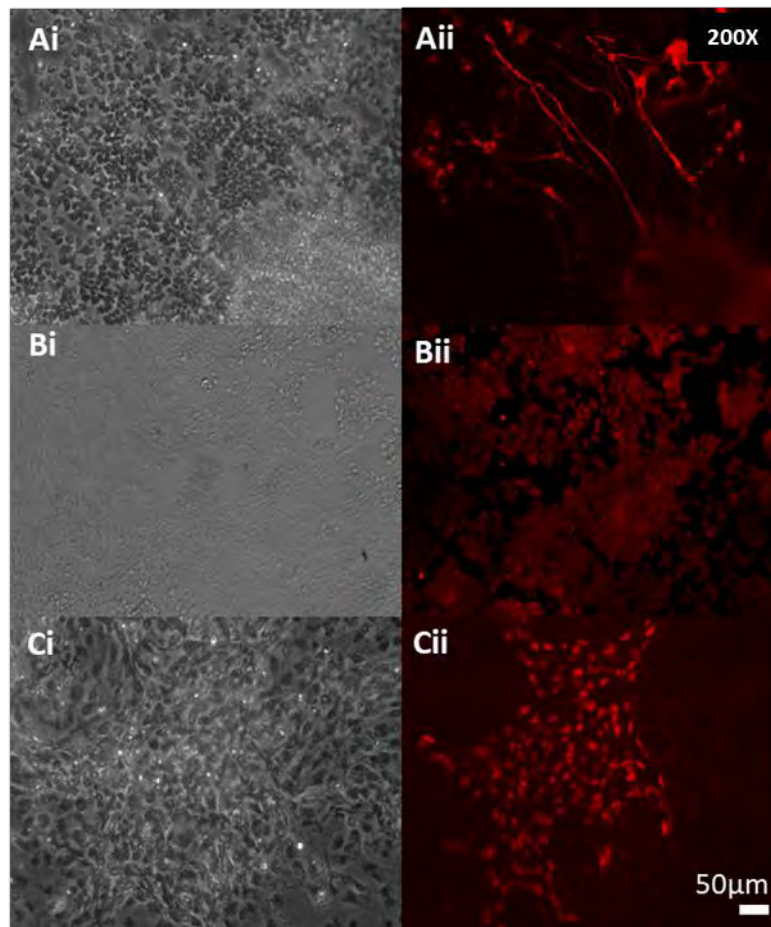


Figure 28. Trilineage differentiation of control iPSC

Control iPSC were differentiated and stained positive for markers of all three germ layers: β -III tubulin (ectoderm), SOX17 (endoderm) and α -SMA (mesoderm). Capacity for differentiation to all three germ layers is a measure of pluripotency. Ai.) Phase-contrast image of control. Aii.) Corresponding fluorescent image for staining with β -III tubulin. Bi.) Phase-contrast image of control. Bii.) Corresponding fluorescent image for staining with α -SMA. Ci.) Phase-contrast image of control. Cii.) Corresponding fluorescent images for staining with SOX-17. All images were taken at 200X magnification using Leica Live Cell Imaging System. Scale bar 50 μ m.

4.3.5 De-differentiation of *PSEN1* NSC to produce *PSEN1* iPSC lines

This project aimed to generate an *in vitro* cell model to investigate differences in human adult neurogenesis between AD and controls. AD and control NSC were purchased from Axol Bioscience to study disease neural differentiation but were not able to generate neural rosettes. Furthermore, it could not be confirmed that both disease and control NSC purchased from an external source were at the same stage in neural differentiation. For this reason, it was decided that each neural specification protocol would be started at the iPSC stage. To begin each neural differentiation process at the iPSC stage, it was necessary to de-differentiate both disease and control lines back to iPSC.

After confirmation of pluripotency in control iPSC, AD neural cells containing FAD mutations *PSEN1* A246E, *PSEN1* M146L, M146L and the variant APOE4 (HOM) were nucleofected with reprogramming factors OCT3/4, SOX2, L-MYC, LIN28 and KLF4 (using an EBNA based system and shP53) to cause them to undergo de-differentiation (Figure 29.). AD neural cell samples containing FAD mutations *PSEN1* A246E, *PSEN1* were de-differentiated to generate large, well characterised cell banks of iPSC. iPSC were generated from AD NSC with the aim of carrying out multiple neural differentiation experiments to compare the process of AD and control neural specification. For de-differentiation, AD neural cells were transduced with an EBNA based cassette containing a combination of four plasmids: pCXWB-EBNA1, pCXLE-hSK, pCXLE-hUL and pCXLE-hOCT3/4-shp53-F which are able to induce de-differentiation in somatic cells for generation of iPSC. Post nucleofection with reprogramming factors, AD NSC were plated onto a feeder layer of iMEFs and cultured for three to four weeks before iPSC colonies began to grow large enough to be visualised using the EVOS® Digital Microscope. iPSC colonies generated from all AD NSC lines phenotypically resembled iPSC and were expanded and frozen down for use in future experiments to investigate AD neurogenesis.

AD iPSC generated varied in their ability to proliferate and APOE iPSC were not able to be amplified up to large enough stores of iPSC to be used for future experiments. iPSC generated from *PSEN1* A246E NSC were analysed to confirm expression of Tra-181, a pluripotency marker that is not expressed as part of the EBNA-based construct used for reprogramming (Figure 31.). *PSEN1* A246E iPSC were also analysed to confirm that they were able to differentiate to cells of all three germ layers (Figure 32.).

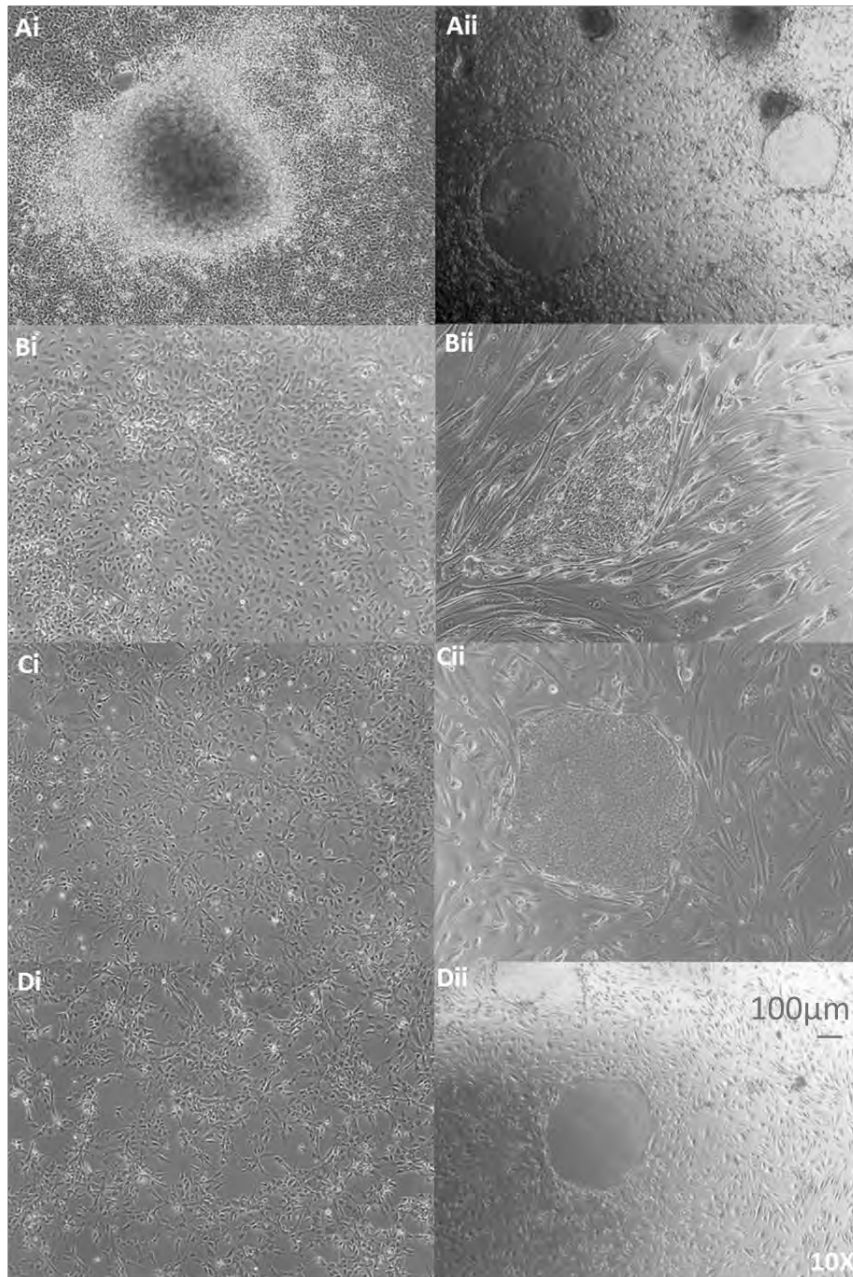


Figure 29. De-differentiation of control and AD NSC to iPSC

De-differentiation of control and AD NSC was carried out using an EBNA based reprogramming cassette which binds episomally to upregulate expression of pluripotency factors. control and AD iPSC generated are shown Ai.) control NSCs. Aii.) control iPSC. Bi.) APOE4 NSCs. Bii.) Corresponding image of APOE4 iPSC. Ci.) *PSEN1* A246E NSCs. Cii.) Corresponding image of *PSEN1* A246E iPSC. Di.) *PSEN1* M146L NSCs. Dii.) Corresponding image of *PSEN1* M146L iPSC. All images were taken at 10X magnification using an EVOS® Digital Microscope.

4.3.6 Production of feeder free iPSC

Feeder free iPSC cultures were generated from *PSEN1* and control iPSC for ease of analysis and for neural differentiation. Initially, iPSC were generated and cultured on a feeder layer of iMEFs, however, neural differentiation and flow cytometry are techniques which require a homogenous population of iPSC without contamination from the feeder layer of iMEFs. To prevent contamination of samples with iMEFs, iPSC colonies were picked and plated onto Matrigel® coated cell culture plates to generate feeder free iPSC (Figure 30.). Feeder free iPSC were passaged a minimum of three times to ensure any iMEF contamination was not carried through to experiments, were expanded and then stored for use in downstream applications such as neural induction and flow cytometry.

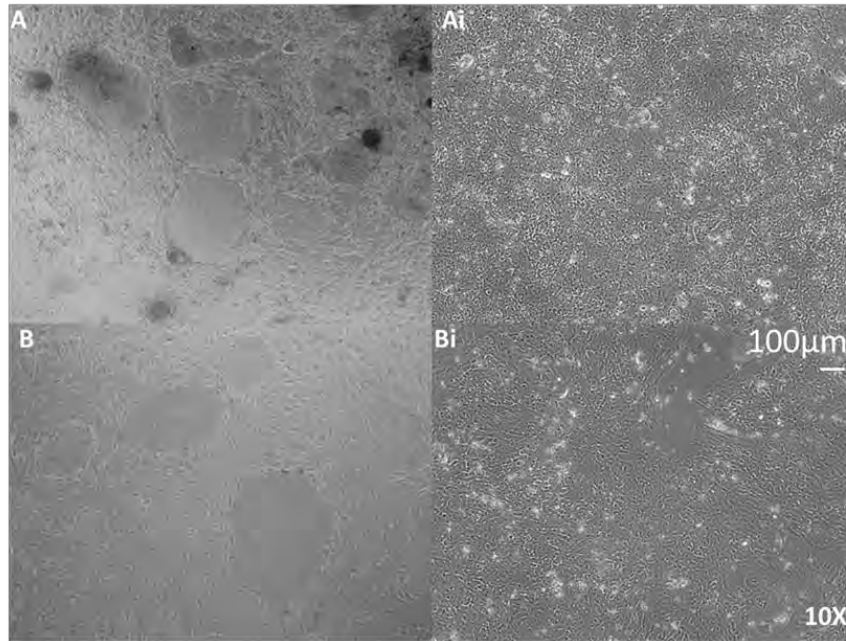


Figure 30. Generation of feeder free iPSC

iPSC colonies were picked and plated onto Matrigel © coated tissue culture plates to generate feeder free iPSC for use in downstream applications. A.) Phase-contrast image of control iPSC on feeders. Ai) FF control iPSC. B.) *PSEN1* A246E AD iPSC on feeders. Bi.) *PSEN1* A246E AD iPSC FF. All images were taken at 10X magnification using an EVOS® Digital Microscope.

4.3.7 Assessment of pluripotency in *PSEN1* iPSC

4.3.7.1 Immunocytochemistry for pluripotency markers in *PSEN1* iPSC

Expression of the pluripotency antigen Tra-1-81 was confirmed in *PSEN1* A246E iPSC using immunocytochemistry. Tra-1-81 is an antigen presented on the cell surface of cells associated with the pluripotent state and is thus an ideal marker to use as confirmation that iPSC generated are pluripotent. iPSC were generated from control and AD NSC for the purpose of generating cells capable of self-renewal, and to enable simultaneous differentiation of control and AD NSC down a neural lineage for investigation of AD neurogenesis. Tra-1-81 pluripotency staining alongside positive SOX2 staining (Figure 31. ICC for pluripotency markers in *PSEN1* iPSC) and successful tri-lineage differentiation was considered sufficient confirmation of stemness in *PSEN1* iPSC.

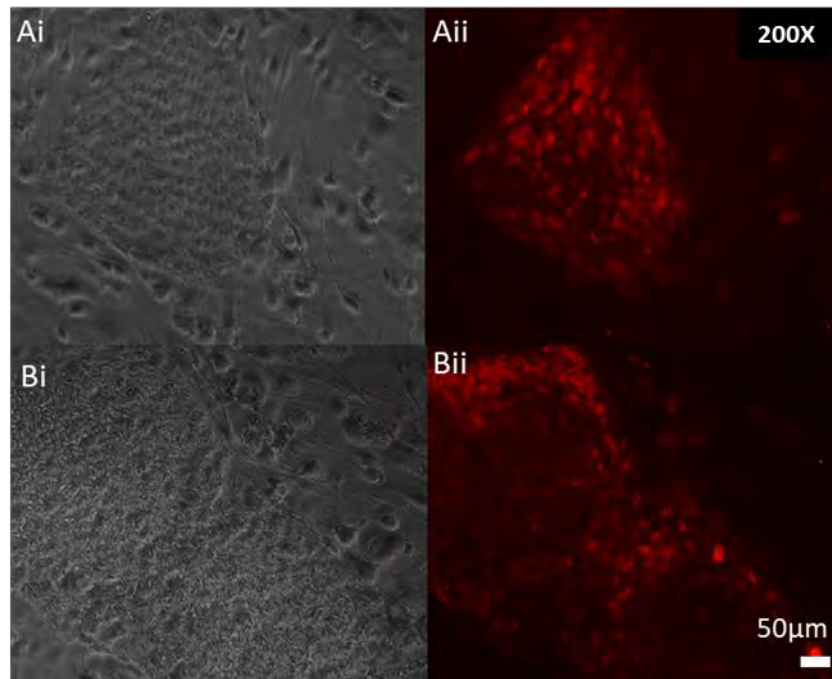


Figure 31. ICC for pluripotency markers in *PSEN1* iPSC

Ai-Aii.) Phase contrast and fluorescent images displaying *PSEN1* A246E iPSC stained positive SOX2.

Bi-Bii.) phase contrast and fluorescent images displaying *PSEN1* A246E iPSC stained positive for

TRA-1-81, an endogenous marker of pluripotency. All images were taken at 200X magnification using Leica Live Cell Imaging System. Scale bar 50 μ m.

4.3.7.2 Trilineage differentiation of *PSEN1* iPSC

Trilineage differentiation was used to differentiate iPSC to cells of all three germ layers. This was carried out to further validate *PSEN1* A246E iPSC as pluripotent stem cells that are capable of differentiating into cells of ectodermal, endodermal, and mesodermal lineages. *PSEN1* A246E iPSC were allowed to differentiate without being directed to differentiate down a particular lineage, they were then stained for markers of all three germ layers: β -III tubulin (ectoderm), SOX17 (endoderm) and α -SMA (mesoderm). Cells derived from *PSEN1* A246E iPSC stained positive for markers of all three germ layers. The ability of *PSEN1* A246E iPSC to differentiate into cells of all three germ layers indicates that they are pluripotent, as only pluripotent (and totipotent) stem cells are capable of differentiation down ectoderm, endoderm, and mesoderm lineages.

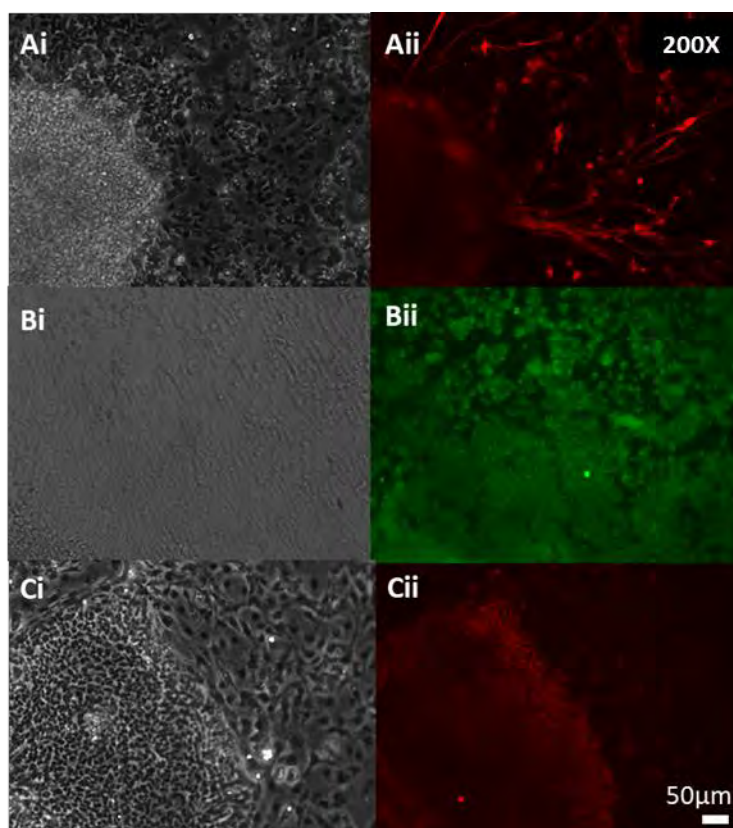


Figure 32. Trilineage differentiation of *PSEN1* iPSC

PSEN1 A246E iPSC were differentiated and stained positive for markers of all three germ layers: Beta-III tubulin (ectoderm), SOX17 (endoderm) and alpha-SMA (mesoderm). Capacity for differentiation to all three germ layers is a measure of pluripotency. Ai.) Phase-contrast image of control. Aii.) Corresponding fluorescent image for staining with Beta-III tubulin. Bi.) Phase-contrast image of control. Bii.) Corresponding fluorescent image for staining with α -SMA. Ci.) Phase-contrast image of control. Cii.) Corresponding fluorescent images for staining with SOX-17. All images were taken at 200X magnification using Leica Live Cell Imaging System. Scale bar 50 μ m.

4.3.7.3 Analysis of OCT3/4 expression in *PSEN1* and control iPSC by flow cytometry

Expression of the pluripotency marker OCT3/4 was measured in *PSEN1* A246E and control iPSC to compare levels of stemness in iPSC prior to initiation of neural differentiation. control and *PSEN1* A246E iPSC were stained with the anti-hOCT3/4 primary antibody and analysed using the DV Verse flow cytometer. The population

of interest was gated to exclude dead cells and debris (Figure 33.A), and then further gated to exclude doublets (Figure 33.B). Unstained samples were run first to enable identification of stained and unstained populations (shown as the orange peaks in the P3 section of both D and E in Figure 33.). Cells were categorised into those which were negative for OCT3/4, those which displayed low expression and those cells which were highly expressing OCT3/4 (Figure 33.C).

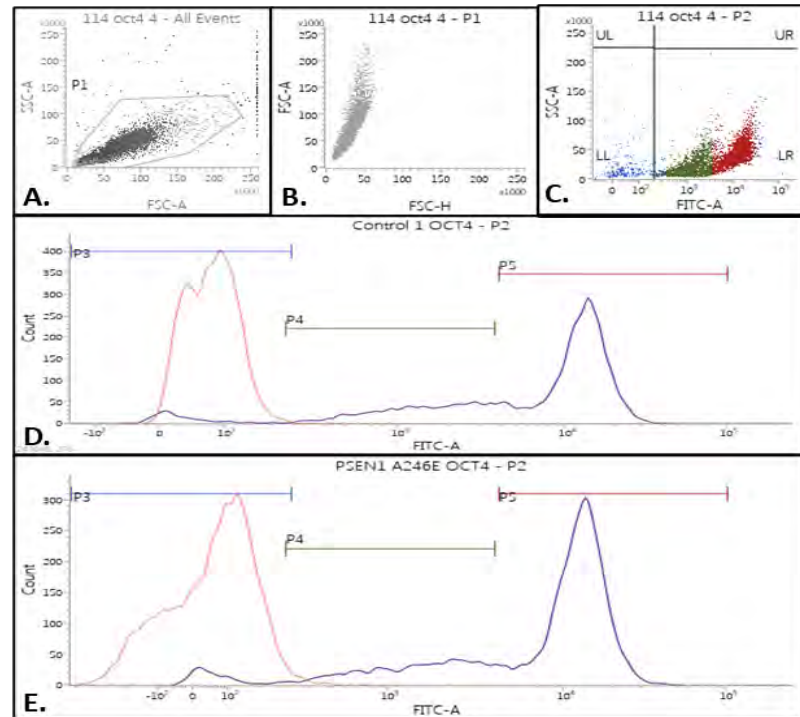


Figure 33. Flow cytometry data displaying OCT4 expression in *PSEN1* and control iPSC

Flow cytometry data displaying OCT4 expression in *PSEN1* A246E iPSC and controls. A.) Initial gating of the population of interest. B.) Gating to exclude doublets. C.) Cells labelled as blue have no expression of OCT4 (unstained samples), cells labelled as green have low expression of OCT4 and cells labelled as red have greater expression of OCT4. D.) Visualisation of these different populations in control iPSC. E.) Visualisation of these different populations in *PSEN1* A246E iPSC.

Data recorded on OCT3/4 expression in control and *PSEN1* A246E iPSC, is shown including raw FITC-A Median values for both unstained and stained samples (Table

28 FITC-A median data acquired from DV Verse flow cytometer displaying unstained and stained values for OCT4 expression.)

Table 28 FITC-A median data acquired from DV Verse flow cytometer displaying unstained and stained values for OCT4 expression.

Sample	FITC-A Median
control 1 FF iPSC unstained P2	82
control 1 FF iPSC OCT4 P2	10407
<i>PSEN1</i> A246E 1 FF iPSC unstained P2	90
<i>PSEN1</i> A246E 1 FF iPSC OCT4 P2	10836
control 2 FF iPSC unstained P2	89
control 2 FF iPSC OCT4 P2	9572
<i>PSEN1</i> A246E 2 FF iPSC unstained P2	96
<i>PSEN1</i> A246E 2 FF iPSC OCT4 P2	9459
control 3 FF iPSC unstained P2	58
control 3 FF iPSC OCT4 P2	7308
<i>PSEN1</i> A246E 3 FF iPSC unstained P2	83
<i>PSEN1</i> A246E 3 FF iPSC OCT4 P2	10621
control 4 FF iPSC unstained P2	83
control 4 FF iPSC OCT4 P2	9239
<i>PSEN1</i> A246E 4 FF iPSC unstained P2	90
<i>PSEN1</i> A246E 4 FF iPSC OCT4 P2	11275

Data displayed in Figure 34. is representative of the average median fluorescence intensity (MFI) of OCT3/4 in control and *PSEN1* iPSC. Results indicated that there was no significant difference ($p=0.112$) in OCT3/4 expression between control and *PSEN1* iPSC (Figure 34.), this indicated that *PSEN1* A246E and control iPSC did not differ significantly in their ability to self-renew and thus, would be beginning the process of neural differentiation from the same stage. Results generated confirmed the expression of pluripotency factors in control and *PSEN1* iPSC and indicated that there was no significant difference between *PSEN1* and control iPSC in terms of their expression of pluripotency markers. Results overall indicate that *PSEN1* and control iPSC will begin neural differentiation at the same stage.

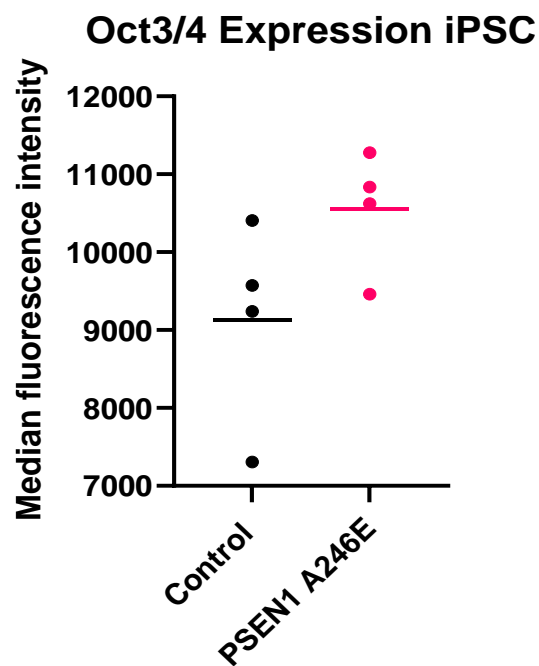


Figure 34. Flow cytometry-based analysis of OCT3/4 expression in control and *PSEN1* A246E iPSC.

Flow cytometry-based analysis of OCT3/4 expression in control and *PSEN1* A246E iPSC. Statistical analysis of data (unpaired t-test) using GraphPad version 9.2.0 indicated no significant differences between expression of OCT3/4 in control and *PSEN1* A246E iPSC ($p=0.112$), ($n=4$). This data indicates no differences in pluripotency between controls and *PSEN1* A246E at the iPSC stage.

4.3.8 Sanger sequencing of iPSC to confirm presence of *PSEN1* A246E mutation

The presence of the *PSEN1* mutation in *PSEN1* A246E iPSC was confirmed using Sanger Sequencing (Figure 35.). DNA was isolated from *PSEN1* A246E iPSC and the primers displayed in 4.2.2 were used to sequence the region of the *PSEN1* gene in which the A246E mutation can be detected. The *PSEN1* A246E mutation is a point, missense mutation in which the base adenine replaces thymine at chromosome 14 position 73659540. Sequencing data displayed in Figure 35. revealed the presence of the GAG codon in place of the GCG codon which would be in this position in the absence of mutation. The mutated base is highlighted in blue in Figure 35.

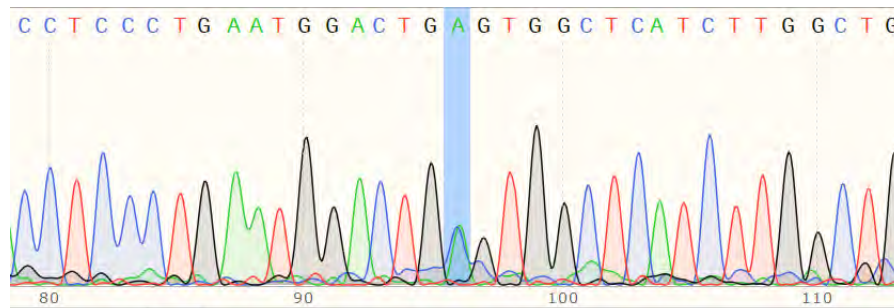


Figure 35. Sanger Sequencing of *PSEN1* A246E iPSC for Mutation Confirmation

Sanger sequencing of *PSEN1* iPSC confirmed the presence of the A246E point, missense mutation in the *PSEN1* gene at position Chr14:73659540 C>A, codon change: GCG to GAG, Exon 7.

4.3.9 Generation of models for investigation of AD neurogenesis

The first aim of this project (1.4) was to generate 2D and 3D neural cell models for the purpose of interrogating mechanisms specific to AD neurogenesis. To generate 2D models for investigation of AD neurogenesis, *PSEN1* and control iPSC were

differentiated to NSC and NPC. To generate 3D models for investigation of AD neurogenesis, *PSEN1* and control iPSC were also differentiated to generate neurospheres.

4.3.9.1 Validation of the neural differentiation protocol using SHEF3

ESC

The neural differentiation protocol which was developed and validated by FitzPatrick *et al.*, (2018) was utilised in this project to generate NSC and NPC for investigation of neural differentiation capacity in AD. SHEF3 ESC are an embryonic stem cell line which were previously used in the McKay by FitzPatrick *et al.*, (2018) to model neural differentiation from ESC to NPC. Each stage in the neural specification model developed by FitzPatrick *et al.*, (2018) was well characterised using microarray data, thus, as their neural differentiation had already been well characterised, SHEF3 ESC were utilised for method optimisation of neural differentiation to NSC and NPC. Following the protocol developed and validated by FitzPatrick *et al.*, (2018), ESC were cultured in V-bottom 96 well plates in NIM media with PVA to encourage formation of embryoid bodies. NIM was made up of DMEMF12 with Glutamax and supplemented with factors N2, FGF2, Heparin and NEAA to initiate neural induction in ESC. The appearance of neural tubes and neural rosettes indicated the presence of NSC (Figure 36.) and these areas containing neural tubes and rosettes were picked and passaged to expand the populations of NSC. The cartoon displayed in Figure 36. displays differentiation of feeder free pluripotent ESC to multipotent NSC and to more lineage specific NPCs. Neural rosettes and neural tubes which formed during the NSC stage are highlighted in (Figure 37).

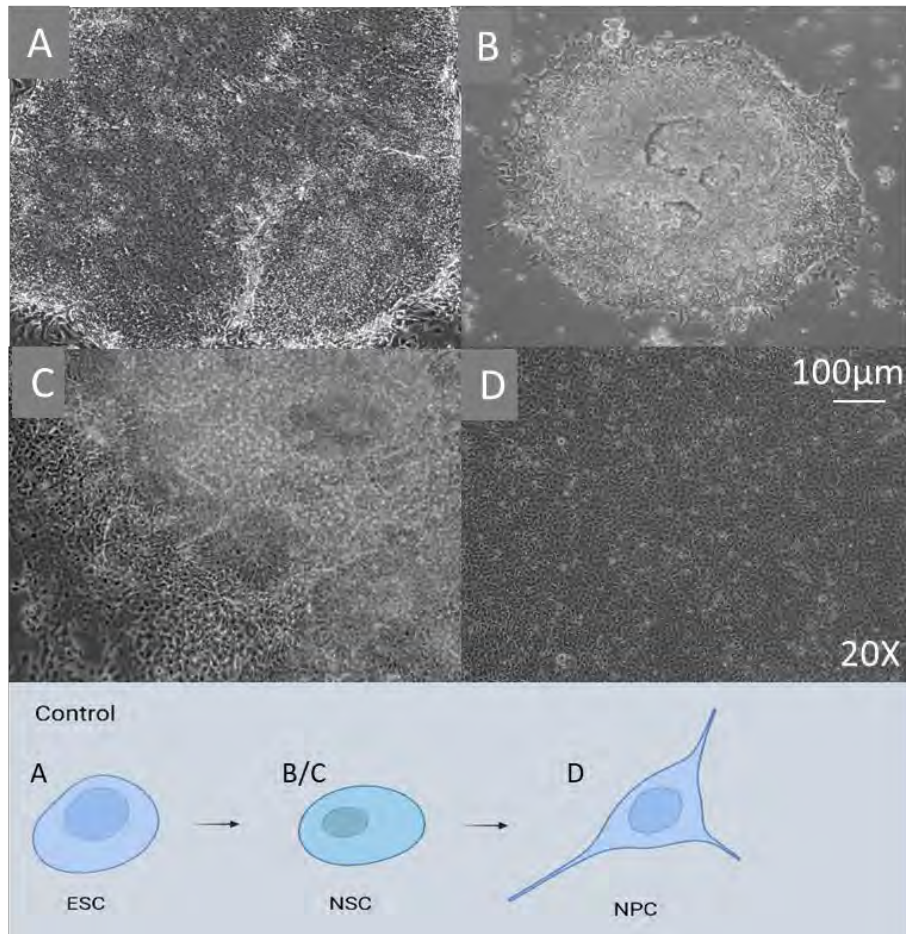


Figure 36. Stages of neural differentiation.

Images and schematic displaying the process of neural differentiation from stem cell to mature neuron. A.) SHEF3 embryonic stem cells (ESCs) prior to neural differentiation. B.) Neuroepithelial cells at day 6 of neural differentiation. C.) Neural rosette forming stem cells at day 10 of neural differentiation. C.) Neural progenitor cells as shown at day 13+ of neural differentiation. All images were taken at 20X magnification using an EVOS® Digital Microscope.

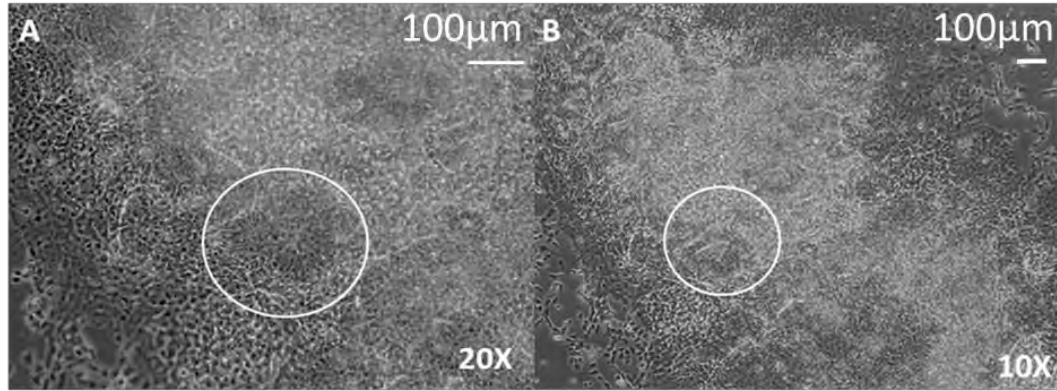


Figure 37. Neural rosettes and tubes

Images A and B display phase-contrast images of SHEF3 NSCs produced during neural differentiation, with circles highlighting areas of neural rosette (A) and neural tube (B) formation. Images were taken at 10X and 20X magnification using an EVOS® Digital Microscope.

4.3.9.2 immunocytochemistry for confirmation of neural phenotype

Immunocytochemistry was employed to assess neural phenotype in SHEF3 NSC. Figure 39. and Figure 40. display staining used alongside phenotypic differences in cells to confirm the stage of the cells during neural differentiation. OCT4 and SOX2 are markers of pluripotency which are highly expressed during the iPSC stage. OCT4 expression is downregulated during the process of neural differentiation. SOX2 expression remains high in NSC but begins to decline as cells mature to NPC. Nestin is a marker expressed in neural stem and in neural progenitor cells. MAP2 is a marker which is expressed in mature neural cells (FitzPatrick *et al.*, 2018). For further maturation of NSC to NPC, cells were passaged enzymatically for separation and the factor B27 was added to encourage attachment of more mature neural cells to the extracellular matrix and thus to encourage differentiation to a more mature neural phenotype. Terminal differentiation of NPC to neurons varied in success (Figure 41.) and thus was not used to generate cells for investigation of disease. NSC generated from SHEF3 ESC were analysed using immunocytochemistry to confirm expression of immature neural markers SOX2 and nestin (Figure 39., Figure 40.).

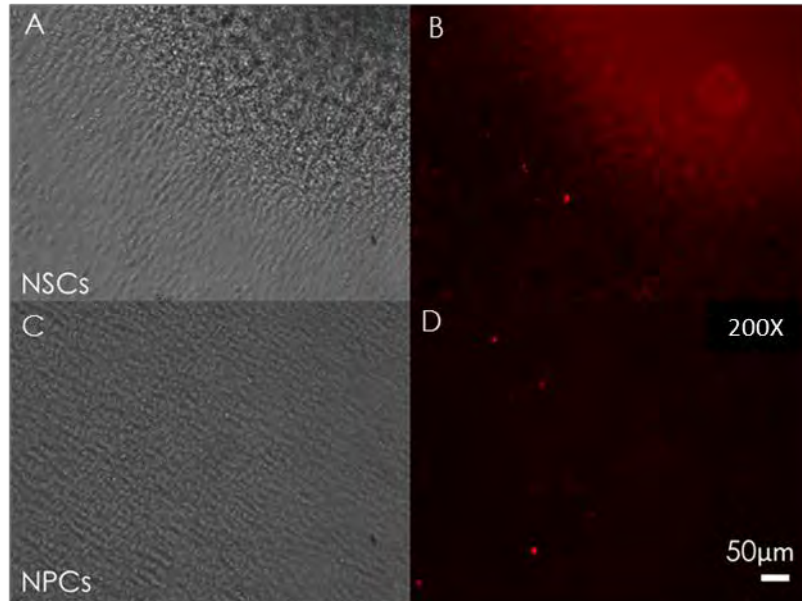


Figure 38. ICC for OCT3/4 expression in SHEF3 NSC and NPC

Staining of NPCs and NSCs for OCT3/4. A.) Phase-contrast image of SHEF3 neural stem cells. B.) SHEF3 Neural stem cells stained for OCT3/4. C.) Phase-contrast image of neural progenitor cells. D.) SHEF3 Neural progenitor cells stained for OCT3/4. OCT3/4 expression appeared to be downregulated as expected during neural differentiation from NSCs to NPCs. All images were taken at 200X magnification using Leica Live Cell Imaging System. Scale bar 50µm.

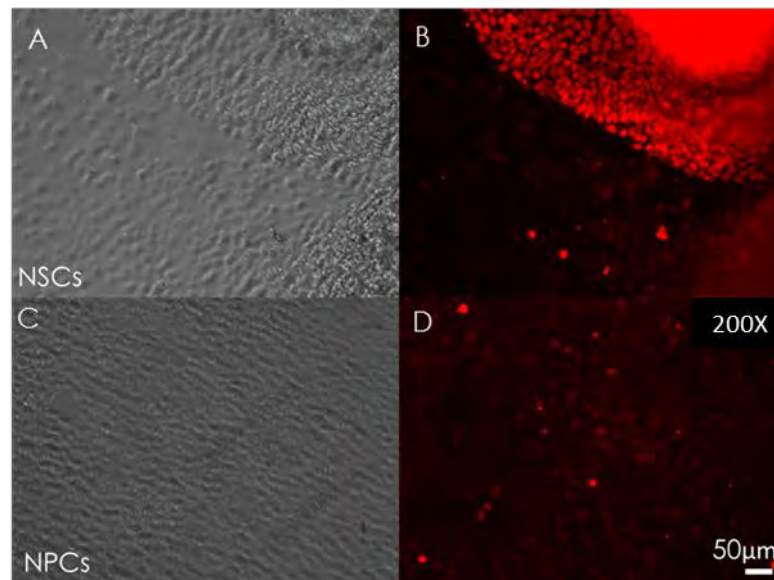


Figure 39. ICC for SOX2 expression in SHEF3 NSC and NPC

Staining of NPCs and NSCs for SOX2. A.) Phase-contrast image of SHEF3 neural stem cells. B.) SHEF3 Neural stem cells stained for SOX2. C.) Phase-contrast image of SHEF3 neural progenitor cells. D.) SHEF3 Neural progenitor cells stained for SOX2. SOX2 expression is downregulated during neural differentiation from NSCs to NPCs. All images were taken at 200X magnification using Leica Live Cell Imaging System. Scale bar 50 μ m.

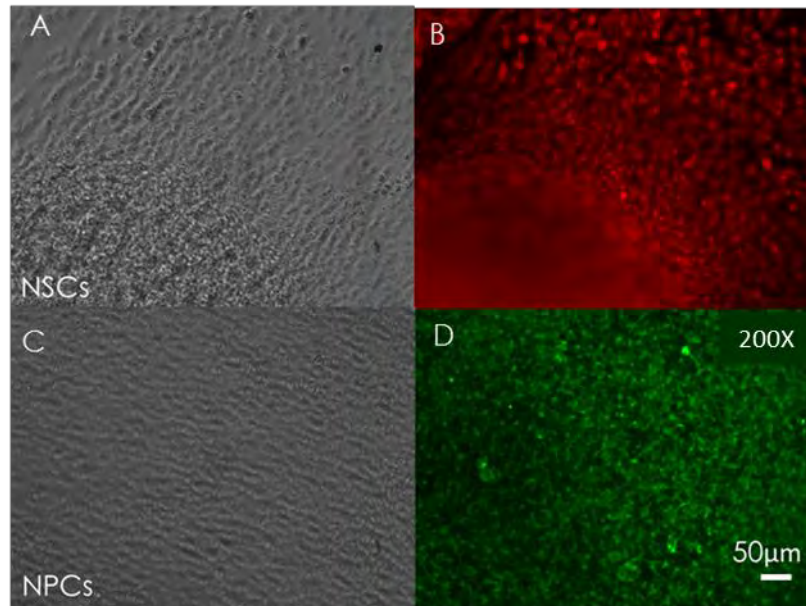


Figure 40. ICC for nestin expression in SHEF3 NSC and NPC

Staining of SHEF3 NPCs and NSCs for nestin. A.) Phase-contrast image of neural stem cells. B.) Neuronal stem cells stained for nestin. C.) Phase-contrast image of neural progenitor cells. D.) Neural progenitor cells stained for nestin. Nestin expression is maintained during neural differentiation from NSCs to NPCs. All images were taken at 200X magnification using Leica Live Cell Imaging System. Scale bar 50 μ m.

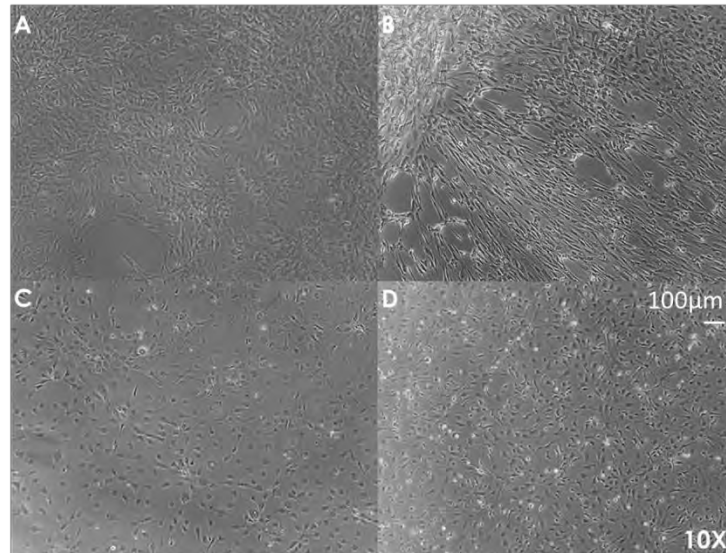


Figure 41. SHEF3 NPC differentiation

A.) Phase-contrast image displaying SHEF3 human NPCs before initiation of neural differentiation. B.) Phase contrast image displaying SHEF3 human NPCs after 14 weeks in terminal differentiation media. C.) Phase contrast image displaying SHEF3 human NPCs after plating at 50,000 cells /cm² in NMM. D.) Phase contrast image displaying SHEF3 human NPCs after plating at 150,000 cells /cm² in NMM. All images were taken at 10X magnification using an EVOS® Digital Microscope.

Results from ICC (Figure 38, Figure 39, Figure 40) display positive staining for nestin and SOX2 in SHEF3 NSC, indicating the presence of cells of an immature neural lineage. The presence of neural rosettes in Figure 37 and Figure 36 also indicated that neural stem cells had been generated in line with the protocol developed by FitzPatrick *et al.*, (2018). This data confirmed that the protocol for neural differentiation could be used for generation of NSC from AD and control iPSC to model AD AHN, and thus to investigate differences in neural specification between AD neural cells and controls, in line with the aims described (1.4).

4.3.9.3 Neural differentiation of *PSEN1* and control iPSC to NSC

After successful differentiation of SHEF3 ESC to NSC and NPC, and validation of the stepwise neural differentiation protocol developed by FitzPatrick *et al.*, (2018),

control and AD iPSC containing mutations *PSEN1* A246E and *PSEN1* M146L were differentiated alongside control iPSC and nHDF iPSC to NSC.(Figure 42. Figure 43.).

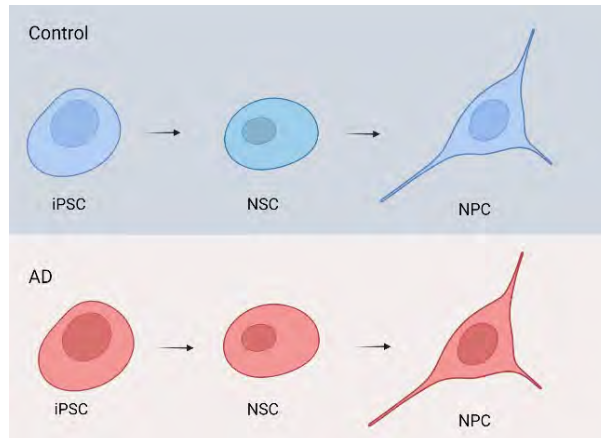


Figure 42. Control and AD neural differentiation to NSC and NPC

Schematic showing control and AD neural differentiation to NSC and NPC. Created in BioRender.com

At P3 post generation of NSC, control, nHDF and *PSEN1* M146L iPSC maintained the ability to generate neural rosettes and tubes, whereas by this stage *PSEN1* A246E NSC had stopped generating neural stem cell rosettes and tubes and had begun to display the presence of neural processes emanating from populations of more immature cells (Figure 43.).

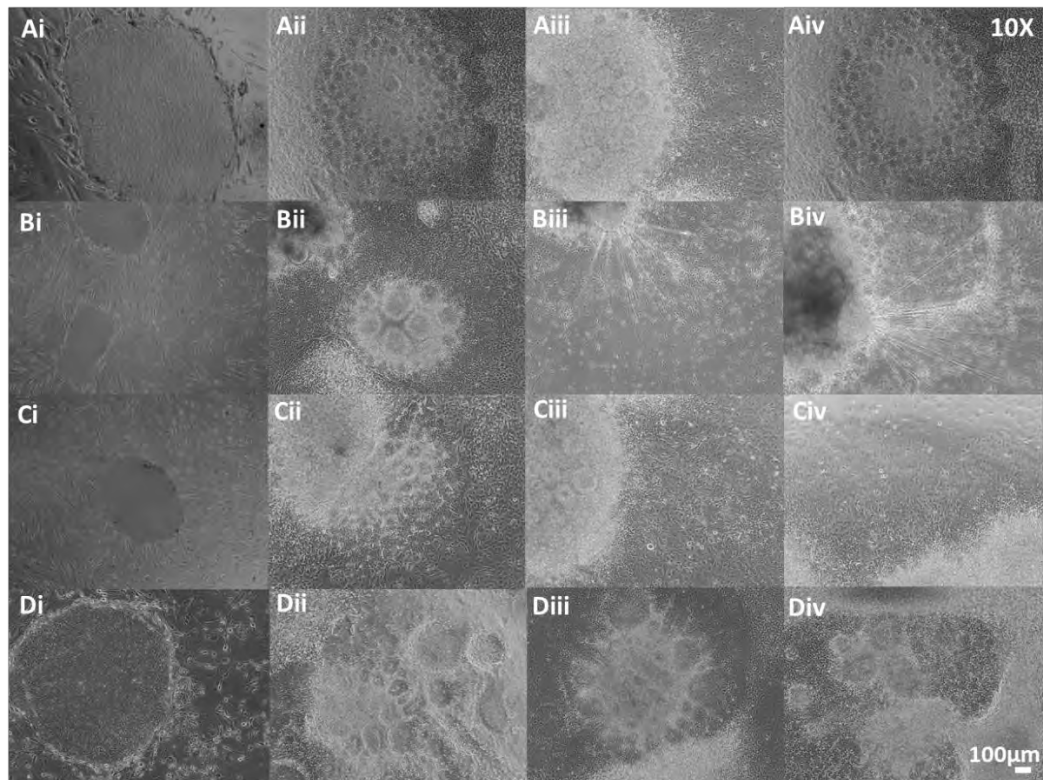


Figure 43. Neural differentiation of *PSEN1* and control iPSC to NSC

Ai-Aiv, display *PSEN1* M146L iPSC undergoing neural differentiation to generate NSC. i.) *PSEN1* M146L iPSC. Aii.) *PSEN1* M146L NSC P2. Aii-Aiv.) *PSEN1* M146L NSC P3. **Bi-Biv** show neural differentiation of *PSEN1* A246E from iPSC to NSC. Bi.) *PSEN1* A246E iPSC. Bii.) *PSEN1* A246E NSC P2. Bii-Biv.) *PSEN1* NSC P3. **Ci-Civ** display neural differentiation of control iPSC to NSC Ci.) control iPSC. Cii.) control NSC P2. Ciii-Civ.) control NSC P3. **Di-Div** show neural differentiation of nHDF iPSC to NSC. Di.) nHDF iPSC. Dii.) nHDF NSC P2. Diii-Div.) nHDF NSC P3. All images were taken at 10X magnification using an EVOS® Digital Microscope.

4.3.9.4 Neural differentiation to NPC

NSC were further differentiated to generate NPC (Figure 44.). This process was used in later experiments to investigate differences between control and *PSEN1* NPC.

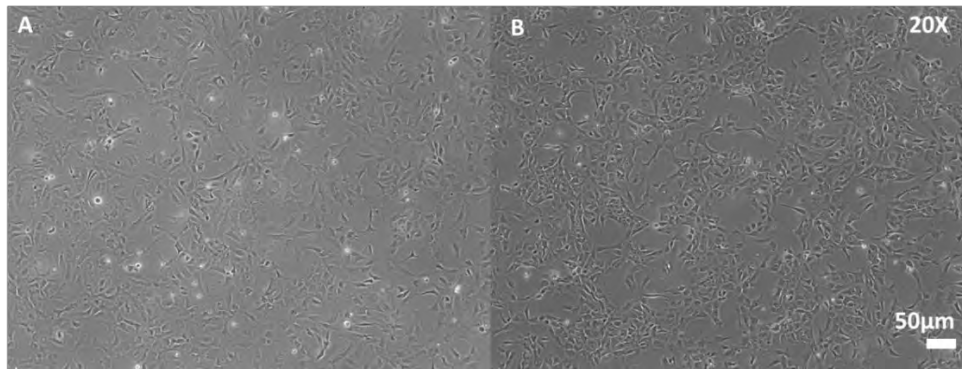


Figure 44. Neural differentiation to NPC

A.) *PSEN1* A246E NPC. B.) control NPC. All images were taken at 20X magnification using an EVOS® Digital Microscope.

4.3.9.5 Validation of *PSEN1* and control NSC and NPC

control NSC, *PSEN1* A246E NSC and *PSEN1* M146L NSC generated using the neural differentiation protocol specified in 4.1.7 were stained for SOX2 and nestin for validation of NSC phenotype and to highlight the neural rosette structures which are characteristic of NSC (Figure 45.). Neural stem cells generated were stained with SOX2 and nestin, which are both markers of early neural stem cells. All *PSEN1* and control NSC stained positive for both SOX2 and nestin, indicating that they were immature neural cells. Co-staining of nestin and SOX2 also functioned to display neural tubes and rosettes, visualisation of these structures was used to further confirm that the cell populations were in the NSC stage of neural differentiation. Figure 45.

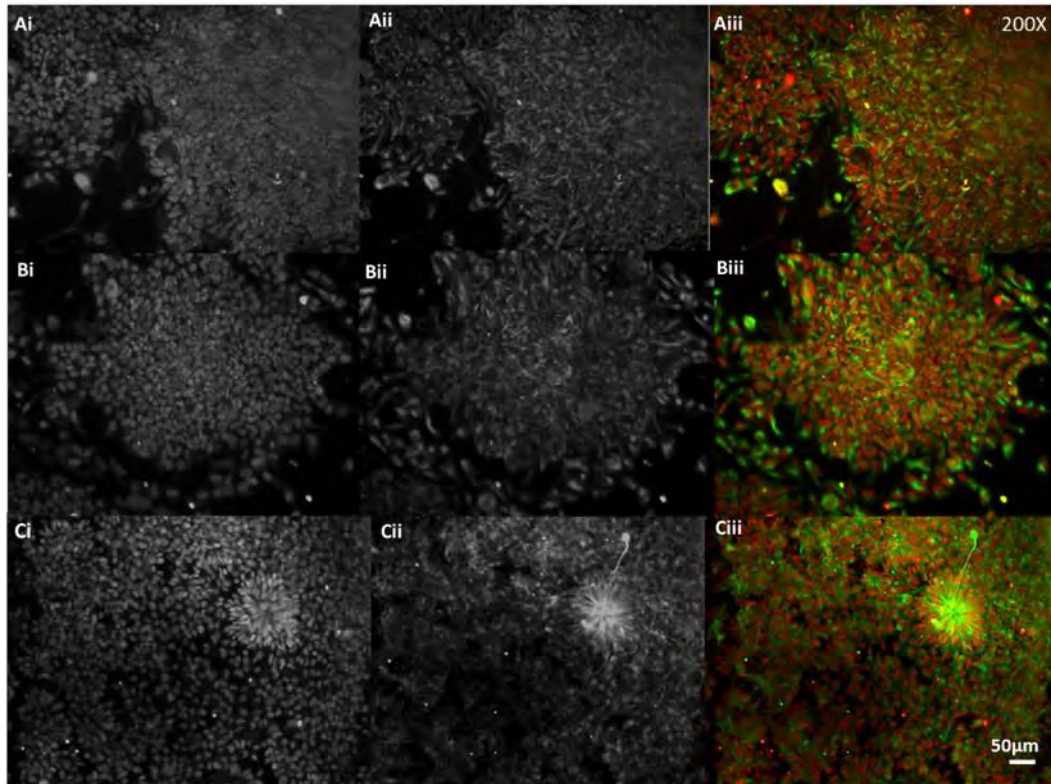


Figure 45. ICC for SOX2 and nestin in *PSEN1* and control NSC

PSEN1 and control NSC stained positive for expression of SOX2 and nestin. Ai.) control NSC stained positive for SOX2, Aii.) control NSC stained positive for nestin. Aiii.) Neural rosettes visible in control NSC with co-staining of SOX2 (red) and nestin (green). Bi.) *PSEN1* A246E NSC stained positive for SOX2. Bii.) *PSEN1* A246E NSC stained positive for nestin. Biii.) Neural rosettes visible in *PSEN1* A246E NSC with co-staining of SOX2 (red) and nestin (green). Ci.) *PSEN1* M146L NSC stained positive for SOX2. Cii.) *PSEN1* M146L NSC stained positive for nestin. Ciii.) Co-staining of *PSEN1* 146L NSC with SOX2 (red) and nestin (green) displays neural rosettes. All images were taken at 200X magnification using Leica Live Cell Imaging System. Scale bar 50µm.

4.3.9.6 Flow cytometry to assess nestin expression in *PSEN1* and control NSC and NPC

Nestin expression in *PSEN1* A246E NSC at P2 and at P3 was assessed using flow cytometry. Flow cytometry was employed to confirm and compare expression of nestin in *PSEN1* and control NSC and NPC. On average, at P2, 98.9 % of *PSEN1* NSC studied were nestin positive and at P3, 97.9% of *PSEN1* NSC were nestin positive (Figure 46). Analysis of this data using an unpaired t-test in GraphPad 9.2.0

revealed no significant difference, but a trend towards downregulated expression of nestin ($p=0.0562$) from P2 to P3. This data shows that at P2 and P3, post generation of NSC, >97% of cells were positive for nestin, and indicates that at this stage in the neural differentiation process, they are immature neural cells. This data also indicates a trend towards declining nestin expression from the NSC to NPC stage, which is in accordance with data generated by FitzPatrick *et al.*, (2018).

Nestin expression in PSEN1 NSC

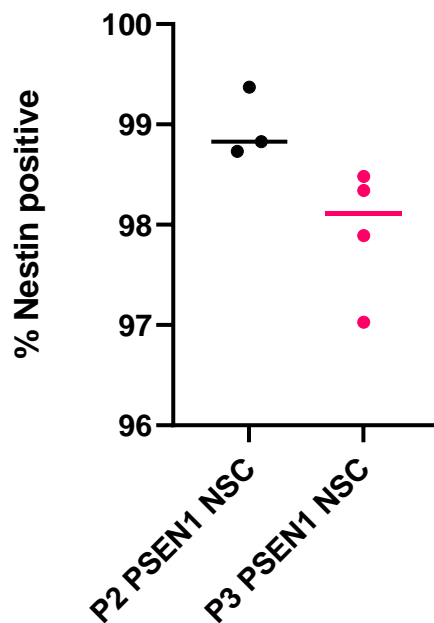


Figure 46. Percentage of Cells which stained positive for nestin expression in *PSEN1* P2 and *PSEN1* P3 NSC

Flow cytometry was used to assess the percentage of cells expressing nestin in *PSEN1* NSC at P2 and P3. Results showed that on average 98.9% of P2 NSC studied were nestin positive and 97.9% of P3 NSC were nestin positive. Differences in the percentage of cells which stained positive for nestin expression were analysed using an unpaired t-test in GraphPad Prism version 9.2.0 for Windows. Results indicate no significant difference in nestin expression between *PSEN1* and control NSC ($p= 0.0562$).

Flow cytometry data (Figure 47) displays the percentage of cells which stained positive for nestin in control and *PSEN1* NPC. control NPC on average were 90.2%

positive for nestin, whereas *PSEN1* NPC were on average only 82.8% positive for nestin. There was no significant difference in nestin expression between samples, but a trend towards reduced expression of nestin in *PSEN1* NPC compared with control NPC ($p=0.0508$). Results indicate that at the NPC stage in the neural differentiation protocol carried out, cells are still highly expressing nestin and thus remain as immature neural cells. The trend towards reduced nestin expression in *PSEN1* NPC compared with control NPC is suggestive of premature differentiation in neural cells containing the *PSEN1* A246E mutation.

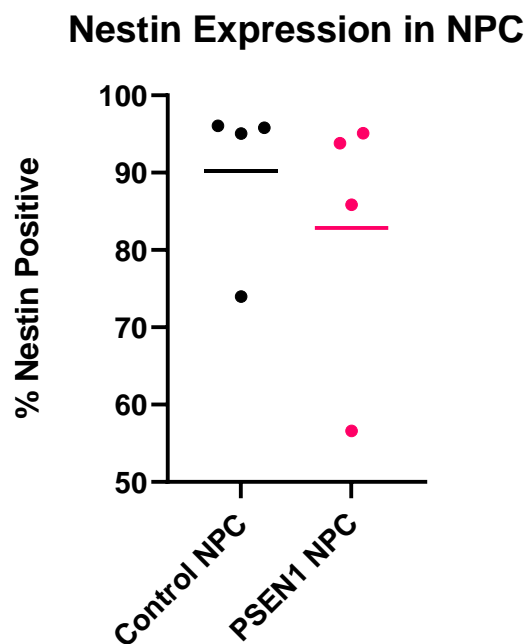


Figure 47. Nestin expression in *PSEN1* and control NPC

Flow cytometry was used to measure nestin expression in control and *PSEN1* NPC. Results showed that on average 90.2 % of control NPC studied were nestin positive and 82.8% of *PSEN1* A246E NPC were nestin positive. Differences in nestin expression were analysed using an unpaired t-test in GraphPad Prism version 9.2.0 for Windows. Results indicate no significant difference in nestin expression between *PSEN1* and control NPC ($p= 0.0508$).

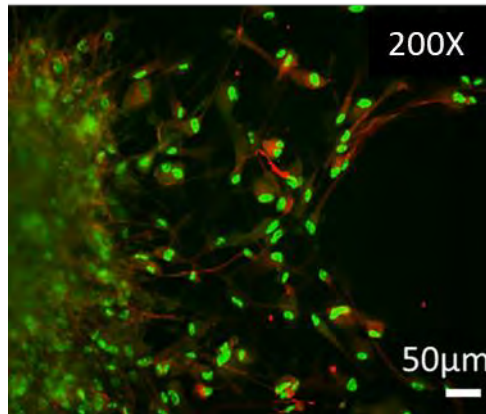


Figure 48. Staining for mature neural markers

PSEN1 NPC were matured further and stained for cytoplasmic β -III tubulin (red), and the neuronal nuclear protein NeuN (green). Positive staining of *PSEN1* derived neural cells with β -III tubulin and NeuN indicates that NSC generated are capable of developing to mature neural cells. Images taken at 200X using Leica Live Cell Imaging System. Scale bar 50 μ m.

4.3.9.7 Generation of neurospheres

Neurospheres were generated from control and *PSEN1* iPSC for further investigation of AD neural differentiation capacity using 3D cell culture (Figure 49). Neurospheres are multicellular organoids that contain a heterogenous cell population which don't differentiate simultaneously through the different states of maturity. The aim of using neurospheres was to enable immature neural cells to undergo untargeted differentiation, to determine if neural cells containing the *PSEN1* mutation were pushed by intra/extracellular signalling to differentiate into different neural cell types. The neurospheres generated were to be analysed on a single cell basis to determine the effect of *PSEN1* mutation on neural differentiation.

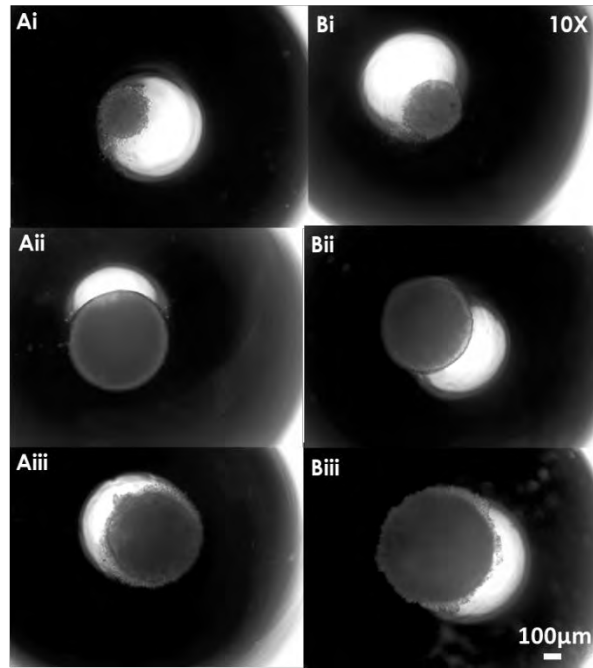


Figure 49. Generation of neurospheres

All images were taken at 10X magnification using an EVOS® Digital Microscope. Ai.) control neurosphere at day 7. Aii.) control neurosphere day 11. Aiii.) control Neurosphere day 21. Bi.) *PSEN1* A246E neurospheres at day 7. Bii.) *PSEN1* A246E neurospheres at day 11. Biii.) *PSEN1* A246E neurospheres at day 21. All images were taken at 10X magnification using an EVOS® Digital Microscope.

Neurospheres generated stained positive for the immature neural marker SOX2 (Figure 50) indicating that they were expressing immature neural markers. Preliminary investigation of transcriptomic changes between *PSEN1* and control neurospheres was carried out using qPCR, however, as neurospheres were to be cultured for a minimum of 21 days before material was taken for analysis, it was determined that generation of sufficient material for investigation would take too long, and further data collection was carried out using neural stem and progenitor cells generated using 2D cell culture.

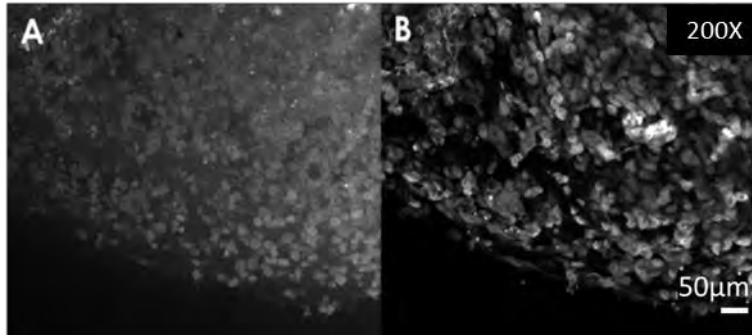


Figure 50. Control neurosphere stained for DAPI (A), SOX2 (B)

Immunocytochemistry was used to interrogate SOX2 expression in control and *PSEN1* neurospheres. SOX2 is a marker which is present in ESC and NSC but is lost by the NPC stage of neural differentiation. Positive staining for SOX2 indicated that at day 11, the neurospheres contained a population of immature neural stem cells. Images taken using an EVOS® Microscope at 200X magnification.

4.3.9.8 Chapter summary

The results from this chapter indicated that control and *PSEN1* iPSC expressed pluripotency factors and were capable of generating cells from endodermal, ectodermal, and mesodermal lineages. Analysis of control and *PSEN1* NSC and NPC confirmed expression of neural precursor markers. All NSC generated neural rosettes and tube structures and expressed SOX2 and nestin. Greater than 97% of *PSEN1* NSC were expressing nestin and greater than 80% of *PSEN1* and control NPC were positive for nestin expression, validating both populations as immature neural cells. The average percentage of nestin positive cells was higher in NSC (98.4%) than in NPC (86.5%) indicating that nestin expression is downregulated as NSC mature to NPC. The percentage of nestin positive *PSEN1* NSC was higher in P2 than in P3 NSC ($p=0.0562$), further indicating that nestin expression is downregulated during neural differentiation. The percentage of nestin positive cells was lower ($p=0.508$) in *PSEN1* NPC compared with control NPC, indicating that *PSEN1* NPC were maturing at a faster rate than control NPC.

5.0 Investigation of AD neurogenesis

5.1.0 Introduction

Neural specification may be directed by different mechanisms, one of which is the shift between symmetric and asymmetric cell division (1.2.2) (Chen *et al.*, 2016; Venkei and Yamashita., 2018). NSC in the niche generally remain in a state of quiescence but can divide by symmetric cell division to generate two immature daughter cells, this method of cell division can help to maintain NSC numbers in the niche. NSC can also be directed by intrinsic or extrinsic factors to divide via asymmetric cell division, leading to one daughter cell acquiring a more mature fate and leaving the NSC niche. The cytoskeleton plays an important role in regulation of cell fate; distribution of cell molecular components between daughter cells is carried out by the mitotic spindle and can tip the scales to push cells towards asymmetric cell division, leading to cell specification (Smith *et al.*, 2017). Cytoskeletal structures may determine cell fate, function, and shape (Fletcher and Mullins., 2010) and the neuronal cytoskeleton is of vital importance in regulating neural cell proliferation, migration and, most importantly, cell specification (Wilhelmsson *et al.*, 2019).

5.1.1 The cytoskeleton

The cytoskeleton is a vital component of eukaryotic cells and regulates cell morphology, motility, spatial organisation, and translocation of intracellular materials, it is composed of a network of regulatory and filamentous proteins. Cytoskeletal molecules can be categorised as microtubules, microfilaments, and intermediate filaments. Molecules classed as microtubules include microtubule associated proteins (MAPs) and β -III tubulin. Intermediate filaments include neurofilaments, lamins, nestins, vimentin and glial fibrillary acidic protein (GFAP). Microfilaments include β -actin and myosin. Cytoskeletal molecules that cannot be categorised into one of those groups include cellular adhesion molecules and catenins such as β -catenin (Figure 51) (Ong *et al.*, 2020).

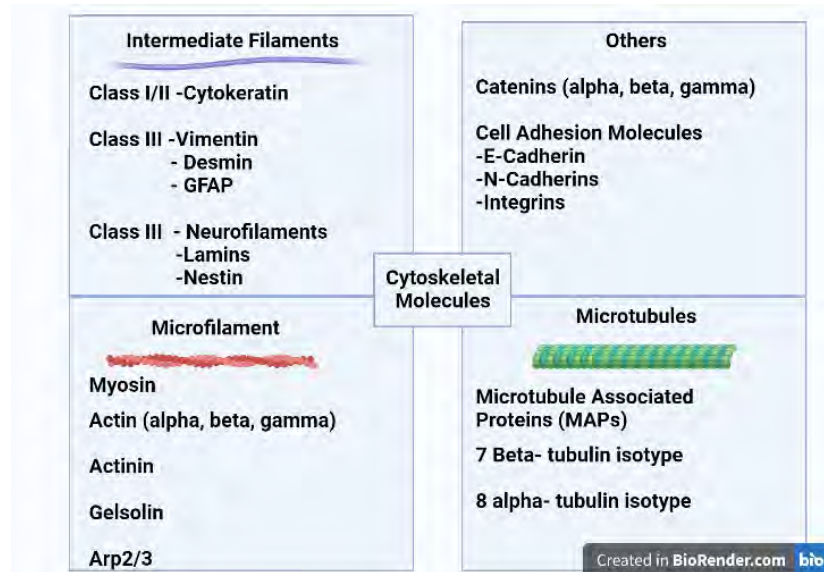


Figure 51. Categorisation of cytoskeletal molecules

Cytoskeletal molecules categorised as microtubules, microfilaments, or intermediate filaments. Cellular adhesion molecules, catenins and actin-related proteins are also cytoskeletal molecules but do not fit into the three primary groups specified (Ong *et al.*, 2020). Figure created in Biorender.com.

The neuronal cytoskeleton is composed primarily of microtubules, intermediate filament proteins and actin filaments. Polymerisation and depolymerisation of microtubules and actin filaments drives morphological changes and guides intracellular organisation. Mature neurons have a membrane-bounded axon which extends from the neural cell body and facilitates transport of signals and materials from the cell body to the axon terminals at the synapse. Neurofilaments are a type of intermediate filament found in neurons, they are present within the axon and form a structural matrix in which microtubules are embedded (Fletcher and Mullins., 2010). Intermediate filaments are expressed in a cell type specific manner, changes in cell phenotype during differentiation can be marked by transition from one intermediate filament type to another, one example of this is the downregulation of nestin expression as NPC mature to neurons (Bernal and Arranz., 2018, FitzPatrick *et*

al., 2018). For this reason, the cytoskeletal molecules expressed by neural cells can be used to determine their stage in neural differentiation.

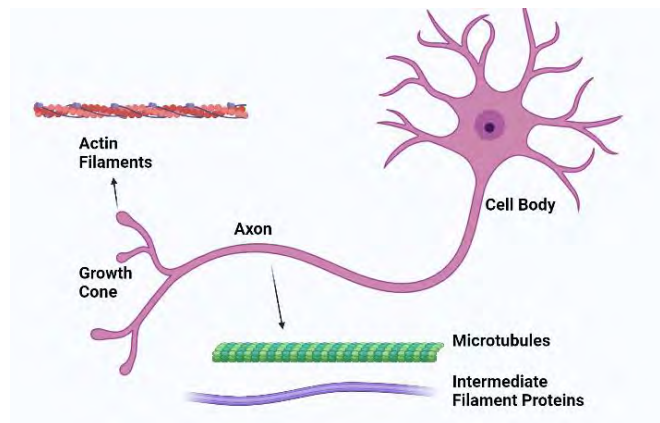


Figure 52. Cytoskeletal components in neurons

Cartoon of a mature neuron displaying the cell body, axon, and growth cone. During neuronal development, the growth cone responds to chemical cues to determine neuronal migration. The cytoskeleton of neurons is made up of microtubules, intermediate filament proteins and actin filaments (Fletcher and Mullins., 2010, Rochlin *et al.*, 1999). Figure created in Biorender.com.

5.1.2 Markers of neural differentiation

Nestin is a cytoskeletal type VI intermediate filament protein which is expressed during the early stages of neural development in mammals (Bernal and Arranz., 2018). Nestin is expressed in neuroepithelial cells and is considered to be a marker of neural stem cells (Lendahl *et al.* 1990; Doetsch *et al.* 1997; Mignone *et al.* 2004, Wilhelmsson *et al.*, 2019). Nestin expression is high in NSC and NPC stages (Bernal and Arranz., 2018) but is replaced by tissue specific intermediate filament proteins as NPC mature to neurons (FitzPatrick *et al.*, 2018). Nestin is expressed in progenitor cells throughout the body, for example, in skin derived precursor cells and in progenitor cells found in the heart and testis, however, nestin is primarily expressed by neural precursor cells. Immature neural cells which express nestin include glial cells such as astrocytes and radial glia as well as NSC and NPC (Bernal and Arranz., 2018, Filippov *et al.* 2003). Intermediate filament proteins, including nestin share a common structure consisting of a central rod domain, an N-terminus head, and a C-

terminus tail. The central rod domain consists of α -helices and is surrounded by a globular head and tail. In Vimentin monomers, the N-terminal head is about 100 amino acids, and the C-terminal tail is about 400 amino acids in length. In nestin, the N-terminal is about 8 amino acids in length and the C-terminal is greater than 1400 amino acids in length. The short N-terminus of nestin prevents its self-assembly so nestin requires other intermediate filaments such as Vimentin to assemble and form dimers (Bernal and Arranz., 2018). Through its position in the cytoskeleton, nestin plays a role in cellular migration, self-renewal, and differentiation. In adult mice, nestin has been shown to play an important role in regulating neurogenesis via Notch signalling (Wilhelmsson *et al.*, 2019). Wilhelmsson *et al.*, (2019) investigated the effect of nestin deficiency on neurogenesis in adult mice. Nestin deficiency did not result in altered proliferation of NPC but did result in enhanced neurogenesis in the DG of the hippocampus. The increase in hippocampal neurogenesis appeared to be caused by nestin deficiency in the NSC niche. Notch signalling was downregulated in nestin deficient astrocytes suggesting that nestin negatively regulates cell survival and neuronal differentiation through its role in Notch signalling. In behavioural studies in adult mice, nestin deficiency was associated with impaired long-term memory (Wilhelmsson *et al.*, 2019).

High levels of microtubule associated proteins (MAP) MAP1, MAP2 and Tau are expressed almost exclusively by neurons, they have a role in stabilising cytoskeletal microtubules and are thought to regulate microtubule networks in neuronal axons and dendrites (Dehmelt and Halpain). MAP interact with tubulin to promote its assembly into microtubules and to stabilise the microtubule network (Iqbal *et al.*, 2010). In mammals, there are two groups of isoforms of MAP2 which are formed by alternative splicing, these are grouped into isoforms with a higher molecular weight (280-270 kDa), termed MAP2a and MAP2b and those with a lower molecular weight (70-75 kDa), termed MAP2c and MAP2d. All isoforms of MAP2 have a proline -rich domain, a tubulin binding domain (made up of 3-4 repeats of 18 amino acids at the C-terminal domain) and have similar N and C-terminal regions. In immature neurons,

MAP2b, MAP2c and MAP2d are the most highly expressed isoforms, whereas in mature neurons, isoforms MAP2a and MAP2d are found at higher concentrations. MAP2 isoforms are able to bind with the C-terminal of tubulin via their proline-rich domain tubulin binding domain, this results in an increase in the rigidity of microtubules, enabling the formation of long neural processes. Due to its structural role in neural cell maturation, MAP2 can be used as an indicator of the functional state of neurons and a marker of differentiation to more mature neural cell types (Korzhevskii *et al.*, 2012). Increased expression of MAP2 during neural differentiation may even play a role in reducing levels of self-renewal as neurons mature. Soltani *et al.*, (2005) showed that expression of MAP2 was induced in primary cutaneous melanoma but was absent in metastatic melanoma, suggesting a role for MAP2 in preventing metastasis. Expression of MAP2 in metastatic melanoma cell lines resulted in stabilisation of microtubules, reduced growth, and cell cycle arrest in G2-M phase and (Soltani *et al.*, 2005).

SOX2 is a marker of neurons in the earliest stages in development and is highly expressed in NSC. Expression of SOX2 and nestin is retained in the postnatal subventricular zone (SVZ) and hippocampal DG Expression of SOX2 is required for NSC self-renewal and maintenance but also plays a dose-dependent role in regulating differentiation to neuronal sub-types. In retinal progenitor cells, SOX2 dosage determined the temporal and spatial regulation of cellular differentiation (Pevny and Nicolis., 2010, Taranova *et al.*, 2006). Defective neural proliferation and differentiation may play a role in the aetiology of neurodegenerative disease; deletion of a neural cell enhancer from SOX2 in mouse models resulted in cerebral malformations such as epilepsy, neuronal abnormalities, such as the presence of protein aggregates in the cytoplasm and cellular degeneration and resulted in the downregulation of self-renewal and differentiation in neuronal precursor cell populations (Ferri *et al.*, 2004). In human glioma cell lines, downregulation of SOX2 via overexpression of SOX21 or using siRNA against SOX2 resulted in an increase in apoptosis (Ferletta *et al.*, 2011).

5.1.3 Self-renewal and differentiation in neural precursors

In the rodent CNS, neurons are derived from three types of neural stem and progenitor cells- basal progenitors, radial glial cells and neuroepithelial cells. Basal progenitors and radial glial cells undergo symmetric neurogenic division, neuroepithelial cells undergo symmetric proliferative division and neuroepithelial cells and radial glial cells undergo asymmetric neurogenic cell division (Gotz and Huttner 2005). In mammals, during the prenatal period, precursor cells in the germinal zone are actively generating new neurons (Wilhelmsson *et al.*, 2019). During embryonic and postnatal periods in mammals, there are high levels of cell division, after which, levels of cell proliferation decline in all tissues except for areas in which long-lived tissue stem cells are maintained (Urbán *et al.*, 2019). The rate of neurogenesis is reduced in the adult mammalian brain, but low levels of neurogenesis persist in areas such as the SVZ of the lateral ventricles and the SGZ of the DG of the hippocampus (Wilhelmsson *et al.*, 2019, Ming and Song 2011, Gotz and Huttner 2005). Post specialisation, the majority of neuronal cells in the mammalian brain are maintained in a state of quiescence, also known as reversible cell cycle arrest (Joseph *et al.*, 2020, Urbán *et al.*, 2019). NSC in the adult mammalian brain are capable of proliferation and differentiation but are located in specialised environments called niches, where they are exposed to signals that generally maintain their quiescence. Changes in the local signalling environment can activate NSC to re-enter the cell cycle and take on a proliferative state (Urbán *et al.*, 2019). Maintenance of NSC reserves and the ability to generate new neurons is dependent on the rate of neurogenesis, which is in turn dependent on the balance between NSC quiescence and activity (Urbán *et al.*, 2019). The transcriptomic profiles of NSC are altered with age; with an increase in age, quiescence is increased to reduce total depletion of the NSC niche (Kalamakis *et al.*, 2019). NSC quiescence is maintained by the niche in older brains via increased inflammation and regulation of Wnt activity. The shift from activation to quiescence in NSC with age is associated with a reduction

in non-canonical Wnt signalling and an increase in inflammation (Kalamakis *et al.*, 2019).

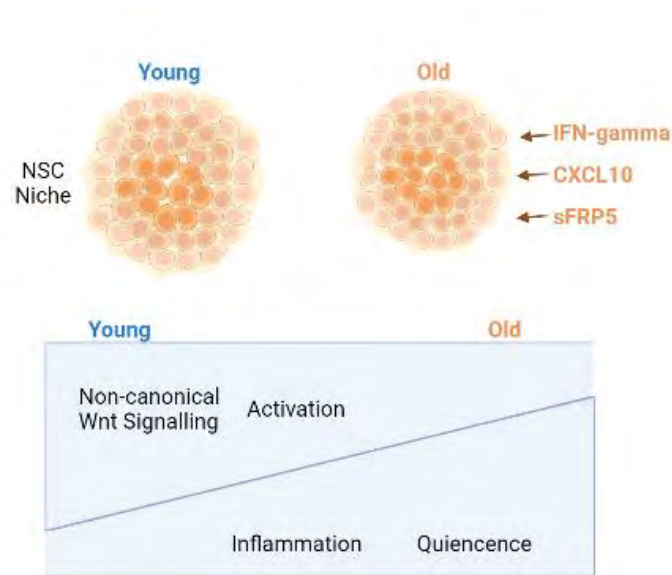


Figure 53. Effects of ageing on the NSC niche

With an increase in age, quiescence is increased in the NSC niche and activation of neural stem cells is decreased to prevent total exhaustion of the NSC niche. With age, there is also a reduction in non-canonical Wnt signalling and an increase in exposure to more inflammatory factors such as IFN-gamma (Kalamakis *et al.*, 2019). Figure created in Biorender referencing data generated by Kalamakis *et al.*, (2019).

Quiescent NSC in the niche can be primed to enter the cell cycle via external stimuli, such as pro-inflammatory mediators. Although pro-inflammatory cytokines can activate NSC, they are generally shown to impair successful neurogenesis, for example, Interleukin-6 and Interleukin-1 β have been described as negative regulators of NSC proliferation (Brett *et al.*, 1995, Kokovay *et al.*, 2012, Belenguer *et al.*, 2021). In mouse models, induction of peripheral inflammation led to the transient activation of primed NSC, occurring via interaction of TNF- α with its receptor TNF receptor 2. Activated NSCs were then returned to quiescence via TNF receptor 1 - dependent signalling, suggesting opposing roles for inflammatory mediators in priming NSC to enter the cell cycle (Belenguer *et al.*, 2021). NSC in a proliferative

state spend approximately 3 hours in G1 phase, and time spent in G1 phase increases by 4-fold as NSC switch to a differentiative phenotype. Inhibition of Cyclin E in these cells led to an extended G1 phase and an earlier switch to a differentiative phenotype. The extended G1 phase may enable intracellular accumulation of transcription factors which induce differentiation (Lange and Calegari., 2010, Lange *et al.*, 2009, Ruijtenberg *et al.*, 2016). Intrinsic factors which regulate cell differentiation and proliferation include SOX2, basic helix -loop-helix Hes genes and small RNA modulators. Extrinsic factors which regulate NSC proliferation and differentiation include Wnt and Notch signalling, TGF α , FGF, EGF and Sonic hedgehog signalling (Shi *et al.*, 2007).

As cell cycle regulation can determine the rate of proliferation and differentiation, cell cycle dysregulation plays a role in the pathogenesis of neurodegenerative disorders. Aberrant cell cycle activation in neurons can be caused by oxidative stress, DNA damage, toxic levels of peptide accumulation and the deprivation of growth factors. Increased intracellular levels of cyclin, proliferating cell nuclear antigen, cyclin-dependent kinases (CDKs) and a decrease in CDK inhibitors can lead to hyperphosphorylation of retinoblastoma protein (Rb) and the release of E2 transcription factor (E2F) which initiates DNA transcription for upregulation of DNA replication. If cells which have undergone DNA replication are not exposed to mitotic signals such as cell division cycle 2 and cyclin A, they do not exit the cell cycle. Duplication of genetic material without the induction of mitosis can result in molecular flaws and the induction of apoptosis, as well as an increase in markers associated with the response to cell stress (Urbán *et al.*, 2019, Joseph *et al.*, 2020).

Inflammation can influence NSC cell cycle re-entry and neuronal specification, (Kalamakis *et al.*, 2019) and may be upregulated in AD by the accumulation of intracellular waste products, caused by impairments in autophagic processing.

5.1.4 Autophagy, inflammation, and the antioxidant response

Neurodegenerative disorders commonly present with chronic inflammation, a decline in the generation of functional neurons as well as impaired autophagy and altered p62 expression (Vivar, 2015; François *et al.*, 2013). Autophagy is an intracellular clearance process by which unwanted and ubiquitinated proteins, as well as damaged organelles, are degraded and recycled (Nixon, 2013). Autophagy regulates cellular homeostasis under nutrient-rich conditions and promotes cell survival during nutrient deprivation (Huang and Liu, 2015). The mammalian target of rapamycin (mTOR) regulates metabolism, translation, and growth as well as proliferation, differentiation, migration, and the formation of dendrites in neural cell types (LiCausi and Hartman). During nutrient depletion, mTOR is inhibited, and the Unc-51-like kinase (ULK)1/2 complex is activated, this induces formation and elongation of the isolation membrane; a membrane which selectively and non-selectively envelopes cytosolic contents for degradation during autophagy (Tooze and Yoshimori, 2010; Kiriyaama and Nochi, 2015).

In neurons, autophagy is the principle mechanism for turnover of unwanted substrates, thus in AD, and other neurodegenerative diseases, defects in autophagic processing can lead to the intraneuronal accumulation of waste products such as A β and proteins such as p62 (Bordi *et al.*, 2016; Brandenstein *et al.*, 2016). p62 is a scaffold protein with a role in regulating key molecular pathways such as autophagy, inflammation, and antioxidant response pathways. p62 regulates the antioxidant response and inflammation in part by indirect interactions with transcription factors NRF2 and NF κ B. p62 binds keap1 via its keap1 interacting region (KIR) and thus, competes with NRF2 for keap1 binding, releasing NRF2 for nuclear translocation and activation of antioxidant response genes (Liu *et al.*, 2016). The N-terminal Phox-BEM1 (PB1) domain of p62 enables its homo-oligomerisation with other molecules of p62 and hetero-oligomerisation with kinases including protein kinase C (PKC), which can then regulate NF κ B signalling and downstream inflammation (Liu *et al.*, 2016). Chronic inflammation exacerbates AD pathology (Wang *et al.*, 2017) and may result

from the accumulation of p62 and subsequent dysregulation of inflammatory and antioxidant response pathways.

5.2 Aims

After generation of models for investigation of FAD as described in 4.0, preliminary work was carried out with the aim to investigate neural differentiation capacity in control and *PSEN1* neural cells as described in 1.4. The purpose of this was to determine if this cellular model would display differences between AD and control neural specification, thus differences in proliferation, growth, cell specification, and cell cycle were to be investigated. Pathways such as inflammation, cell stress and autophagy were also to be investigated to determine if AD NSC presented with increased inflammation, cell stress and impaired autophagy, all of which are patterns that have been associated with AD in numerous publications (Bordi *et al.*, 2016; Brandenstein *et al.*, 2016; Vivar, 2015; François *et al.*, 2013; Urbán *et al.*, 2019; Joseph *et al.*, 2020).

This chapter aimed to repeatedly differentiate control and *PSEN1* iPSC simultaneously to NSC and NPC to generate material for analysis, the material was to be used for analysis of differences between control and *PSEN1* NSC. As described in 4.0, *PSEN1* and control iPSC were simultaneously differentiated to generate NSC and NPC. For interrogation of *PSEN1* neural specification:

- qPCR was to be used to investigate markers related to proliferation and neural specification to understand if these differed between *PSEN1* NSC and controls, and to determine if *PSEN1* NSC were more pre-disposed to differentiate prematurely compared with controls.
- Flow cytometry was to be used to investigate the percentage of cells in different stages of the cell cycle, to investigate whether *PSEN1* NSC were more likely to be entering the cell cycle and leaving the state of quiescence in which NSC in the stem cell niche typically reside.

- qPCR was also to be used to measure expression of markers related to inflammation, cell stress and autophagy to determine if these were altered as expected in *PSEN1* NSC compared with control NSC.

5.3 Results

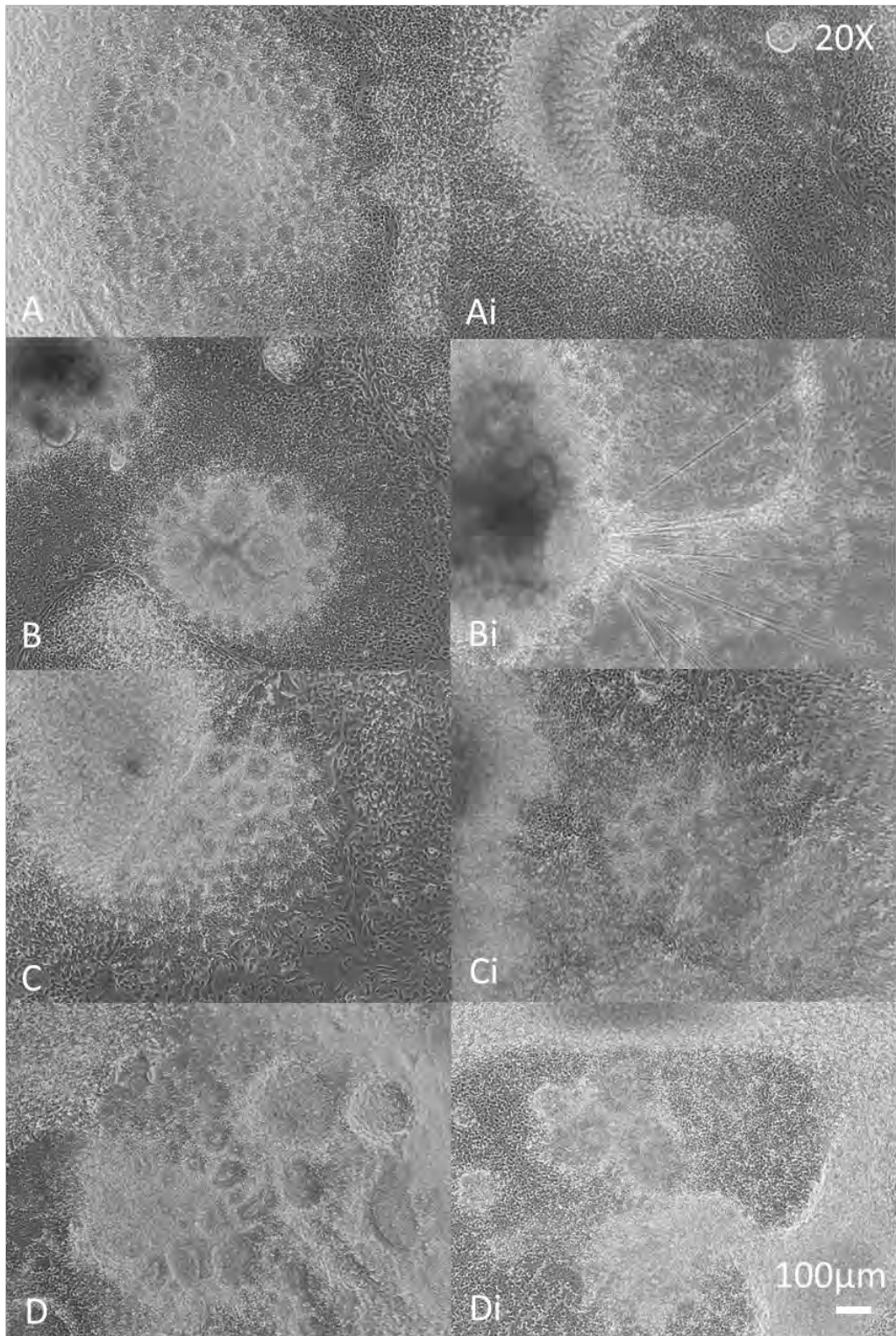
NSC containing the *PSEN1* A246E mutation were repeatedly less capable of proliferating to generate more progeny and displayed smaller and fewer neural stem cell rosettes (Figure 54.). NSC which contained the *PSEN1* A246E mutation also displayed neural-like processes stretching across the cell culture plate. These phenotypic changes suggested that *PSEN1* A246E were primed to differentiate prematurely when compared with control NSC. To work towards elucidating the causes of this premature neural differentiation, RNA was extracted from control and *PSEN1* NSC at P2 and P3 and qPCR was used to analyse markers related to aberrant neural differentiation, these included markers of normal neural differentiation, proliferation, inflammation, cell stress and autophagy. Preliminary analysis of autophagy in *PSEN1* A246E NSC indicated a trend towards downregulation of autophagy related markers Beclin-1, MTOR and LC3 compared with controls, and a trend towards upregulation of P62 expression compared with controls (Figure 55 A). Preliminary analysis of autophagy related gene expression in *PSEN1* M146L displayed a trend towards upregulation of Beclin-1, MTOR and LC3 when compared with controls (Figure 55 B). These results indicated that there were variations in autophagy between NSC containing different *PSEN1* mutations. Altered Wnt signalling in *PSEN1* NSC was investigated using probes for expression of LEF-1, CTNNB1, GSK3-beta, *AXIN2* and JAG1. Data displayed a trend towards increased expression of Wnt-related markers LEF-1, CTNNB1, GSK3-beta and *AXIN2* in both *PSEN1* A246E NSC and *PSEN1* M146L when compared with controls (Figure 56 A, Figure 56 B). Data also displayed a trend towards downregulated expression of JAG1 in *PSEN1* A246E NSC and a trend towards upregulated expression of JAG1 in *PSEN1* M146L NSC when compared with controls.

Gene expression related to different signalling pathways varied between the two different *PSEN1* mutations, (Figure 55, Figure 56) for that reason, further experiments were carried out using only *PSEN1* A246E NSC and control NSC. NSC and neurosphere models were compared to investigate the effect of different culture methods on the detection of differences between *PSEN1* and control immature neural cell populations (Figure 57, Figure 58) Analysis of inflammation and the antioxidant response in *PSEN1* NSC and neurospheres indicated little difference between *PSEN1* A246E NSC and control NSC. In *PSEN1* neurospheres, however, there was a trend towards upregulation of NRF2, HIF, *NQO1* and STAT3 compared with control neurospheres (Figure 57). Preliminary analysis of markers of neural differentiation was carried out in *PSEN1* A246E NSC and *PSEN1* A246E neurospheres. Results displayed a trend towards upregulated MAP2 and nestin expression in *PSEN1* NSC compared with control NSC, but little difference in SOX2 expression between control and *PSEN1* A246E NSC. Investigation of normal neural differentiation in neurospheres indicated a trend towards increased expression of SOX2 and MAP2 and decreased expression of nestin in neurospheres with the *PSEN1* A246E mutation compared with control neurospheres (Figure 58).

After preliminary investigation of pathways related to normal and dysregulated neural differentiation in disease, further analysis was carried out to validate and to further investigate the changes seen in markers related to neural differentiation. To generate samples for investigation, control and *PSEN1* A246E iPSC were differentiated simultaneously to NSC three times and RNA was harvested from the NSC generated when they reached P2, P3 and P8. *PSEN1* A246E samples were investigated for expression of markers of neural differentiation: SOX2, nestin and MAP2 as they matured. There was no significant difference ($p=0.719$) in expression of SOX2, nestin ($p>0.9999$) or MAP2 (0.155) between *PSEN1* and control NSC. There was, however, a strong trend towards an increase in MAP2 gene expression in *PSEN1* NSC compared with control NSC (Figure 59). MAP2 expression was lowest in samples taken from P2 NSC and highest from samples taken from P8 NSC, indicating that

MAP2 increases in NSC as they mature. In each sample pair -consisting of *PSEN1* and control NSC at P2, P3 and P8, MAP2 expression was consistently higher in the *PSEN1* mutation containing NSC than in control NSC. The trend towards increasing MAP2 in *PSEN1* NSC supports the notion that *PSEN1* A246E NSC were undergoing neural differentiation at a faster rate than control NSC. Samples from control and *PSEN1* NSC which displayed the highest levels of nestin were both taken from NSC at P8. Expression of nestin did not differ to a large degree between control and *PSEN1* NSC at P2 and P3, however, at P8, there was a greater difference between nestin expression in *PSEN1* and control NSC, this can be seen by the difference between the highest data points for nestin expression in *PSEN1* and control NSC. SOX2 expression in control NSC displayed very low levels of variation between biological replicates, higher intra-sample variation was seen between *PSEN1* biological replicates (Figure 61). Variability in SOX2 expression in *PSEN1* biological replicates may be indicative of the primary stages of dysregulated neural differentiation in disease (Figure 59).

It was hypothesised that altered cell division and altered cell cycle progression could influence the progeny generated during neural differentiation, for this reason, cell cycle progression was investigated in control and *PSEN1* NSC and NPC using propidium iodide staining and flow cytometry. Cell cycle analysis results displayed no significant difference in the proportion of cells in G1 ($p=0.388$), G2 ($p=0.234$) or S-phases ($p=0.113$), and no significant difference between sample levels of DNA fragmentation ($p=0.1$) but did indicate trends towards an increase in the proportion of *PSEN1* NSC in G1, a decrease in the proportion of *PSEN1* NSC in G2 and S-phases and a trend towards an increase in the percentage of DNA fragmentation in *PSEN1* NSC compared with control NSC.



Repeated simultaneous differentiation of control and *PSEN1* iPSC to NSC, consistently revealed phenotypic differences between *PSEN1* and control NSC. As *PSEN1* NSC matured, they generated fewer neural rosettes and tubes, and began to extend neuronal-like processes across the cell culture plate. These phenotypic differences indicated a more rapid maturation/differentiation in *PSEN1* A246E NSC compared with controls. *PSEN1* M146L did not display the same phenotypic changes during neural differentiation and were similar to controls in their ability to proliferate and generate new neural stem cells in their rosettes. *PSEN1* M146L NSC at P2 (A) and P3 (Ai), *PSEN1* A246E NSC at P2 (B) and P3 (Bi), control 1 NSC at P2 (C) and P3 (Ci), control 2 NSC at P2 (D) and P3 (Di). All images were taken at 20X magnification using an EVOS® Digital Microscope.

5.3.1 qPCR-based analyses of *PSEN1* NSC and neurospheres

Initial qPCR-based analysis of *PSEN1* NSC focused on investigating the role of autophagy in disease neurogenesis. Both 2D and 3D models of neural differentiation were used to investigate disease neurogenesis, these included NSC generated from disease and control lines as well as neurospheres generated from the same immortalised stem cell lines. The markers Beclin-1, MTOR, LC3 and P62 were selected for qPCR-based analysis of autophagy in control and *PSEN1* NSC. Preliminary analysis indicated a downregulation in expression of Beclin-1, MTOR and LC3 and an upregulation in expression of P62 in *PSEN1* A246E NSC when compared with controls (Figure 55 A). In *PSEN1* M146L NSC, expression of Beclin-1, MTOR and LC3 was upregulated compared with controls (Figure 55 B). These results indicated that there were variations in autophagy between NSC containing different *PSEN1* mutations.

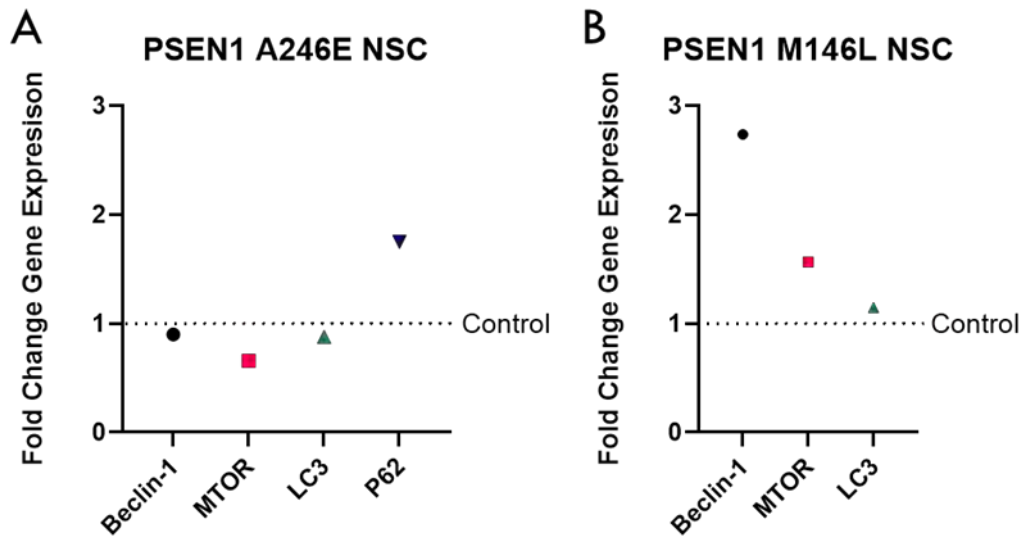


Figure 55. qPCR based analysis of autophagy in *PSEN1* NSC

Fold change gene expression in *PSEN1* A246E NSC (P3) compared with controls. B.) Fold change gene expression in *PSEN1* M146L NSC (P3) compared with controls. For *PSEN1* samples, n=1 biological repeat with 3 technical repeats, for control samples, n=2 biological repeats with 3 technical repeats. Beclin-1 gene expression was lower in *PSEN1* A246E NSC than in controls (A) but was much higher in *PSEN1* M146L NSC than in controls (B). MTOR gene expression was reduced in *PSEN1* A246E NSC compared with controls (A) but increased in *PSEN1* M146L NSC compared with controls (B). LC3 gene expression was reduced in *PSEN1* A246E compared with controls but increased in *PSEN1* M146L NSC compared with controls. P62 gene expression was increased in *PSEN1* A246E NSC compared with controls. Gene expression varied widely between the two different *PSEN1* mutations, results indicate variations in autophagy between NSC containing different *PSEN1* mutations. Fold Change Gene Expression was calculated using the Delta-Delta Ct method.

Altered Wnt signalling in *PSEN1* NSC was hypothesised to be a potential cause of the differences in proliferation and differentiation seen between *PSEN1* and control NSC. Probes selected for investigation of Wnt signalling included LEF-1, CTNNB1, GSK3-beta, *AXIN2* and *JAG1*. Expression of LEF-1, CTNNB1, GSK3-beta and *AXIN2* was higher in both *PSEN1* A246E NSC and *PSEN1* M146L than in controls (Figure 56 A, B), expression of *JAG1* was lower in *PSEN1* A246E NSC than in controls and higher in

PSEN1 M146L NSC than in controls. Results indicated that gene expression related to Wnt signalling increased in *PSEN1* NSC compared with controls.

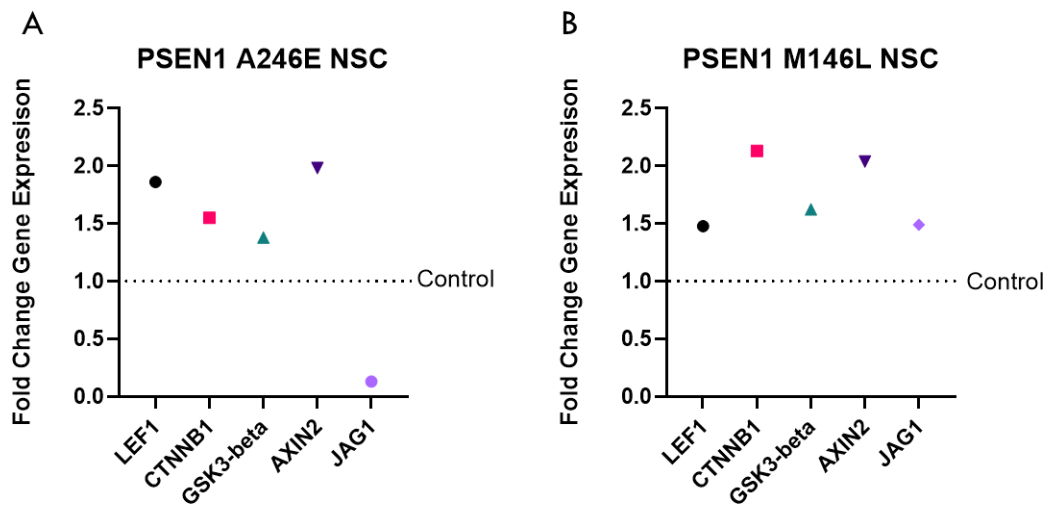


Figure 56. Expression of markers related to Wnt signalling

A.) Fold change gene expression in *PSEN1* A246E NSC (P3) (n=1) compared with controls (n=2). B.) Fold change gene expression in *PSEN1* M146L NSC (P3) (n=1) compared with controls (n=2). Expression of LEF-1, CTNNB1, GSK3-beta and *AXIN2* was higher in both *PSEN1* A246E NSC and *PSEN1* M146L than in controls (A), expression of *JAG1* was lower in *PSEN1* A246E NSC than in controls and higher in *PSEN1* M146L NSC than in controls. Overall, results indicate that gene expression related to Wnt signalling increased in *PSEN1* NSC compared with controls.

PSEN1 A246E NSC were compared against control NSC for differences in levels of oxidative stress and inflammation. Markers selected for investigation of oxidative stress and inflammation were NRF2, HIF1, *NQO1* and STAT3. There was a trend towards upregulation of NRF2 and *NQO1* in *PSEN1* A246E NSC, a trend towards downregulation of STAT3 in *PSEN1* A246E NSC and no detectable difference between *PSEN1* A246E and control NSC in expression of HIF (Figure 57 A), (Figure 57 B).

The variation in gene expression between *PSEN1* M146L and *PSEN1* A246E NSC led to the decision to focus on one *PSEN1* mutation, thus further investigations were carried out using *PSEN1* A246E NSC and control cell lines. Neurospheres generated

from control and *PSEN1* A246E iPSC were analysed alongside *PSEN1* A246E and control NSC to determine if the model used led to differences in gene expression. In *PSEN1* A246E NSC, there was a trend towards upregulation of *NRF2* and *NQO1* and downregulation of *STAT3* compared with controls. There was no detectable difference between *PSEN1* A246E and control NSC in expression of *HIF* (Figure 57 A). In *PSEN1* A246E Neurospheres, there was a trend towards upregulation of *NRF2*, *HIF*, *NQO1* and *STAT3* compared with control neurospheres (Figure 57 B).

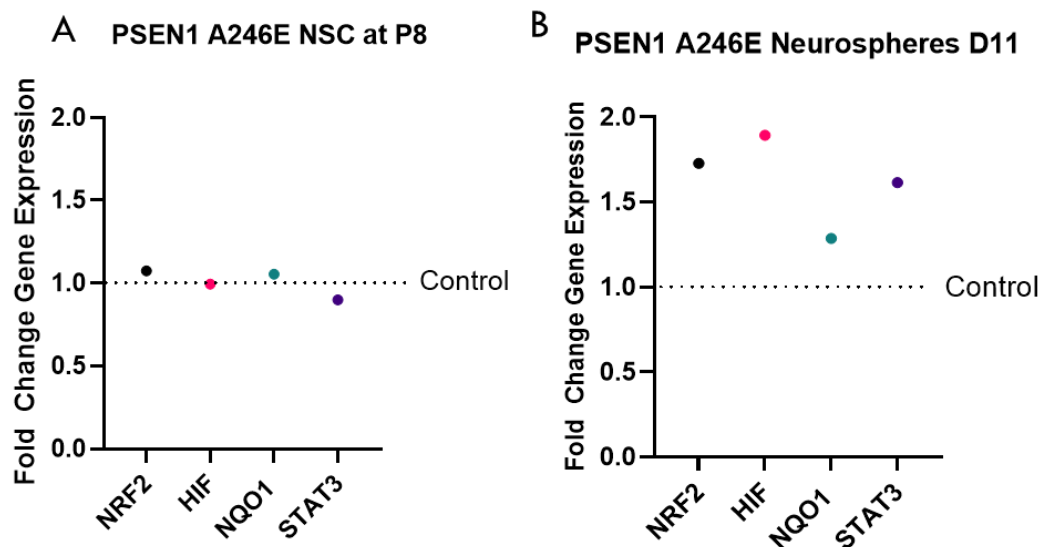


Figure 57. qPCR based analysis of antioxidant-response and inflammation-related gene expression in NSC and neurospheres

A.) *PSEN1* A246E NSC compared with control NSC. Results indicated a trend towards upregulation of *NRF2* and *NQO1* and downregulation of *STAT3* compared with controls. There was no detectable difference between *PSEN1* A246E and control NSC in expression of *HIF*. B.) *PSEN1* A246E neurospheres compared with control neurospheres, there was a trend towards upregulation of *NRF2*, *HIF*, *NQO1* and *STAT3* in *PSEN1* A246E neurospheres compared with control neurospheres.

Preliminary investigation of markers related to neural differentiation was carried out in *PSEN1* A246E NSC compared with control NSC (Figure 58). *SOX2* is a marker which is highly expressed by immature NSC and is downregulated as NSC mature to NPC

and even further downregulated as NSC mature to neurons. Nestin is a marker which is highly expressed by neural stem and progenitor cells but is downregulated as NSC differentiate to neurons. Microtubule associated protein 2 (MAP2) is a marker which is upregulated as NSC mature to NPC and further to mature neurons. Results displayed a trend towards upregulated MAP2 and nestin expression in *PSEN1* NSC compared with control NSC. There was no difference detected in SOX2 expression between control and *PSEN1* A246E NSC. Investigation of normal neural differentiation in neurospheres indicated a trend towards increased expression of SOX2 and MAP2 and decreased expression of nestin.

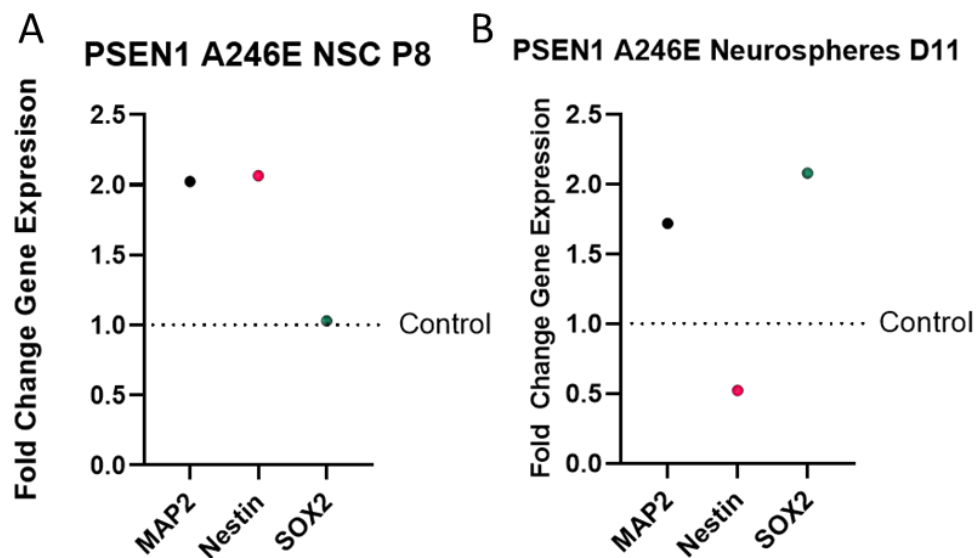


Figure 58. qPCR based analysis of markers of neural differentiation in NSC and neurospheres

Preliminary qPCR data comparing expression of markers MAP2, nestin and SOX2 in NSC and in neurospheres. A.) Results indicated a trend towards upregulation of MAP2 and nestin gene expression in *PSEN1* A246E NSC (n=1) at P8 compared with controls (n=2) at P8. A.) Results indicated that there was no difference in expression of SOX2 between *PSEN1* and control NSC P8. B.) Results indicated a trend towards upregulation of MAP2 and SOX2 gene expression and downregulation of nestin gene expression in *PSEN1* A246E neurospheres (n=1) at D11 compared with controls (n=2) at D11.

After preliminary investigation of pathways related to normal and dysregulated neural differentiation in disease, control and *PSEN1* iPSC were differentiated simultaneously to NSC three times and RNA was harvested from the NSC generated when they reached P2, P3 and P8. RNA collected from *PSEN1* and control NSC at P2, P3 and P8 was investigated for markers of neural differentiation using qPCR for expression of markers MAP2, nestin and SOX2 (Figure 59). There was no significant difference ($p=0.719$) in expression of SOX2, nestin ($p>0.9999$) or MAP2 (0.155) between *PSEN1* and control NSC. There was, however, a strong trend towards an increase in MAP2 gene expression in *PSEN1* NSC compared with control NSC. MAP2 expression was lowest in samples taken from P2 NSC and highest from samples taken from P8 NSC, indicating that MAP2 increases in NSC as they mature. In each sample pair -consisting of *PSEN1* and control NSC at P2, P3 and P8, MAP2 expression was consistently higher in the *PSEN1* mutation containing NSC than in control NSC. The trend towards increasing MAP2 in *PSEN1* NSC supports the notion that *PSEN1* A246E NSC were undergoing neural differentiation at faster rate than control NSC. Samples from control and *PSEN1* NSC which displayed the highest levels of nestin were both taken from NSC at P8. Expression of nestin did not differ to a large degree between control and *PSEN1* NSC at P2 and P3, however, at P8, there was a greater difference between nestin expression in *PSEN1* and control NSC, this can be seen by the difference between the highest data points for nestin expression in *PSEN1* and control NSC. SOX2 expression in control NSC displayed very low levels of variation between biological replicates, higher intra-sample variation was seen between *PSEN1* biological replicates (Figure 59). Variability in SOX2 expression in *PSEN1* biological replicates may be indicative of the primary stages of dysregulated neural differentiation in disease.

Markers of Neural Differentiation

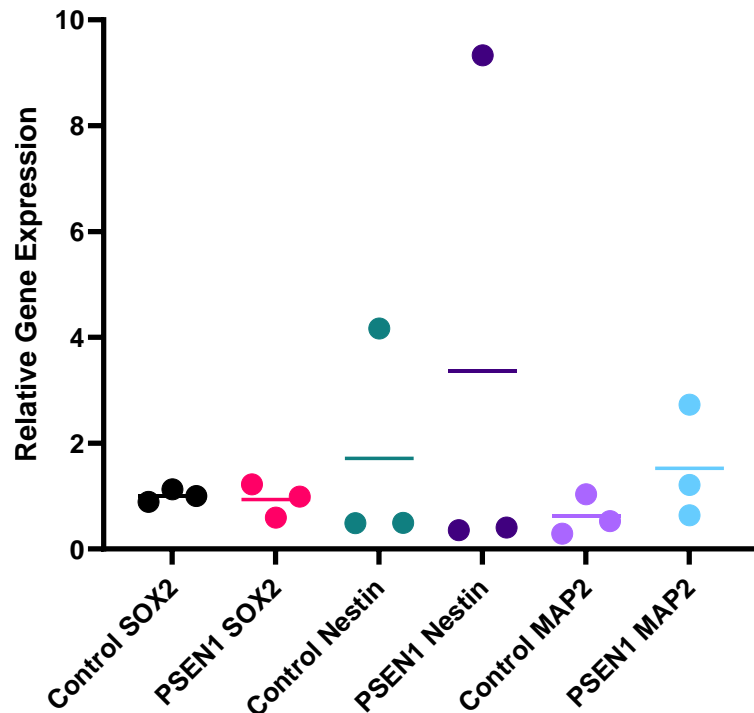


Figure 59. qPCR based investigation of markers of neural differentiation

Early and more mature markers of neural differentiation were compared in *PSEN1* and control NSC. Samples were taken from NSC at P2, P3 and P8. Data points which display higher levels of nestin were both taken from NSC at P8. For each pair of samples taken (at P2, P3 and P8), MAP2 expression was higher in *PSEN1* NSC than in control NSC in every sample pair. MAP2 expression was also higher as NSC matured from P2 to P8. There was no significant difference ($p=0.719$) in expression of SOX2, nestin ($p>0.9999$) or MAP2 (0.155) between *PSEN1* and control NSC. There was, however, a strong trend towards an increase in MAP2 gene expression in *PSEN1* NSC compared with control NSC. Normality tests, Paired T-tests and the Wilcoxon test were carried out using GraphPad Prism 9.2.0. The graph was made using GraphPad Prism 9.2.0 and displays individual data points with the mean value indicated by a horizontal line.

5.3.2 Cell cycle analysis in *PSEN1* and control NSC

Differences in cell cycle progression may lead to altered proliferation and differentiation in *PSEN1* A246E NSC. For this reason, cell cycle progression was analysed in NSC generated from *PSEN1* A246E and control lines. control and *PSEN1* iPSC were differentiated simultaneously to NSC in triplicate and 1×10^6 cells were

harvested from the NSC generated when they reached P3. *PSEN1* and control NSC collected were stained with propidium iodide and analysed using flow cytometry to investigate the proportion of cells in each stage of the cell cycle. Figure 60. A. displays differences seen between *PSEN1* and control NSC in Forward scatter (FSC) vs side scatter (SSC) gating. In *PSEN1* NSC, cell density is highest closer to the lower ends of each axis, this indicates an increase in debris and cell death in *PSEN1* NSC compared with control NSC.

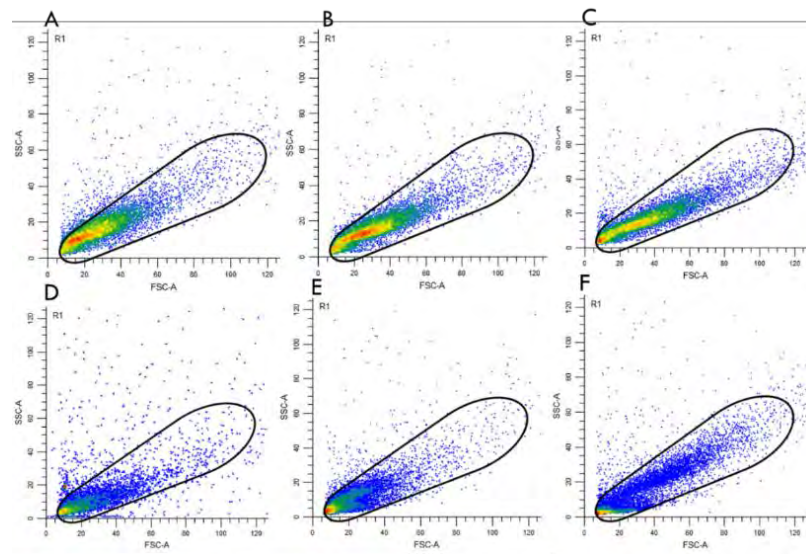


Figure 60. Forward scatter vs side scatter differences in *PSEN1* NSC

Forward scatter (FSC) vs side scatter (SSC) gating was used to identify cells of interest based on size and granularity. Warmer colours indicated a greater cell density. A-C represent three biological repeats of control NSC. D-F represent three biological repeats of *PSEN1* A246E NSC. In control NSC, the majority of cells are located higher up the forward and side scatter plot, whereas in *PSEN1* A246E NSC, the majority of cells are found closer to the bottom of both axes, indicating an increase in debris and cell death in *PSEN1* A246E NSC.

After gating based on cell population, cells were gated further for exclusion of doublets before analysis of PI staining results. Figure 61 A-C represent the distribution of cells in the cell cycle in three biological repeats of control NSC. Figure 61 D-F represent the distribution of *PSEN1* A246E NSC in the different stages of the

cell cycle. The graphs shown for the control NSC biological repeats (A-C) resemble expected cell cycle results, with a high G0/G1 peak, which is representative of cells in quiescence or in the G1 phase of the cell cycle, a smaller G2 peak, to represent cells with twice amount of DNA that have undergone DNA replication, and a lower, more widely spread peak between the G0/G1 and G2 peaks which represents cells in the S-phase undergoing DNA replication that have somewhere between one copy and two copies of DNA. Graphs shown for the *PSEN1* A246E NSC biological repeats do not resemble normal cell cycle plots, on average they display a much lower number of cells in the G0/G1 phase of the cell cycle than seen in control NSC, a lower number of cells in the G2 phase of the cell cycle and a lower number of cells in the S-phase of the cell cycle than seen in control NSC, these differences are plotted in Figure 62.

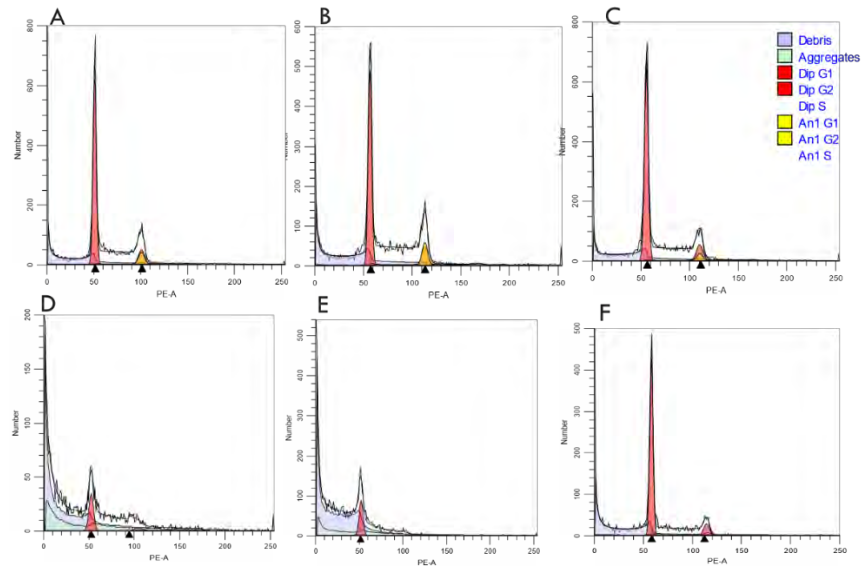


Figure 61. Distribution of control and *PSEN1* A246E NSC in cell cycle plots

A-C represent the distribution of cells in the cell cycle in three biological repeats of control NSC. D-F represent the distribution of *PSEN1* A246E NSC in the different stages of the cell cycle. The graphs shown for the control NSC biological repeats (A-C) resemble expected cell cycle results, with a high G0/G1 peak, to represent cells in quiescence or in G1 phase of the cell cycle, a smaller G2 peak, to represent cells with twice amount of DNA that have undergone DNA replication, and number of cells in between the G0/G1 and G2 peaks which are undergoing DNA replication and have somewhere between one copy and two copies of DNA (S-phase). Graphs shown for the *PSEN1* A246E NSC biological repeats do not resemble normal cell cycle plots, on average they have a much lower number of cells in the G0/G1 phase of the cell cycle than seen in control NSC, a much lower number of cells in the G2 phase of the cell cycle and a lower number of cells in the S-phase of the cell cycle. Cell cycle plots were generated using ModFit LT™.

Results from cell cycle analysis using PI, flow cytometry and ModFit LT™ were analysed to investigate differences in cell cycle progression between *PSEN1* and control NSC at P3. Figure 62 displays the percentage of *PSEN1* A246E and control NSC at P3 in different stages of the cell cycle Figure 62 A, displays the proportion of NSC in the G1 phase of the cell cycle, Figure 62 B. displays the proportion of NSC in the G2 phase of the cell cycle, Figure 62 C. displays the percentage of NSC in the S-phase of the cell cycle, Figure 62. Cell cycle analysis of *PSEN1* A246E and control NSC D. displays the percentage of DNA fragmentation seen in *PSEN1* NSC compared with

control NSC. There was no significant difference ($p=0.3881$) between the percentage of *PSEN1* and control NSC in G1 of the cell cycle, but there was a trend ($p=0.3881$) towards an increase in the proportion of *PSEN1* NSC in the G1 phase of the cell cycle compared with controls (Figure 62 A). There was no significant difference (0.234) in the percentage of cells in the G2 phase of the cell cycle, but there was a trend (0.234) towards a smaller proportion of *PSEN1* NSC reaching the G2 phase of the cell cycle when compared with control NSC. There was no significant difference ($p=0.113$) between the percentage of *PSEN1* and control NSC in the S-Phase of the cell cycle, but there was a trend ($p=0.113$) towards a decrease in the proportion of *PSEN1* NSC in the S-phase of the cell cycle compared with control NSC (Figure 62 C). There was no significant difference ($p=0.1$) in percentage DNA fragmentation in *PSEN1* NSC compared with control NSC, but there was a trend ($p=0.1$) towards increased DNA fragmentation in *PSEN1* NSC at P3 compared with *PSEN1* NSC at P2.

Percentage of *PSEN1* NSC in the G1 phase of the cell cycle ranged from 47- 78% with an SEM of 8.5. Percentage of control NSC in the G1 phase of the cell cycle ranged from 49- 59% with an SEM of 2.7. This data indicates that there was greater variance between samples containing the *PSEN1* mutation than control samples. The percentage of *PSEN1* NSC in the S-phase of the cell cycle ranged from 22-45% with an SEM of 7.0, whereas the percentage of control NSC in the S-phase of the cell cycle ranged from 33 to 43% with an SEM of 2.6, this data indicates that there is more variance between *PSEN1* samples than control samples. The percentage of *PSEN1* NSC in G2 phase of the cell cycle ranged from 0-7.5% with an SEM of 2.32 whereas the percentage of control NSC in G2 phase was 8.0% with no variation between samples and thus an SEM of 0. This indicates again that there is more variation between *PSEN1* samples than controls in terms of their progression through the cell cycle, this data also indicates that a greater proportion of control NSC reached the G2 phase of the cell cycle than seen in *PSEN1* samples. The percentage of DNA fragmentation in *PSEN1* NSC ranged from 36 to 72% with an SEM of 10.2, whereas

the percentage of DNA fragmentation seen in control NSC ranged from 24 to 31% with an SEM of 2.15.

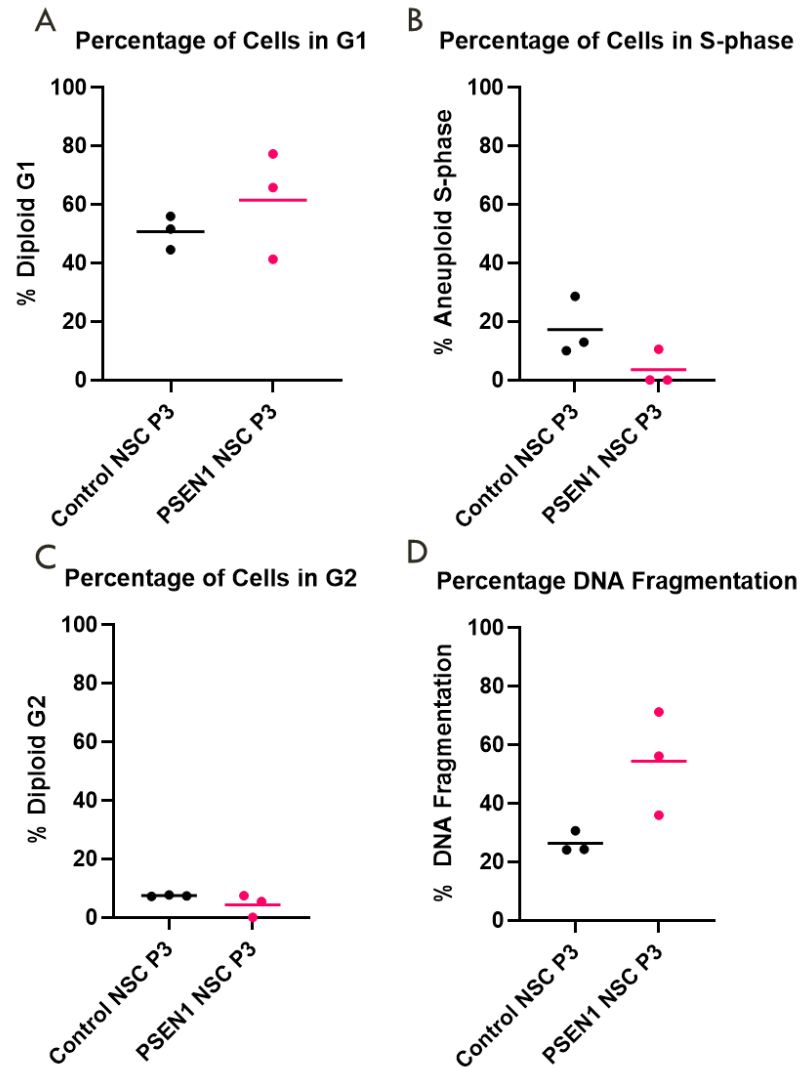


Figure 62. Cell cycle analysis of *PSEN1* A246E and control NSC

Cell cycle analysis of *PSEN1* and control NSC. Flow Cytometry was used to investigate differences in cell cycle progression between *PSEN1* and control NSC at P3. A.) displays the percentage of P3 NSC in phase G1 of the cell cycle, there was no significant difference ($p=0.388$) between the percentage of *PSEN1* and control NSC in G1 of the cell cycle, but there was a trend towards a greater proportion of *PSEN1* NSC being in the G1 phase of the cell cycle compared with the proportion of control. B.) displays the percentage of P3 NSC in the S-phase of the cell cycle, there was no significant difference ($p=0.1125$) between the percentage of *PSEN1* and control NSC in the S-Phase of the cell cycle, but there was a trend towards a decrease in the proportion of *PSEN1* NSC in the S-phase of the cell cycle compared with control NSC. C.) displays the percentage of control and *PSEN1* NSC in the G2 phase of the cell cycle. There was no significant difference ($p=0.234$) in the percentage of cells in the G2 phase of the cell cycle, but there was a trend towards fewer *PSEN1* NSC reaching the G2

phase of the cell cycle when compared with control NSC. D.) displays the percentage of DNA fragmentation seen in *PSEN1* NSC compared with control NSC, there was no significant difference ($p=0.1$) in percentage DNA fragmentation in *PSEN1* NSC compared with control NSC, but there was a trend towards increased DNA fragmentation in *PSEN1* NSC at P3 compared with *PSEN1* NSC at P2. Normality tests, T-tests and Man-Whitney U tests were carried out using GraphPad Prism 9.2.0. Graph made using GraphPad Prism displays individual data points with the mean value indicated by a horizontal line.

5.3.3 Chapter summary

The data shown in this chapter indicate trends towards dysregulation of pathways related to Wnt signalling, autophagy and neural differentiation in *PSEN1* NSC. Cell cycle analysis results indicated a trend towards an increase in the proportion of *PSEN1* NSC in G1, and a decrease in the proportion of *PSEN1* NSC in G2 and S-phases, these results suggested impairments in cell cycle progression in *PSEN1* NSC. Cell cycle results also displayed a trend towards an increase in the percentage of DNA fragmentation in *PSEN1* NSC compared with control NSC, which may be indicative of increased apoptosis or necrosis in AD. Pathway dysregulation in *PSEN1* required further analysis on a wider scale to enable a full screen of transcriptomic differences occurring between *PSEN1* and control NSC. For this reason, it was decided that RNA sequencing would be carried out on control and *PSEN1* NSC at multiple stages in neural differentiation, to enable investigation of the transcriptomic changes which were occurring exclusively during *PSEN1* neural differentiation and pushing them towards a more neural phenotype.

6. RNA sequencing

6.1 Introduction

6.1.1 Overview of RNA sequencing

RNA sequencing is a useful tool for bulk transcriptomic analysis of a cell population. RNA is isolated, purified and fragmented before conversion to cDNA. Adapters are ligated to cDNA fragments to enable binding to a flow cell, after which the sequencing library is run to generate reads, which are mapped onto a reference genome (Figure 63). The Illumina TruSeq Stranded Total RNA protocol can be used for generation of a cDNA library for RNA Sequencing. Purification of Poly-A containing mRNA molecules is carried out using poly-T-oligo attached magnetic beads, fragmentation of mRNA is then carried out using divalent cations at a high temperature. First strand synthesis of cDNA is carried out using random primers and the enzyme reverse transcriptase. Addition of actinomycin to the first strand synthesis mix improves strand specificity as it prevents DNA dependent synthesis but allows RNA-dependent synthesis. Second strand synthesis of cDNA is carried out using DNA polymerase I and RNase H. To achieve strand specificity, in the second strand marking mix, dTTP is replaced by dUTP, during amplification, the second strand is quenched by the presence of dUTP. After generation of cDNA, 3' ends are adenylated to prevent ligation with other blunt fragments during adaptor ligation. A Thymine nucleotide on the 3' end of the adapter enables complementary binding of adapter with fragment. The ligation of adaptors to fragments allows the double stranded cDNA generated to hybridise to the flow cell. Post ligation of adaptors to cDNA fragments, cDNA is amplified using PCR. The assay uses a DNA polymerase that stops incorporating bases at dUTP, this quenches the second strand of cDNA during enrichment. Bead based purification of enriched DNA products is carried out before quality control (QC) and quantification of the final library. The LS library which was used in this project has a single index adaptor.

RNA Sequencing

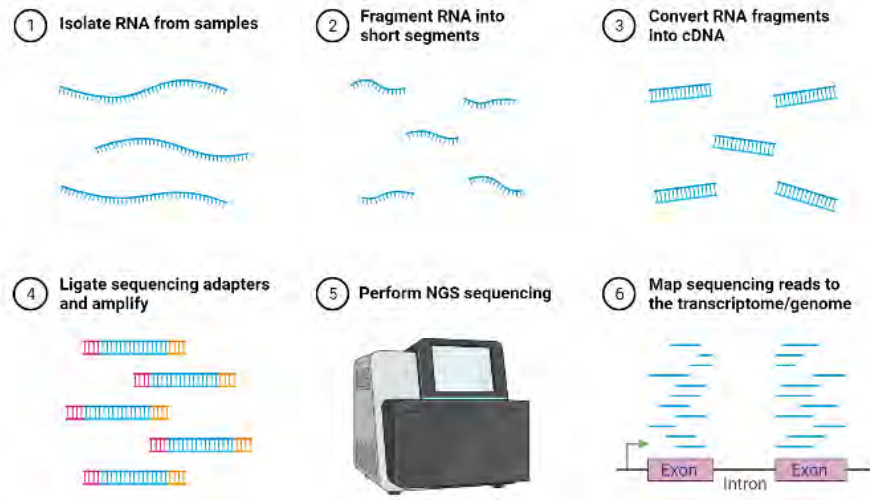


Figure 63. Overview of library preparation and RNA sequencing

Overview of the library preparation stages of RNA Sequencing. 1.) RNA is isolated from samples, 2.) RNA is fragmented into short segments. 3.) RNA fragments are converted into cDNA. 4.) Sequencing adaptors are ligated, and cDNA fragments are amplified. 5.) The cDNA library is loaded to a flow cell and Next Generation Sequencing is carried out. 6.) Reads are alignment to a reference genome to generate read counts that can be compared between samples to investigate differences in gene expression (Created in BioRender.com).

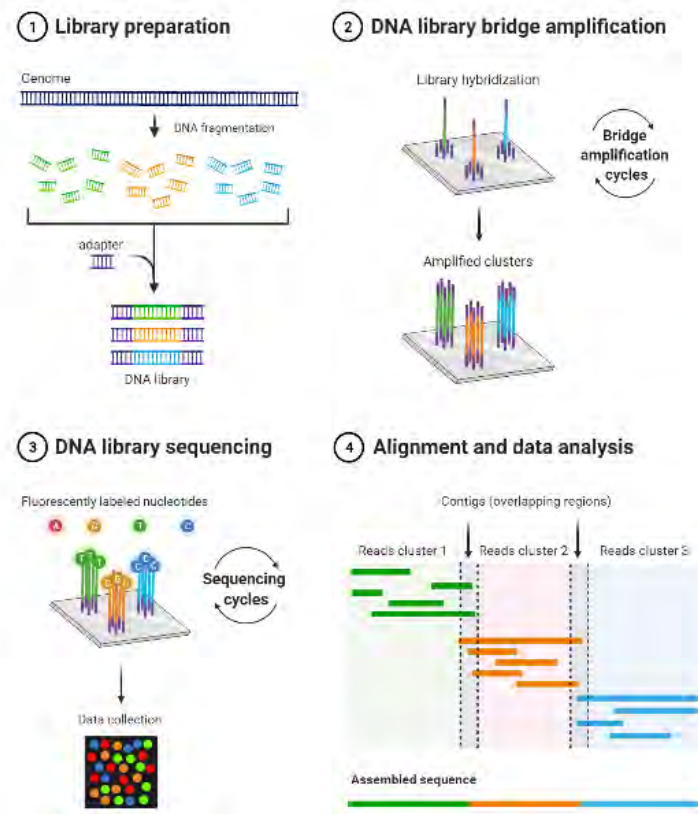


Figure 64. Overview of RNA sequencing

Overview of Illumina’s RNA sequencing process. 1.) cDNA library is prepared from RNA samples. 2.) The cDNA library binds to the flow cell and clusters are amplified. 3.) Fluorescent labelling of nucleotides enables accurate cDNA sequencing. 4.) Sequencing results are processed for quality control and then aligned to a reference genome, after which, read counts are generated and used to interrogate differences in gene expression between samples (Created in BioRender.com).

Cluster generation and sequencing of Read 1- reads map to the antisense strand in read 1 and map to the sense strand in Read 2. Fragments with no adapters cannot hybridize to surface-bound primers in the flow cell. Fragments with an adapter on 1 end can hybridize to surface bound primers but cannot form clusters.

RNA SEQ ADAPTERS

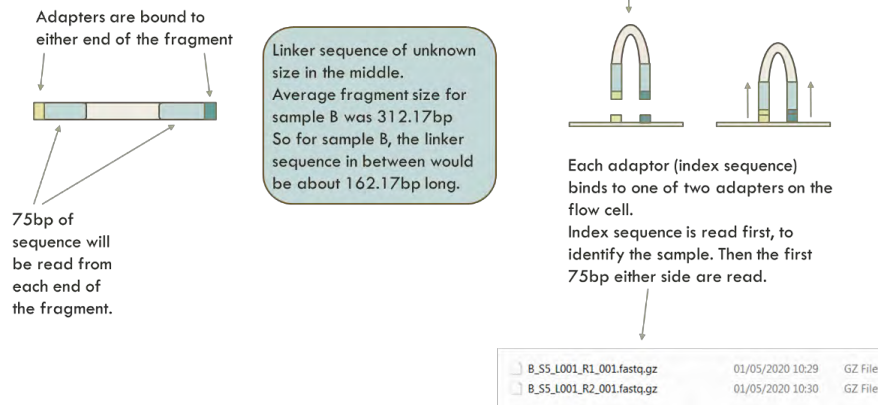


Figure 65. RNA sequencing adapters

RNA Sequencing adaptors are bound to cDNA fragments for attachment to the flow cell

6.1.2 Quality control of RNA seq data

Sequencing problems often occur in RNA seq data, and include low sequencing quality of raw reads, contamination from other species, residual degradation and varied read coverage. Each sample file contains the 75bp of sequenced read, a sequence ID, and a quality score. The quality score or Q score is represented as an ASCII character to save data. The tools FastQC and MultiQC can interpret the ASCII symbols to present a quality score for the calling of each base. QC including trimming and filtering was carried out on the initial sequencing data, on reads post alignment to the reference genome and on DESeq2 results.

6.2 Aims

The overarching aim of chapter 3 was to use RNA sequencing to investigate transcriptomic differences between control and *PSEN1* NSC at P2 and P3, and thus to analyse the transcriptomic differences between control and *PSEN1* neural differentiation. Analysis using RNA sequencing enabled large scale transcriptome wide analysis of *PSEN1* and control NSC and required a relatively low quantity of starting material. The objectives of chapter 3 were:

1. Preparation of cDNA libraries for sequencing from RNA isolated from *PSEN1* and control NSC at P2 and P3
 - Extraction of RNA and DNase digestion
 - Analysis of RNA prior to initiation of library preparation
 - Library preparation following the Illumina TruSeq Stranded Total RNA protocol
 - Analysis and quantification of cDNA libraries prior to running on the RNA-sequencing

2. Running cDNA libraries on the Illumina RNA Sequencer 500
 - Preparation of libraries for addition to the flow cell

3. Quality control (QC) and Processing of data
 - QC of sequencing data
 - Alignment to a reference genome
 - QC of alignment
 - Generation of read counts
 - Analysis of RNA seq data- using DESeq2, Reactome and Panther for pathway analysis

6.3 Results

RNA sequencing was used to investigate transcriptomic differences between control and *PSEN1* A246E NSC at P2 and P3. Investigation of differences in transcription between control and *PSEN1* A246E NSC at P2 and P3 was carried out to investigate differences in neurogenesis. Biological repeats were generated from the same initial cell lines -Axol119 control and Axol114 *PSEN1* A246E and were classed as biological repeats because each repeat was generated from a separate neural differentiation protocol. Three separate experiments were conducted in which A246E iPSC and control iPSC were differentiated simultaneously to NSC and harvested at P2 and P3.

Variation was seen between biological repeats which did not differ genetically, this highlights the variations that can be seen between different neural differentiations which were carried out in exactly the same manner and highlights the importance of simultaneously differentiating AD and control lines for investigation of differences occurring in disease neurogenesis. *PSEN1* A246E NSC samples will herein be referred to as *PSEN1* NSC.

RNA Sequencing Workflow

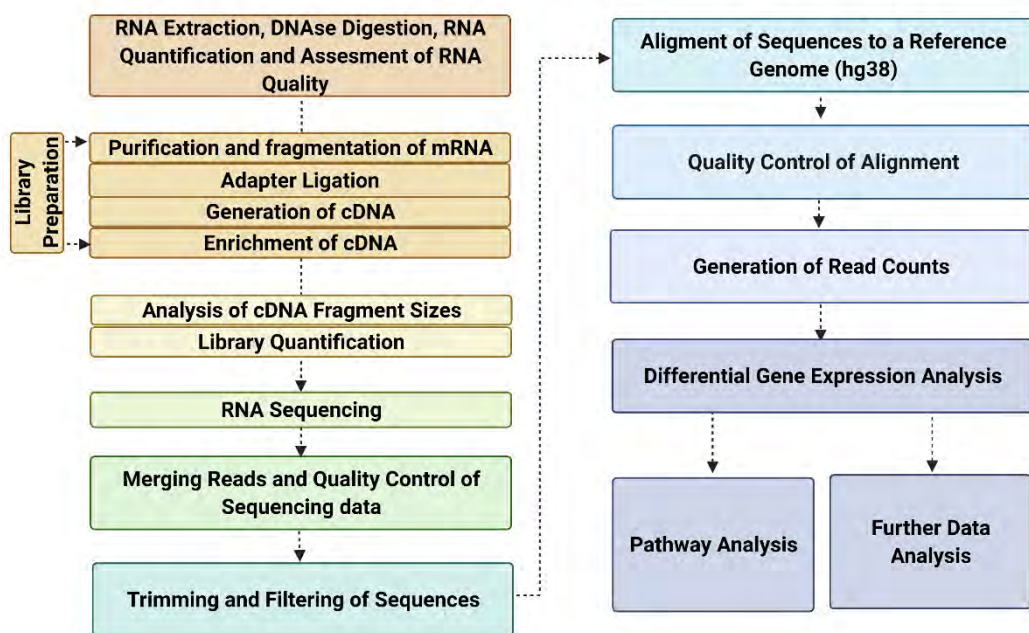


Figure 66. RNA sequencing workflow

Workflow to show library preparation for RNA Sequencing, QC, and analysis post sequencing. RNA was extracted from control and *PSEN1* A246E NSC at P2 and P3 and DNase digestion was carried out to prevent genomic contamination in RNA samples. All RNA samples were quantified and assessed to determine quality before initiation of library preparation. Library preparation involved purification and fragmentation of mRNA before adapter ligation, generation of cDNA and enrichment of cDNA using PCR. RNA sequencing was carried out using the Illumina NextSeq 500 and data generated underwent QC, which included trimming and filtering of low-quality bases and sequences. After QC of data, sequences were aligned to a reference genome, and the quality of this alignment was assessed. Read counts were generated and differential gene expression analysis was carried out to investigate differences in gene expression between samples. Pathway analysis was

carried out along with further analysis of differences in gene expression (Figure Created in BioRender.com).

6.3.1 Analysis of cDNA fragment sizes post library preparation

After simultaneous generation of NSC from *PSEN1* and control iPSC, RNA was extracted at P2 and P3. DNase digestion was used to degrade both double-stranded and single-stranded DNA to prevent genomic contamination in RNA samples. RNA samples were quantified and assessed to determine quality before library preparation. Library preparation was carried out using the Illumina TruSeq Stranded mRNA workflow and consisted of purification and fragmentation of mRNA, adapter ligation, generation of cDNA and enrichment of cDNA using PCR (Figure 66).

The first cDNA library generated using the Illumina TruSeq Stranded mRNA protocol was assessed using the 2100 Bioanalyzer system by Agilent to determine quality and fragment sizes of cDNA samples. cDNA fragment sizes were expected to range from 200-500 bp, however, along with cDNA fragments in the expected range, there were also larger cDNA fragments seen at >1000 bp (Figure 101). The presence of samples with these larger fragment sizes was thought to be due to bead contamination, so further wash steps were carried out using beads, however this did not lead to removal of the larger cDNA fragments.

After attempts to remove larger fragments were unsuccessful, RNA samples were processed again for library preparation. The second library preparation resulted in the generation of cDNA fragments within the expected range (200-500bp) (Figure 67). The issues seen with the first library preparation may have been due to plates being placed on ice in between steps.

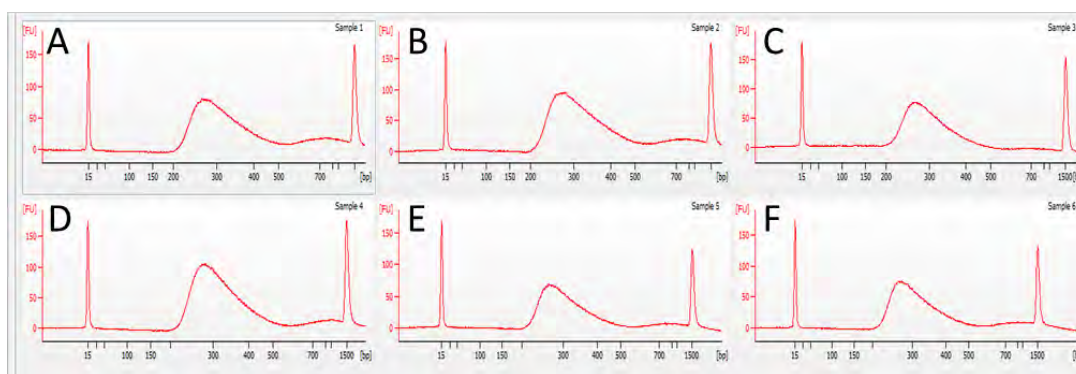


Figure 67. Bioanalyzer traces displaying cDNA used for RNA sequencing

Screen capture of Agilent 2100 Bioanalyzer electropherograms

Bioanalyzer traces were used to check cDNA fragment sizes after completion of the second library preparation. The second library preparation performed displayed fragment sizes within the expected range of 200-500bp in all 12 samples tested. A, B, C display control P3 NSC, D, E, F display *PSEN1* A246E P3 NSC.

6.3.2 Processing of RNA sequencing data

RNA sequencing was carried out using the Illumina NextSeq 500 and data generated was assessed for quality, prior to processing for data analysis. The RNA sequencing run was successful and generated a total of 144,239,762 reads, from which, clusters which could not clearly be identified were filtered out, leaving 136,681,764 reads - 93.6% of the total read count. The PhiX control is a ready to use library to be used as a control for RNA sequencing runs. Reads 1 and 3 displayed the PhiX control, the alignment percentages of which were 5.1% and 5.03% indicating high quality normalisation and quantification of the library. 97.3% of the indexed library had a Q score greater than 30. 5 billion reads had a Q score between 30 and 35, and 35 billion reads had a Q score which was in the range 35-40. A Q score of 40 indicates that there is a 1:10,000 chance that the base reading was incorrect, this gives a probability value (p) of 0.0001. This data indicates that the quality of sequencing reads was high.

For analysis of sequencing reads, the 12 samples sequenced were divided into the four groups *PSEN1* A246E NSC P2, *PSEN1* A246E NSC P3, control NSC P2 and control

NSC P3, with each group containing three biological repeats. A one-way ANOVA was used to compare percentage reads identified between samples using GraphPad Prism 9.2.0. There was no significant difference in percentage reads identified between groups ($p= 0.0757$). A one-way ANOVA was also carried out to determine if the number of identified reads differed significantly between groups, there was no significant difference between the number of identified reads between groups ($p=0.0715$) (Figure 68). These results indicated that sequencing was not significantly affected by variations in the cDNA concentration loaded and indicated that library quantification prior to sequencing was successful. The lower percentage of reads identified in control P3 may have led to a reduction in the identification of lowly expressed genes meaning that small changes may have been missed. The higher percentage of reads identified in *PSEN1* A246E P3 compared with *PSEN1* A246E P2 could have resulted in the loss of data on genes which are upregulated to a smaller degree from P2 to P3 and indicates that genes which are seen to be upregulated in P3 compared with P2 may be upregulated to an even greater degree than is seen in the data. The mean of all three biological repeats is indicated on the graph. All reads were further filtered prior to analysis.

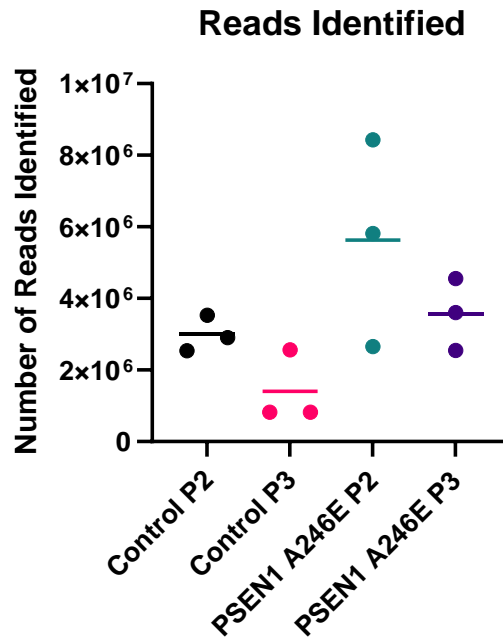


Figure 68. Number of reads identified per group

RNA Sequencing reads were grouped as control P3, *PSEN1* A246E P3, control P2 and *PSEN1* A246E P2. The number of reads identified is plotted for each sample group. There was a trend towards an increase in number of reads identified for the group *PSEN1* A246E P2 relative to other groups. A one-way ANOVA was carried out on all four groups using GraphPad Prism 9.2.0. There was no significant difference in the number of reads identified between groups ($p=0.0757$). The mean of all three biological repeats is indicated on the graph. B.) A one-way ANOVA was used to compare the number of reads identified between samples. There was no significant difference in the number of reads identified between groups ($p=0.0715$).

RNA sequencing data generated underwent quality control (QC) prior to analysis, QC included trimming and filtering of low-quality bases and sequences. After QC of reads, sequences were aligned to a reference genome, and the quality of this alignment was assessed. Read counts were generated and differential gene expression analysis was carried out to investigate differences in gene expression between samples. Pathway analysis was carried out along with further analysis of differences in gene expression between samples. All QC, formatting and analysis of RNA sequencing data was done using the galaxy wrapper for each program. The

sequencing data were uploaded to the Galaxy web platform and the public server was used at usegalaxy.org for all data analysis.

6.3.3 Quality control of RNA sequencing data

RNA sequencing data underwent quality control (QC) assessment prior to analysis, QC included trimming and filtering of low-quality bases and sequences. Individual Fastq files were analysed for quality control using the programs FastQC and MultiQC. Samples were analysed for their Average Per Base Sequence Quality for every position in the read (total 75 bp) (Figure 103). At every position in the read, all samples had a Q score of >30 indicating high quality base identification. Samples were analysed to determine their overall per base sequence content (Figure 103 B). The first 10 bases of this sample display an uneven distribution of A/T/G/C. These first 10 bases are not sequenced incorrectly as their quality score was above 30, the uneven base distribution at the start of each read was likely due to the use of random hexamers in first strand synthesis. Samples were analysed for their per base N content (Figure 103 C), all samples displayed a per base N content of 0%. Samples were analysed for per tile sequence quality (Figure 103 D), a small number of samples displayed warm coloured tiles which may have been the result of bubbles or debris in the flow cell lane, however this issue only occurred for a whole 75 bp sequence on one tile for affected samples, meaning that the low-quality sequences could be filtered out. Samples were analysed for adapter content (Figure 103). All samples analysed passed this module and did not present with a significant amount of adapter present. Samples were analysed for their per sequence quality scores, (Figure 103) the average quality per read for all samples was >30. Samples were analysed for sequence length distribution (Figure 103). All fragments were sequenced to between 72 and 76 bp, with most fragments at 75bp. Samples were analysed for their levels of sequence duplication (Figure 103), biological duplication is expected in RNA sequencing and is indicative of levels of gene expression. All samples were analysed for their per sequence GC content (Figure 103) which was normally distributed in all samples, with most samples having a mean GC content of 50%. All samples were also

analysed for the presence of overrepresented sequences, most samples had no overrepresented sequences but those that did had adaptor sequences and long strings of G's, which meant that the machine had detected no signal and had run out of template (Table 35). All samples underwent trimming and filtering using the tool Trimmomatic which resulted in the removal of poor-quality bases, poor-quality sequences, and contaminants (Appendix 3. Table 36).

6.3.4 Alignment, generation of read counts and data analysis

After QC of reads, sequences were aligned to the reference genome (Hg38), and the quality of this alignment was assessed. Read counts were generated and statistical analyses were carried out to determine if differences in the number of reads aligned per sample group had a significant effect on downstream analyses and results. The rate of alignment was >90% for all samples, which indicated successful alignment of all samples to the reference genome (Appendix 3. Figure 101). Post alignment of sequences to the reference genome Hg38, aligned BAM files were filtered to leave only reads which were paired, mapped in a proper pair, and had a mapping quality above 20 on the Phred scale. After aligning genes to the reference genome (Hg38) and quality-based filtering, the number of reads mapping to each gene were counted (Table 42). The number of reads assigned to the reference genome post filtering was compared between samples (Figure 69). There was no significant difference ($p=0.0624$) in the number of reads assigned between samples, this indicated that results generated from further analyses would not be affected by differences in the number of reads assigned to the reference genome per sample group. Generation of read counts enabled analysis of differential gene expression between samples.

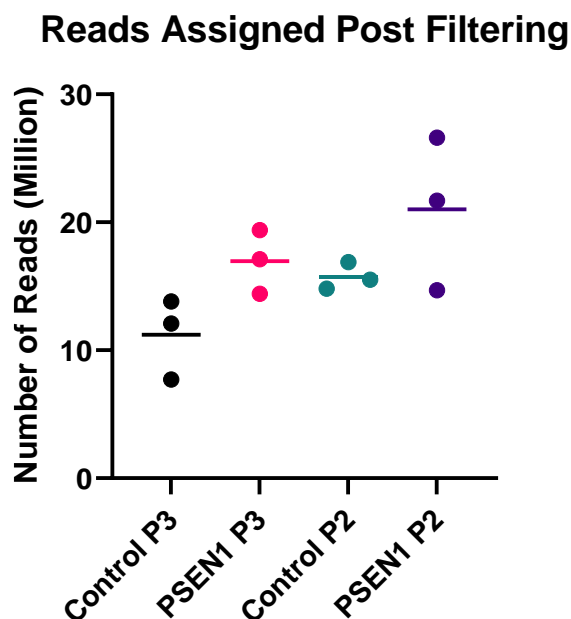


Figure 69. Number of reads assigned to the reference genome post-filtering

Post QC of alignment, the number of remaining reads assigned to the reference genome was compared between sample groups. There was no significant difference ($p=0.0624$) in the number of reads assigned per group post filtering. These results indicated that the number of reads assigned per sample group did not affect downstream data analysis. Statistical analysis was carried out using a one way ANOVA using GraphPad Prism 9.2.0.

6.3.5 Analysis of variance in rna sequencing data

Differential gene expression analysis was carried out to investigate differences in gene expression between samples. DESeq2 was used to identify genes which were differentially expressed between sample groups. Differentially expressed genes (DEGs) were generated for each group comparison i.e., *PSEN1* P2 vs *PSEN1* P3, control P2 vs control P3, *PSEN1* P2 vs control P2 and *PSEN1* P3 vs control P3. Information on differentially expressed genes (DEGs) was utilised to investigate the variance between samples and to carry out pathway analysis. Variance between sample groups sequenced was assessed using a principal component analysis (PCA) plot (Figure 71.), a Sample-to-Sample Distances Heatmap (Figure 72.) and a Dispersion Estimates graph (Figure 73.).

Principal component analysis (PCA) was carried out using DESeq2 through the galaxy wrapper to elucidate the similarity of gene expression between samples. The PCA plot generated displays the variation between the transcriptomic profiles captured for each sample in their principal components -principal component 1 (PC1) and principal component 2 (PC2) (Figure 70). The PCA plot was used to visualise the overall effect of batch effects and experimental covariates. Each sample was plotted on the 2D graph based on its relative variance to the other samples. The distance between two points on an axis was proportional to the variance in gene expression between those points i.e., points further apart on an axis were more divergent in gene expression within that principal component. control NSC samples at P2 and P3 cluster closely together on the PCA plot, and when grouped, display some overlap. control NSC at P2 and P3 do not display high levels of variance in PC1 and PC2, this indicates that gene expression profiles do not differ greatly between control NSC at P2 and at P3. *PSEN1* NSC samples at P2 cluster closely together and display low levels of variance from control samples in PC1 and PC2, but do not overlap with control samples when grouped together. *PSEN1* NSC samples at P3 display high levels of variance between all biological repeats in both PC1 and PC2 and vary from *PSEN1* P2 NSC in both PC1 and PC2. When grouped together, gene expression profiles of *PSEN1* NSC at P3 do not overlap with *PSEN1* P2 samples or with control samples. This data indicates that more transcriptional changes have occurred during a single passage in *PSEN1* NSC than in control NSC, indicating that there are more changes in gene expression during disease neural differentiation than there are in control neural differentiation. The high levels of variance seen between *PSEN1* P3 samples may also indicate that neural differentiation in FAD is not as carefully regulated as in control NSC.

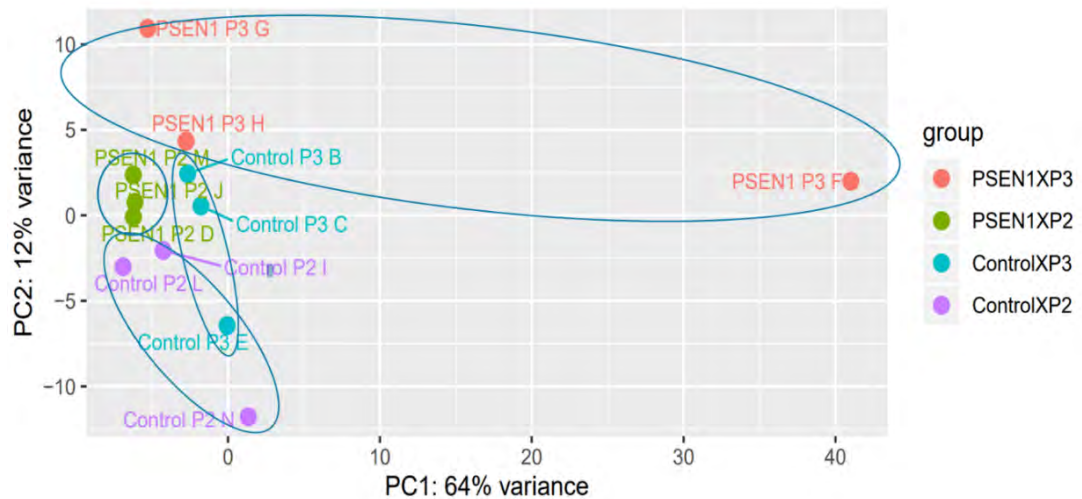


Figure 70. PCA plot displaying variance between RNA seq samples

The Principal Component Analysis (PCA) plot was generated using DESeq2 through the galaxy wrapper. The PCA plot displays variance in gene expression between sequencing samples. Principal component 1 was plotted on the x-axis against principal component 2 on the y-axis. The distance between two points on an axis was proportional to the variance in gene expression between those points. Control NSC samples at P2 and P3 cluster closely together on the PCA plot, and when grouped, gene expression profiles for control NSC at P2 and P3 display some overlap.

The Sample-Sample distances plot (Figure 72.) is a clear means by which to interrogate the similarities and differences between each individual samples. This enables investigation of similarities and dissimilarities between biological repeats as well as between samples under the different conditions. The heatmap of the distance matrix gives an overview of similarities between samples. A hierarchical clustering based on the sample distances was added to the heatmap. The sample *PSEN1* P3 F is dissimilar to all other samples including other *PSEN1* P3 samples and all samples are most dissimilar to this sample. This data may indicate that the sample *PSEN1* P2 F should be removed from analysis, however as sample sizes were small ($n=3$) for each variable, this sample was not removed. Other biological repeats displayed greater similarities with other samples in that group and greater differences with samples from other groups.

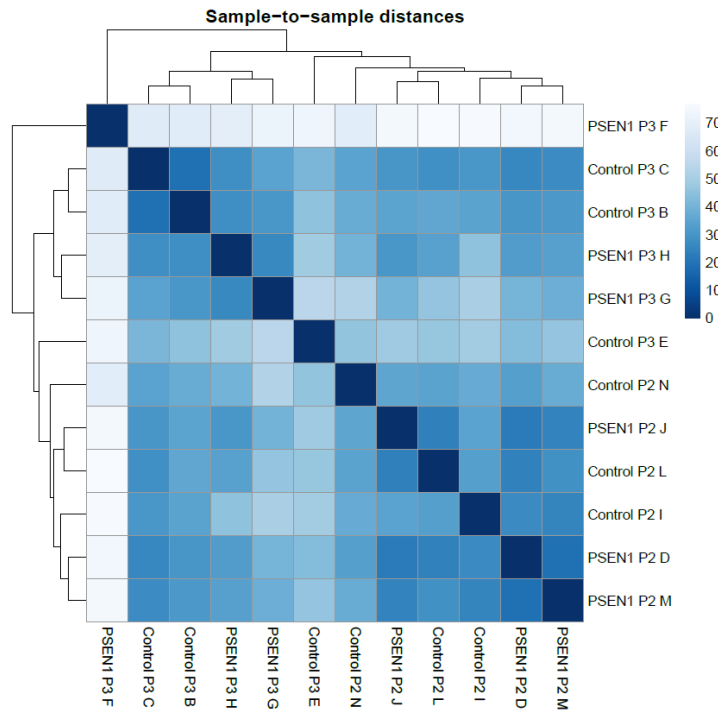


Figure 71. Sample-to-sample distances heatmap

The Sample-to-Sample Distances Heatmap gives an overview of similarities and differences between samples. Hierarchical clustering was added to the heatmap based on sample distances. Samples are plotted on both the x and y-axis for comparison with all other samples. No differences between samples is shown by a dark blue colour, for example, there is no difference between the sample *PSEN1* P2 M and *PSEN1* P2 M, because these are the same sample.

The dispersion plot (Figure 72) displays the spread or variability in the RNA sequencing data set. DESeq2 assumes similar levels of dispersion for genes with similar expression levels. Gene-wise dispersion estimates were shrunk to the expected dispersion values, thus reducing the likelihood of false positives. Outliers were not shrunk towards the fitted values as this can increase the risk of false positives. The dispersion estimate plot displayed negative correlation between dispersion levels and mean normalised counts, this indicated no contamination or outlier samples were present in the sequencing data.

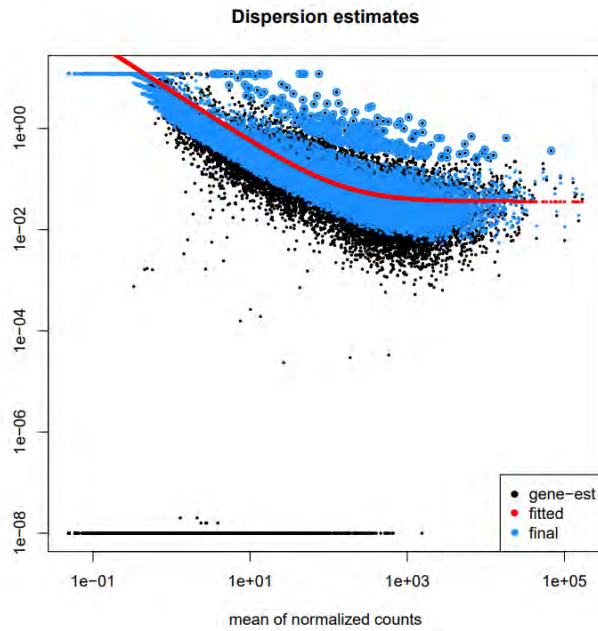


Figure 72. Dispersion estimates RNA sequencing data

6.3.6 Analysis of differential gene expression in rna sequencing data

DESeq2 was used to identify genes which were differentially expressed between sample groups. Histograms were used to compare the p-values for DEGs between samples (Figure 73) and MA-plots were used to display log fold-change attributable to a given variable, plotted against the mean of normalised counts for all samples in the data set (Figure 74). Volcano plots were used to display significant ($p < 0.05$) DEGs from P2 to P3 in *PSEN1* and control NSC (Figure 76).

p-Value Histograms for DEGs display few significant DEGs when control NSC are compared at P2 and P3 (A) but displays a much greater number of significant DEGs when *PSEN1* NSC are compared at P2 and P3 (B). This indicates that there are more changes occurring in *PSEN1* neural differentiation than in control neural differentiation. Data displays few significant DEGs between control and *PSEN1* NSC at P2 (C) but a much greater number of significant DEGs between control and *PSEN1* NSC at P3 (D). This indicates that at the earlier passage, control and *PSEN1* NSC do

not vary significantly, but that as they mature, control and *PSEN1* NSC become more divergent in their gene expression.

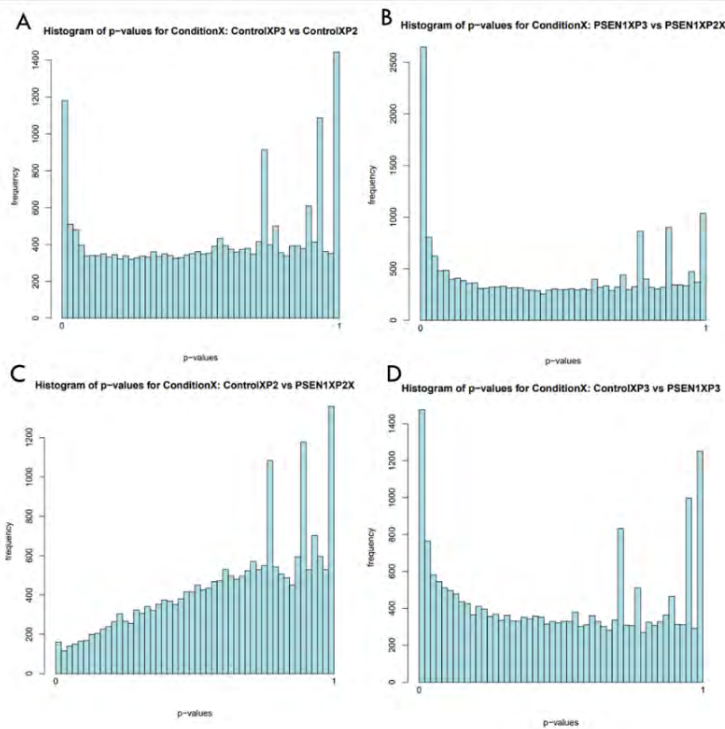


Figure 73. p-value histograms for DEGs

Histograms of p-values for DEGs between samples. The y-axis shows p-values, and the x-axis displays the frequency of that p-value occurring. A.) Histogram of p-values for control P3 vs control P2. B.) Histogram of p-values for *PSEN1* P3 vs *PSEN1* P3. C.) Histogram of p-values for control P2 vs *PSEN1* P2. D.) Histogram of p-values for control P3 vs *PSEN1* P3. The data displays few significant DEGs when control NSC are compared at P2 and P3 (A) but displays a much greater number of significant DEGs when *PSEN1* NSC are compared at P2 and P3 (B). This indicates that there are more changes occurring in *PSEN1* neural differentiation than in control neural differentiation. Data displays few significant DEGs between control and *PSEN1* NSC at P2 (C) but a much greater number of significant DEGs between control and *PSEN1* NSC at P3 (D). This indicates that at the earlier passage, control and *PSEN1* NSC do not vary significantly, but that as they mature, control and *PSEN1* NSC become more divergent in their gene expression.

MA-plots are 2D scatter plots which were used to aid visualisation of gene expression changes in RNA sequencing data between two different conditions, for example, control vs *PSEN1* or early passage vs later passage. MA-plots display log fold-change

attributable to a given variable, plotted against the mean of normalised counts for all samples in the data set. Genes which have similar expression values in both conditions are shown to cluster around $M=0$ on the y-axis, this indicates no significant changes in gene expression between the two conditions. Genes which are upregulated from one condition to another are shown above the $M=0$ line, genes which are downregulated from one condition to the other are shown below $M=0$ on the y-axis. Red points indicate the adjusted p-value is < 0.1 . MA-plots do not consider p-values, nor do they consider adjusted p-values, for this reason, MA-plots cannot be used to accurately visualise statistical significance in gene expression.

DESeq2 computes fold change of factor level 1 against factor level 2, meaning that genes in factor level 2 are upregulated or downregulated compared with genes in factor level 1. (Figure 74 A). displays genes which were differentially expressed in control P2 NSC when compared with control P3 NSC. (Figure 74 B). displays genes which were differentially expressed in *PSEN1* NSC at P2 when compared with *PSEN1* NSC at P3. Changes in gene expression occurred in both control and *PSEN1* neural differentiation (P2 NSC to P3 NSC). Many genes were upregulated during neural differentiation from P2 to P3 and are displayed here as downregulated from P3 to P2. When analysed further, many of the genes differentially expressed from P2 to P3 NSC in both control and *PSEN1* samples were genes associated with neural differentiation. The differences visualised between MA-plots A. and B. indicate that the number of DEGs with an adjusted p-value of < 0.1 is much greater in *PSEN1* neural differentiation (P2 to P3) than in control neural differentiation (P2 to P3), indicating that there are more changes in gene expression occurring in *PSEN1* neural differentiation than in control neural differentiation. Figure 74 C. displays genes which were upregulated and downregulated in *PSEN1* P2 NSC when compared with control P2 NSC. Figure 74 D. shows genes which were upregulated and downregulated in *PSEN1* P3 NSC when compared with control P3 NSC. Figure 74 C. displays a small number of DEGs with an adjusted p-value of < 0.1 when *PSEN1* and control NSC are compared at P2, whereas (Figure 74 D). shows this number increasing

greatly when the same cells are compared one passage later at P3. These data indicate that gene expression does not vary greatly between *PSEN1* and control NSC at earlier stages in neural differentiation, but that as NSC mature, there is an increase in transcriptomic differences between cells containing the *PSEN1* mutation and controls.

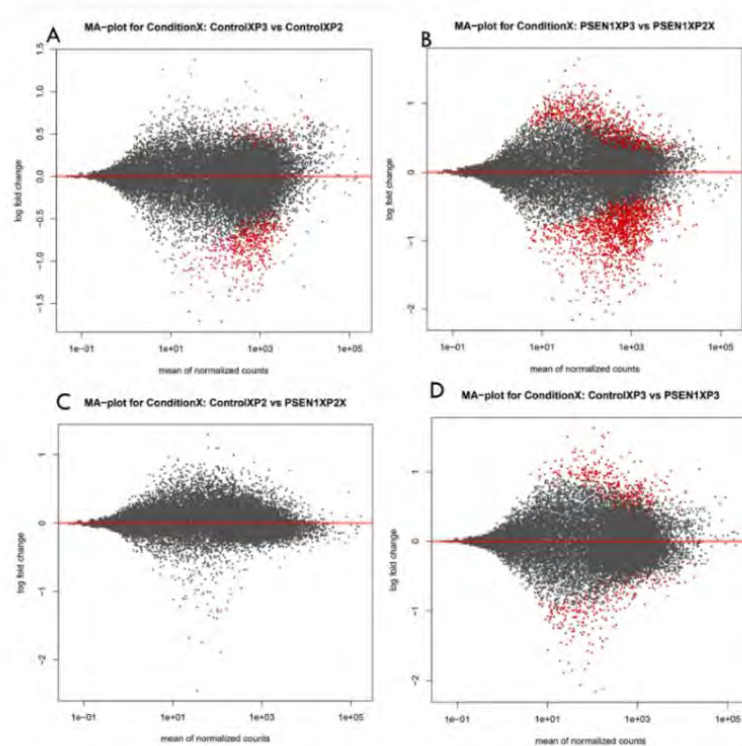


Figure 74. MA-plots for RNA sequencing data

MA-plots display log fold-change attributable to a given variable, plotted against the mean of normalised counts for all samples in the data set. Genes with similar expression values in both conditions are shown to cluster around $M=0$ on the y-axis, genes which are upregulated from one condition to another are shown above the $M=0$ line, genes which are downregulated from one condition to the other are shown below $M=0$ on the y-axis. Red points indicate the adjusted p-value is < 0.1 . A.) Log fold change values for gene expression changes between control P3 and control P2 NSC. This plot shows genes which were upregulated and downregulated in control P2 NSC when compared with control P3 NSC. B.) Log fold change values for gene expression changes between *PSEN1* P3 and *PSEN1* P2 NSC. This plot shows genes which were upregulated and downregulated in *PSEN1* P2 NSC when compared with control P3 NSC. Many genes were upregulated during neural

differentiation from P2 to P3 and are displayed here as downregulated from P3 to P2. Changes in gene expression occurred in both control and *PSEN1* neural differentiation (P2 NSC to P3 NSC). The differences visualised between MA-plots A and B indicate that the number of DEGs with an adjusted p-value of <0.1 is much greater in *PSEN1* neural differentiation (P2 to P3) than in control neural differentiation (P2 to P3). This indicates that there are more changes in gene expression occurring in *PSEN1* neural differentiation than in control neural differentiation. C.) Log fold change values for gene expression changes occurring in *PSEN1* P2 NSC when compared with control P2 NSC. This plot shows genes which were upregulated and downregulated in *PSEN1* P2 NSC when compared with control P2 NSC. D.) Log fold change values for gene expression changes between *PSEN1* P3 and control P3 NSC.

Genes which were differentially expressed between sample groups were filtered for fold change >1 and significance ($p < 0.05$), after which the number of DEGs per sample group comparison was plotted (Figure 75). Between *PSEN1* NSC at P2 and *PSEN1* NSC at P3, 409 genes were differentially expressed. Between control NSC at P2 and control NSC at P3, 87 genes were differentially expressed. The number of genes which were differentially expressed during *PSEN1* neural differentiation (from P2 to P3) was 4.7 fold higher than the number of genes seen to be differentially expressed during control neural differentiation (from P2 to P3). When the sample group control P2 NSC was compared to the sample group *PSEN1* P2 NSC, there were 12 DEGs. When the sample group *PSEN1* P3 NSC was compared with the sample group control P3 NSC, there were 119 DEGs. The number of genes which were differentially expressed when comparing control and *PSEN1* NSC at P3 was 9.92 fold higher than when comparing control and *PSEN1* NSC at P2. Results indicated that the greatest number of DEGs were seen between *PSEN1* NSC at P2 and *PSEN1* NSC at P3. The second largest number of DEGs was seen when comparing control NSC at P3 and *PSEN1* NSC at P3.

Number of DEGs Per Sample Group Comparison

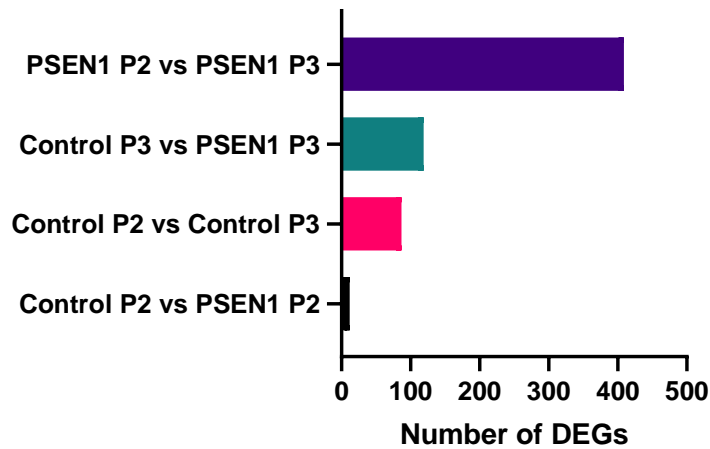


Figure 75. Number of DEGs per sample group comparison

Post filtering of DEGs for fold change >1 and significance ($p < 0.05$), the number of DEGs per sample group comparison were plotted. Using DESeq2, comparison between *PSEN1* NSC at P2 and *PSEN1* NSC at P3 generated 409 DEGs, comparison between control NSC at P3 and *PSEN1* NSC at P3 generated 119 DEGs, comparison between control NSC at P2 and control NSC at P3 generated 87 DEGs and comparison between control P2 NSC and *PSEN1* P2 NSC generated 12 DEGs. Results indicate that the greatest number of DEGs were seen between *PSEN1* NSC at P2 and *PSEN1* NSC at P3. The second largest number of DEGs was seen when comparing control NSC at P3 and *PSEN1* NSC at P3. The number of DEGs seen during *PSEN1* neural differentiation was 4.7 fold higher than the number of DEGs seen in control neural differentiation. The number of DEGs seen when comparing control and *PSEN1* NSC at P3 was 9.92 fold higher than the number of DEGs seen when comparing *PSEN1* and control NSC at P2.

MA-plots do not consider p-values nor adjusted p-values so cannot be used to visualise statistical significance in gene expression, for this reason, volcano plots were generated to indicate genes with statistically significant differences. DEGs determined by DESeq2 were filtered based on $p < 0.05$ and a fold change of >1 , after which, volcano plots were generated to display the overall number of genes which were dysregulated to a statistically significant degree between samples.

Volcano plots (**Figure 76**) display a much greater number of statistically significant ($p < 0.05$) DEGs between *PSEN1* NSC P2 and *PSEN1* NSC P3 (B) than between control NSC P2 and control NSC P3 (A). This indicates that there are more statistically significant ($p < 0.05$) changes occurring during *PSEN1* neural differentiation than occur during control neural differentiation. A greater number of genes are upregulated during both control (A) and disease (B) neural differentiation than are downregulated. The most upregulated genes in control neural differentiation (A.) are *PLEC*, *ANO8*, *CCDC85B*, *ADAMTS7* and *ZDHHC8*. The most upregulated genes in *PSEN1* neural differentiation (B.) are *PLEC*, *CORO1B*, *BTBD2*, *LRFN4* and *NDUFS7*. With the exception of *CORO1B*, these genes are all upregulated in both *PSEN1* and control neural differentiation, and almost all are upregulated to a higher degree in *PSEN1* neural differentiation.

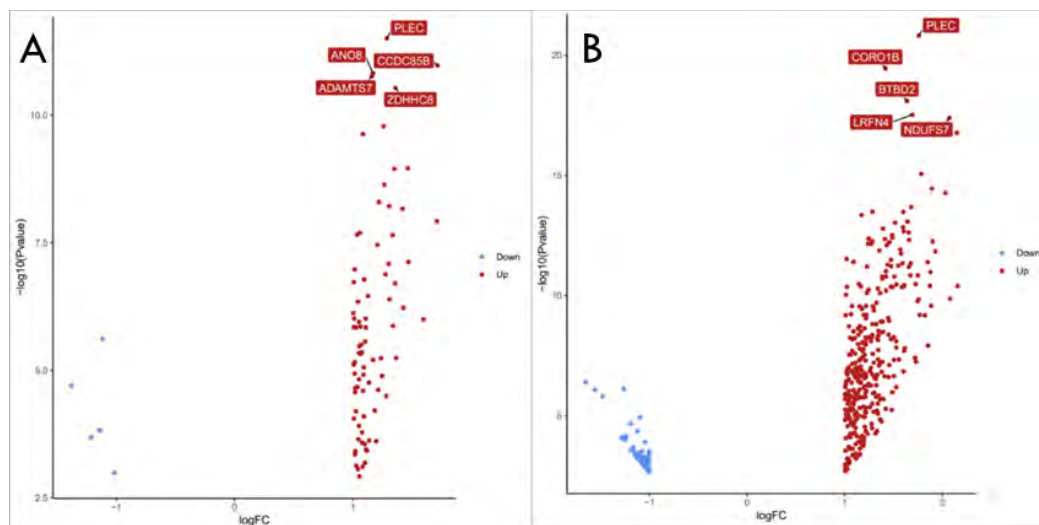


Figure 76. Volcano plots for DEGs

Volcano plots display significant ($p < 0.05$) DEGs from P2 to P3 in *PSEN1* and control NSC. Blue dots represent genes which were significantly ($p < 0.05$) downregulated in P3 compared with P2 and red dots represent genes which were significantly ($p < 0.05$) upregulated in P3 compared with P2. A.) Volcano plot displaying statistically significant ($p < 0.05$) DEGs from P2 to P3 in control NSC. B.) Volcano plot displaying statistically significant ($p < 0.05$) DEGs from P2 to P3 in *PSEN1* NSC. Data displayed a much greater number of statistically significant ($p < 0.05$) DEGs between *PSEN1* NSC P2

and *PSEN1* NSC P3 (B) than between control NSC P2 and control NSC P3 (A). A greater number of genes were upregulated during both control (A) and disease (B) neural differentiation than are downregulated. The five most upregulated genes in control neural differentiation (A.) were *PLEC*, *ANO8*, *CCDC85B*, *ADAMTS7* and *ZDHHC8*. The five most upregulated genes in *PSEN1* neural differentiation (B.) were *PLEC*, *CORO1B*, *BTBD2*, *LRFN4* and *NDUFS7*.

6.3.6 Analysis of pathways and molecular functions altered in *PSEN1* and control neural differentiation

Analysis of the pathways, molecular functions and biological processes dysregulated in *PSEN1*, and control neural differentiation was carried out using Gene Ontology (GO), the protein annotation through evolutionary relationship (PANTHER) classification system and the Reactome Database.

Prior to pathway analysis, DEGs generated from differential gene expression analysis were filtered based on $p < 0.05$ and a fold change of > 1 . Gene Ontology results indicated that the molecular functions protein binding and binding were significantly upregulated in *PSEN1* NSC at P3 compared with *PSEN1* NSC at P2 (FDR $p < 0.05$) (Figure 77).

Analysis Type:	PANTHER Overrepresentation Test (Released 20220202)						
Annotation Version and Release Date:	GO Ontology database DOI: 10.5281/zenodo.5725227 Released 2020-11-01						
Analysed List:	upload_1 (Homo sapiens)						
Reference List:	Homo sapiens (all genes in database)						
Test Type:	FISHER						
Correction:	FDR						
GO molecular function complete	Homo sapiens - REFLIST (20589)	Number	Expected	Fold Enrichment	+	Raw p-Value	FDR
protein binding (GO:0005515)	14398	324	279.02	+	1.16	4.42E-07	2.16E-03
binding (GO:0005488)	16554	355	320.8	+	1.11	6.91E-06	1.69E-02

Figure 77. significantly dysregulated molecular functions in *PSEN1* neural differentiation.

GO results display molecular functions which were up or downregulated in *PSEN1* NSC at P3 compared with *PSEN1* NSC at P2. Processes which are up or down regulated in *PSEN1* NSC compared with control NSC are denoted by a + or a – symbol.

Gene Ontology results indicated that there were no statistically significant dysregulated pathways seen between control P2 NSC and control P3 NSC, and no statistically significant dysregulated pathways seen between *PSEN1* P2 and *PSEN1* P3 NSC. Pathway dysregulation which was seen to be significant as a raw p-value lost significance when the false discovery rate cut-off of <0.05 was applied. Non-significant trends seen in pathway dysregulation were investigated using the Reactome database, significant DEGs were projected onto the human genome in an aim to elucidate trends in pathway dysregulation and expression data used by Reactome was obtained from the Gene Expression Atlas. Analysis of control neural differentiation using Reactome (Figure 78) revealed trends in dysregulation of pathways related to extracellular matrix organisation, metabolism, gene expression (transcription), developmental biology, DNA repair and programmed cell death.

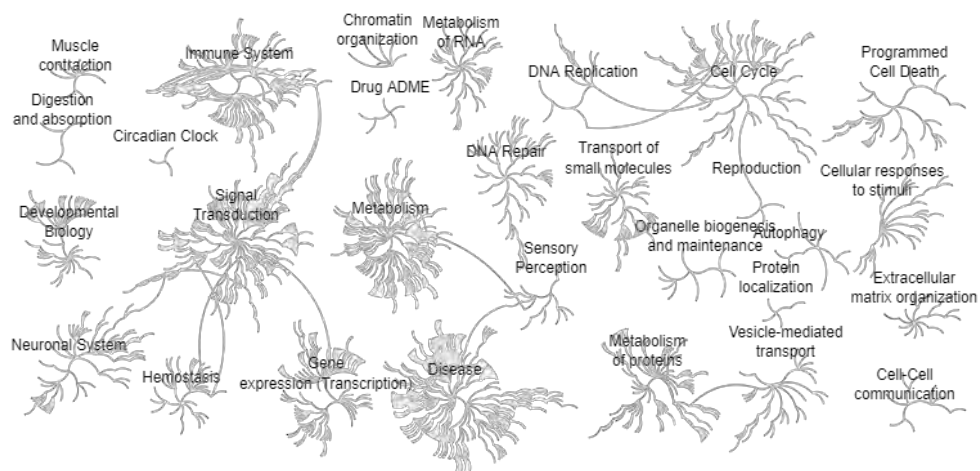


Figure 78. Pathway alterations during control neural differentiation

The Reactome database was used to visualise trends in pathways dysregulated during neural differentiation in control NSC. Pathways dysregulated in control neural differentiation included metabolism, gene expression (transcription), extracellular matrix organisation, developmental biology, and programmed cell death. Diagram generated using Reactome.

P3. Between control NSC at P2 and P3, pathways altered included Wnt signalling, integrin signalling, VEGF signalling and p38 MAPK signalling pathways, along with pathways related to development and angiogenesis (Figure 80). DEGs related to Alzheimer’s disease presenilin pathway included *LRP5*, *LRP3*, *MMP17*, *PCSK4* and *DVL1*, all of which were all upregulated from P2 to P3 NSC. DEGs related to Wnt signalling included *LRP5* and *DVL1*, which were both upregulated from P2 to P3 NSC. In relation to angiogenesis, *PKD1* and *DVL1* were upregulated during control neurogenesis.

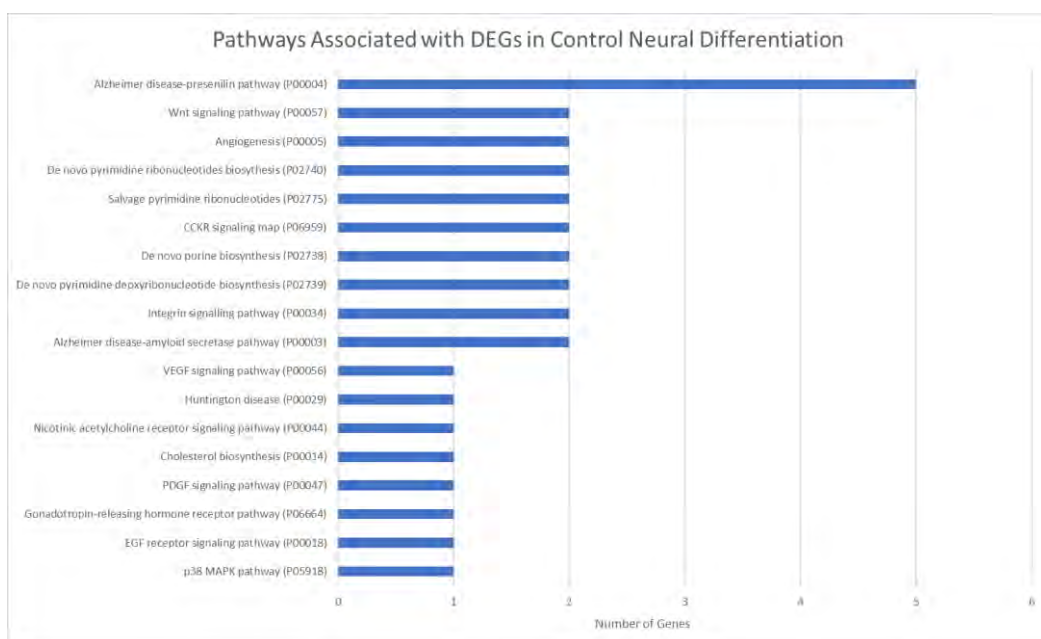


Figure 80. Pathway Analysis of DEGs in control Neural Differentiation

Pathway analysis of DEGs in control neural differentiation was carried out using PANTHER. Between control NSC at P2 and P3, pathways altered included Wnt signalling, integrin signalling, VEGF signalling, p38 MAPK signalling pathways and angiogenesis.

Between *PSEN1* NSC at P2 and P3, pathways dysregulated included Wnt signalling, angiogenesis, Huntington disease and pathways related to Alzheimer’s disease presenilin pathway. DEGs related to the Alzheimer’s disease presenilin pathway were *DVL1*, *ACTG2*, *PUF60*, *LRP3*, *MMP17*, *PCSK4*, *ERBB4* and *FZD9*. DEGs related to Notch

signalling were *NCOR2*, *HEY1*, *JAG2* and *RFNG*. *RFNG*, *NCOR2*, *JAG2* were upregulated in P3 NSC compared with P2 NSC and *HEY1* was downregulated in P3 NSC compared with P2 NSC in cells with the *PSEN1* mutation (Figure 81).

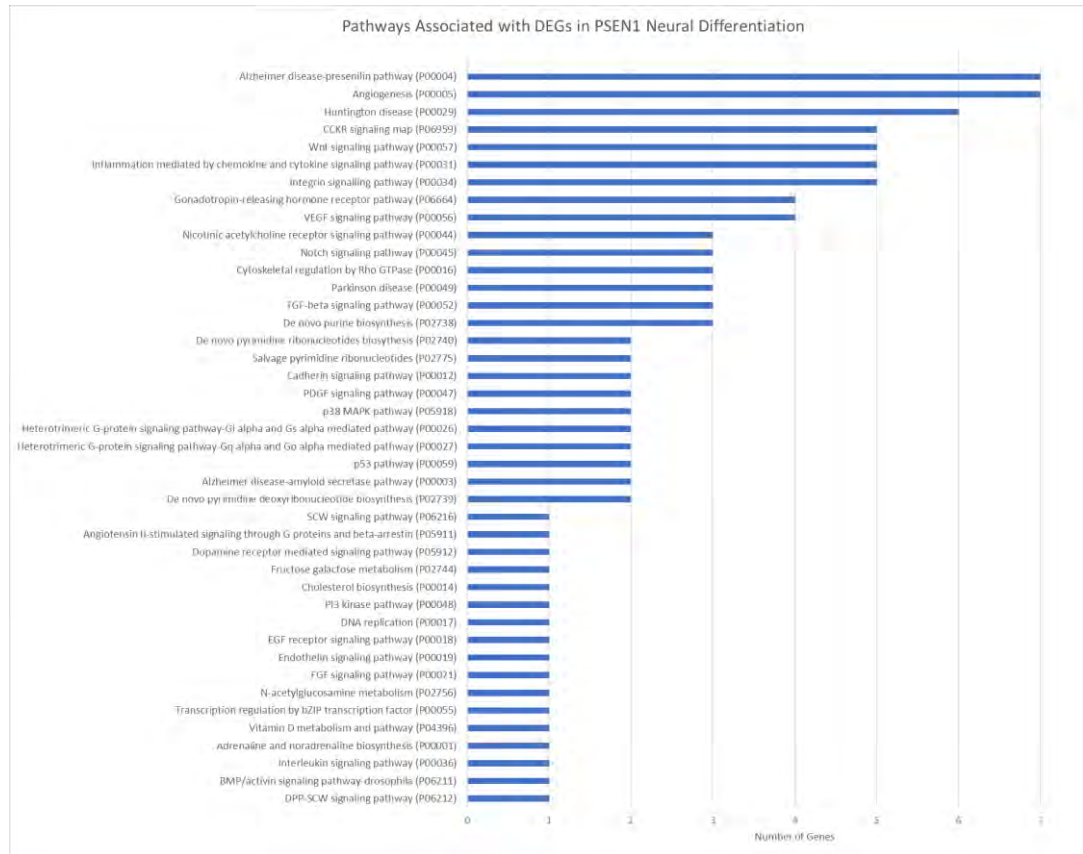


Figure 81. Pathway analysis of DEGs in *PSEN1* neural differentiation

Analysis was carried out using the Panther Classification System to investigate pathways associated with DEGs dysregulated during *PSEN1* neural differentiation. Between *PSEN1* NSC at P2 and P3, pathways dysregulated included Wnt signalling, Notch signalling, angiogenesis, Alzheimer’s disease presenilin pathway and inflammation mediated by chemokine and cytokine signalling.

Biological processes dysregulated in control neural differentiation were analysed using the PANTHER classification system. Dysregulated biological processes included cellular processes, metabolic processes, processes related to biological regulation, localisation, response to stimulus, signalling and developmental process. DEGs associated with development included *PLEC*, *ERF*, *METR1*, *BTBD2* and *MAP1S*, all of

which were significantly upregulated during control neural differentiation. DEGs associated with cellular processes included JPH4, SIVA1, MIB2, TRAPPC5, ERF, *PLEC* and TPGS1, all of which were significantly upregulated during control neural differentiation.

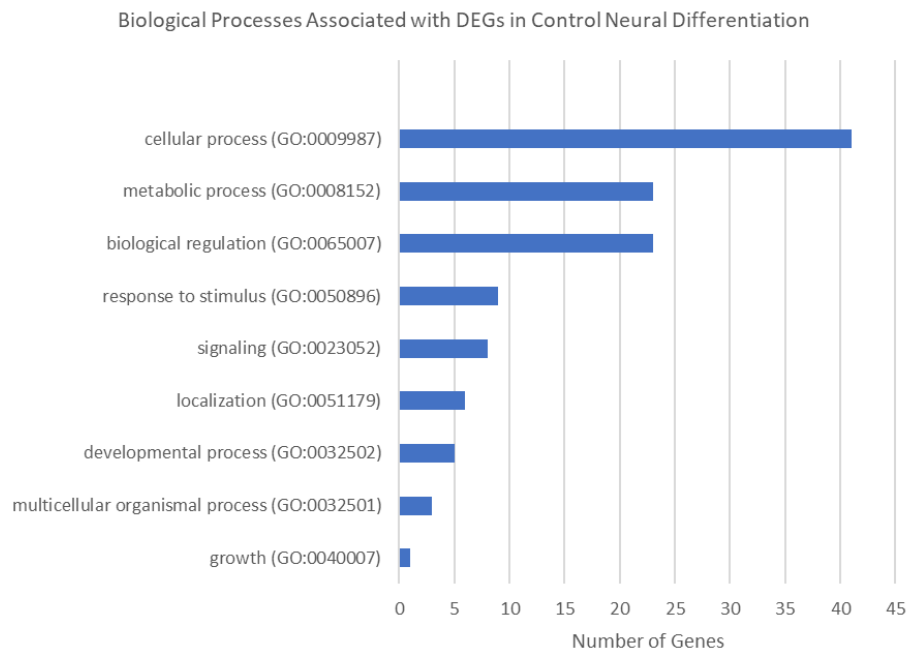


Figure 82. Biological processes associated with DEGs in control neural differentiation

Biological processes associated with DEGs in control neural differentiation were analysed using the PANTHER classification system. Biological processes which were dysregulated during control neural differentiation included cellular processes, metabolic processes, biological regulation, developmental processes, and growth. DEGs associated with processes of the immune system included EOMES, ZFPM1, ZBTB17, CACTIN and UNC93B1.

Biological processes dysregulated in *PSEN1* neural differentiation were analysed using the PANTHER classification system. Dysregulated biological processes in *PSEN1* neural differentiation included cellular processes, metabolic processes, processes related to biological regulation, localisation, response to stimulus, signalling and

developmental process (Figure 83). DEGs associated with immune system processes included EOMES, ZFPM1, ZBTB17, CACTIN and UNC93B1. The DEGs associated with development seen in control neural differentiation were also significantly upregulated in disease neural differentiation, however, in *PSEN1* neural differentiation, there were 6 fold more DEGs associated with development, indicating upregulation of pathways related to development in disease. DEGs in *PSEN1* neural differentiation included CEND1, which plays a role in cell cycle exit and neuronal differentiation and was significantly upregulated in *PSEN1* neural differentiation, *CDH20* which was significantly downregulated in *PSEN1* neural differentiation, FGFR4 -fibroblast growth factor receptor 4- which was significantly upregulated in *PSEN1* P3 compared with P2 and ERG which codes for the ERG protein – a transcriptional regulator that plays a role in regulation of embryonic development, cellular proliferation, differentiation, and apoptosis. ERG was downregulated in *PSEN1* neural differentiation. The gene *SEMA6B* was significantly upregulated in *PSEN1* neural differentiation and is associated with growth and axon guidance.

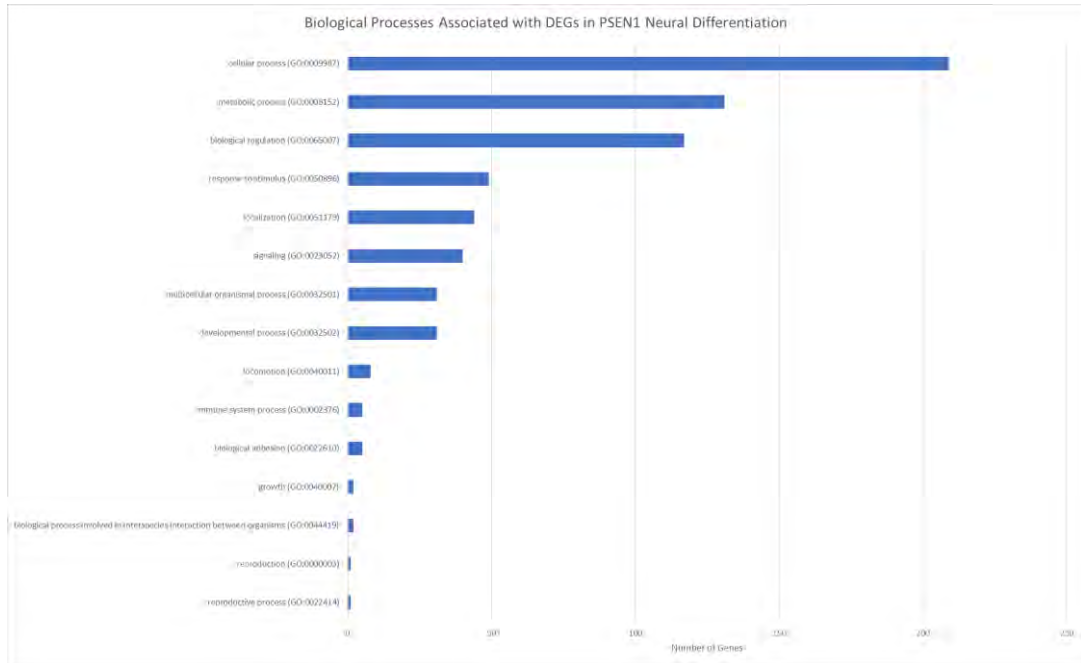


Figure 83. Biological processes associated with DEGs in *PSEN1* neural differentiation

Biological processes associated with DEGs in *PSEN1* neural differentiation were analysed using the PANTHER classification system. Biological processes which were dysregulated in *PSEN1* neural differentiation included cellular processes, metabolic processes, processes related to biological regulation, localisation, response to stimulus, signalling and developmental process.

Genes related to cell cycle regulation which were significantly up and downregulated from P2 to P3 in *PSEN1* A246E NSC were collected and analysed to interrogate mechanisms behind cell cycle dysregulation in disease NSC (Table 29)

Table 29. Log2(FC) Values for significant DEGs Related to Cell Cycle Regulation

Gene	Log2(FC)
<i>SCRIB</i>	2.15
PIDD1	1.64
<i>FZD9</i>	1.58
E4F1	1.39
NOS3	1.32
FBXW5	1.28
MIIP	1.27
ZBTB17	1.26
DOT1L	1.24
PKD1	1.23
DGKZ	1.22
BOP1	1.19
JUNB	1.14
CEP131	1.14
TP53I13	1.10
GADD45G	1.09
CDT1	1.09
CDK18	1.04
AURKAIP1	1.00
MSX1	-1.01
CABLES1	-1.08
MECOM	-1.19
EDN3	-1.28

For analysis of DEGs specific to *PSEN1* neural differentiation, DEGs found in both control and *PSEN1* neural differentiations were removed and DEGs which were specific to *PSEN1* neural differentiation were manually organised into four categories: cell signalling, cytoskeletal, nuclear and metabolism (Figure 84). The majority of DEGs specific to *PSEN1* neural differentiation were involved in biological processes occurring in the nucleus (43%), for example, transcriptional activators and repressors, 29% of DEGs specific to *PSEN1* neural differentiation were associated

with cell signalling, 14% of DEGs were associated with metabolism and 14% of DEGs specific to *PSEN1* neural differentiation were associated with cytoskeletal processes.

Categorisation of DEGs

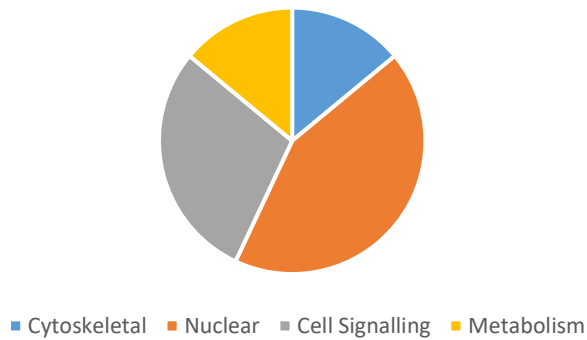


Figure 84. Analysis of DEGs exclusively found in *PSEN1* neural differentiation

DEGs exclusive to *PSEN1* neural differentiation were isolated and grouped into four categories: cell signalling, cytoskeletal, nuclear and metabolism. The majority (43%) of DEGs were exclusive to *PSEN1* neural differentiation were associated with the nucleus, 29% of DEGs specific to *PSEN1* neural differentiation were associated with cell signalling, 14% of DEGs were associated with metabolism and 14% were associated with cytoskeletal processes.

Further analysis of DEGs specific to *PSEN1* neural differentiation revealed significant dysregulation ($p < 0.05$) of a subset of genes related to Wnt and Notch signalling. DEGs related to Wnt signalling which were significantly ($p < 0.05$) upregulated during *PSEN1* neural differentiation included *FZD9*, *LRP3* and *CSNK1G2*. *DKK2*, *CDH2* and *ACTG2* were significantly ($p < 0.05$) downregulated in *PSEN1* neural differentiation (Figure 85). DEGs linked with Notch signalling that were significantly ($p < 0.05$) upregulated during *PSEN1* neural differentiation included *JAG2*, *CHAC1*, *NCOR2* and *RFNG*. *HEY1* was significantly downregulated ($p < 0.05$) during *PSEN1* neural differentiation.

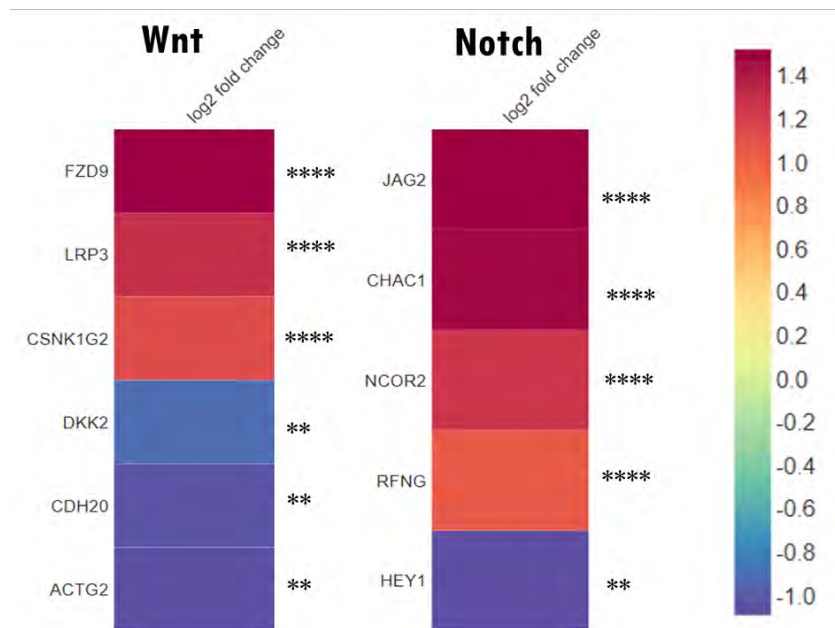


Figure 85. DEGs in *PSEN1* neural differentiation linked with Wnt and Notch signalling

DEGs related to Wnt signalling which were significantly ($p < 0.05$) upregulated during *PSEN1* neural differentiation included *FZD9*, *LRP3* and *CSNK1G2*. *DKK2*, *CDH2* and *ACTG2* were significantly ($p < 0.05$) downregulated in *PSEN1* neural differentiation. DEGs linked with Notch signalling that were significantly ($p < 0.05$) upregulated during *PSEN1* neural differentiation included *JAG2*, *CHAC1*, *NCOR2* and *RFNG*. *HEY1* was significantly downregulated ($p < 0.05$) during *PSEN1* neural differentiation. Colder colours relate to downregulation and warmer colours relate to upregulation. The numbers refer to log₂ fold change values, so blue colours are downregulated by a maximum log fold change of -1 and warmer colours are upregulated by a maximum log fold change of 1.4.

6.3.7 Analysis of pathways and molecular functions altered between *PSEN1* and control NSC at P3

Analysis of DEGs between *PSEN1* and control NSC at P3 was carried out using the Gene Ontology (GO) database. The purpose of this analysis was to interrogate differences in more mature NSC containing the *PSEN1* mutation compared with controls. Results from GO analysis (Table 30) indicate biological processes which are significantly (FDR $p < 0.05$) dysregulated between control and *PSEN1* NSC at P3. GO analysis revealed that many biological processes which were significantly (FDR

p<0.05) dysregulated were associated with nuclear processes such as transcription. Significantly dysregulated biological processes include regulation of transcription by RNA polymerase II, regulation of gene expression, metabolic processes, and cellular processes.

Table 30. Gene ontology results for biological processes dysregulated between control NSC P3 and *PSEN1* NSC P3.

Homo sapiens (REF)	upload_1 (Hierarchy NEW!)						
	#	#	expected	Fold Enrichment	+/-	raw P value	FDR
GO biological process complete							
regulation of transcription by RNA polymerase II	2597	35	12.86	2.72	+	1.56E-08	6.10E-05
regulation of transcription, DNA-templated	3429	42	16.98	2.47	+	4.55E-09	7.12E-05
regulation of gene expression	4783	50	23.69	2.11	+	2.16E-08	4.84E-05
regulation of macromolecule metabolic process	6133	55	30.37	1.81	+	5.80E-07	6.49E-04
regulation of metabolic process	6654	57	32.95	1.73	+	1.15E-06	1.20E-03
regulation of nucleic acid-templated transcription	3430	42	16.99	2.47	+	4.59E-09	3.59E-05
regulation of RNA biosynthetic process	3439	42	17.03	2.47	+	4.96E-09	2.59E-05
regulation of macromolecule biosynthetic process	3953	43	19.58	2.2	+	1.02E-07	1.78E-04
regulation of biosynthetic process	4172	44	20.66	2.13	+	1.80E-07	2.35E-04
regulation of RNA metabolic process	3724	43	18.44	2.33	+	1.72E-08	5.40E-05
regulation of nucleobase-containing compound metabolic process	3973	45	19.68	2.29	+	1.73E-08	4.52E-05
regulation of nitrogen compound metabolic process	5586	53	27.67	1.92	+	1.37E-07	2.14E-04
regulation of cellular metabolic process	5983	52	29.63	1.75	+	4.90E-06	4.27E-03
regulation of primary metabolic process	5747	53	28.46	1.86	+	3.56E-07	4.29E-04
regulation of cellular biosynthetic process	4113	44	20.37	2.16	+	1.38E-07	1.97E-04

regulation of cellular macromolecule biosynthetic process	3925	43	19.44	2.21	+	8.59E-08	1.68E-04
nitrogen compound metabolic process	6455	14	31.97	0.44	-	6.02E-05	4.29E-02
metabolic process	7968	17	39.46	0.43	-	1.88E-06	1.74E-03
primary metabolic process	6969	15	34.52	0.43	-	2.04E-05	1.60E-02
cellular metabolic process	7094	15	35.13	0.43	-	1.33E-05	1.09E-02
cellular process	15139	55	74.98	0.73	-	2.41E-05	1.80E-02
organic substance metabolic process	7506	15	37.17	0.4	-	1.46E-06	1.43E-03

Results display biological processes which are significantly (FDR $p < 0.05$) dysregulated between control and *PSEN1* NSC at P3. Significantly dysregulated processes include regulation of transcription by RNA polymerase II, regulation of gene expression, metabolic processes, and cellular processes. GO results indicated that these biological processes are upregulated in *PSEN1* NSC at P3 compared with control NSC at P3. Only results with FDR $p < 0.05$ are displayed. Processes which are up or down regulated in *PSEN1* NSC compared with control NSC are denoted by a + or a – symbol.

Biological processes which were dysregulated between *PSEN1* and control NSC at P3 were analysed using the PANTHER classification system. Biological processes dysregulated between *PSEN1* and control NSC at P3 were categorised into one of the following groups: cellular processes, metabolic processes, biological regulation, signalling, response to stimulus, multicellular organismal processes, developmental processes, localisation, biological processes involving interspecies interaction between organisms, immune system processes, reproduction, and reproductive processes. DEGs associated with processes of the immune system included EOMES, ZFPM1, ZBTB17, CACTIN and UNC93B1.

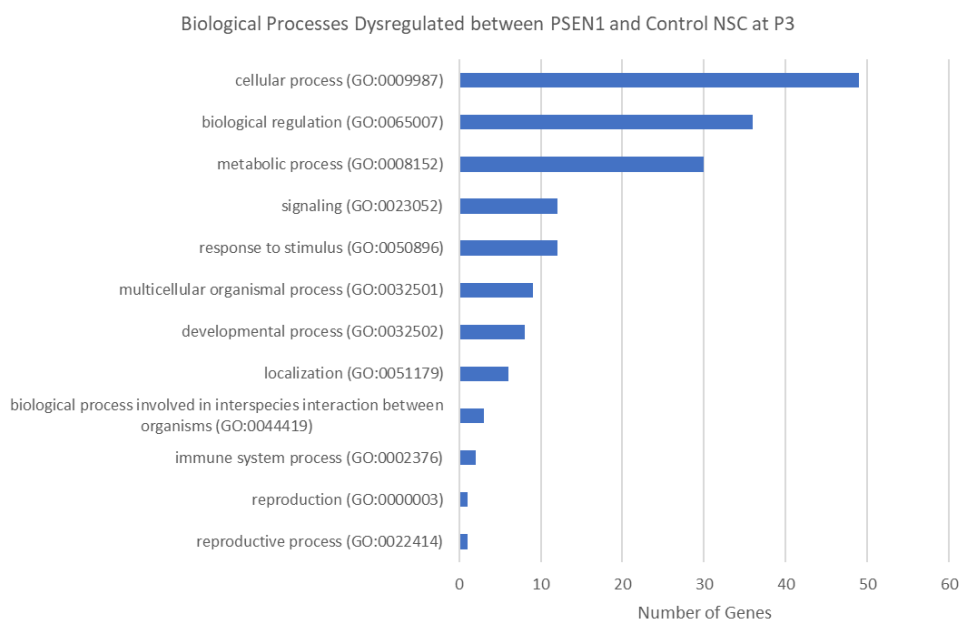


Figure 86. Biological processes dysregulated between *PSEN1* and control NSC at P3

Biological processes which were dysregulated between *PSEN1* and control NSC at P3 were analysed using the PANTHER classification system. Biological processes dysregulated between *PSEN1* and control NSC at P3 were categorised into one of the following groups: cellular processes, metabolic processes, biological regulation, signalling, response to stimulus, multicellular organismal processes, developmental processes, localisation, biological processes involving interspecies interaction between organisms, immune system processes, reproduction, and reproductive processes. DEGs associated with processes of the immune system included EOMES, ZFPM1, ZBTB17, CACTIN and UNC93B1.

Molecular functions which were dysregulated in *PSEN1* NSC at P3 compared with control NSC at P3 were analysed using the PANTHER classification system via Gene Ontology. Results from GO and PANTHER based analysis (Table 30, Table 31) indicate molecular functions which are significantly (FDR $p < 0.05$) dysregulated between control and *PSEN1* NSC at P3. GO analysis revealed that many molecular functions which were significantly dysregulated were associated with nuclear processes such as transcription. Significantly dysregulated molecular functions include DNA transcription factor binding activity, RNA polymerase II transcription regulatory region sequence specific DNA binding and transcription regulator activity.

Table 31 Molecular functions significantly dysregulated in *PSEN1* P3 NSC compared with control NSC at P3.

Analysis Type:	PANTHER Overrepresentation Test (Released 20220202)						
Annotation Version and Release Date:	GO Ontology database DOI: 10.5281/zenodo.5725227 Released 2020-11-01						
Analysed List:	upload_1 (Homo sapiens)						
Reference List:	Homo sapiens (all genes in database)						
Test Type:	FISHER						
Correction:	FDR						
GO molecular function complete	Homo sapiens - REFLIST (20589)	upload_1 (102)	upload_1 (expected)	upload_1 (over/under)	upload_1 (fold Enrichment)	upload_1 (raw P-value)	upload_1 (FDR)
DNA-binding transcription factor activity, RNA polymerase II-specific (GO:0000981)	1390	34	6.89	+	4.94	2.79E-15	1.36E-11
RNA polymerase II transcription regulatory region sequence-specific DNA binding (GO:0000977)	1435	34	7.11	+	4.78	6.97E-15	1.71E-11
DNA-binding transcription factor activity (GO:0003700)	1444	34	7.15	+	4.75	8.34E-15	1.36E-11
transcription cis-regulatory region binding (GO:0000976)	1531	34	7.58	+	4.48	4.42E-14	5.41E-11
transcription regulatory region nucleic acid binding (GO:0001067)	1533	34	7.59	+	4.48	4.59E-14	4.49E-11
sequence-specific double-stranded DNA binding (GO:1990837)	1588	34	7.87	+	4.32	1.24E-13	1.01E-10
double-stranded DNA binding (GO:0003690)	1686	34	8.35	+	4.07	6.64E-13	4.64E-10
sequence-specific DNA binding (GO:0043565)	1694	34	8.39	+	4.05	7.57E-13	4.64E-10
RNA polymerase II cis-regulatory region sequence-specific DNA binding (GO:0000978)	1208	24	5.98	+	4.01	4.88E-09	1.99E-06
cis-regulatory region sequence-specific DNA binding (GO:0000987)	1230	24	6.09	+	3.94	6.89E-09	2.60E-06
transcription regulator activity (GO:0140110)	1953	35	9.68	+	3.62	7.57E-12	4.12E-09
DNA binding (GO:0003677)	2498	36	12.38	+	2.91	1.48E-09	7.25E-07
metal ion binding (GO:0046872)	4287	48	21.24	+	2.26	4.43E-09	1.97E-06
nucleic acid binding (GO:0003676)	3997	44	19.8	+	2.22	4.81E-08	1.57E-05
cation binding (GO:0043169)	4376	48	21.68	+	2.21	7.44E-09	2.60E-06
ion binding (GO:0043167)	6077	51	30.11	+	1.69	1.66E-05	5.08E-03
heterocyclic compound binding (GO:1901363)	5968	48	29.57	+	1.62	1.15E-04	3.32E-02

organic cyclic compound binding (GO:0097159)	6043	48	29.94	+	1.6	1.81E-04	4.93E-02
---	------	----	-------	---	-----	----------	----------

Analysis carried out by PANTHER Overrepresentation Test revealed significant dysregulation (FDR $p < 0.05$) of pathways related to DNA binding, transcription factor activity, organic cyclic compound binding and metal ion binding. Processes which are up or down regulated in *PSEN1* NSC compared with control NSC are denoted by a + or a – symbol.

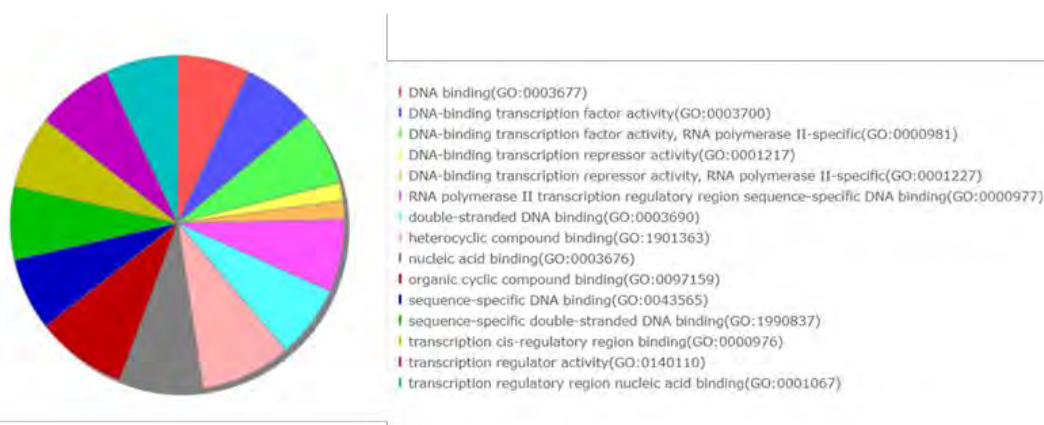


Figure 87. Pie graph to represent molecular functions significantly dysregulated in *PSEN1* NSC at P3 compared with controls

Analysis carried out by PANTHER Overrepresentation Test revealed significant dysregulation (FDR $p < 0.05$) of molecular functions related to DNA binding, transcription factor activity, organic cyclic compound binding and metal ion binding. PANTHER analysis is presented as a pie graph for ease of interpretation.

Results from PANTHER based analysis of *PSEN1* P3 NSC compared with control P3 NSC (Figure 88) indicated dysregulation of molecular functions related to binding, transcription regulator activity and catalytic activity as well as molecular transducer activity, molecular function regulator, transporter activity, molecular adapter activity and ATP-dependent activity.

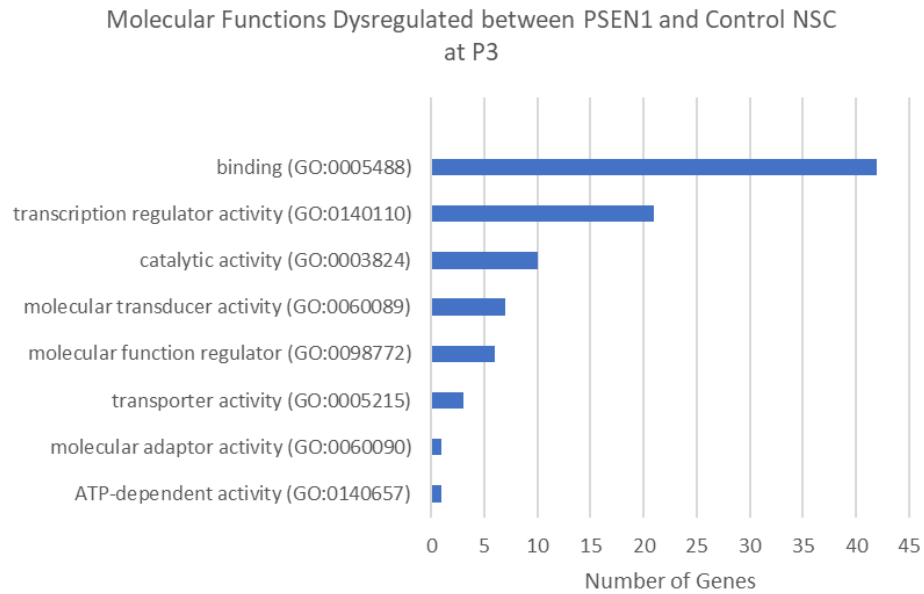


Figure 88. Molecular functions dysregulated between *PSEN1* and control NSC at P3

Molecular functions which were dysregulated in *PSEN1* NSC at P3 compared with control NSC at P3 were analysed using the PANTHER classification system, results indicated dysregulation of molecular functions related to binding, transcription regulator activity and catalytic activity as well as molecular transducer activity, molecular function regulator, transporter activity, molecular adapter activity and ATP-dependent activity.

Pathways which were dysregulated between *PSEN1* and control NSC at P3 were analysed using the PANTHER classification system. Pathways dysregulated between *PSEN1* and control NSC at P3 were categorised into one of the following groups: Wnt Signalling pathways, Integrin signalling, Endothelin signalling pathways, Alzheimer’s disease presenilin pathway, PI3 kinase pathway, Parkinson disease, 5-hydroxytryptamine degradation, Heterotrimeric G-protein signalling pathway- Gq alpha and GO alpha mediated pathway, VEGF signalling pathway, Inflammation mediated by chemokine signalling pathway, Huntington disease and interleukin signalling pathway.

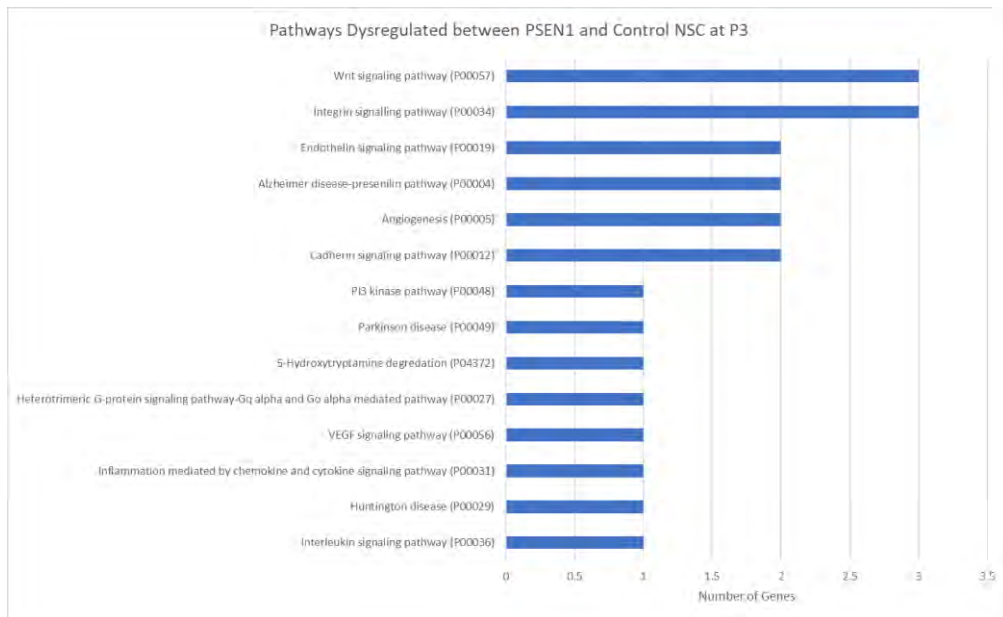


Figure 89. Pathways dysregulated between *PSEN1* and control NSC at P3

Pathways which were dysregulated between *PSEN1* and control NSC at P3 were analysed using the PANTHER classification system. Pathways dysregulated between *PSEN1* and control NSC at P3 were categorised into one of the following groups: Wnt Signalling pathways, Integrin signalling, Endothelin signalling pathways, Alzheimer’s disease presenilin pathway, PI3 kinase pathway, Parkinson disease, 5-hydroxytryptamine degradation, Heterotrimeric G-protein signalling pathway- Gq alpha and GO alpha mediated pathway, VEGF signalling pathway, Inflammation mediated by chemokine signalling pathway, Huntington disease and interleukin signalling pathway.

Trends seen in pathway dysregulation between *PSEN1* NSC at P3 and control NSC at P3 were investigated using the Reactome database, significant DEGs were projected onto the human genome in an aim to elucidate trends in pathway dysregulation and expression data used by Reactome was obtained from the Gene Expression Atlas. Analysis using Reactome (Figure 90Figure 78. Pathway alterations during control neural differentiation Figure 78) revealed significant dysregulation (FDR $p < 0.05$) of pathways related to gene expression, specifically transcription related pathways, extracellular matrix organisation, disease related pathways, pathways related to developmental biology and pathways related to the immune system, specifically the IPAF inflammasome.

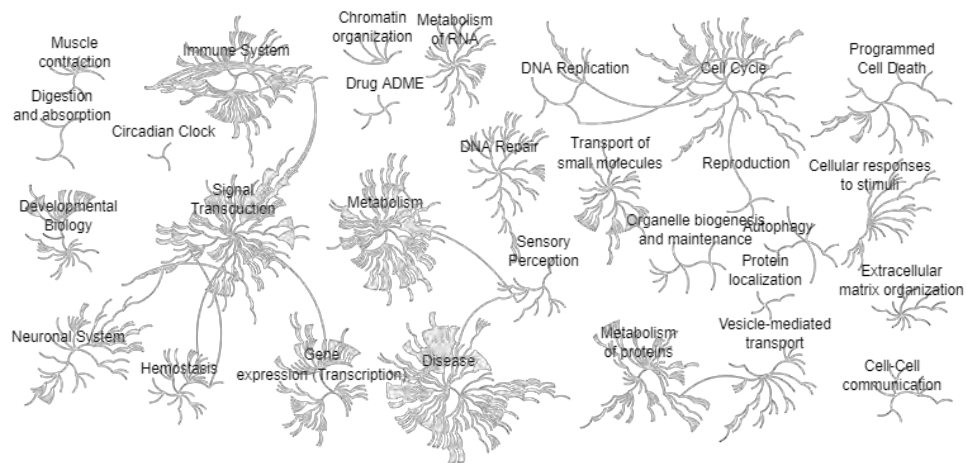


Figure 90. Pathway dysregulation between *PSEN1* and control NSC at P3

Pathways which were dysregulated between *PSEN1* and control NSC at P3 were visualised using the Reactome database. Pathways which are significantly (FDR $p < 0.05$) dysregulated in *PSEN1* NSC at P3 compared with control NSC at P3 are indicated with a copper colour. Gene expression, specifically transcription related pathways was significantly dysregulated in *PSEN1* NSC at P3 compared with control NSC at P3. Gene expression related to extracellular matrix organisation was dysregulated in *PSEN1* NSC at P3 compared with controls as were disease related pathways, pathways related to developmental biology and the immune system, specifically the IPAF inflammasome. Pathways related to programmed cell death and cell cycle were also dysregulated between *PSEN1* and control NSC at P3. Diagram generated using Reactome.

6.3.8 Chapter summary

RNA sequencing was carried out to generate differential gene expression data for transcriptome-based comparison of *PSEN1* and control NSC during neural differentiation. Results from RNA sequencing analysis of *PSEN1* and control NSC at P2 and P3 indicated that there were 4.7-fold more gene expression changes occurring during *PSEN1* neural differentiation compared with control neural differentiation (Figure 75). Volcano plots also indicate that in both control and *PSEN1* neural differentiation (from P2 NSC to P3 NSC), the majority of DEGs were upregulated, and only a small number of DEGs were downregulated. The five most upregulated genes

in *PSEN1* neural differentiation were *PLEC*, *CORO1B*, *BTBD2*, *LRFN4* and *NDUFS7*. With the exception of *CORO1B*, these genes were all upregulated in both *PSEN1* and control neural differentiation, and almost all were upregulated to a higher degree in *PSEN1* neural differentiation (Figure 76).

Pathway analysis carried out using GO indicated that Binding and Protein binding molecular functions were significantly upregulated (FDR $p < 0.05$) during *PSEN1* neural differentiation (Figure 77).

There were no statistically significant dysregulated pathways seen between *PSEN1* P2 and *PSEN1* P3 NSC, but trends appeared towards dysregulation of pathways such as Wnt signalling in both control and *PSEN1* neural differentiation (Figure 80, Figure 81) and Notch signalling, which was specific to *PSEN1* neural differentiation (Figure 81).

Analysis using Reactome indicated that during *PSEN1* neural differentiation, there were trends towards dysregulation of pathways related to disease, gene expression (transcription), metabolism, signal transduction, DNA repair, programmed cell death and the neuronal system. DEGs exclusive to *PSEN1* neural differentiation included genes which play a role in Wnt and Notch signalling pathways. DEGs related to Wnt signalling which were significantly ($p < 0.05$) upregulated during *PSEN1* neural differentiation included *FZD9*, *LRP3* and *CSNK1G2*. *DKK2*, *CDH2* and *ACTG2* were significantly ($p < 0.05$) downregulated in *PSEN1* neural differentiation. DEGs linked with Notch signalling that were significantly ($p < 0.05$) upregulated during *PSEN1* neural differentiation included *JAG2*, *CHAC1*, *NCOR2* and *RFNG*. *HEY1* was significantly downregulated ($p < 0.05$) during *PSEN1* neural differentiation (Figure 85).

GO results indicated that there were a range of biological processes which were significantly dysregulated between control NSC at P3 and *PSEN1* NSC at P3 (Table 30). The biological process that was most significantly upregulated between *PSEN1* and control NSC at P3 was regulation of transcription by RNA polymerase II (FDR

$p < 0.0001$). GO results indicated that there were a range of molecular functions which were also altered between *PSEN1* NSC at P3 and control NSC at P3 (Table 31). The molecular function which was most significantly upregulated between *PSEN1* and control NSC at P3 was DNA-binding transcription factor activity, RNA polymerase II-specific ($p < 0.0001$).

Biological processes which were dysregulated in *PSEN1* NSC at P3 compared with control NSC at P3 were further analysed using the PANTHER classification system, results indicated dysregulation of biological processes related to cellular processes, metabolic processes, biological regulation, signalling, response to stimulus, multicellular organismal processes, developmental processes, localisation, biological processes involving interspecies interaction between organisms, immune system processes, reproduction and reproductive processes (Figure 86).

Molecular functions which were dysregulated in *PSEN1* NSC at P3 compared with control NSC at P3 were further analysed using the PANTHER classification system, results indicated dysregulation of molecular functions related to binding, transcription regulator activity and catalytic activity as well as molecular transducer activity, molecular function regulator, transporter activity, molecular adapter activity and ATP-dependent activity (Figure 87, Figure 88).

Trends in pathway dysregulation between *PSEN1* and control NSC at P3 were further investigated using PANTHER and Reactome. Pathways dysregulated between *PSEN1* and control NSC at P3 as indicated by PANTHER based analysis (Figure 89) were categorised into one of the following groups: Wnt Signalling pathways, Integrin signalling, Endothelin signalling pathways, Alzheimer's disease presenilin pathway, PI3 kinase pathway, Parkinson disease, 5-hydroxytryptamine degradation, Heterotrimeric G-protein signalling pathway- Gq alpha and GO alpha mediated pathway, VEGF signalling pathway, Inflammation mediated by chemokine signalling pathway, Huntington disease and interleukin signalling pathway.

Analysis using Reactome (Figure 90) indicated that Gene expression, specifically transcription related pathways were significantly dysregulated in *PSEN1* NSC at P3 compared with control NSC at P3. Gene expression related to extracellular matrix organisation was dysregulated in *PSEN1* NSC at P3 compared with controls as were disease related pathways, pathways related to developmental biology and the immune system, specifically the IPAF inflammasome.

7.0 Interrogation of RNA sequencing results

7.1 Introduction

The work in this chapter was carried out to validate results shown in **5.3.2**, **6.3.6** and **6.3.7**. RNA sequencing data analysis indicated a trend towards dysregulation of Wnt signalling pathways between *PSEN1* NSC at P2 and *PSEN1* NSC at P3 (Figure 81). To validate and interrogate Wnt and Notch pathway dysregulation in *PSEN1* neural differentiation, DEGs which play a role in Notch and Wnt signalling were identified from RNA sequencing data for analysis using qPCR. Results of RNA sequencing indicated that Wnt related genes *FZD9*, *LRP3* and *CSNK1G2* were significantly upregulated in *PSEN1* neural differentiation and that *CDH20*, *DKK2* and *ACTG2* were significantly downregulated in *PSEN1* neural differentiation. Notch related genes *JAG2*, *CHAC1*, *NCOR2* and *RFNG* were significantly upregulated in *PSEN1* neural differentiation, whereas *HEY1* was significantly downregulated (Figure 85). DEGs selected for qPCR-based analysis were dysregulated exclusively in *PSEN1* neural differentiation and were all up or downregulated by a fold change of >1 with a p-value of <0.05. DEGs selected for investigation of Wnt signalling were *FZD9*, *ACTG2*, *CSNK1G2* and *CDH20* and DEGs selected for investigation of Notch signalling pathways were *JAG2*, *HEY1* and *RFNG*. qPCR primers were selected for the DEGs related to Wnt and Notch signalling, and primer efficiency tests were used to ensure primer sets were between 90-110% efficient.

7.2 Aims

This chapter aimed to investigate and validate RNA sequencing results and to further investigate previous cell cycle results using a combination of transcriptomic and protein-based methods, to this end, qPCR was employed to validate transcriptomic alterations in *PSEN1* NSC and flow cytometry was used to investigate alterations in apoptosis in live, nestin positive *PSEN1* NSC.

7.3 Results

7.3.1 Wnt and Notch signalling in *PSEN1* neural differentiation

qPCR was used to validate and interrogate the changes in gene expression seen in RNA sequencing data. qPCR primers were selected for *CSNK1G2*, *FZD9*, *CDH20* and *ACTG2* underwent primer efficiency tests to ensure primer sets were between 90-110% efficient. NSC were generated from *PSEN1* lines in three separate neural differentiations and were harvested at P2 and P3 for extraction of RNA. RNA used for RNA sequencing was also generated from three separate neural differentiations and was measured alongside RNA generated from the newer neural differentiations of *PSEN1* NSC. Results of qPCR based analysis of *PSEN1* NSC at P2 and P3 (Figure 92.) indicated no significant differences between *PSEN1* NSC at P2 and P3 in *FZD9* ($p=0.387$), *ACTG2* ($p= 0.156$), *CSNK1G2* ($p=0.776$) or *CDH20* ($p= 0.132$) between P2 and P3 NSC but did indicate a trend towards increased expression of *ACTG2*, *CSNK1G2* and *CDH20* in P3 NSC compared with P2 NSC. Results of *FZD9* expression may indicate dysregulation of *FZD9* in *PSEN1* NSC as they mature.

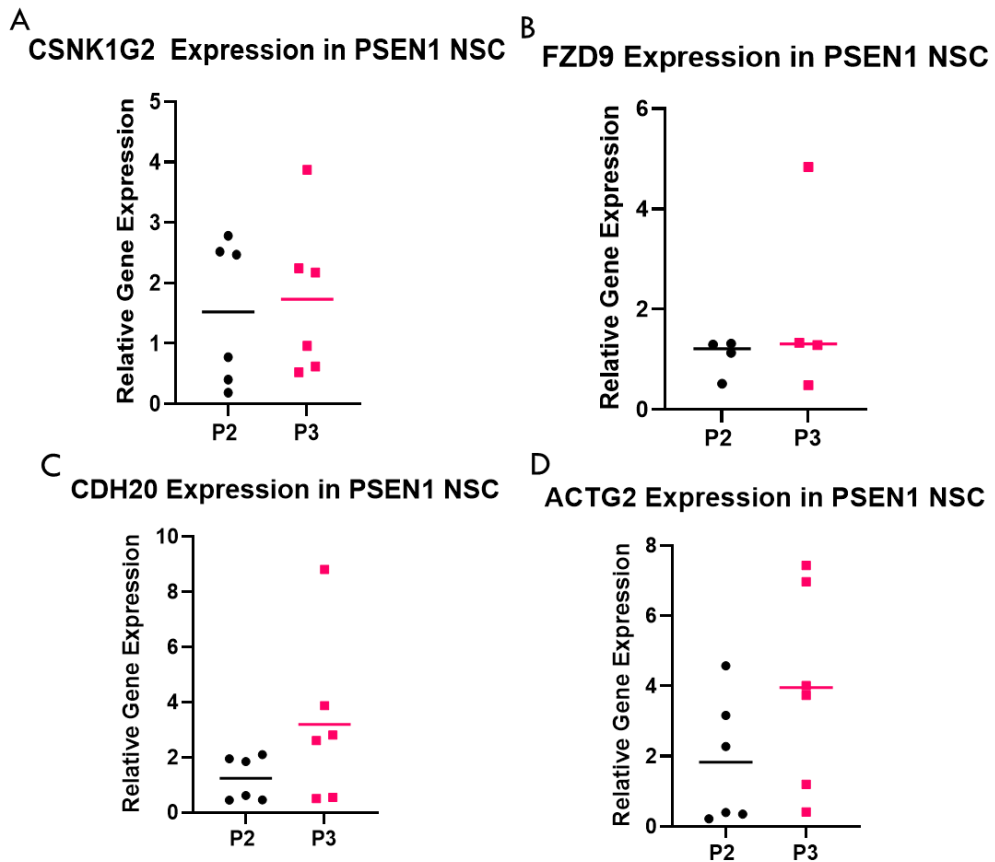


Figure 91. qPCR based interrogation of Wnt signalling in *PSEN1* neural differentiation

qPCR based interrogation of Wnt signalling indicated no significant differences between *PSEN1* NSC at P2 and P3 in *CSNK1G2* ($p=0.776$), *FZD9* ($p=0.387$), *CDH20* ($p=0.132$) or *ACTG2* ($p=0.156$), between P2 and P3 NSC but did indicate a trend towards increased expression of *ACTG2* ($p=0.156$), *CSNK1G2* ($p=0.776$), and *CDH20* ($p=0.132$) in P3 NSC compared with P2 NSC. Results of *FZD9* expression may indicate dysregulation of *FZD9* in *PSEN1* NSC as they mature. Normality tests, T-tests and Man-Whitney U tests were carried out using GraphPad Prism 9.2.0. Graph made using GraphPad Prism displays individual sample values with the mean value indicated by a horizontal line.

Results of qPCR-based analysis of *PSEN1* NSC at P2 and P3 (Figure 92) indicated a significant increase in *RFNG* ($p=0.0430$) gene expression between *PSEN1* NSC at P2

and P3. There were no significant differences in *JAG2* ($p=0.7143$) or *HEY1* ($p=0.344$) between *PSEN1* NSC at P2 and P3, but results did indicate a trend towards increased expression of *JAG2* and *HEY1* in *PSEN1* NSC at P3 compared with *PSEN1* NSC at P2.

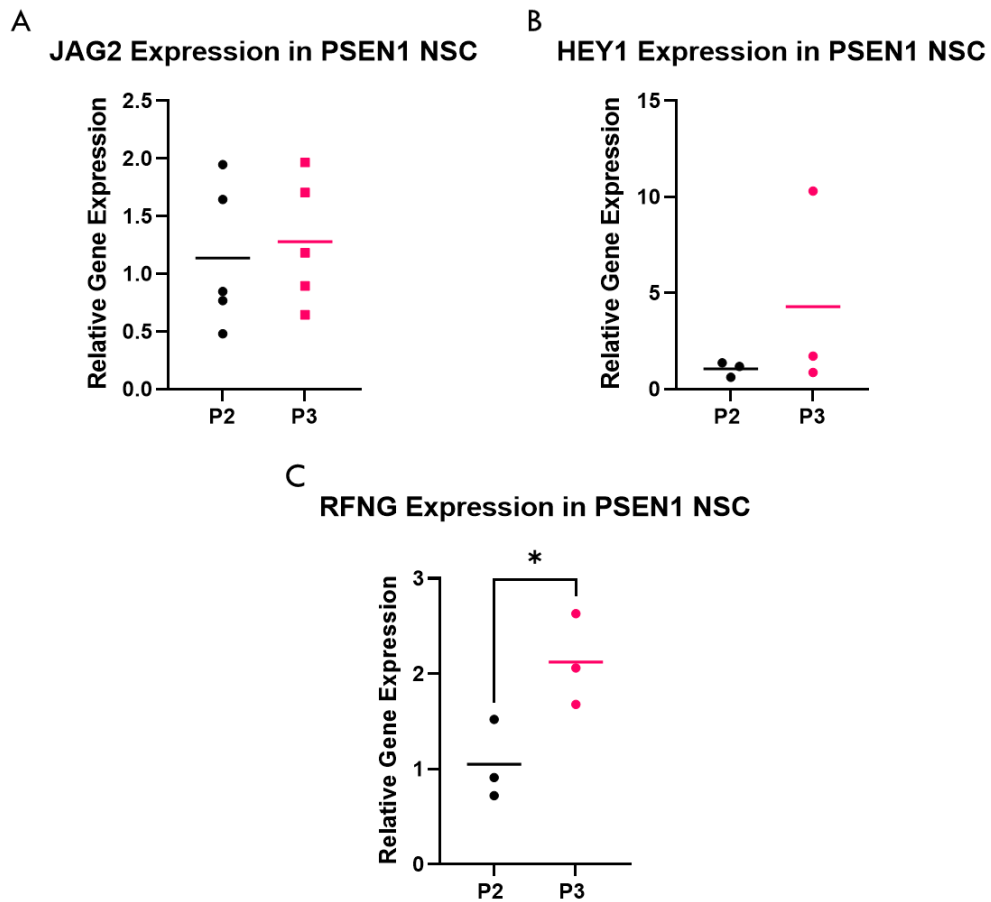


Figure 92. qPCR based interrogation of Notch signalling in *PSEN1* neural differentiation

qPCR based interrogation of Notch signalling indicated that there was a significant increase in *RFNG* ($p=0.0430$) gene expression between *PSEN1* NSC at P2 and P3. There were no significant differences in *JAG2* ($p=0.7143$) or *HEY1* ($p=0.344$) between *PSEN1* NSC at P2 and P3, but results did indicate a trend towards increased expression of *JAG2* and *HEY1* in *PSEN1* NSC at P3 compared with *PSEN1* NSC at P2. Normality tests, T-tests and Man-Whitney U tests were carried out using GraphPad Prism 9.2.0. Graph made using GraphPad Prism displays individual sample values with the mean value indicated by a horizontal line.

7.3.2 Apoptosis in *PSEN1* neural differentiation

Analysis of RNA sequencing results revealed genes which were differentially expressed from P2 to P3 in *PSEN1* NSC that were associated with programmed cell death (Figure 79

Figure 79. Pathway alterations during *PSEN1* neural differentiation). Alterations in apoptosis between *PSEN1* and control early neural cells and between *PSEN1* NSC P2 and P3 were investigated using flow cytometry. Apotracker Green was used alongside a fixable viability dye (eFluor™ 780) to enable exclusion of dead cells. The nestin monoclonal antibody (MA1-110) was used to isolate only nestin positive NPC for investigation of apoptosis. In this way, it was ensured that only live, nestin positive NSC and NPC which were undergoing apoptosis were included in results. Results indicated no significant difference ($p=0.334$) in the percentage of cells which were positive for apotracker between *PSEN1* NSC at P2 and *PSEN1* NSC at P3. However, a trend ($p=0.334$) was seen towards increasing numbers of apotracker positive cells as *PSEN1* NSC matured from P2 to P3 (Figure 93).

Apoptosis in *PSEN1* Neural Differentiation

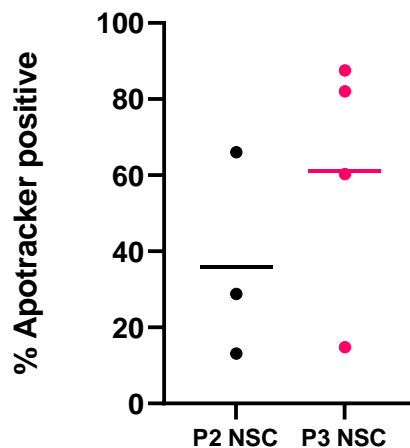


Figure 93. Apoptosis in *PSEN1* neural differentiation

Flow Cytometry was used to investigate differences in apoptosis between *PSEN1* NSC at P2 and P3. The cell stain Apotracker was used along with a viability dye to ensure that only live cells which were undergoing apoptosis were included in these results. The nestin monoclonal antibody (MA1-

110) was used to isolate only nestin positive NPC for investigation of apoptosis. Results indicated no significant difference ($p=0.334$) in the percentage of cells which were positive for apotracker between *PSEN1* NSC at P2 and *PSEN1* NSC at P3. However, a trend was seen towards increasing numbers of apotracker positive cells as *PSEN1* NSC matured from P2 to P3. Normality tests and a Students T-test were carried out using GraphPad Prism 9.2.0. Graph made using GraphPad Prism displays individual sample values with the mean value indicated by a horizontal line.

Analysis of RNA sequencing results revealed genes which were differentially expressed between control and *PSEN1* NPC that were associated with programmed cell death (Figure 90). *PSEN1* and control NSC at P3). control and *PSEN1* NPC were analysed for differences in the percentage of cells undergoing apoptosis. Results indicated no significant difference ($p=0.143$) in the percentage of cells which were positive for apotracker between *PSEN1* NPC and control NPC, but a trend ($p=0.143$) was seen towards increasing numbers of apotracker positive cells in *PSEN1* NPC when compared with controls (Figure 94).

Apoptosis in Control and *PSEN1* NPC

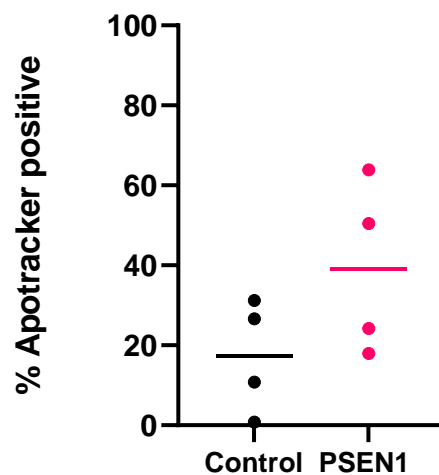


Figure 94. Apoptosis in *PSEN1* NPC compared with controls

Flow Cytometry was used to investigate differences in apoptosis between *PSEN1* and control NPC. The cell stain Apotracker was used along with a viability dye to ensure that only live cells which were undergoing apoptosis were included in these results. The nestin monoclonal antibody (MA1-

110) was used to isolate only nestin positive NPC for investigation of apoptosis. Results indicated no significant difference ($p=0.143$) in the percentage of cells which stained positive for apotracker between control and *PSEN1* NPC. Results however, displayed a trend towards increasing numbers of apotracker positive cells in *PSEN1* NPC compared with control NSC. Normality tests, T-tests and Man-Whitney U tests were carried out using GraphPad Prism 9.2.0. Graph made using GraphPad Prism displays individual sample values with the mean value indicated by a horizontal line.

7.3.3 Chapter summary

Results from qPCR-based analysis of Wnt related DEGs indicated no significant difference between *PSEN1* NSC at P2 and P3, but a trend towards upregulation of *ACTG2*, *CSNK1G2* and *CDH20* in P3 *PSEN1* NSC (Figure 82). Results from analysis of Notch related signalling pathways indicated a significant increase in *RFNG* gene expression ($p=0.0430$) in *PSEN1* NSC at P3 compared with *PSEN1* NSC at P2. There was no significant difference in *JAG2* and *HEY1* gene expression in *PSEN1* NSC at P3 compared with P2 but a trend towards increased expression of both genes during *PSEN1* neural differentiation (Figure 92).

PSEN1 NSC at P2 and P3 were analysed for differences in the percentage of cells undergoing apoptosis. Results indicated no significant difference ($p=0.334$) in the percentage of cells which were positive for apoptotracker between *PSEN1* NSC at P2 and *PSEN1* NSC at P3. However, a trend was seen towards increasing numbers of apoptotracker positive cells as *PSEN1* NSC matured from P2 to P3 (Figure 94.). control and *PSEN1* NPC were analysed for differences in the percentage of cells undergoing apoptosis. Results indicated no significant difference ($p=0.143$) in the percentage of cells which were positive for apoptotracker between *PSEN1* NPC and control NPC, but a trend was seen towards increasing numbers of apoptotracker positive cells in *PSEN1* NPC when compared with controls (Figure 95.).

8.0 Discussion

8.1 Adult hippocampal neurogenesis

This study generated iPSC from mutation confirmed AD and control donor cells and employed a pre-validated neural differentiation protocol (FitzPatrick *et al.*, 2018) to differentiate iPSC to NSC and NPC. The purpose of this study was to interrogate neural differentiation capacity in AD and controls to improve understanding of AHN in AD. In vitro and in vivo models of AD commonly display dysregulation of self-renewal and/or differentiation in neural precursor cells (Appel *et al.*, 2018; Scopa *et al.*, 2020). Many AD subtypes present with impaired neurogenesis resulting from either an increase or decrease in neural differentiation, often resulting in a loss of functional mature neurons. Premature neural differentiation in particular, may be a trait that occurs more commonly in conjunction with mutations in *PSEN1* and these *PSEN1* specific effects may be due to the role of *PSEN1* in activation of Notch signalling. In this study, *PSEN1* (A246E and M146L) and control NSC iPSC were repeatedly differentiated to NSC and NPC and continuously displayed phenotypic differences corresponding with a more mature phenotype in populations containing the *PSEN1* A246E mutation. These *PSEN1* NSC had a reduced capacity for self-renewal and an increased propensity for differentiation (Figure 42). This premature differentiation was also seen by Yang *et al.*, (2017) who found that NPC derived from patients with the *PSEN1* A246E mutation were more predisposed to undergo premature neural differentiation and increased apoptosis than controls. This correlates with flow cytometry data from this study which indicated apoptosis was increased in live, nestin+ NPC containing the *PSEN1* mutation (Figure 94) compared with controls at the same stage in neural specification.

AD mutations have been shown to reduce Notch signalling by reducing γ -secretase mediated Notch cleavage (Chávez-Gutiérrez *et al.*, 2012; Song *et al.*, 1999), and this reduced Notch signalling may drive dysregulated AHN in humans (Arber *et al.*, 2021). In cell models, inhibition of Notch signalling results in a loss of neural rosettes and

premature neural differentiation (Main *et al.*, 2013). Dysregulation of Notch signalling was seen in this study in RNA sequencing data specific to *PSEN1* neural differentiation (Figure 78, Figure 79). Notch related DEGs significantly upregulated ($p < 0.05$) in *PSEN1* NSC at P3 compared with P2 included *NCOR2*, *JAG2*, *CHAC1* and *RFNG*. qPCR based validation displayed significant upregulation of *RFNG* ($p = 0.04$) in *PSEN1* NSC at P3 compared with *PSEN1* NSC at P2, and indicated a trend towards upregulation of *JAG2* expression, correlating with RNA sequencing data (Figure 92).

This study is unique in that it compares the transcriptomic profiles of *PSEN1* and control NSC as they progress through neural specification. This study design generated data on both control and *PSEN1* neural differentiation to allow for comparison between the two at early (P2) and later (P3) time-points. The number of DEGs ($p < 0.05$) between *PSEN1* and control NSC at P3 was 9.92-fold higher than the number of DEGs between *PSEN1* and control NSC at P2 (Figure 75), suggesting transcriptomic differences between *PSEN1* and control NSC become more pronounced as cells specify further down the neural lineage. This finding links back to data generated by (Arber *et al.*, 2021) using the BrainSpan reference atlas which indicated differences in spatiotemporal expression of β and γ -secretase subunits during human development, with enrichment of *PSEN1* and *APH1A* in cells which were capable of self-renewal, and enrichment of *PSEN2* and *APH1A* in neurons that had undergone terminal differentiation. The findings from this study, coupled with the findings from Arber *et al.*, (2021) suggest that expression of *PSEN1* varies depending on the stage of neural specification and that there are different *PSEN1* related requirements from neural stem and progenitor cells as they pass through different stages of maturity, leading to disease specific effects only being detected at discrete stages in differentiation.

8.2 Dysregulated neural differentiation in AD NSC/NPC

This project generated evidence for premature neural differentiation in AD NSC and NPC showing trends towards reduced nestin expression in *PSEN1* NPC compared with

controls (Figure 47, Figure 58, Figure 59) and trends towards reduced nestin expression in *PSEN1* NSC as they mature (Figure 46, Figure 59). Nestin is a cytoskeletal type VI intermediate filament protein, expressed during the early stages of neural development in mammals (Bernal and Arranz., 2018). Nestin is expressed in neuroepithelial cells and is considered to be a marker of neural stem cells (Lendahl et al. 1990; Doetsch et al. 1997; Mignone et al. 2004, Wilhelmsson *et al.*, 2019). Nestin expression is high in NSC and NPC stages (Bernal and Arranz., 2018) but is replaced by tissue specific intermediate filament proteins as NPC mature to neurons (FitzPatrick *et al.*, 2018). Downregulation of nestin expression in *PSEN1* neural cells (Figure 47) indicates that mutations in *PSEN1* may induce a premature neural differentiation phenotype. MAP2 isoforms are able to bind with tubulin and increase in the rigidity of microtubules, enabling the formation of long neural processes. Due to its structural role in neural cell maturation, MAP2 can be used as an indicator of the functional state of neurons and a marker of differentiation to more mature neural cell types (Korzhevskii *et al.*, 2012). Increased expression of MAP2 during neural differentiation may even play a role in reducing levels of self-renewal as neurons mature. Soltani *et al.*, (2005) showed that expression of MAP2 was induced in primary cutaneous melanoma but was absent in metastatic melanoma, suggesting a role for MAP2 in preventing metastasis. Expression of MAP2 in metastatic melanoma cell lines resulted in stabilisation of microtubules, reduced growth, and cell cycle arrest in G2-M phase (Soltani *et al.*, 2005). Both AD and control NSC showed trends towards increased expression of MAP2 with maturation (Figure 59), and at all timepoints measured (P2, P3, P8), MAP2 was increased in *PSEN1* NSC compared with controls (Figure 58, Figure 59), suggesting a more differentiated phenotype in *PSEN1* NSC and neurospheres than in controls at the same stage. MAP2 is a MAP with similar functions to tau, however tau localises to neural axons to stabilise microtubules, whereas MAP2 localises to cell bodies and dendrites.

This data provides novelty in that MAP2 expression was measured in *PSEN1* and control NSC at multiple timepoints during neural differentiation and at every

timepoint MAP2 expression was higher in PSEN1 NSC (Figure 59), providing further support to the hypothesis that the mutation PSEN1 A246E promotes neural specification in NSC.

8.3 Altered Cell Signalling in AD NSC/ NPC

Signalling pathways which are known to be affected by AD and which may play a role in causing premature neural differentiation in *PSEN1* were investigated in this project and displayed trends towards dysregulation of Wnt signalling, autophagy and antioxidant response pathways in AD (Figure 55, Figure 56, Figure 57). Yang *et al.*, (2017) suggested a role of altered Notch and Wnt signalling in dysregulating neurogenesis. With the exception of JAG1, genes associated with Wnt signalling were increased in both *PSEN1* A246E and *PSEN1* M146L NSC compared with controls (Figure 56) JAG1 is a regulator of Notch signalling via the Notch ligand Jagged1. Using a transgenic mouse model, Marathe *et al.*, (2017) showed that targeted loss of Jagged1 expression during adulthood caused a reduction in exploration-dependent Notch activation and induced spatial memory loss (Marathe *et al.*, 2017). Work by Sargin *et al.*, (2013) showed that mice with a heterozygous mutation resulting in reduced expression of Jag1 displayed impairments in spatial memory formation indicating the importance of Jag1-Notch signalling in memory formation in the adult brain (Sargin *et al.*, 2013). Downregulation of JAG1 in *PSEN1* A246E NSC may contribute to reduced Notch signalling and dysregulated AHN in AD. JAG1 was actually upregulated in *PSEN1* M146L NSC which may explain the lack of premature differentiation seen in *PSEN1* M146L NSC. Transcription of Wnt related genes is regulated in part by the interaction of β -catenin with TCF/LEF. Both *PSEN1* A246E and *PSEN1* M146L NSC displayed upregulated expression of *LEF1* and CTNNB1 which codes for the protein β -catenin (Figure 56). Upregulated expression of these important Wnt related factors is indicative of enhanced Wnt signalling in AD (Jia *et al.*, 2019). AXIN forms part of the β -catenin destruction complex which prevents β -catenin nuclear translocation and transcription of Wnt target genes. Upregulation of *AXIN2* leads to β -catenin degradation. Wnt/ β -Catenin/*LEF1* signalling promotes

cellular proliferation (Mu *et al.*, 2019), however the increase in β -Catenin and *LEF1* in *PSEN1* NSC may be regulated by the increased *AXIN2*. Neurodegenerative disorders commonly present with chronic inflammation, a decline in the generation of functional neurons as well as impaired autophagy and altered p62 expression (Vivar, 2015; François *et al.*, 2013). In neurons, autophagy is the principle mechanism for turnover of unwanted substrates, thus in AD, and other neurodegenerative diseases, defects in autophagic processing can lead to the intraneuronal accumulation of waste products such as $A\beta$ and proteins such as p62 (Bordi *et al.*, 2016; Brandenstein *et al.*, 2016). Beclin-1 and LC3 play an important role in formation of autophagosomes for autophagy and were downregulated in *PSEN1* A246E but upregulated in *PSEN1* M146L NSC compared with controls (Figure 55). Pickford *et al.*, (2008) revealed reduced expression of Beclin-1 in mouse models of AD associated with a reduction in clearance of waste materials and $A\beta$ (Pickford *et al.*, 2008). Downregulation of Beclin-1 and LC3 is indicative of reduced autophagy in *PSEN1* A246E NSC compared with controls. MTOR regulates metabolism, translation, and growth as well as proliferation, differentiation, migration, and the formation of dendrites in neural cell types (LiCausi and Hartman). During nutrient depletion, MTOR is inhibited, and the Unc-51-like kinase (ULK)1/2 complex is activated, this induces formation and elongation of the isolation membrane; a membrane which selectively and non-selectively envelopes cytosolic contents for degradation during autophagy (Tooze and Yoshimori, 2010; Kiriyaama and Nochi, 2015). P62 gene expression was upregulated in *PSEN1* A246E NSC compared with controls (Figure 55), downregulated mTOR and upregulated p62 would indicate an increase in autophagy, thus results indicate a trend towards dysregulation of autophagy in disease. p62 regulates the antioxidant response and inflammation in part by indirect interactions with transcription factors NRF2 and NF κ B. p62 binds keap1 via its keap1 interacting region (KIR) and thus, competes with NRF2 for keap1 binding, releasing NRF2 for nuclear translocation and activation of antioxidant response genes (Liu *et al.*, 2016). The N-terminal Phox-BEM1 (PB1) domain of p62 enables its homo-oligomerisation

with other molecules of p62 and hetero-oligomerisation with kinases including protein kinase C (PKC), which can then regulate NF κ B signalling and downstream inflammation (Liu *et al.*, 2016). Chronic inflammation exacerbates AD pathology (Wang *et al.*, 2017) and may result from the accumulation of p62 and subsequent dysregulation of inflammatory and antioxidant response pathways. Analysis of genes related to inflammation and the antioxidant response displayed little variation between *PSEN1* A246E and control NSC, but NRF2, HIF1, *NQO1* and STAT3 were upregulated in *PSEN1* A246E neurospheres compared with control neurospheres (Figure 57) These results show that culturing cells of the same cell lines using different cell culture methodology can lead to disparate effects on cell signalling. The increase in inflammatory markers in neurospheres could be more representative of disease or could be a result of hypoxia and inflammation in cells within the neurosphere that have limited access to nutrients. These results show novelty in that gene expression of *PSEN1* NSC was compared in two different cell culture models and results showed that the cell model used for investigation of AD can affect results.

8.4 Dysregulated Cell Cycle Progression and Apoptosis in AD NSC and NPC

NSC in the niche are generally maintained in a state of quiescence (Cheung *et al.*, 2013), but can be primed to enter the cell cycle via external stimuli, such as pro-inflammatory mediators. Although pro-inflammatory cytokines can activate NSC, they are generally shown to impair successful neurogenesis, for example, Interleukin-6 and Interleukin-1 β have been described as negative regulators of NSC proliferation (Brett *et al.*, 1995, Kokovay *et al.*, 2012, Belenguer *et al.*, 2021). NSC in a proliferative state spend approximately 3 hours in G1 phase, time spent in G1 phase increases by 4-fold as NSC switch to a differentiative phenotype. Inhibition of Cyclin E in these cells led to an extended G1 phase and an earlier switch to a differentiative phenotype. The extended G1 phase may enable intracellular accumulation of transcription factors which induce differentiation (Lange and Calegari., 2010, Lange

et al., 2009, Ruijtenberg *et al.*, 2016). Cell cycle analysis of *PSEN1* A246E NSC revealed trends towards an increased proportion of cells in G0/G1 phases and a decrease in the proportion of *PSEN1* NSC in G2 and S-phases compared with controls (Figure 63.). Results were generated from three biological repeats of control and *PSEN1* A246E NSC and in all measurements, *PSEN1* NSC biological repeats displayed greater variation between samples than controls. A greater number of biological repeats displaying the same results would likely yield significant results. Trends in results (Figure 62) indicate impaired cell cycle progression in *PSEN1* NSC. As cell cycle regulation can determine the rate of proliferation and differentiation, cell cycle dysregulation plays a role in the pathogenesis of neurodegenerative disorders.

Cell cycle progression is regulated by cyclins, cyclin-dependent kinases (CDK) and a CDK (cyclin-dependent kinase) inhibitors (CDKI). The interaction between Cyclin D and CDK4 or CDK6 forms a CDK4/6-cyclin D complex, the formation of this complex regulates cell entry into G1 phase. Formation of the CDK4/6-cyclin D complex results in phosphorylation of Rb and the release of E2F for activation of DNA transcription. Inhibitors such as members of the Cip/Kip family and the INK4 family can prevent cell cycle progression. Cell cycle regulators including cyclins, CDKs, cip/kip family of inhibitors, caspases, bax and p53 have been identified to be involved in impaired cell cycle regulation and associated with neural pathology (Wang *et al.*, 2019).

GO analysis of RNA sequencing data revealed significant dysregulation of genes with a role in cell cycle regulation (**Error! Reference source not found.**), *CABLES1* Cdk5 and Abl enzyme substrate 1 expression were significantly downregulated in *PSEN1* NSC at P3 compared with the same cells at P2. Growth arrest and DNA damage inducible gamma (*GADD45G*) was significantly upregulated in *PSEN1* NSC at P3 compared with *PSEN1* NSC at P2. Expression of this gene is associated with stress-related growth arrest and DNA damage. Genes *MIIP*, *ZBTB17*, *DGKZ*, *CDT1*, *PIDD1*, *SCRIB*, *AURKAIP1*, *DOT1L* and *TP53I13* were all significantly upregulated in *PSEN1* NSC at P3 compared with *PSEN1* NSC at P2 and are all associated with negative regulation of cell cycle (Table 29). RNA sequencing data also revealed dysregulation of pathways

associated with Chk1/Chk2(Cds1) mediated inactivation of the Cyclin B:Cdk1 complex (Figure 91.). The MKRN3 gene was significantly downregulated in *PSEN1* NSC at P3 compared with control NSC at P3 and regulates cell proliferation via ubiquitination of PABPC1. Prevention of PABPC1 ubiquitination via inactivation of MKRN3 has been shown to prevent cell cycle arrest at the G2/M transition and to enhance transcription of PABPC1 target genes (Li *et al.*, 2021).

In AD, terminally differentiated neurons can be activated to enter the cell cycle, ultimately leading to their death (Wang *et al.*, 2019). Altered expression of cell cycle regulators has been seen in brain regions affected by AD, such as the hippocampus, for example, neurons in the hippocampus with NFT have also displayed positive staining for cdk1 and cyclin B1. Presence of these markers indicates that cells passed the G1/S phase checkpoint and underwent cell cycle arrest at G2 phase (Atwood and Bowen., 2015, Busser *et al.*, 1998). Aberrant cell cycle activation in neurons can be caused by oxidative stress, DNA damage, toxic levels of peptide accumulation and the deprivation of growth factors. Altered activation of cell cycle regulators plays a role in a range of CNS disorders. In CNS disease, activation of the cell cycle in astrocytes and microglia leads to proliferation and is associated with glial scar formation and the production of inflammatory cytokines. In mature neurons however, instead of inducing proliferation, unregulated cell cycle re-entry results in neuronal cell death. Apoptosis is often increased in CNS injury and is associated with a cell cycle blockade at the G1-S phase. In some subtypes of AD, some neurons undergo DNA synthesis but are prevented from completing the cell cycle due to cell cycle arrest at the transition from G2 to M-phase (Wang *et al.*, 2009). Cell cycle abnormalities play a major role in both LOAD and EOAD/FAD and appear prior to the accumulation of A β plaques and tau NFT, therefore represent an important target to prevent neuronal loss in AD (Atwood and Bowen., 2015).

Pathway analysis of RNA sequencing results displayed trends in dysregulation of pathways related to programmed cell death in *PSEN1* neural differentiation, (Figure 79.) programmed cell death related pathways were also dysregulated during control

neural differentiation (Figure 80.) and were seen to be dysregulated between control and *PSEN1* NSC at P3 (Figure 91.). DEGs associated with apoptosis included *CARD8* and *MKRN3*, *Card8* is caspase recruitment domain family member 8, and was significantly downregulated in *PSEN1* compared with control NSC at P3. *MKRN3* codes for expression of Makorin ring finger protein 3 and was also significantly downregulated in *PSEN1* compared with control NSC at P3. In control Neural differentiation *PLEC* and *BBC3* were both significantly upregulated from p2 to p3 and are associated with apoptosis. Cell cycle analysis of *PSEN1* and control NSC at P3 also revealed a trend towards an increased percentage of DNA fragmentation in *PSEN1* NSC compared with controls (Figure 63.). Increased DNA fragmentation in disease may be a result of apoptosis; if cells which have undergone DNA replication are not exposed to mitotic signals such as cell division cycle 2 and cyclin A, they do not exit the cell cycle. Duplication of genetic material without the induction of mitosis can result in molecular flaws and the induction of apoptosis, as well as an increase in markers associated with the response to cell stress (Urbán *et al.*, 2019, Joseph *et al.*, 2020). Neural cells exposed to stress/DNA damage may attempt to re-enter cell cycle but begin to undergo apoptosis at the G1/S phase checkpoint (Frade and Ovejero-Benito, 2014). In analysis by flow cytometry, nestin positive, live *PSEN1* NSC displayed a trend towards increased apoptosis as they matured from P2 to P3 (Figure 94), *PSEN1* NPC also displayed a trend towards an increase in the percentage of nestin positive live cells undergoing apoptosis when compared with control NPC at the same passage (Figure 95). These results provide further, novel evidence to the hypothesis that apoptosis is increased in *PSEN1* immature neural cells compared with controls and is also increased as *PSEN1* neural cells mature -increased apoptosis in *PSEN1* NSC may be a result of cell cycle dysregulation.

8.5 Comparison of *PSEN1* and control Neural Differentiation

The transcriptomic profiles of *PSEN1* A246E and control NSC at P2 and P3 were compared to look for differences in neural differentiation between *PSEN1* and control NSC. Interestingly, the number of genes which were differentially expressed

during *PSEN1* neural differentiation (from P2 to P3) was 4.7-fold higher than the number of genes seen to be differentially expressed during control neural differentiation (from P2 to P3) (Figure 74, Figure 77). This data indicates that there is a much greater number of transcriptomic changes occurring in *PSEN1* neural differentiation when compared with controls at the same stage. The majority of DEGs in both *PSEN1* and control neural differentiation were upregulated. The five most upregulated genes in control neural differentiation (A.) were *PLEC*, *ANO8*, *CCDC85B*, *ADAMTS7* and *ZDHHC8*. The five most upregulated genes in *PSEN1* neural differentiation (B.) were *PLEC*, *CORO1B*, *BTBD2*, *LRFN4* and *NDUFS7*. With the exception of *CORO1B*, these genes were all upregulated in both *PSEN1* and control neural differentiation, and almost all were upregulated to a higher degree in *PSEN1* neural differentiation (Figure 77.). Many genes were differentially expressed in both *PSEN1* and control neural differentiation and were indicative of normal neural differentiation. DEGs associated with development in control neural differentiation were *PLEC*, *ERF*, *METRNL*, *BTBD2* and *MAP1S*, all of which were significantly upregulated during control neural differentiation (Figure 83). The DEGs associated with development seen in control neural differentiation were also significantly upregulated in disease neural differentiation, however, in *PSEN1* neural differentiation, there were 6-fold more DEGs associated with development, indicating upregulation of pathways related to development in disease (Figure 84). Other interesting DEGs in *PSEN1* neural differentiation included *CEND1*, which plays a role in cell cycle exit and neuronal differentiation and was significantly upregulated in *PSEN1* neural differentiation, *CDH20*, *FGFR4* and *ERG*. *ERG* codes for the ERG protein which regulates transcription and in particular, plays a role in regulation of embryonic development, cellular proliferation, differentiation, and apoptosis. *ERG* was downregulated in *PSEN1* neural differentiation. Downregulation of *ERG* along with *FLI1* in endothelial cells has been shown to trigger endothelial-to-mesenchymal transition (Nagai *et al.*, 2018), suggesting that downregulation of *ERG* in *PSEN1* neural differentiation may be contributing to the premature neural differentiation seen in

disease. *SEMA6B* was another DEG associated with growth and was significantly upregulated in *PSEN1* neural differentiation. *SEMA6B* encodes a member of the semaphorin family of proteins which have an important role in axon guidance, therefore upregulation of *SEMA6B* may contribute to the neural phenotype in *PSEN1* NSC.

The pathway cytoskeletal regulation by Rho GTPase was dysregulated during *PSEN1* neural differentiation, DEGs included *ACTG2*, *PUF60*, *MYH14* and *ARPC1B*, all of which were upregulated from P2 to P3 (Figure 81). This pathway was not shown to be dysregulated during control neural differentiation. Polymerisation of actin and interactions between actin and myosin have been shown to modulate differentiation of stem cells to more mature mesodermal and endodermal lineages (Boraas *et al.*, 2018). In neurons, actin filaments play a role in axon integrity (Arnold and Gallo., 2014). Myosins are motor proteins which are able to produce mechanical forces to drive actin cytoskeletal dynamics. In the brain, interactions between actin and non-muscle myosin II contribute to neural morphology, polarisation, and migration during development (Javier-Torrent and Saura., 2020). *MYH14* is a non-muscle myosin and *ARPC1B* is a component of the Arp2/3 complex which plays a role in actin polymerisation and cell motility. Upregulation of these components indicates cytoskeletal changes in *PSEN1* neural differentiation which are not occurring in control neural differentiation and may play a role in the premature neural differentiation seen in *PSEN1* NSC.

GO analysis of dysregulated molecular functions in *PSEN1* neural differentiation indicated that binding and protein binding were significantly dysregulated during *PSEN1* neural differentiation (Figure 77), 335 significantly dysregulated DEGs were associated with binding. Proteins encoded by these DEGs were diverse and included growth arrest and DNA damage inducible proteins interacting protein 1, autophagy related protein2 homolog A, Apoptosis regulatory protein Siva, cell polarity related proteins and transcriptional regulators.

Between *PSEN1* NSC at P2 and P3, pathways dysregulated included Wnt signalling, angiogenesis, Huntington disease and pathways related to Alzheimer's disease presenilin pathway. The most dysregulated pathway in both *PSEN1* and control neural differentiation was the Alzheimer's Disease Presenilin Pathway (Figure 81, Figure 82). In control neural differentiation, DEGs in this pathway were *LRP5*, *LRP3*, *MMP17*, *PCSK4* and *DVL1*, all of which were all upregulated from P2 to P3 NSC. In *PSEN1* neural differentiation, DEGs related to the Alzheimer's disease presenilin pathway were *DVL1*, *ACTG2*, *PUF60*, *LRP3*, *MMP17*, *PCSK4*, *ERBB4* and *FZD9*, all of which were upregulated from P2 to P3, excluding *ACTG2* and *ERBB4*. *ACT2* encodes the protein Actin γ -2, actin filaments play an important role in cytoskeletal maintenance. In AD, actin filaments can interact with proteins such as APP, presenilin, tau and apolipoprotein E which may contribute to neurodegeneration (Ostrowski *et al.*, 2005). *ERBB4* is a member of the epidermal growth factor receptor subfamily and plays a role in proliferation. The proteins described as being members of this pathway have been reported to be dysregulated during AD, however, also play important roles in healthy cells. Interestingly, the amyloid beta precursor protein binding family A member 3 *APBA3* was upregulated in both *PSEN1* and control neural differentiation but was upregulated to a greater degree in *PSEN1* neural differentiation ($p < 0.0001$) than in control neural differentiation ($p < 0.001$).

DEGs shown in both *PSEN1*, and control neural differentiation were said to be associated with normal neural differentiation. DEGs exclusive to *PSEN1* neural differentiation were isolated and manually categorised as fitting into either nuclear, cytoskeletal, cell signalling or metabolism-related categories (Figure 85.) The majority (43%) of DEGs exclusive to *PSEN1* neural differentiation were associated with the nucleus, 29% were associated with cell signalling, 14% were associated with metabolism and the remaining 14% were associated with cytoskeletal processes.

Notch signalling pathways were dysregulated in *PSEN1* neural differentiation (Figure 81) but were not shown to be dysregulated during control neural differentiation (Figure 80), suggesting the *PSEN1* A246E mutation leads to dysregulated Notch

signalling in *PSEN1* neural differentiation. DEGs related to Notch signalling which were significantly upregulated during *PSEN1* neural differentiation included *NCOR2*, *HEY1*, *JAG2*, *CHAC1* and *RFNG*. *HEY1* gene expression was significantly downregulated in P3 NSC compared with P2 NSC containing the *PSEN1* mutation (Figure 81, Figure 85. DEGs in *PSEN1* neural differentiation linked with Wnt and Notch signalling).

Regulation of Notch signalling is critical during development, Notch signalling determines the timing and duration of neural progenitor proliferation and differentiation and thus plays a pivotal role in brain development (Hansen *et al.*, 2010). In particular, Notch signalling has been shown to regulate neural rosette polarity, playing a role in determining symmetric vs asymmetric cell division and ultimately, cell fate. Dysregulation of notch and Wnt signalling plays a role in altered neural specification in *PSEN1* NSC and NPC, recent research describes a link between mutations in *PSEN1*, reduced Notch signalling and premature differentiation (Arber *et al.*, 2021).

Wnt signalling pathways were shown to be dysregulated during both *PSEN1* and control neural differentiation. Upon isolation of DEGs which were exclusive to *PSEN1* neural differentiation, a subset of Wnt genes which were only dysregulated in *PSEN1* neural differentiation were identified (Figure 85). DEGs related to Wnt signalling which were significantly upregulated ($p < 0.05$) during *PSEN1* neural differentiation included *FZD9*, *LRP3* and *CSNK1G2*. DEGs which were significantly downregulated ($p < 0.05$) during neural differentiation included *DKK2*, *CDH2* and *ACTG2*.

Gene ontology (GO) analysis of differentially expressed genes (DEGs) specific to AD neural differentiation revealed significant dysregulation (FDR $p < 0.05$) of genes related to neurogenesis, apoptosis, cell cycle, transcriptional control, and cell growth/maintenance as *PSEN1* NSC matured from P2 to P3. The majority of DEGs in both *PSEN1* and control neural differentiation were upregulated, this indicated that neural specification involves more upregulation of gene expression than

downregulation. That the number of upregulated genes was much greater in *PSEN1* neural differentiation than in control and that the topmost upregulated genes in *PSEN1* neural differentiation (*PLEC*, *CORO1B*, *BTBD2*, *LRFN4* and *NDUFS7*) are associated with neural differentiation (cytoskeletal changes, movement of cells, promotion of neurite outgrowth in hippocampal neurons, metabolic shifts from glycolysis to oxidative phosphorylation) indicates that presence of the *PSEN1* mutation results in the initiation of more transcriptomic changes during neural differentiation, those which likely lead to the premature neural differentiation phenotype seen in *PSEN1* lines (Figure 42, Figure 43). This data provides novel evidence of pathway dysregulation during *PSEN1* neural differentiation, particularly related to the upregulation of pathways which promote neural differentiation. This data supports the hypothesis that the *PSEN1* mutation promotes premature neural specification.

8.6 Comparison of *PSEN1* and control NSC at P3

GO analysis of DEGs between *PSEN1* and control NSC at P3 was carried out to interrogate differences in more mature NSC containing the *PSEN1* mutation compared with controls. Comparison of *PSEN1* and control NSC at P3 revealed significant dysregulation of a range of pathways and molecular functions.

Biological processes which were most significantly dysregulated between *PSEN1* and control NSC at P3 were associated with regulation of transcription and gene expression, these pathways were shown to be significantly upregulated in *PSEN1* NSC at P3 compared with control NSC at P3. After this, pathways associated with regulation of metabolic processes were the most significantly dysregulated. Regulation of metabolic processes was upregulated, whereas metabolic processes themselves were downregulated in *PSEN1* NSC compared with control NSC (

Results display biological processes which are significantly (FDR $p < 0.05$) dysregulated between control and *PSEN1* NSC at P3. Significantly dysregulated processes include regulation of transcription by RNA polymerase II, regulation of gene expression,

metabolic processes, and cellular processes. GO results indicated that these biological processes are upregulated in *PSEN1* NSC at P3 compared with control NSC at P3. Only results with FDR $p < 0.05$ are displayed. Molecular functions that were most significantly dysregulated between *PSEN1* and control NSC at P3 were related to DNA-binding transcription factor activity, RNA polymerase II specific. After this, the most significantly dysregulated molecular functions were related to transcriptional regulation and DNA binding, all of these molecular functions related to DNA binding and transcription were shown to be upregulated in *PSEN1* NSC at P3 compared with control NSC at P3 (Figure 87).

Analysis using the PANTHER classification system revealed trends in pathway dysregulation (Figure 89). The topmost dysregulated pathway between *PSEN1* and control NSC at P3 was the Wnt signalling pathway. After this, was integrin and endothelin signalling pathways, Alzheimer's disease-presenilin pathway, angiogenesis, and cadherin signalling. Pathways which were dysregulated between *PSEN1* and control NSC at P3 were visualised using the Reactome database and indicated significant dysregulation of gene expression (specifically transcription), extracellular matrix organisation, developmental biology, pathways related to the immune system and pathways related to programmed cell death (Figure 90). A greater number of gene expression changes were occurring during *PSEN1* neural differentiation than during control neural differentiation (Figure 76). Results from GO analyses show that there was an increase in expression of genes associated with transcription in *PSEN1* compared with control NSC at P3 (Figure 87). This increase in transcription and DNA binding in *PSEN1* NSC may have led to an increase in expression of genes related to developmental pathways, pushing *PSEN1* NSC towards neural specification. This data provides novel evidence of significantly upregulated gene expression during *PSEN1* neural differentiation and supports the hypothesis that disease causing changes which occur in AD may be a result of abnormal AHN and impaired neural specification.

8.7 Limitations and further study

Data generated is limited by the number of biological replicates used. For each experiment, the NSC utilised were produced using three biological repeats of control and *PSEN1* A246E, each of which were generated from a separate neural differentiation procedure. Flow cytometry-based analysis of cell cycle progression, apoptosis and nestin expression in *PSEN1* NSC generated results which displayed clear trends towards cell cycle dysregulation, increased apoptosis and decreased nestin expression in *PSEN1* NSC. qPCR results displayed trends towards enhanced *MAP2* expression with maturation in *PSEN1* NSC compared with controls, as well as dysregulation of Wnt signalling. The addition of further biological replicates in the study would have enhanced the power and reproducibility of results, however, the onset of the SARS-CoV-2 pandemic and subsequent lab closure hindered the undertaking of lengthy neural differentiation procedures, and thus prevented generation of sufficient material for further repetitions.

Another important limitation to the study is the interpretation of Gene ontology results. Initial GO/Panther analysis of RNA sequencing data was carried out on DEGs specific to *PSEN1* neural differentiation. Within this data set, pathway dysregulation of Wnt and Notch signalling was identified (Figure 81) and led to the prioritisation of qPCR-based validation to confirm dysregulation of Wnt and Notch related genes between *PSEN1* NSC at P2 and P3. Dysregulation of Wnt and Notch signalling pathways was only highlighted in *PSEN1* neural differentiation due to a total of 8 DEGs, which upon validation via RNA sequencing did not display the same significant results seen in the RNA sequencing data. Upon later GO/Panther re-analysis of RNA sequencing results, comparison between *PSEN1* NSC at P3 and control NSC at P3 revealed significant upregulation (FDR<0.0000259) of 5 biological processes related to transcription and gene expression as well as significant upregulation (FDR<0.000000725) of 12 molecular functions related to DNA binding and transcription factor activity. The number of significantly upregulated biological processes and biological pathways which are related to the same or similar processes

and functions means that these results are more likely to be true and to be able to be validated through further transcriptomic/ proteomic work. Thus, in further study, the significant dysregulations in metabolism and transcription related processes which were seen in *PSEN1* NSC compared with control NSC would be interrogated to confirm the specific transcription factors driving these changes in *PSEN1* neural differentiation.

8.8 Conclusion and Impact

The findings described in this work indicate that the mutation *PSEN1* A246E predisposes immature neural cells to neural specification at a faster rate than is seen in controls. The 4.7-fold increase in DEGs ($p < 0.05$) during *PSEN1* neural differentiation compared with controls (Figure 75, Figure 76) indicates that the *PSEN1* A246E mutation has a major effect on early neural specification. If hippocampal neurogenesis does occur in adults, this data indicates that it is significantly altered in patients with the *PSEN1* A246E mutation. Data generated in this study point towards *PSEN1* NSC being pushed to differentiate prematurely (Figure 43, Figure 60, Figure 62, Figure 81). This premature neural specification may result in depletion of the neural stem cell niche in patients with the *PSEN1* mutation, reducing their ability for regenerative repair and increasing the rate of disease progression. Accelerated loss of the NSC niche may accelerate the effects of inter and intra- neuronal A β and Tau, resulting in the faster rate of disease progression seen in FAD patients compared with patients with LOAD. These data indicate that along with targeting A β and Tau accumulation, treatment of FAD also requires therapies targeted at maintaining the NSC niche and preventing premature differentiation of the NSC reserves within it.

Restoration of functional AHN in the early stages of AD has the potential to delay disease onset, improving quality of life for patients and reducing healthcare costs. In terms of LOAD, delaying disease onset by 5 years is predicted to lower disease prevalence by 41% and associated healthcare costs by 40% by the year 2050

(Zissimopoulos *et al.*, 2014). Improved treatment of FAD will undoubtedly lead to improved treatment of LOAD, which will benefit millions worldwide.

Improved understanding of the mechanisms which lead to NSC depletion and impaired neurogenesis in AD will aid the identification of therapeutic targets for treatment. Therapeutic agents currently in use for treatment of AD, including AChEi and the NMDA receptor agonist Memantine, act to improve neuronal communication, survival, and plasticity. These agents focus on reducing disease symptoms rather than treating the cause of disease, primarily because disease mechanisms are still not fully understood. Therapeutic agents targeted at reducing inter and intraneuronal A β have been in development for several decades with little success (Aghaizu *et al.*, 2020; Behl *et al.*, 2020), suggesting that A β is not the primary disease-causing agent in AD. BACE inhibitors and inhibitors of γ -secretase which are both focused on reducing inter and intraneuronal levels of A β have not yet shown beneficial effects on reducing disease progression but have displayed major side effects, including hippocampal atrophy and worsened cognition, these negative effects are likely due to the widespread roles of BACE and γ -secretase in neural function (Nash *et al.*, 2021; Coric *et al.*, 2012). In FAD mutations which result in impaired γ -secretase cleavage, overexpression of γ -secretase could be beneficial, however, as γ -secretase has such a varied range of substrates, adverse effects would be likely.

Pathway analysis of RNA sequencing data generated in this study indicates that altered *PSEN1* neural specification may be directed by dysregulated Notch and Wnt signalling (Figure 79). The trends towards increased apoptosis in *PSEN1* NSC (Figure 93, Figure 94) may occur as a result of altered cell cycle regulation (Figure 62), which may be another effect of enhanced neural specification and dysregulated Wnt and Notch signalling in FAD. Wnt signalling pathways have been targeted in AD models with some success, with activation of Wnt signalling -by molecules such as the GSK3- β inhibitor LiCl- achieving results such as enhanced neuronal survival, a reduction in soluble and insoluble A β , rescued memory retention, restored myelination, restored

retention of short and long-term memory, protection against dendritic spine loss mediated by Dkk1, increased microglial cell number in the hippocampus and cortex, increased excitatory synapse numbers and an increase in cell cycle markers c-Myc and Cyclin D1 (Zhang *et al.*, 2019; Zheng *et al.*, 2017; Cerpa *et al.*, 2010; Alvarez *et al.*, 2004; Marzo *et al.*, 2016; Salcedo-Tello *et al.*, 2014; Vargas *et al.*, 2014; Sellers *et al.*, 2018). Synapse degeneration is a feature of AD which is correlated with cognitive decline. Dickkopf-1 (Dkk1) is a Wnt agonist that is increased in AD and plays a role in synaptic failure mediated by A β . Restoration of Wnt signalling in adult transgenic mice which inducibly express Dkk1 in the hippocampus, was shown to reverse synapse degeneration in the hippocampus and to improve learning and memory deficits (Marzo *et al.*, 2016), this research indicates that restoration of normal Wnt signalling is a viable therapeutic option for reducing neuronal loss and enhancing patient cognition and survival.

This work highlights a new and pressing need for therapies that prevent premature neural specification in AD and promote maintenance of hippocampal NSC reserves. Further analysis of *PSEN1* and control NSC is required to identify key therapeutic targets in Notch and Wnt signalling pathways. Restoration of normal Notch and Wnt signalling in *PSEN1* immature neural cells has the potential to prevent neuronal loss and reduce the rate of disease progression.

9.0 Bibliography

Acar, A., Hidalgo-Sastre, A., Leverentz, M. K., Mills, C. G., Woodcock, S., Baron, M., Collu, G. M. and Brennan, K. (2021) 'Inhibition of Wnt signalling by Notch via two distinct mechanisms.' *Sci Rep*, 11(1), 04 27, 20210427, p. 9096.

Aghaizu, N. D., Jin, H. and Whiting, P. J. (2020) 'Dysregulated Wnt Signalling in the Alzheimer's Brain.' *Brain Sci*, 10(12), Nov 24, 20201124,

Ahmadi-Abhari S , Guzman-Castillo M , Bandosz P , Shipley M J , Muniz-Terrera G and al., S.-M. A. e. (2017) 'Temporal trend in dementia incidence since 2002 and projections for prevalence in England and Wales to 2040: modelling study.' p. 358 :j2856.

Alvarez, A. R., Godoy, J. A., Mullendorff, K., Olivares, G. H., Bronfman, M. and Inestrosa, N. C. (2004) 'Wnt-3a overcomes beta-amyloid toxicity in rat hippocampal neurons.' *Exp Cell Res*, 297(1), Jul 01, pp. 186-196.

Alvarez-Buylla, A. and Garcia-Verdugo, J. M. (2002) 'Neurogenesis in adult subventricular zone.' *J Neurosci*, 22(3), Feb 01, pp. 629-634.

Appel, J. R., Ye, S., Tang, F., Sun, D., Zhang, H., Mei, L. and Xiong, W. C. (2018) 'Increased Microglial Activity, Impaired Adult Hippocampal Neurogenesis, and Depressive-like Behavior in Microglial VPS35-Depleted Mice.' *J Neurosci*, 38(26), Jun, 2018/05/31, pp. 5949-5968.

Arber, C., Lovejoy, C., Harris, L., Willumsen, N., Alatz, A., Casey, J. M., Lines, G., Kerins, C., et al. (2021) 'Familial Alzheimer's Disease Mutations in PSEN1 Lead to Premature Human Stem Cell Neurogenesis.' *Cell Rep*, 34(2), 01 12, p. 108615.

Arnold, D. B. and Gallo, G. (2014) 'Structure meets function: actin filaments and myosin motors in the axon.' *J Neurochem*, 129(2), Apr, 20131119, pp. 213-220.

Atwood, C. S. and Bowen, R. L. (2015) 'A Unified Hypothesis of Early- and Late-Onset Alzheimer's Disease Pathogenesis.' *J Alzheimers Dis*, 47(1) pp. 33-47.

Ayodele, T., Rogaeva, E., Kurup, J. T., Beecham, G. and Reitz, C. (2021) 'Early-Onset Alzheimer's Disease: What Is Missing in Research?' *Curr Neurol Neurosci Rep*, 21(2), 01 19, 20210119, p. 4.

Baldacci, F., Lista, S., Cavedo, E., Bonuccelli, U. and Hampel, H. (2017) 'Diagnostic function of the neuroinflammatory biomarker YKL-40 in Alzheimer's disease and other neurodegenerative diseases.' *Expert Rev Proteomics*, 14(4), 04, 2017/03/20, pp. 285-299.

Barnett, D. W., Garrison, E. K., Quinlan, A. R., Strömberg, M. P. and Marth, G. T. (2011) 'BamTools: a C++ API and toolkit for analyzing and managing BAM files.' *Bioinformatics*, 27(12), Jun 15, 20110414, pp. 1691-1692.

Baron, O., Boudi, A., Dias, C., Schilling, M., Nölle, A., Vizcay-Barrena, G., Rattray, I., Jungbluth, H., et al. (2017) 'Stall in Canonical Autophagy-Lysosome Pathways Prompts Nucleophagy-Based Nuclear Breakdown in Neurodegeneration.' *Curr Biol*, 27(23), Dec, 2017/11/22, pp. 3626-3642.e3626.

Beel, A. J. and Sanders, C. R. (2008) 'Substrate specificity of gamma-secretase and other intramembrane proteases.' *Cell Mol Life Sci*, 65(9), May, pp. 1311-1334.

Behl, T., Kaur, I., Fratila, O., Brata, R. and Bungau, S. (2020) 'Exploring the Potential of Therapeutic Agents Targeted towards Mitigating the Events Associated with Amyloid- β Cascade in Alzheimer's Disease.' *Int J Mol Sci*, 21(20), Oct 09, 20201009,

Belenguer, G., Duart-Abadia, P., Jordán-Pla, A., Domingo-Muelas, A., Blasco-Chamarro, L., Ferrón, S. R., Morante-Redolat, J. M. and Fariñas, I. (2021) 'Adult Neural Stem Cells Are Alerted by Systemic Inflammation through TNF- α Receptor Signaling.' *Cell Stem Cell*, 28(2), 02 04, 20201117, pp. 285-299.e289.

Bernal, A. and Arranz, L. (2018) 'Nestin-expressing progenitor cells: function, identity and therapeutic implications.' *Cell Mol Life Sci*, 75(12), 06, 20180314, pp. 2177-2195.

- Bolger, A. M., Lohse, M. and Usadel, B. (2014) 'Trimmomatic: a flexible trimmer for Illumina sequence data.' *Bioinformatics*, 30(15), Aug 01, 20140401, pp. 2114-2120.
- Boraas, L. C., Pineda, E. T. and Ahsan, T. (2018) 'Actin and myosin II modulate differentiation of pluripotent stem cells.' *PLoS One*, 13(4) 20180417, p. e0195588.
- Borchelt, D. R., Thinakaran, G., Eckman, C. B., Lee, M. K., Davenport, F., Ratovitsky, T., Prada, C. M., Kim, G., et al. (1996a) 'Familial Alzheimer's disease-linked presenilin 1 variants elevate A β 1-42/1-40 ratio in vitro and in vivo.' *Neuron*, 17(5), Nov, pp. 1005-1013.
- Borchelt, D. R., Thinakaran, G., Eckman, C. B., Lee, M. K., Davenport, F., Ratovitsky, T., Prada, C. M., Kim, G., et al. (1996b) 'Familial Alzheimer's disease-linked presenilin 1 variants elevate A β 1-42/1-40 ratio in vitro and in vivo.' *Neuron*, 17(5), Nov, pp. 1005-1013.
- Bordi, M., Berg, M. J., Mohan, P. S., Peterhoff, C. M., Alldred, M. J., Che, S., Ginsberg, S. D. and Nixon, R. A. (2016) 'Autophagy flux in CA1 neurons of Alzheimer hippocampus: Increased induction overburdens failing lysosomes to propel neuritic dystrophy.' *Autophagy*, 12(12), Dec, 2016/11/04, pp. 2467-2483.
- Borghese, L., Dolezalova, D., Opitz, T., Haupt, S., Leinhaas, A., Steinfarz, B., Koch, P., Edenhofer, F., et al. (2010) 'Inhibition of notch signaling in human embryonic stem cell-derived neural stem cells delays G1/S phase transition and accelerates neuronal differentiation in vitro and in vivo.' *Stem Cells*, 28(5), May, pp. 955-964.
- Brandenstein, L., Schweizer, M., Sedlacik, J., Fiehler, J. and Storch, S. (2016) 'Lysosomal dysfunction and impaired autophagy in a novel mouse model deficient for the lysosomal membrane protein Cln7.' *Hum Mol Genet*, 25(4), Feb, 2015/12/17, pp. 777-791.
- Bray, S. J. (2006) 'Notch signalling: a simple pathway becomes complex.' *Nat Rev Mol Cell Biol*, 7(9), Sep, pp. 678-689.

Brett, F. M., Mizisin, A. P., Powell, H. C. and Campbell, I. L. (1995) 'Evolution of neuropathologic abnormalities associated with blood-brain barrier breakdown in transgenic mice expressing interleukin-6 in astrocytes.' *J Neuropathol Exp Neurol*, 54(6), Nov, pp. 766-775.

Bruni, A. C., Bernardi, L., Colao, R., Rubino, E., Smirne, N., Frangipane, F., Terni, B., Curcio, S. A., et al. (2010) 'Worldwide distribution of PSEN1 Met146Leu mutation: a large variability for a founder mutation.' *Neurology*, 74(10), Mar, 2010/02/17, pp. 798-806.

Buckles, V. D., Xiong, C., Bateman, R. J., Hassenstab, J., Allegri, R., Berman, S. B., Chhatwal, J. P., Danek, A., et al. (2021) 'Different rates of cognitive decline in autosomal dominant and late-onset Alzheimer disease.' *Alzheimers Dement*, Dec 02, 20211202,

Buckley, S. M., Delhove, J. M., Perocheau, D. P., Karda, R., Rahim, A. A., Howe, S. J., Ward, N. J., Birrell, M. A., et al. (2015) 'In vivo bioimaging with tissue-specific transcription factor activated luciferase reporters.' *Sci Rep*, 5, Jul, 2015/07/03, p. 11842.

Busser, J., Geldmacher, D. S. and Herrup, K. (1998) 'Ectopic cell cycle proteins predict the sites of neuronal cell death in Alzheimer's disease brain.' *J Neurosci*, 18(8), Apr 15, pp. 2801-2807.

Butler, M. T. and Wallingford, J. B. (2017) 'Planar cell polarity in development and disease.' *Nat Rev Mol Cell Biol*, 18(6), 06, 20170315, pp. 375-388.

Camp, A. J. and Wijesinghe, R. (2009) 'Calretinin: modulator of neuronal excitability.' *Int J Biochem Cell Biol*, 41(11), Nov, 20090518, pp. 2118-2121.

Castilla-Ortega, E., Pedraza, C., Estivill-Torrús, G. and Santín, L. J. (2011a) 'When is adult hippocampal neurogenesis necessary for learning? evidence from animal research.' *Rev Neurosci*, 22(3) 20110513, pp. 267-283.

Castilla-Ortega, E., Hoyo-Becerra, C., Pedraza, C., Chun, J., Rodríguez De Fonseca, F., Estivill-Torrús, G. and Santín, L. J. (2011b) 'Aggravation of chronic stress effects on hippocampal neurogenesis and spatial memory in LPA₁ receptor knockout mice.' *PLoS One*, 6(9) 20110929, p. e25522.

Cerpa, W., Farías, G. G., Godoy, J. A., Fuenzalida, M., Bonansco, C. and Inestrosa, N. C. (2010) 'Wnt-5a occludes Abeta oligomer-induced depression of glutamatergic transmission in hippocampal neurons.' *Mol Neurodegener*, 5, Jan 18, 20100118, p. 3.

Cheignon, C., Tomas, M., Bonnefont-Rousselot, D., Faller, P., Hureau, C. and Collin, F. (2018) 'Oxidative stress and the amyloid beta peptide in Alzheimer's disease.' *Redox Biol*, 14, 04, 20171018, pp. 450-464.

Chen, C., Fingerhut, J. M. and Yamashita, Y. M. (2016) 'The ins(ide) and outs(ide) of asymmetric stem cell division.' *Curr Opin Cell Biol*, 43, 12, 20160616, pp. 1-6.

Chen, E., Xu, D., Lan, X., Jia, B., Sun, L., Zheng, J. C. and Peng, H. (2013) 'A novel role of the STAT3 pathway in brain inflammation-induced human neural progenitor cell differentiation.' *Curr Mol Med*, 13(9), Nov, pp. 1474-1484.

Chen, G. F., Xu, T. H., Yan, Y., Zhou, Y. R., Jiang, Y., Melcher, K. and Xu, H. E. (2017) 'Amyloid beta: structure, biology and structure-based therapeutic development.' *Acta Pharmacol Sin*, 38(9), Sep, 20170717, pp. 1205-1235.

Chong, C. M., Ke, M., Tan, Y., Huang, Z., Zhang, K., Ai, N., Ge, W., Qin, D., et al. (2018) 'Presenilin 1 deficiency suppresses autophagy in human neural stem cells through reducing γ -secretase-independent ERK/CREB signaling.' *Cell Death Dis*, 9(9), Aug, 2018/08/29, p. 879.

Chávez-Gutiérrez, L., Bammens, L., Benilova, I., Vandersteen, A., Benurwar, M., Borgers, M., Lismont, S., Zhou, L., et al. (2012a) 'The mechanism of γ -Secretase dysfunction in familial Alzheimer disease.' *EMBO J*, 31(10), May 16, 20120413, pp. 2261-2274.

Chávez-Gutiérrez, L., Bammens, L., Benilova, I., Vandersteen, A., Benurwar, M., Borgers, M., Lismont, S., Zhou, L., et al. (2012b) 'The mechanism of γ -Secretase dysfunction in familial Alzheimer disease.' *EMBO J*, 31(10), May 16, 20120413, pp. 2261-2274.

Colović, M. B., Krstić, D. Z., Lazarević-Pašti, T. D., Bondžić, A. M. and Vasić, V. M. (2013) 'Acetylcholinesterase inhibitors: pharmacology and toxicology.' *Curr Neuropharmacol*, 11(3), May, pp. 315-335.

Conesa, A., Madrigal, P., Tarazona, S., Gomez-Cabrero, D., Cervera, A., McPherson, A., Szcześniak, M. W., Gaffney, D. J., et al. (2016) 'A survey of best practices for RNA-seq data analysis.' *Genome Biol*, 17, Jan 26, 20160126, p. 13.

Congdon, E. E. and Sigurdsson, E. M. (2018) 'Tau-targeting therapies for Alzheimer disease.' *Nat Rev Neurol*, 14(7), 07, pp. 399-415.

Coric, V., van Dyck, C. H., Salloway, S., Andreasen, N., Brody, M., Richter, R. W., Soininen, H., Thein, S., et al. (2012) 'Safety and tolerability of the γ -secretase inhibitor avagacestat in a phase 2 study of mild to moderate Alzheimer disease.' *Arch Neurol*, 69(11), Nov, pp. 1430-1440.

Costamagna, G., Andreoli, L., Corti, S. and Faravelli, I. (2019) 'iPSCs-Based Neural 3D Systems: A Multidimensional Approach for Disease Modeling and Drug Discovery.' *Cells*, 8(11), 11 14, 20191114,

Cummings, J. L., Morstorf, T. and Zhong, K. (2014) 'Alzheimer's disease drug-development pipeline: few candidates, frequent failures.' *Alzheimers Res Ther*, 6(4) 20140703, p. 37.

D'Souza, B., Meloty-Kapella, L. and Weinmaster, G. (2010) 'Canonical and non-canonical Notch ligands.' *Curr Top Dev Biol*, 92 pp. 73-129.

Dehmelt, L. and Halpain, S. (2005) 'The MAP2/Tau family of microtubule-associated proteins.' *Genome Biol*, 6(1) 20041223, p. 204.

Deng, W., Aimone, J. B. and Gage, F. H. (2010) 'New neurons and new memories: how does adult hippocampal neurogenesis affect learning and memory?' *Nat Rev Neurosci*, 11(5), May, 20100331, pp. 339-350.

Dent, E. W., Tang, F. and Kalil, K. (2003) 'Axon guidance by growth cones and branches: common cytoskeletal and signaling mechanisms.' *Neuroscientist*, 9(5), Oct, pp. 343-353.

Dent, E. W., Merriam, E. B. and Hu, X. (2011) 'The dynamic cytoskeleton: backbone of dendritic spine plasticity.' *Curr Opin Neurobiol*, 21(1), Feb, 20100909, pp. 175-181.

Dobrowolski, R., Vick, P., Ploper, D., Gumper, I., Snitkin, H., Sabatini, D. D. and De Robertis, E. M. (2012) 'Presenilin deficiency or lysosomal inhibition enhances Wnt signaling through relocalization of GSK3 to the late-endosomal compartment.' *Cell Rep*, 2(5), Nov 29, 20121101, pp. 1316-1328.

Doetsch, F., García-Verdugo, J. M. and Alvarez-Buylla, A. (1997) 'Cellular composition and three-dimensional organization of the subventricular germinal zone in the adult mammalian brain.' *J Neurosci*, 17(13), Jul 01, pp. 5046-5061.

Doody, R. S., Raman, R., Farlow, M., Iwatsubo, T., Vellas, B., Joffe, S., Kieburtz, K., He, F., et al. (2013) 'A phase 3 trial of semagacestat for treatment of Alzheimer's disease.' *N Engl J Med*, 369(4), Jul 25, pp. 341-350.

Duan, W., Zhang, Y. P., Hou, Z., Huang, C., Zhu, H., Zhang, C. Q. and Yin, Q. (2016) 'Novel Insights into NeuN: from Neuronal Marker to Splicing Regulator.' *Mol Neurobiol*, 53(3), Apr, 20150214, pp. 1637-1647.

Duff, K., Eckman, C., Zehr, C., Yu, X., Prada, C. M., Perez-tur, J., Hutton, M., Buee, L., et al. (1996) 'Increased amyloid-beta₄₂(43) in brains of mice expressing mutant presenilin 1.' *Nature*, 383(6602), Oct 24, pp. 710-713.

Duggan, S. P. and McCarthy, J. V. (2016) 'Beyond γ -secretase activity: The multifunctional nature of presenilins in cell signalling pathways.' *Cell Signal*, 28(1), Jan, 2015/10/21, pp. 1-11.

Dzamba, D., Harantova, L., Butenko, O. and Anderova, M. (2016) 'Glial Cells - The Key Elements of Alzheimer's Disease.' *Curr Alzheimer Res*, 13(8) pp. 894-911.

Egan, M. F., Kost, J., Tariot, P. N., Aisen, P. S., Cummings, J. L., Vellas, B., Sur, C., Mukai, Y., et al. (2018a) 'Randomized Trial of Verubecestat for Mild-to-Moderate Alzheimer's Disease.' *N Engl J Med*, 378(18), May 03, pp. 1691-1703.

Egan, M. F., Kost, J., Tariot, P. N., Aisen, P. S., Cummings, J. L., Vellas, B., Sur, C., Mukai, Y., et al. (2018b) 'Randomized Trial of Verubecestat for Mild-to-Moderate Alzheimer's Disease.' *N Engl J Med*, 378(18), May 03, pp. 1691-1703.

Egan, M. F., Kost, J., Voss, T., Mukai, Y., Aisen, P. S., Cummings, J. L., Tariot, P. N., Vellas, B., et al. (2019) 'Randomized Trial of Verubecestat for Prodromal Alzheimer's Disease.' *N Engl J Med*, 380(15), Apr 11, pp. 1408-1420.

Ethell, D. W. (2010) 'An amyloid-notch hypothesis for Alzheimer's disease.' *Neuroscientist*, 16(6), Dec, 20100630, pp. 614-617.

Ferguson, S. M. (2018) 'Axonal transport and maturation of lysosomes.' *Curr Opin Neurobiol*, 51, Aug, 2018/03/09, pp. 45-51.

Ferletta, M., Caglayan, D., Mokvist, L., Jiang, Y., Kastemar, M., Uhrbom, L. and Westermarck, B. (2011) 'Forced expression of Sox21 inhibits Sox2 and induces apoptosis in human glioma cells.' *Int J Cancer*, 129(1), Jul 01, 20101109, pp. 45-60.

Ferri, A. L., Cavallaro, M., Braida, D., Di Cristofano, A., Canta, A., Vezzani, A., Ottolenghi, S., Pandolfi, P. P., et al. (2004) 'Sox2 deficiency causes neurodegeneration and impaired neurogenesis in the adult mouse brain.' *Development*, 131(15), Aug, 20040707, pp. 3805-3819.

Fiddes, I. T., Lodewijk, G. A., Mooring, M., Bosworth, C. M., Ewing, A. D., Mantalas, G. L., Novak, A. M., van den Bout, A., et al. (2018) 'Human-Specific NOTCH2NL Genes Affect Notch Signaling and Cortical Neurogenesis.' *Cell*, 173(6), 05 31, 20180531, pp. 1356-1369.e1322.

Filippov, V., Kronenberg, G., Pivneva, T., Reuter, K., Steiner, B., Wang, L. P., Yamaguchi, M., Kettenmann, H., et al. (2003) 'Subpopulation of nestin-expressing progenitor cells in the adult murine hippocampus shows electrophysiological and morphological characteristics of astrocytes.' *Mol Cell Neurosci*, 23(3), Jul, pp. 373-382.

Finch, C. E. (2005) 'Developmental origins of aging in brain and blood vessels: an overview.' *Neurobiol Aging*, 26(3), Mar, pp. 281-291.

FitzPatrick, L. M., Hawkins, K. E., Delhove, J. M. K. M., Fernandez, E., Soldati, C., Bullen, L. F., Nohturfft, A., Waddington, S. N., et al. (2018a) 'NF- κ B Activity Initiates Human ESC-Derived Neural Progenitor Cell Differentiation by Inducing a Metabolic Maturation Program.' *Stem Cell Reports*, 10(6), 06 05, 20180419, pp. 1766-1781.

FitzPatrick, L. M., Hawkins, K. E., Delhove, J. M. K. M., Fernandez, E., Soldati, C., Bullen, L. F., Nohturfft, A., Waddington, S. N., et al. (2018b) 'NF- κ B Activity Initiates Human ESC-Derived Neural Progenitor Cell Differentiation by Inducing a Metabolic Maturation Program.' *Stem Cell Reports*, 10(6), Jun, 2018/04/19, pp. 1766-1781.

Fletcher, D. A. and Mullins, R. D. (2010) 'Cell mechanics and the cytoskeleton.' *Nature*, 463(7280), Jan 28, pp. 485-492.

Folke, J., Pakkenberg, B. and Brudek, T. (2019) 'Impaired Wnt Signaling in the Prefrontal Cortex of Alzheimer's Disease.' *Mol Neurobiol*, 56(2), Feb, 20180526, pp. 873-891.

Foroutan, N., Hopkins, R. B., Tarride, J. E., Florez, I. D. and Levine, M. (2019) 'Safety and efficacy of active and passive immunotherapy in mild-to-moderate Alzheimer's

disease: A systematic review and network meta-analysis.' *Clin Invest Med*, 42(1), 03 23, 20190323, pp. E53-E65.

Frade, J. M. and Ovejero-Benito, M. C. (2015a) 'Neuronal cell cycle: the neuron itself and its circumstances.' *Cell Cycle*, 14(5) pp. 712-720.

Frade, J. M. and Ovejero-Benito, M. C. (2015b) 'Neuronal cell cycle: the neuron itself and its circumstances.' *Cell Cycle*, 14(5) pp. 712-720.

Fradkin, L. G., Dura, J. M. and Noordermeer, J. N. (2010) 'Ryks: new partners for Wnts in the developing and regenerating nervous system.' *Trends Neurosci*, 33(2), Feb, 20091211, pp. 84-92.

François, A., Terro, F., Janet, T., Rioux Bilan, A., Paccalin, M. and Page, G. (2013a) 'Involvement of interleukin-1 β in the autophagic process of microglia: relevance to Alzheimer's disease.' *J Neuroinflammation*, 10, Dec, 2013/12/13, p. 151.

François, A., Terro, F., Janet, T., Rioux Bilan, A., Paccalin, M. and Page, G. (2013b) 'Involvement of interleukin-1 β in the autophagic process of microglia: relevance to Alzheimer's disease.' *J Neuroinflammation*, 10, Dec, 2013/12/13, p. 151.

Frieden, C. (2015) 'ApoE: the role of conserved residues in defining function.' *Protein Sci*, 24(1), Jan, 2014/12/09, pp. 138-144.

Galceran, J., Miyashita-Lin, E. M., Devaney, E., Rubenstein, J. L. and Grosschedl, R. (2000) 'Hippocampus development and generation of dentate gyrus granule cells is regulated by LEF1.' *Development*, 127(3), Feb, pp. 469-482.

Ghim, C. M., Lee, S. K., Takayama, S. and Mitchell, R. J. (2010) 'The art of reporter proteins in science: past, present and future applications.' *BMB Rep*, 43(7), Jul, pp. 451-460.

Giau, V. V., Bagyinszky, E., An, S. S. and Kim, S. Y. (2015) 'Role of apolipoprotein E in neurodegenerative diseases.' *Neuropsychiatr Dis Treat*, 11 2015/07/16, pp. 1723-1737.

Gil-Perotín, S., Duran-Moreno, M., Cebrián-Silla, A., Ramírez, M., García-Belda, P. and García-Verdugo, J. M. (2013) 'Adult neural stem cells from the subventricular zone: a review of the neurosphere assay.' *Anat Rec (Hoboken)*, 296(9), Sep, 20130731, pp. 1435-1452.

Gong, J., Muñoz, A. R., Chan, D., Ghosh, R. and Kumar, A. P. (2014) 'STAT3 down regulates LC3 to inhibit autophagy and pancreatic cancer cell growth.' *Oncotarget*, 5(9), May, pp. 2529-2541.

Gu, L. and Guo, Z. (2013) 'Alzheimer's A β 42 and A β 40 peptides form interlaced amyloid fibrils.' *J Neurochem*, 126(3), Aug, 20130312, pp. 305-311.

Guarnieri, F. C., de Chevigny, A., Falace, A. and Cardoso, C. (2018) 'Disorders of neurogenesis and cortical development.' *Dialogues Clin Neurosci*, 20(4), 12, pp. 255-266.

Guo, Q., Zheng, X., Yang, P., Pang, X., Qian, K., Wang, P., Xu, S., Sheng, D., et al. (2019) 'Small interfering RNA delivery to the neurons near the amyloid plaques for improved treatment of Alzheimer's disease.' *Acta Pharm Sin B*, 9(3), May, 20181230, pp. 590-603.

Götz, A., Mylonas, N., Högel, P., Silber, M., Heinel, H., Menig, S., Vogel, A., Feyrer, H., et al. (2019) 'Modulating Hinge Flexibility in the APP Transmembrane Domain Alters γ -Secretase Cleavage.' *Biophys J*, 116(11), 06 04, 20190503, pp. 2103-2120.

Güner, G. and Lichtenthaler, S. F. (2020) 'The substrate repertoire of γ -secretase/presenilin.' *Semin Cell Dev Biol*, 105, 09, 20200629, pp. 27-42.

Hampel, H., Toschi, N., Babiloni, C., Baldacci, F., Black, K. L., Bokde, A. L. W., Bun, R. S., Cacciola, F., et al. (2018) 'Revolution of Alzheimer Precision Neurology. Passageway of Systems Biology and Neurophysiology.' *J Alzheimers Dis*, 64(s1) pp. S47-S105.

Hansen, D. V., Lui, J. H., Parker, P. R. and Kriegstein, A. R. (2010) 'Neurogenic radial glia in the outer subventricular zone of human neocortex.' *Nature*, 464(7288), Mar 25, pp. 554-561.

Hardy, J. (1992) 'An 'anatomical cascade hypothesis' for Alzheimer's disease.' *Trends Neurosci*, 15(6), Jun, pp. 200-201.

Hardy, J. and Selkoe, D. J. (2002) 'The amyloid hypothesis of Alzheimer's disease: progress and problems on the road to therapeutics.' *Science*, 297(5580), Jul 19, pp. 353-356.

Hardy, J. A. and Higgins, G. A. (1992) 'Alzheimer's disease: the amyloid cascade hypothesis.' *Science*, 256(5054), Apr 10, pp. 184-185.

Heilig, E. A., Xia, W., Shen, J. and Kelleher, R. J. (2010) 'A presenilin-1 mutation identified in familial Alzheimer disease with cotton wool plaques causes a nearly complete loss of gamma-secretase activity.' *J Biol Chem*, 285(29), Jul 16, 20100511, pp. 22350-22359.

Heilig, E. A., Gutti, U., Tai, T., Shen, J. and Kelleher, R. J. (2013) 'Trans-dominant negative effects of pathogenic PSEN1 mutations on γ -secretase activity and A β production.' *J Neurosci*, 33(28), Jul 10, pp. 11606-11617.

Henley, D., Raghavan, N., Sperling, R., Aisen, P., Raman, R. and Romano, G. (2019) 'Preliminary Results of a Trial of Atabecestat in Preclinical Alzheimer's Disease.' *N Engl J Med*, 380(15), Apr 11, pp. 1483-1485.

Hernández-Ortega, K., Quiroz-Baez, R. and Arias, C. (2011) 'Cell cycle reactivation in mature neurons: a link with brain plasticity, neuronal injury and neurodegenerative diseases?' *Neurosci Bull*, 27(3), Jun, pp. 185-196.

Hirabayashi, Y. and Gotoh, Y. (2005) 'Stage-dependent fate determination of neural precursor cells in mouse forebrain.' *Neurosci Res*, 51(4), Apr, pp. 331-336.

Hitzenberger, M. and Zacharias, M. (2019) 'Structural Modeling of γ -Secretase A β .' *ACS Chem Neurosci*, 10(3), 03 20, 20190130, pp. 1826-1840.

Ho, S. M., Hartley, B. J., Tcw, J., Beaumont, M., Stafford, K., Slesinger, P. A. and Brennand, K. J. (2016) 'Rapid Ngn2-induction of excitatory neurons from hiPSC-derived neural progenitor cells.' *Methods*, 101, 05, 2015/11/25, pp. 113-124.

Hofmann, J. W., McBryan, T., Adams, P. D. and Sedivy, J. M. (2014) 'The effects of aging on the expression of Wnt pathway genes in mouse tissues.' *Age (Dordr)*, 36(3), Jun, 20140201, p. 9618.

Hollands, C., Tobin, M. K., Hsu, M., Musaraca, K., Yu, T. S., Mishra, R., Kernie, S. G. and Lazarov, O. (2017) 'Depletion of adult neurogenesis exacerbates cognitive deficits in Alzheimer's disease by compromising hippocampal inhibition.' *Mol Neurodegener*, 12(1), 09 08, 20170908, p. 64.

Hsiao, K., Chapman, P., Nilsen, S., Eckman, C., Harigaya, Y., Younkin, S., Yang, F. and Cole, G. (1996) 'Correlative memory deficits, A β elevation, and amyloid plaques in transgenic mice.' *Science*, 274(5284), Oct 04, pp. 99-102.

Hu, J., Yu, J., Gan, J., Song, N., Shi, L., Liu, J., Zhang, Z. and Du, J. (2020) 'Notch1/2/3/4 are prognostic biomarker and correlated with immune infiltrates in gastric cancer.' *Aging (Albany NY)*, 12(3), 02 06, 20200206, pp. 2595-2609.

Hunsberger, H. C., Pinky, P. D., Smith, W., Suppiramaniam, V. and Reed, M. N. (2019) 'The role of APOE4 in Alzheimer's disease: strategies for future therapeutic interventions.' *Neuronal Signal*, 3(2), 06, 20190418, p. NS20180203.

Iadecola, C. (2004) 'Neurovascular regulation in the normal brain and in Alzheimer's disease.' *Nat Rev Neurosci*, 5(5), May, pp. 347-360.

Iqbal, K., Liu, F., Gong, C. X. and Grundke-Iqbal, I. (2010) 'Tau in Alzheimer disease and related tauopathies.' *Curr Alzheimer Res*, 7(8), Dec, pp. 656-664.

Ittner, L. M., Fath, T., Ke, Y. D., Bi, M., van Eersel, J., Li, K. M., Gunning, P. and Götz, J. (2008) 'Parkinsonism and impaired axonal transport in a mouse model of frontotemporal dementia.' *Proc Natl Acad Sci U S A*, 105(41), Oct 14, 20081002, pp. 15997-16002.

Janicki, S. M., Stabler, S. M. and Monteiro, M. J. (2000) 'Familial Alzheimer's disease presenilin-1 mutants potentiate cell cycle arrest.' *Neurobiol Aging*, 21(6), 2000 Nov-Dec, pp. 829-836.

Jarmas, A. E., Brunskill, E. W., Chaturvedi, P., Salomonis, N. and Kopan, R. (2021) 'Progenitor translatoe changes coordinated by Tsc1 increase perception of Wnt signals to end nephrogenesis.' *Nat Commun*, 12(1), 11 03, 20211103, p. 6332.

Javier-Torrent, M. and Saura, C. A. (2020) 'Conventional and Non-Conventional Roles of Non-Muscle Myosin II-Actin in Neuronal Development and Degeneration.' *Cells*, 9(9), 08 19, 20200819,

Jia, L., Piña-Crespo, J. and Li, Y. (2019) 'Restoring Wnt/ β -catenin signaling is a promising therapeutic strategy for Alzheimer's disease.' *Mol Brain*, 12(1), 12 04, 20191204, p. 104.

Jin, K., Peel, A. L., Mao, X. O., Xie, L., Cottrell, B. A., Henshall, D. C. and Greenberg, D. A. (2004) 'Increased hippocampal neurogenesis in Alzheimer's disease.' *Proc Natl Acad Sci U S A*, 101(1), Jan 06, 20031205, pp. 343-347.

Joseph, C., Mangani, A. S., Gupta, V., Chitranshi, N., Shen, T., Dheer, Y., Kb, D., Mirzaei, M., et al. (2020a) 'Cell Cycle Deficits in Neurodegenerative Disorders: Uncovering Molecular Mechanisms to Drive Innovative Therapeutic Development.' *Aging Dis*, 11(4), Jul, 20200723, pp. 946-966.

Joseph, C., Mangani, A. S., Gupta, V., Chitranshi, N., Shen, T., Dheer, Y., Kb, D., Mirzaei, M., et al. (2020b) 'Cell Cycle Deficits in Neurodegenerative Disorders: Uncovering Molecular Mechanisms to Drive Innovative Therapeutic Development.' *Aging Dis*, 11(4), Jul, 20200723, pp. 946-966.

Kabir, M. T., Uddin, M. S., Setu, J. R., Ashraf, G. M., Bin-Jumah, M. N. and Abdel-Daim, M. M. (2020) 'Exploring the Role of PSEN Mutations in the Pathogenesis of Alzheimer's Disease.' *Neurotox Res*, 38(4), Dec, 20200618, pp. 833-849.

Kalamakis, G., Brüne, D., Ravichandran, S., Bolz, J., Fan, W., Ziebell, F., Stiehl, T., Catalá-Martinez, F., et al. (2019) 'Quiescence Modulates Stem Cell Maintenance and Regenerative Capacity in the Aging Brain.' *Cell*, 176(6), 03 07, 20190228, pp. 1407-1419.e1414.

Kang, D. E., Soriano, S., Frosch, M. P., Collins, T., Naruse, S., Sisodia, S. S., Leibowitz, G., Levine, F., et al. (1999) 'Presenilin 1 facilitates the constitutive turnover of beta-catenin: differential activity of Alzheimer's disease-linked PS1 mutants in the beta-catenin-signaling pathway.' *J Neurosci*, 19(11), Jun 01, pp. 4229-4237.

Karalay, O., Doberauer, K., Vadodaria, K. C., Knobloch, M., Berti, L., Miquelajauregui, A., Schwark, M., Jagasia, R., et al. (2011) 'Prospero-related homeobox 1 gene (Prox1) is regulated by canonical Wnt signaling and has a stage-specific role in adult hippocampal neurogenesis.' *Proc Natl Acad Sci U S A*, 108(14), Apr 05, 20110321, pp. 5807-5812.

Katsetos, C. D., Legido, A., Perentes, E. and Mörk, S. J. (2003) 'Class III beta-tubulin isotype: a key cytoskeletal protein at the crossroads of developmental neurobiology and tumor neuropathology.' *J Child Neurol*, 18(12), Dec, pp. 851-866; discussion 867.

Kempermann, G. (2002) 'Why new neurons? Possible functions for adult hippocampal neurogenesis.' *J Neurosci*, 22(3), Feb 01, pp. 635-638.

Kempermann, G., Jessberger, S., Steiner, B. and Kronenberg, G. (2004) 'Milestones of neuronal development in the adult hippocampus.' *Trends Neurosci*, 27(8), Aug, pp. 447-452.

Kim, D., Langmead, B. and Salzberg, S. L. (2015) 'HISAT: a fast spliced aligner with low memory requirements.' *Nat Methods*, 12(4), Apr, 20150309, pp. 357-360.

Kiriyama, Y. and Nochi, H. (2015) 'The Function of Autophagy in Neurodegenerative Diseases.' *Int J Mol Sci*, 16(11), Nov, 2015/11/09, pp. 26797-26812.

Kokovay, E., Wang, Y., Kusek, G., Wurster, R., Lederman, P., Lowry, N., Shen, Q. and Temple, S. (2012) 'VCAM1 is essential to maintain the structure of the SVZ niche and acts as an environmental sensor to regulate SVZ lineage progression.' *Cell Stem Cell*, 11(2), Aug 03, pp. 220-230.

Kopan, R. (2012) 'Notch signaling.' *Cold Spring Harb Perspect Biol*, 4(10), Oct 01, 20121001,

Kopan, R. and Ilagan, M. X. (2009) 'The canonical Notch signaling pathway: unfolding the activation mechanism.' *Cell*, 137(2), Apr 17, pp. 216-233.

Korzhevskii, D. E., Karpenko, M. N. and Kirik, O. V. (2011) '[Microtubule-associated proteins as markers of nerve cell differentiation and functional status].' *Morfologija*, 139(1) pp. 13-21.

Kwart, D., Gregg, A., Scheckel, C., Murphy, E. A., Paquet, D., Duffield, M., Fak, J., Olsen, O., et al. (2019) 'A Large Panel of Isogenic APP and PSEN1 Mutant Human iPSC Neurons Reveals Shared Endosomal Abnormalities Mediated by APP β -CTFs, Not A β .' *Neuron*, 104(5), Dec 04, p. 1022.

Ladrón de Guevara-Miranda, D., Moreno-Fernández, R. D., Gil-Rodríguez, S., Rosell-Valle, C., Estivill-Torrús, G., Serrano, A., Pavón, F. J., Rodríguez de Fonseca, F., et al. (2019) 'Lysophosphatidic acid-induced increase in adult hippocampal neurogenesis facilitates the forgetting of cocaine-contextual memory.' *Addict Biol*, 24(3), 05, 20180226, pp. 458-470.

Lancaster, M. A., Renner, M., Martin, C. A., Wenzel, D., Bicknell, L. S., Hurles, M. E., Homfray, T., Penninger, J. M., et al. (2013) 'Cerebral organoids model human brain development and microcephaly.' *Nature*, 501(7467), Sep, 2013/08/28, pp. 373-379.

Lange, C. and Calegari, F. (2010) 'Cdks and cyclins link G1 length and differentiation of embryonic, neural and hematopoietic stem cells.' *Cell Cycle*, 9(10), May 15, 20100515, pp. 1893-1900.

Lange, C., Huttner, W. B. and Calegari, F. (2009) 'Cdk4/cyclinD1 overexpression in neural stem cells shortens G1, delays neurogenesis, and promotes the generation and expansion of basal progenitors.' *Cell Stem Cell*, 5(3), Sep 04, pp. 320-331.

Lasser, M., Tiber, J. and Lowery, L. A. (2018) 'The Role of the Microtubule Cytoskeleton in Neurodevelopmental Disorders.' *Front Cell Neurosci*, 12 20180614, p. 165.

Lattanzi, V., André, I., Gasser, U., Dubackic, M., Olsson, U. and Linse, S. (2021) 'Amyloid β 42 fibril structure based on small-angle scattering.' *Proc Natl Acad Sci U S A*, 118(48), 11 30,

Lavado, A. and Oliver, G. (2007) 'Prox1 expression patterns in the developing and adult murine brain.' *Dev Dyn*, 236(2), Feb, pp. 518-524.

Lazarov, O. and Hollands, C. (2016) 'Hippocampal neurogenesis: Learning to remember.' *Prog Neurobiol*, 138-140, 2016 Mar-May, 20160206, pp. 1-18.

Lazutkin, A., Podgorny, O. and Enikolopov, G. (2019) 'Modes of division and differentiation of neural stem cells.' *Behav Brain Res*, 374, 11 18, 20190729, p. 112118.

Lee, S. M., Tole, S., Grove, E. and McMahon, A. P. (2000) 'A local Wnt-3a signal is required for development of the mammalian hippocampus.' *Development*, 127(3), Feb, pp. 457-467.

Lendahl, U., Zimmerman, L. B. and McKay, R. D. (1990) 'CNS stem cells express a new class of intermediate filament protein.' *Cell*, 60(4), Feb 23, pp. 585-595.

- Leng, F. and Edison, P. (2021) 'Neuroinflammation and microglial activation in Alzheimer disease: where do we go from here?' *Nat Rev Neurol*, 17(3), 03, 20201214, pp. 157-172.
- Li, K., Zheng, X., Tang, H., Zang, Y. S., Zeng, C., Liu, X., Shen, Y., Pang, Y., et al. (2021) 'E3 ligase MKRN3 is a tumor suppressor regulating PABPC1 ubiquitination in non-small cell lung cancer.' *J Exp Med*, 218(8), 08 02, 20210618,
- Liao, Y., Smyth, G. K. and Shi, W. (2014) 'featureCounts: an efficient general purpose program for assigning sequence reads to genomic features.' *Bioinformatics*, 30(7), Apr 01, 20131113, pp. 923-930.
- LiCausi, F. and Hartman, N. W. (2018) 'Role of mTOR Complexes in Neurogenesis.' *Int J Mol Sci*, 19(5), May 22, 20180522,
- Liu, C. C., Zhao, N., Fu, Y., Wang, N., Linares, C., Tsai, C. W. and Bu, G. (2017a) 'ApoE4 Accelerates Early Seeding of Amyloid Pathology.' *Neuron*, 96(5), Dec, pp. 1024-1032.e1023.
- Liu, C. C., Zhao, N., Fu, Y., Wang, N., Linares, C., Tsai, C. W. and Bu, G. (2017b) 'ApoE4 Accelerates Early Seeding of Amyloid Pathology.' *Neuron*, 96(5), Dec, pp. 1024-1032.e1023.
- Liu, W. J., Ye, L., Huang, W. F., Guo, L. J., Xu, Z. G., Wu, H. L., Yang, C. and Liu, H. F. (2016) 'p62 links the autophagy pathway and the ubiquitin-proteasome system upon ubiquitinated protein degradation.' *Cell Mol Biol Lett*, 21 2016/12/13, p. 29.
- Livak, K. J. and Schmittgen, T. D. (2001) 'Analysis of relative gene expression data using real-time quantitative PCR and the 2(-Delta Delta C(T)) Method.' *Methods*, 25(4), Dec, pp. 402-408.
- Logan, C. Y. and Nusse, R. (2004) 'The Wnt signaling pathway in development and disease.' *Annu Rev Cell Dev Biol*, 20 pp. 781-810.

- Long, J. M. and Holtzman, D. M. (2019) 'Alzheimer Disease: An Update on Pathobiology and Treatment Strategies.' *Cell*, 179(2), 10 03, 20190926, pp. 312-339.
- Main, H., Radenkovic, J., Jin, S. B., Lendahl, U. and Andersson, E. R. (2013) 'Notch signaling maintains neural rosette polarity.' *PLoS One*, 8(5) 20130510, p. e62959.
- Marathe, S., Jaquet, M., Annoni, J. M. and Alberi, L. (2017) 'Jagged1 Is Altered in Alzheimer's Disease and Regulates Spatial Memory Processing.' *Front Cell Neurosci*, 11 20170809, p. 220.
- Marzo, A., Galli, S., Lopes, D., McLeod, F., Podpolny, M., Segovia-Roldan, M., Ciani, L., Purro, S., et al. (2016) 'Reversal of Synapse Degeneration by Restoring Wnt Signaling in the Adult Hippocampus.' *Curr Biol*, 26(19), 10 10, 20160901, pp. 2551-2561.
- Masters, C. L., Bateman, R., Blennow, K., Rowe, C. C., Sperling, R. A. and Cummings, J. L. (2015) 'Alzheimer's disease.' *Nat Rev Dis Primers*, 1, 10 15, 20151015, p. 15056.
- Mattson, M. P. (2004) 'Pathways towards and away from Alzheimer's disease.' *Nature*, 430(7000), Aug 05, pp. 631-639.
- Medoro, A., Bartollino, S., Mignogna, D., Passarella, D., Porcile, C., Pagano, A., Florio, T., Nizzari, M., et al. (2018) 'Complexity and Selectivity of γ -Secretase Cleavage on Multiple Substrates: Consequences in Alzheimer's Disease and Cancer.' *J Alzheimers Dis*, 61(1) pp. 1-15.
- Meyer, E. P., Ulmann-Schuler, A., Staufenbiel, M. and Krucker, T. (2008) 'Altered morphology and 3D architecture of brain vasculature in a mouse model for Alzheimer's disease.' *Proc Natl Acad Sci U S A*, 105(9), Mar 04, 20080227, pp. 3587-3592.
- Ming, G. L. and Song, H. (2011) 'Adult neurogenesis in the mammalian brain: significant answers and significant questions.' *Neuron*, 70(4), May 26, pp. 687-702.
- Miskinyte, G., Grønning Hansen, M., Monni, E., Lam, M., Bengzon, J., Lindvall, O., Ahlenius, H. and Kokaia, Z. (2018) 'Transcription factor programming of human ES

cells generates functional neurons expressing both upper and deep layer cortical markers.' *PLoS One*, 13(10) 2018/10/11, p. e0204688.

Moreno-Jiménez, E. P., Flor-García, M., Terreros-Roncal, J., Rábano, A., Cafini, F., Pallas-Bazarra, N., Ávila, J. and Llorens-Martín, M. (2019) 'Adult hippocampal neurogenesis is abundant in neurologically healthy subjects and drops sharply in patients with Alzheimer's disease.' *Nat Med*, 25(4), 04, 20190325, pp. 554-560.

Mu, F., Huang, J., Xing, T., Jing, Y., Cui, T., Guo, Y., Yan, X., Li, H., et al. (2019) 'The Wnt/ β -Catenin/LEF1 Pathway Promotes Cell Proliferation at Least in Part Through Direct Upregulation of miR-17-92 Cluster.' *Front Genet*, 10 20190529, p. 525.

Musich, R., Cadle-Davidson, L. and Osier, M. V. (2021) 'Comparison of Short-Read Sequence Aligners Indicates Strengths and Weaknesses for Biologists to Consider.' *Front Plant Sci*, 12 20210416, p. 657240.

Muñoz, S. S., Garner, B. and Ooi, L. (2018) 'Understanding the Role of ApoE Fragments in Alzheimer's Disease.' *Neurochem Res*, Sep, 2018/09/17,

Nagai, N., Ohguchi, H., Nakaki, R., Matsumura, Y., Kanki, Y., Sakai, J., Aburatani, H. and Minami, T. (2018) 'Downregulation of ERG and FLI1 expression in endothelial cells triggers endothelial-to-mesenchymal transition.' *PLoS Genet*, 14(11), 11, 20181130, p. e1007826.

Nah, J., Yuan, J. and Jung, Y. K. (2015) 'Autophagy in neurodegenerative diseases: from mechanism to therapeutic approach.' *Mol Cells*, 38(5), May, 2015/04/20, pp. 381-389.

Naseri, N. N., Wang, H., Guo, J., Sharma, M. and Luo, W. (2019) 'The complexity of tau in Alzheimer's disease.' *Neurosci Lett*, 705, 07 13, 20190425, pp. 183-194.

Nash, A., Gijzen, H. J. M., Hrupka, B. J., Teng, K. S., Lichtenthaler, S. F., Takeshima, H., Gunnensen, J. M. and Munro, K. M. (2021) 'BACE inhibitor treatment of mice induces

hyperactivity in a Seizure-related gene 6 family dependent manner without altering learning and memory.' *Sci Rep*, 11(1), 07 23, 20210723, p. 15084.

Nicaise, A. M., Willis, C. M., Crocker, S. J. and Pluchino, S. (2020) 'Stem Cells of the Aging Brain.' *Front Aging Neurosci*, 12 20200806, p. 247.

Nile, A. H., Mukund, S., Stanger, K., Wang, W. and Hannoush, R. N. (2017) 'Unsaturated fatty acyl recognition by Frizzled receptors mediates dimerization upon Wnt ligand binding.' *Proc Natl Acad Sci U S A*, 114(16), 04 18, 20170404, pp. 4147-4152.

Obernier, K., Cebrian-Silla, A., Thomson, M., Parraguez, J. I., Anderson, R., Guinto, C., Rodas Rodriguez, J., Garcia-Verdugo, J. M., et al. (2018) 'Adult Neurogenesis Is Sustained by Symmetric Self-Renewal and Differentiation.' *Cell Stem Cell*, 22(2), 02 01, pp. 221-234.e228.

Ohno, S. (2007a) 'Extrinsic Wnt signalling controls the polarity component aPKC.' *Nat Cell Biol*, 9(7), Jul, pp. 738-740.

Ohno, S. (2007b) 'Extrinsic Wnt signalling controls the polarity component aPKC.' *Nat Cell Biol*, 9(7), Jul, pp. 738-740.

Okamoto, M., Inoue, K., Iwamura, H., Terashima, K., Soya, H., Asashima, M. and Kuwabara, T. (2011) 'Reduction in paracrine Wnt3 factors during aging causes impaired adult neurogenesis.' *FASEB J*, 25(10), Oct, 20110711, pp. 3570-3582.

Okita, K., Matsumura, Y., Sato, Y., Okada, A., Morizane, A., Okamoto, S., Hong, H., Nakagawa, M., et al. (2011) 'A more efficient method to generate integration-free human iPS cells.' *Nat Methods*, 8(5), May, 20110403, pp. 409-412.

Ong, M. S., Deng, S., Halim, C. E., Cai, W., Tan, T. Z., Huang, R. Y., Sethi, G., Hooi, S. C., et al. (2020) 'Cytoskeletal Proteins in Cancer and Intracellular Stress: A Therapeutic Perspective.' *Cancers (Basel)*, 12(1), Jan 18, 20200118,

- Ostrowski, M., Grzanka, A. and Izdebska, M. (2005) '[The role of actin in Alzheimer's disease].' *Postepy Hig Med Dosw (Online)*, 59, Jun 03, pp. 224-228.
- Ottoboni, L., von Wunster, B. and Martino, G. (2020) 'Therapeutic Plasticity of Neural Stem Cells.' *Front Neurol*, 11 20200320, p. 148.
- Ovejero-Benito, M. C. and Frade, J. M. (2013) 'Brain-derived neurotrophic factor-dependent cdk1 inhibition prevents G2/M progression in differentiating tetraploid neurons.' *PLoS One*, 8(5) 20130531, p. e64890.
- Palomer, E., Buechler, J. and Salinas, P. C. (2019a) 'Wnt Signaling Deregulation in the Aging and Alzheimer's Brain.' *Front Cell Neurosci*, 13 20190522, p. 227.
- Palomer, E., Buechler, J. and Salinas, P. C. (2019b) 'Wnt Signaling Deregulation in the Aging and Alzheimer's Brain.' *Front Cell Neurosci*, 13 20190522, p. 227.
- Paroni, G., Bisceglia, P. and Seripa, D. (2019) 'Understanding the Amyloid Hypothesis in Alzheimer's Disease.' *J Alzheimers Dis*, 68(2) pp. 493-510.
- Penke, B., Paragi, G., Gera, J., Berkecz, R., Kovács, Z., Crul, T. and Vigh, L. (2018) 'The Role of Lipids and Membranes in the Pathogenesis of Alzheimer's Disease: A Comprehensive View.' *Curr Alzheimer Res*, Sep, 2018/09/11,
- Penna, I., Vella, S., Gigoni, A., Russo, C., Cancedda, R. and Pagano, A. (2011a) 'Selection of candidate housekeeping genes for normalization in human postmortem brain samples.' *Int J Mol Sci*, 12(9) 20110826, pp. 5461-5470.
- Penna, I., Vella, S., Gigoni, A., Russo, C., Cancedda, R. and Pagano, A. (2011b) 'Selection of candidate housekeeping genes for normalization in human postmortem brain samples.' *Int J Mol Sci*, 12(9) 20110826, pp. 5461-5470.
- Pevny, L. H. and Nicolis, S. K. (2010) 'Sox2 roles in neural stem cells.' *Int J Biochem Cell Biol*, 42(3), Mar, 20090903, pp. 421-424.
- Phng, L. K. and Gerhardt, H. (2009) 'Angiogenesis: a team effort coordinated by notch.' *Dev Cell*, 16(2), Feb, pp. 196-208.

Phng, L. K., Potente, M., Leslie, J. D., Babbage, J., Nyqvist, D., Lobov, I., Ondr, J. K., Rao, S., et al. (2009) 'Nrarp coordinates endothelial Notch and Wnt signaling to control vessel density in angiogenesis.' *Dev Cell*, 16(1), Jan, pp. 70-82.

Quartu, M., Serra, M. P., Boi, M., Ibba, V., Melis, T. and Del Fiacco, M. (2008) 'Polysialylated-neural cell adhesion molecule (PSA-NCAM) in the human trigeminal ganglion and brainstem at prenatal and adult ages.' *BMC Neurosci*, 9, Nov 06, 20081106, p. 108.

Quinn, E. M. and McManus, R. (2015) 'Quality Control and Analysis of NGS RNA Sequencing Data.' *Methods Mol Biol*, 1326 pp. 217-232.

Rapp, J., Jaromi, L., Kvell, K., Miskei, G. and Pongracz, J. E. (2017) 'WNT signaling - lung cancer is no exception.' *Respir Res*, 18(1), 09 05, 20170905, p. 167.

Rashidian, J., Iyirhiaro, G., Aleyasin, H., Rios, M., Vincent, I., Callaghan, S., Bland, R. J., Slack, R. S., et al. (2005) 'Multiple cyclin-dependent kinases signals are critical mediators of ischemia/hypoxic neuronal death in vitro and in vivo.' *Proc Natl Acad Sci U S A*, 102(39), Sep 27, 20050915, pp. 14080-14085.

Reya, T. and Clevers, H. (2005) 'Wnt signalling in stem cells and cancer.' *Nature*, 434(7035), Apr 14, pp. 843-850.

Ricciarelli, R. and Fedele, E. (2017) 'The Amyloid Cascade Hypothesis in Alzheimer's Disease: It's Time to Change Our Mind.' *Curr Neuropharmacol*, 15(6) pp. 926-935.

Ring, L., Neth, P., Weber, C., Steffens, S. and Faussner, A. (2014) ' β -Catenin-dependent pathway activation by both promiscuous "canonical" WNT3a-, and specific "noncanonical" WNT4- and WNT5a-FZD receptor combinations with strong differences in LRP5 and LRP6 dependency.' *Cell Signal*, 26(2), Feb, 20131121, pp. 260-267.

- Rochlin, M. W., Dailey, M. E. and Bridgman, P. C. (1999) 'Polymerizing microtubules activate site-directed F-actin assembly in nerve growth cones.' *Mol Biol Cell*, 10(7), Jul, pp. 2309-2327.
- Rosso, S. B., Sussman, D., Wynshaw-Boris, A. and Salinas, P. C. (2005) 'Wnt signaling through Dishevelled, Rac and JNK regulates dendritic development.' *Nat Neurosci*, 8(1), Jan, 20041219, pp. 34-42.
- Rothman, S. M. and Olney, J. W. (1986) 'Glutamate and the pathophysiology of hypoxic--ischemic brain damage.' *Ann Neurol*, 19(2), Feb, pp. 105-111.
- Rovelet-Lecrux, A., Hannequin, D., Raux, G., Le Meur, N., Laquerrière, A., Vital, A., Dumanchin, C., Feuillette, S., et al. (2006a) 'APP locus duplication causes autosomal dominant early-onset Alzheimer disease with cerebral amyloid angiopathy.' *Nat Genet*, 38(1), Jan, 20051220, pp. 24-26.
- Rovelet-Lecrux, A., Hannequin, D., Raux, G., Le Meur, N., Laquerrière, A., Vital, A., Dumanchin, C., Feuillette, S., et al. (2006b) 'APP locus duplication causes autosomal dominant early-onset Alzheimer disease with cerebral amyloid angiopathy.' *Nat Genet*, 38(1), Jan, 20051220, pp. 24-26.
- Ruijtenberg, S. and van den Heuvel, S. (2016) 'Coordinating cell proliferation and differentiation: Antagonism between cell cycle regulators and cell type-specific gene expression.' *Cell Cycle*, 15(2) pp. 196-212.
- Rydbirk, R., Folke, J., Winge, K., Aznar, S., Pakkenberg, B. and Brudek, T. (2016) 'Assessment of brain reference genes for RT-qPCR studies in neurodegenerative diseases.' *Sci Rep*, 6, 11 17, 20161117, p. 37116.
- Salcedo-Tello, P., Hernández-Ortega, K. and Arias, C. (2014) 'Susceptibility to GSK3 β -induced tau phosphorylation differs between the young and aged hippocampus after Wnt signaling inhibition.' *J Alzheimers Dis*, 39(4) pp. 775-785.

Sargin, D., Botly, L. C., Higgs, G., Marsolais, A., Frankland, P. W., Egan, S. E. and Josselyn, S. A. (2013) 'Reprint of: disrupting Jagged1-Notch signaling impairs spatial memory formation in adult mice.' *Neurobiol Learn Mem*, 105, Oct, 20130709, pp. 20-30.

Scheuner, D., Eckman, C., Jensen, M., Song, X., Citron, M., Suzuki, N., Bird, T. D., Hardy, J., et al. (1996) 'Secreted amyloid beta-protein similar to that in the senile plaques of Alzheimer's disease is increased in vivo by the presenilin 1 and 2 and APP mutations linked to familial Alzheimer's disease.' *Nat Med*, 2(8), Aug, pp. 864-870.

Schulte, G. and Bryja, V. (2007) 'The Frizzled family of unconventional G-protein-coupled receptors.' *Trends Pharmacol Sci*, 28(10), Oct, 20070919, pp. 518-525.

Scopa, C., Marrocco, F., Latina, V., Ruggeri, F., Corvaglia, V., La Regina, F., Ammassari-Teule, M., Middei, S., et al. (2020) 'Impaired adult neurogenesis is an early event in Alzheimer's disease neurodegeneration, mediated by intracellular A β oligomers.' *Cell Death Differ*, 27(3), 03, 20191007, pp. 934-948.

Selkoe, D. J. and Hardy, J. (2016a) 'The amyloid hypothesis of Alzheimer's disease at 25 years.' *EMBO Mol Med*, 8(6), 06, 20160601, pp. 595-608.

Selkoe, D. J. and Hardy, J. (2016b) 'The amyloid hypothesis of Alzheimer's disease at 25 years.' *EMBO Mol Med*, 8(6), 06, 20160601, pp. 595-608.

Serrano-Pozo, A., Das, S. and Hyman, B. T. (2021) 'APOE and Alzheimer's disease: advances in genetics, pathophysiology, and therapeutic approaches.' *Lancet Neurol*, 20(1), 01, pp. 68-80.

Shi, Y., Sun, G., Zhao, C. and Stewart, R. (2008) 'Neural stem cell self-renewal.' *Crit Rev Oncol Hematol*, 65(1), Jan, 20070723, pp. 43-53.

Shi, Y., Yamada, K., Liddel, S. A., Smith, S. T., Zhao, L., Luo, W., Tsai, R. M., Spina, S., et al. (2017) 'ApoE4 markedly exacerbates tau-mediated neurodegeneration in a mouse model of tauopathy.' *Nature*, 549(7673), 09, 2017/09/20, pp. 523-527.

Shimada, I. S., Badgandi, H., Somatilaka, B. N. and Mukhopadhyay, S. (2017) 'Using Primary Neurosphere Cultures to Study Primary Cilia.' *J Vis Exp*, (122), 04, 2017/04/14,

Silva-Vargas, V., Delgado, A. C. and Doetsch, F. (2018) 'Symmetric Stem Cell Division at the Heart of Adult Neurogenesis.' *Neuron*, 98(2), 04 18, pp. 246-248.

Slepek, T. I., Salay, L. D., Lemmon, V. P. and Bixby, J. L. (2012a) 'Dyrk kinases regulate phosphorylation of doublecortin, cytoskeletal organization, and neuronal morphology.' *Cytoskeleton (Hoboken)*, 69(7), Jul, 20120307, pp. 514-527.

Slepek, T. I., Salay, L. D., Lemmon, V. P. and Bixby, J. L. (2012b) 'Dyrk kinases regulate phosphorylation of doublecortin, cytoskeletal organization, and neuronal morphology.' *Cytoskeleton (Hoboken)*, 69(7), Jul, 20120307, pp. 514-527.

Smith, P., Azzam, M. and Hinck, L. (2017) 'Extracellular Regulation of the Mitotic Spindle and Fate Determinants Driving Asymmetric Cell Division.' *Results Probl Cell Differ*, 61 pp. 351-373.

Sokolov, M. V., Panyutin, I. V., Onyshchenko, M. I., Panyutin, I. G. and Neumann, R. D. (2010) 'Expression of pluripotency-associated genes in the surviving fraction of cultured human embryonic stem cells is not significantly affected by ionizing radiation.' *Gene*, 455(1-2), May, 2010/02/01, pp. 8-15.

Soltani, M. H., Pichardo, R., Song, Z., Sangha, N., Camacho, F., Satyamoorthy, K., Sanguenza, O. P. and Setaluri, V. (2005) 'Microtubule-associated protein 2, a marker of neuronal differentiation, induces mitotic defects, inhibits growth of melanoma cells, and predicts metastatic potential of cutaneous melanoma.' *Am J Pathol*, 166(6), Jun, pp. 1841-1850.

Somavarapu, A. K. and Kepp, K. P. (2016) 'The dynamic mechanism of presenilin-1 function: Sensitive gate dynamics and loop unplugging control protein access.' *Neurobiol Dis*, 89, May, 20160204, pp. 147-156.

Song, P., Li, S., Wu, H., Gao, R., Rao, G., Wang, D., Chen, Z., Ma, B., et al. (2016) 'Parkin promotes proteasomal degradation of p62: implication of selective vulnerability of neuronal cells in the pathogenesis of Parkinson's disease.' *Protein Cell*, 7(2), Feb, 2016/01/08, pp. 114-129.

Song, W., Nadeau, P., Yuan, M., Yang, X., Shen, J. and Yankner, B. A. (1999a) 'Proteolytic release and nuclear translocation of Notch-1 are induced by presenilin-1 and impaired by pathogenic presenilin-1 mutations.' *Proc Natl Acad Sci U S A*, 96(12), Jun 08, pp. 6959-6963.

Song, W., Nadeau, P., Yuan, M., Yang, X., Shen, J. and Yankner, B. A. (1999b) 'Proteolytic release and nuclear translocation of Notch-1 are induced by presenilin-1 and impaired by pathogenic presenilin-1 mutations.' *Proc Natl Acad Sci U S A*, 96(12), Jun 08, pp. 6959-6963.

Sorrells, S. F., Paredes, M. F., Zhang, Z., Kang, G., Pastor-Alonso, O., Biagiotti, S., Page, C. E., Sandoval, K., et al. (2021) 'Positive Controls in Adults and Children Support That Very Few, If Any, New Neurons Are Born in the Adult Human Hippocampus.' *J Neurosci*, 41(12), 03 24, pp. 2554-2565.

Stenovec, M., Trkov Bobnar, S., Smolič, T., Kreft, M., Parpura, V. and Zorec, R. (2018) 'Presenilin PS1ΔE9 disrupts mobility of secretory organelles in rat astrocytes.' *Acta Physiol (Oxf)*, 223(2), Jun, 2018/02/19, p. e13046.

Suchting, S., Freitas, C., le Noble, F., Benedito, R., Bréant, C., Duarte, A. and Eichmann, A. (2007) 'The Notch ligand Delta-like 4 negatively regulates endothelial tip cell formation and vessel branching.' *Proc Natl Acad Sci U S A*, 104(9), Feb 27, 20070212, pp. 3225-3230.

Sun, A., Liu, M., Nguyen, X. V. and Bing, G. (2003) 'P38 MAP kinase is activated at early stages in Alzheimer's disease brain.' *Exp Neurol*, 183(2), Oct, pp. 394-405.

Sun, L., Zhou, R., Yang, G. and Shi, Y. (2017) 'Analysis of 138 pathogenic mutations in presenilin-1 on the in vitro production of A β 42 and A β 40 peptides by γ -secretase.' *Proc Natl Acad Sci U S A*, 114(4), 01 24, 20161205, pp. E476-E485.

Sung, P. S., Lin, P. Y., Liu, C. H., Su, H. C. and Tsai, K. J. (2020) 'Neuroinflammation and Neurogenesis in Alzheimer's Disease and Potential Therapeutic Approaches.' *Int J Mol Sci*, 21(3), Jan 21, 20200121,

Sur, C., Kost, J., Scott, D., Adamczuk, K., Fox, N. C., Cummings, J. L., Tariot, P. N., Aisen, P. S., et al. (2020) 'BACE inhibition causes rapid, regional, and non-progressive volume reduction in Alzheimer's disease brain.' *Brain*, 143(12), Dec 01, pp. 3816-3826.

Takagi-Niidome, S., Sasaki, T., Osawa, S., Sato, T., Morishima, K., Cai, T., Iwatsubo, T. and Tomita, T. (2015) 'Cooperative roles of hydrophilic loop 1 and the C-terminus of presenilin 1 in the substrate-gating mechanism of γ -secretase.' *J Neurosci*, 35(6), Feb 11, pp. 2646-2656.

Takahashi, K. and Yamanaka, S. (2006) 'Induction of pluripotent stem cells from mouse embryonic and adult fibroblast cultures by defined factors.' *Cell*, 126(4), Aug, 2006/08/10, pp. 663-676.

Taranova, O. V., Magness, S. T., Fagan, B. M., Wu, Y., Surzenko, N., Hutton, S. R. and Pevny, L. H. (2006) 'SOX2 is a dose-dependent regulator of retinal neural progenitor competence.' *Genes Dev*, 20(9), May 01, pp. 1187-1202.

Teixeira, C. M., Pallas-Bazarra, N., Bolós, M., Terreros-Roncal, J., Ávila, J. and Llorens-Martín, M. (2018) 'Untold New Beginnings: Adult Hippocampal Neurogenesis and Alzheimer's Disease.' *J Alzheimers Dis*, 64(s1) pp. S497-S505.

Teo, J. L., Ma, H., Nguyen, C., Lam, C. and Kahn, M. (2005) 'Specific inhibition of CBP/beta-catenin interaction rescues defects in neuronal differentiation caused by a presenilin-1 mutation.' *Proc Natl Acad Sci U S A*, 102(34), Aug 23, 20050810, pp. 12171-12176.

Thordardottir, S., Kinhult Ståhlbom, A., Almkvist, O., Thonberg, H., Eriksson, M., Zetterberg, H., Blennow, K. and Graff, C. (2017) 'The effects of different familial Alzheimer's disease mutations on APP processing in vivo.' *Alzheimers Res Ther*, 9(1), Feb, 2017/02/16, p. 9.

Tincer, G., Mashkaryan, V., Bhattarai, P. and Kizil, C. (2016) 'Neural stem/progenitor cells in Alzheimer's disease.' *Yale J Biol Med*, 89(1), 03, 2016/03/24, pp. 23-35.

Tiwari, S., Atluri, V., Kaushik, A., Yndart, A. and Nair, M. (2019) 'Alzheimer's disease: pathogenesis, diagnostics, and therapeutics.' *Int J Nanomedicine*, 14 20190719, pp. 5541-5554.

Tobin, M. K., Musaraca, K., Disouky, A., Shetti, A., Bheri, A., Honer, W. G., Kim, N., Dawe, R. J., et al. (2019a) 'Human Hippocampal Neurogenesis Persists in Aged Adults and Alzheimer's Disease Patients.' *Cell Stem Cell*, 24(6), 06 06, 20190523, pp. 974-982.e973.

Tobin, M. K., Musaraca, K., Disouky, A., Shetti, A., Bheri, A., Honer, W. G., Kim, N., Dawe, R. J., et al. (2019b) 'Human Hippocampal Neurogenesis Persists in Aged Adults and Alzheimer's Disease Patients.' *Cell Stem Cell*, 24(6), 06 06, 20190523, pp. 974-982.e973.

Tooze, S. A. and Yoshimori, T. (2010) 'The origin of the autophagosomal membrane.' *Nat Cell Biol*, 12(9), Sep, pp. 831-835.

Turner, P. R., O'Connor, K., Tate, W. P. and Abraham, W. C. (2003) 'Roles of amyloid precursor protein and its fragments in regulating neural activity, plasticity and memory.' *Prog Neurobiol*, 70(1), May, pp. 1-32.

Uddin, M. S., Hasana, S., Hossain, M. F., Islam, M. S., Behl, T., Perveen, A., Hafeez, A. and Ashraf, G. M. (2021) 'Molecular Genetics of Early- and Late-Onset Alzheimer's Disease.' *Curr Gene Ther*, 21(1) pp. 43-52.

- Urbán, N., Blomfield, I. M. and Guillemot, F. (2019) 'Quiescence of Adult Mammalian Neural Stem Cells: A Highly Regulated Rest.' *Neuron*, 104(5), 12 04, pp. 834-848.
- Vaz, M. and Silvestre, S. (2020) 'Alzheimer's disease: Recent treatment strategies.' *Eur J Pharmacol*, 887, Nov 15, 20200915, p. 173554.
- Venkei, Z. G. and Yamashita, Y. M. (2018) 'Emerging mechanisms of asymmetric stem cell division.' *J Cell Biol*, 217(11), 11 05, 20180919, pp. 3785-3795.
- Veugelen, S., Saito, T., Saido, T. C., Chávez-Gutiérrez, L. and De Strooper, B. (2016a) 'Familial Alzheimer's Disease Mutations in Presenilin Generate Amyloidogenic A β Peptide Seeds.' *Neuron*, 90(2), 04 20, pp. 410-416.
- Veugelen, S., Saito, T., Saido, T. C., Chávez-Gutiérrez, L. and De Strooper, B. (2016b) 'Familial Alzheimer's Disease Mutations in Presenilin Generate Amyloidogenic A β Peptide Seeds.' *Neuron*, 90(2), 04 20, pp. 410-416.
- Viale, B., Song, L., Petrenko, V., Wenger Combremont, A. L., Contestabile, A., Bocchi, R., Salmon, P., Carleton, A., et al. (2019) 'Transient Deregulation of Canonical Wnt Signaling in Developing Pyramidal Neurons Leads to Dendritic Defects and Impaired Behavior.' *Cell Rep*, 27(5), 04 30, pp. 1487-1502.e1486.
- Vivar, C. (2015) 'Adult Hippocampal Neurogenesis, Aging and Neurodegenerative Diseases: Possible Strategies to Prevent Cognitive Impairment.' *Curr Top Med Chem*, 15(21) pp. 2175-2192.
- Wang, L., Wang, S. and Li, W. (2012) 'RSeQC: quality control of RNA-seq experiments.' *Bioinformatics*, 28(16), Aug 15, 20120627, pp. 2184-2185.
- Wang, Q., Wu, H., Hu, J., Fu, H., Qu, Y., Yang, Y., Cai, K. Q., Efimov, A., et al. (2021) 'Nestin Is Required for Spindle Assembly and Cell-Cycle Progression in Glioblastoma Cells.' *Mol Cancer Res*, 19(10), 10, 20210622, pp. 1651-1665.
- Wang, R. and Reddy, P. H. (2017) 'Role of Glutamate and NMDA Receptors in Alzheimer's Disease.' *J Alzheimers Dis*, 57(4) pp. 1041-1048.

Wang, W., Bu, B., Xie, M., Zhang, M., Yu, Z. and Tao, D. (2009) 'Neural cell cycle dysregulation and central nervous system diseases.' *Prog Neurobiol*, 89(1), Sep, 20090204, pp. 1-17.

Wang, Y., Shi, Y. and Wei, H. (2017) 'Calcium Dysregulation in Alzheimer's Disease: A Target for New Drug Development.' *J Alzheimers Dis Parkinsonism*, 7(5), Aug, 2017/09/15,

Watanabe, H. and Shen, J. (2017) 'Dominant negative mechanism of.' *Proc Natl Acad Sci U S A*, 114(48), 11 28, 20171115, pp. 12635-12637.

Wessels, A. M., Lines, C., Stern, R. A., Kost, J., Voss, T., Mozley, L. H., Furtek, C., Mukai, Y., et al. (2020a) 'Cognitive outcomes in trials of two BACE inhibitors in Alzheimer's disease.' *Alzheimers Dement*, 16(11), Nov, 20201013, pp. 1483-1492.

Wessels, A. M., Tariot, P. N., Zimmer, J. A., Selzler, K. J., Bragg, S. M., Andersen, S. W., Landry, J., Krull, J. H., et al. (2020b) 'Efficacy and Safety of Lanabecestat for Treatment of Early and Mild Alzheimer Disease: The AMARANTH and DAYBREAK-ALZ Randomized Clinical Trials.' *JAMA Neurol*, 77(2), Feb 01, pp. 199-209.

Wilhelmsson, U., Lebkuechner, I., Leke, R., Marasek, P., Yang, X., Antfolk, D., Chen, M., Mohseni, P., et al. (2019a) 'Nestin Regulates Neurogenesis in Mice Through Notch Signaling From Astrocytes to Neural Stem Cells.' *Cereb Cortex*, 29(10), 09 13, pp. 4050-4066.

Wilhelmsson, U., Lebkuechner, I., Leke, R., Marasek, P., Yang, X., Antfolk, D., Chen, M., Mohseni, P., et al. (2019b) 'Nestin Regulates Neurogenesis in Mice Through Notch Signaling From Astrocytes to Neural Stem Cells.' *Cereb Cortex*, 29(10), 09 13, pp. 4050-4066.

Wolfe, M. S. (2020) 'Unraveling the complexity of γ -secretase.' *Semin Cell Dev Biol*, 105, 09, 20200121, pp. 3-11.

Woo, S. M., Kim, J., Han, H. W., Chae, J. I., Son, M. Y., Cho, S., Chung, H. M., Han, Y. M., et al. (2009) 'Notch signaling is required for maintaining stem-cell features of neuroprogenitor cells derived from human embryonic stem cells.' *BMC Neurosci*, 10, Aug 17, 20090817, p. 97.

Xia, D., Kelleher, R. J. and Shen, J. (2016) 'Loss of A β 43 Production Caused by Presenilin-1 Mutations in the Knockin Mouse Brain.' *Neuron*, 90(2), 04 20, pp. 417-422.

Xia, D., Watanabe, H., Wu, B., Lee, S. H., Li, Y., Tsvetkov, E., Bolshakov, V. Y., Shen, J., et al. (2015) 'Presenilin-1 knockin mice reveal loss-of-function mechanism for familial Alzheimer's disease.' *Neuron*, 85(5), Mar 04, pp. 967-981.

Xu, T. H., Yan, Y., Kang, Y., Jiang, Y., Melcher, K. and Xu, H. E. (2016) 'Alzheimer's disease-associated mutations increase amyloid precursor protein resistance to γ -secretase cleavage and the A β 42/A β 40 ratio.' *Cell Discov*, 2 20160823, p. 16026.

Yang, J., Zhao, H., Ma, Y., Shi, G., Song, J., Tang, Y., Li, S., Li, T., et al. (2017) 'Early pathogenic event of Alzheimer's disease documented in iPSCs from patients with PSEN1 mutations.' *Oncotarget*, 8(5), Jan 31, pp. 7900-7913.

Yin, Y. and Wang, Z. (2018) 'ApoE and Neurodegenerative Diseases in Aging.' *Adv Exp Med Biol*, 1086 pp. 77-92.

Yoshinaga, Y., Kagawa, T., Shimizu, T., Inoue, T., Takada, S., Kuratsu, J. and Taga, T. (2010) 'Wnt3a promotes hippocampal neurogenesis by shortening cell cycle duration of neural progenitor cells.' *Cell Mol Neurobiol*, 30(7), Oct, 20100630, pp. 1049-1058.

You, L., Wang, Z., Li, H., Shou, J., Jing, Z., Xie, J., Sui, X., Pan, H., et al. (2015a) 'The role of STAT3 in autophagy.' *Autophagy*, 11(5) pp. 729-739.

You, L., Wang, Z., Li, H., Shou, J., Jing, Z., Xie, J., Sui, X., Pan, H., et al. (2015b) 'The role of STAT3 in autophagy.' *Autophagy*, 11(5) pp. 729-739.

Yuan, L. and Hassan, B. A. (2014) 'Neurogenins in brain development and disease: an overview.' *Arch Biochem Biophys*, 558, Sep, 2014/06/17, pp. 10-13.

Zaletel, I., Schwirtlich, M., Perović, M., Jovanović, M., Stevanović, M., Kanazir, S. and Puškaš, N. (2018) 'Early Impairments of Hippocampal Neurogenesis in 5xFAD Mouse Model of Alzheimer's Disease Are Associated with Altered Expression of SOXB Transcription Factors.' *J Alzheimers Dis*, 65(3) pp. 963-976.

Zbinden, A., Canté-Barrett, K., Pike-Overzet, K. and Staal, F. J. T. (2021) 'Stem Cell-Based Disease Models for Inborn Errors of Immunity.' *Cells*, 11(1), Dec 30, 20211230,

Zechner, D., Fujita, Y., Hülsken, J., Müller, T., Walther, I., Taketo, M. M., Crenshaw, E. B., Birchmeier, W., et al. (2003) 'beta-Catenin signals regulate cell growth and the balance between progenitor cell expansion and differentiation in the nervous system.' *Dev Biol*, 258(2), Jun 15, pp. 406-418.

Zhang, D., Lu, Z., Man, J., Cui, K., Fu, X., Yu, L., Gao, Y., Liao, L., et al. (2019) 'Wnt-3a alleviates neuroinflammation after ischemic stroke by modulating the responses of microglia/macrophages and astrocytes.' *Int Immunopharmacol*, 75, Oct, 20190717, p. 105760.

Zhang, N., Parr, C. J. C., Birch, A. M., Goldfinger, M. H. and Sastre, M. (2018) 'The amyloid precursor protein binds to β -catenin and modulates its cellular distribution.' *Neurosci Lett*, 685, 10 15, 20180831, pp. 190-195.

Zhang, S., Cai, F., Wu, Y., Bozorgmehr, T., Wang, Z., Huang, D., Guo, J., Shen, L., et al. (2018) 'A presenilin-1 mutation causes Alzheimer disease without affecting Notch signaling.' *Mol Psychiatry*, Jun, 2018/06/18,

Zhang, X., Zhu, J., Yang, G. Y., Wang, Q. J., Qian, L., Chen, Y. M., Chen, F., Tao, Y., et al. (2007) 'Dishevelled promotes axon differentiation by regulating atypical protein kinase C.' *Nat Cell Biol*, 9(7), Jul, 20070610, pp. 743-754.

Zhao, J., Davis, M. D., Martens, Y. A., Shinohara, M., Graff-Radford, N. R., Younkin, S. G., Wszolek, Z. K., Kanekiyo, T., et al. (2017) 'APOE ϵ 4/ ϵ 4 diminishes neurotrophic function of human iPSC-derived astrocytes.' *Hum Mol Genet*, 26(14), 07, pp. 2690-2700.

Zheng, H., Jia, L., Liu, C. C., Rong, Z., Zhong, L., Yang, L., Chen, X. F., Fryer, J. D., et al. (2017) 'TREM2 Promotes Microglial Survival by Activating Wnt/ β -Catenin Pathway.' *J Neurosci*, 37(7), 02 15, 20170111, pp. 1772-1784.

Zhong, L., Xie, Y. Z., Cao, T. T., Wang, Z., Wang, T., Li, X., Shen, R. C., Xu, H., et al. (2016) 'A rapid and cost-effective method for genotyping apolipoprotein E gene polymorphism.' *Mol Neurodegener*, 11, Jan, 2016/01/12, p. 2.

Zhou, R., Yang, G., Guo, X., Zhou, Q., Lei, J. and Shi, Y. (2019) 'Recognition of the amyloid precursor protein by human γ -secretase.' *Science*, 363(6428), Feb 15, 20190110,

Zhu, A. J. and Watt, F. M. (1999) 'beta-catenin signalling modulates proliferative potential of human epidermal keratinocytes independently of intercellular adhesion.' *Development*, 126(10), May, pp. 2285-2298.

Zissimopoulos, J., Crimmins, E. and St Clair, P. (2014) 'The Value of Delaying Alzheimer's Disease Onset.' *Forum Health Econ Policy*, 18(1), Nov, 20141104, pp. 25-39.

10.0 Apendices

10.1 Appendix 1

10.1.1 Plasmid maps for plasmids used in iPSC reprogramming

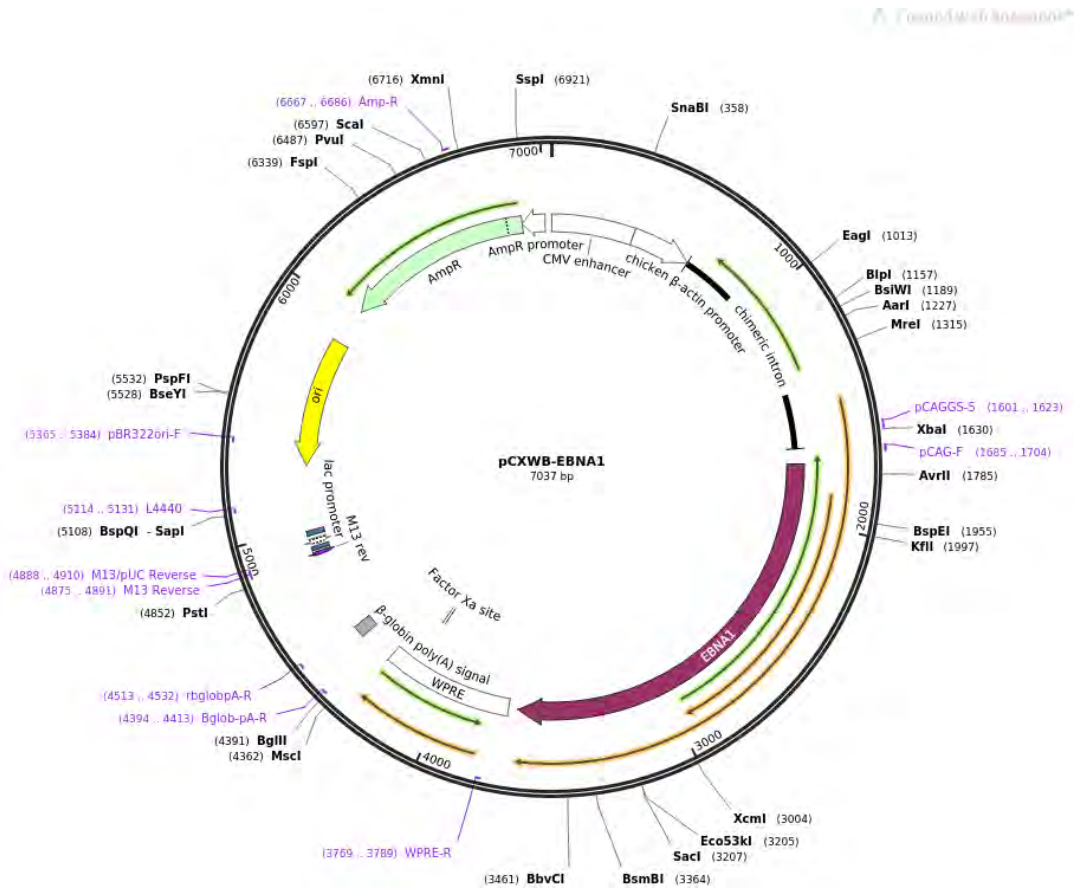


Figure 95. Full sequence map for pCXWB-EBNA1.

Full Sequence Map for pCXWB-EBNA1.

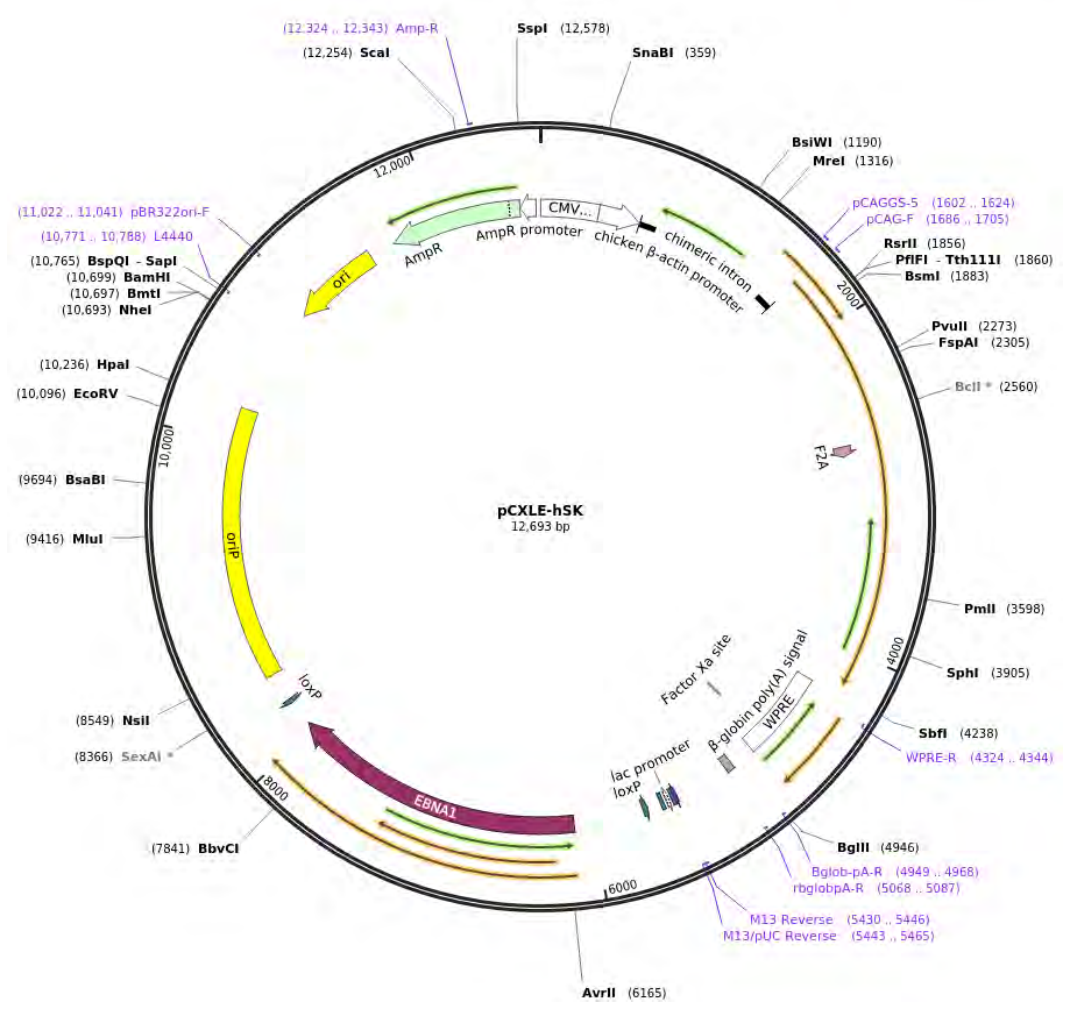


Figure 96. Full sequence map for pCXLE-hSK.

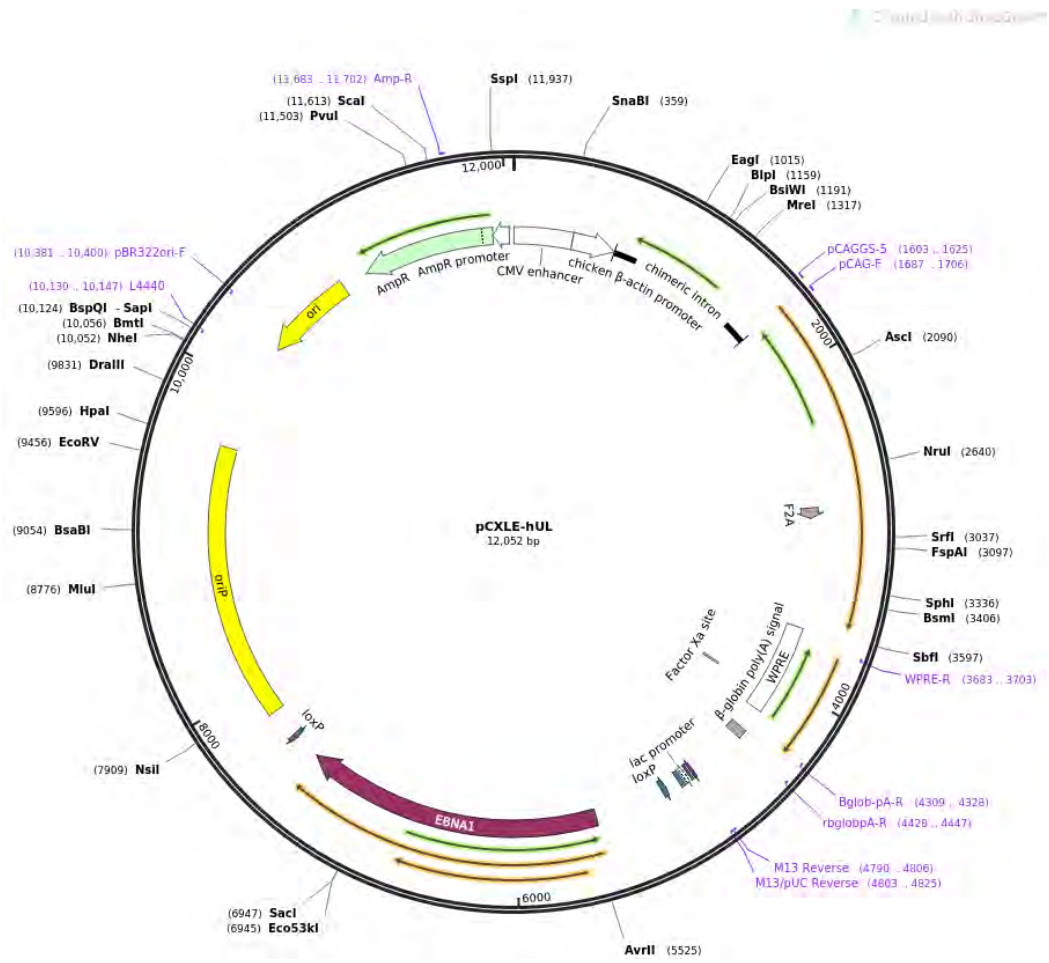


Figure 97. Full sequence map for pCXLE-hUL.

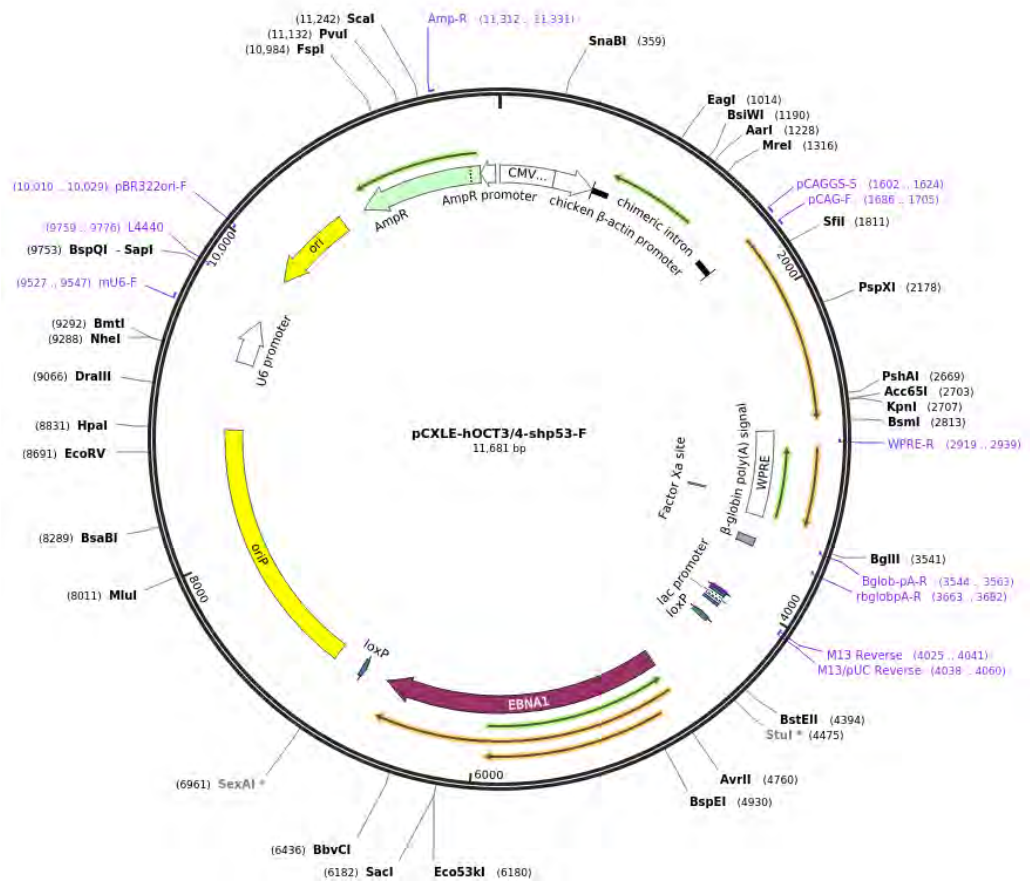


Figure 98. Full sequence map for pCXLE-hOCT3/4-shp53-F.

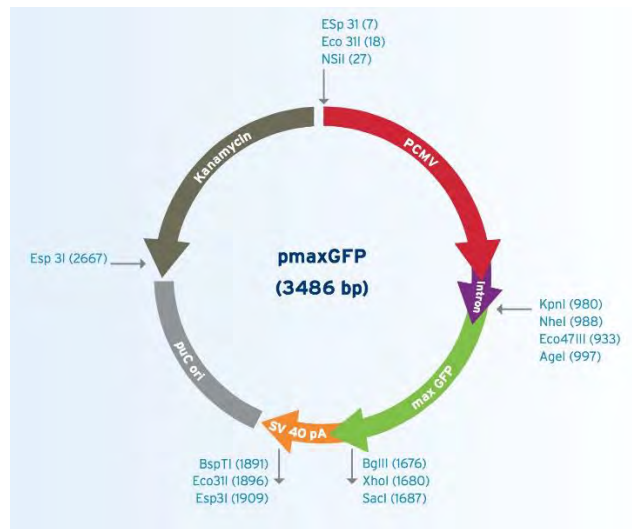


Figure 99. Vector map for the pmax GFP™ Vector

The pmax GFP™ Vector has a human CMV promoter, this is a strong promoter and enables high-level constitutive expression of GFP. The pmax GFP™ Vector also has a gene which enables resistance to Kanamycin.

10.2 Appendix 3: RNA sequencing data analysis

10.2.1 Bioanalyser traces of cDNA fragments post library preparation

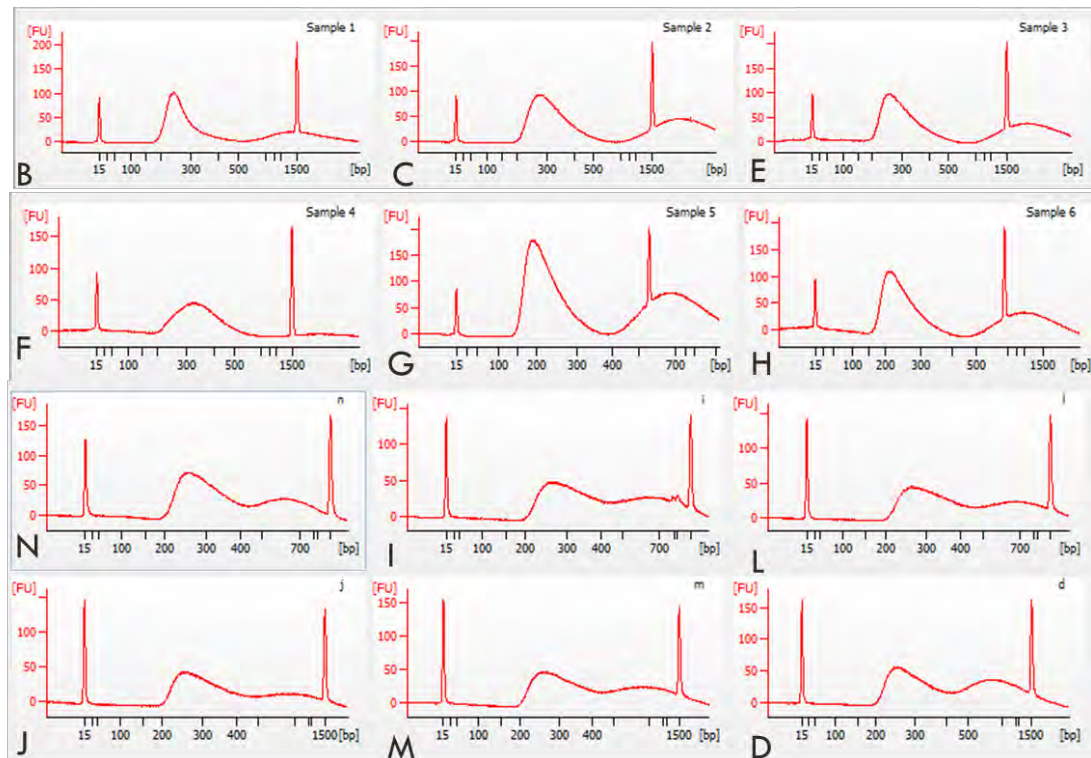


Figure 100. Bioanalyzer traces displaying cDNA fragment size of samples

Screen capture of Agilent 2100 Bioanalyzer electropherograms. Bioanalyzer traces were used to check cDNA fragment sizes after completion of library preparation. The initial library preparation performed displayed small quantities of fragments with sizes above 1000bp. B, C, E display control P3 NSC, F,G,H display *PSEN1* A246E NSC, N, I, L, display control NSC at P2, J, M, D display *PSEN1* NSC at P3.

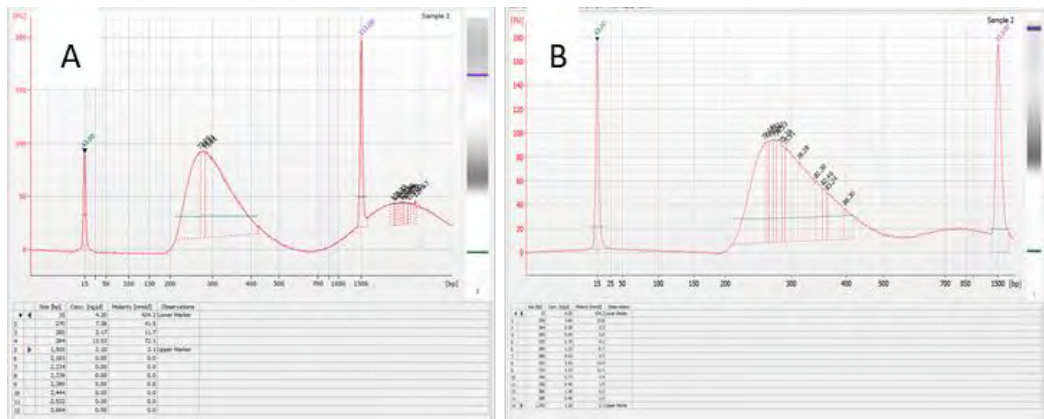


Figure 101. Example of contamination with larger DNA fragments

Screen capture of Agilent 2100 Bioanalyzer electropherograms. A.) Larger DNA fragments of >1000 bp were detected in sample C. B.) In the second library preparation, in all samples, all fragment sizes detected were in the range 200-500bp.

10.2.2 Initial quality data for sequencing reads

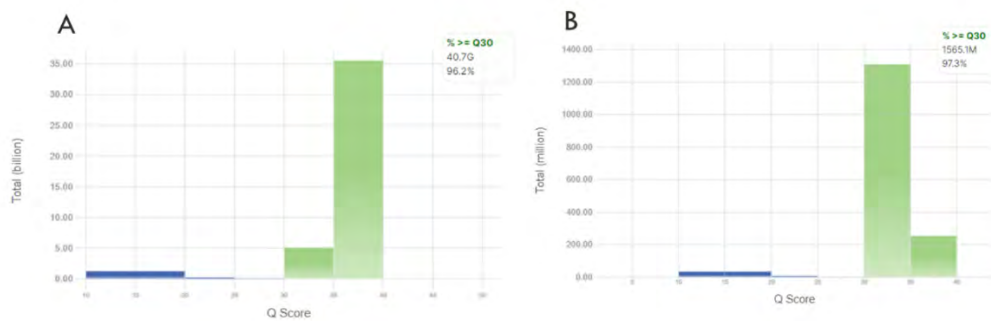


Figure 102. Q score of sequencing reads

A.) Overall Q Score for all samples sequenced (including the PhiX control). 5 billion reads had a Q score between 30 and 35, and 35 billion reads had a Q score which was in the range 35-40. B.) Overall Q Score for All Indexed Samples (*PSEN1* A246E and control NSC). 1309.329 million reads had a Q Score of 30-35. 255.7556 million reads had a Q score of 35-40. Samples with a lower Q score were filtered out. 97.19% of the library had a Q score greater than 30, this indicated that sample reads had less than a 1:1000 chance of being incorrect.

Table 32. Index sequences and reads identified per index

Index Number	Index Sequence	Sample ID	Percentage Reads Identified (PF) Per Index	Number of reads	Number of reads Identified
1	GAGTGG	N	7.3817	39,378,352	2,906,792
2	TAGCTT	F	9.2222	49,358,484	4,551,938
3	ACTTGA	C	6.9201	36,978,912	2,558,978
4	GATCAG	E	3.9307	20,987,656	824,962
5	TTAGGC	B	5.9588	31,812,204	1,895,626
6	GTGGCC	H	6.894	36,886,982	2,542,989
7	GGCTAC	D	12.5691	67,074,004	8,430,599
8	ACTGAT	J	7.0502	37,696,268	2,657,662
9	ATTCCT	M	10.4196	55,751,512	5,809,085
10	GTTTCG	L	6.8913	36,854,614	2,539,762
11	CGTACG	G	8.2077	43,890,034	3,602,362
12	ATCACG	I	8.1283	43,436,142	3,530,620

10.2.2.1 Table 33. ASCII character quality score

Symbol	ASCII Code	Q-Score	Symbol	ASCII Code	Q-Score
!	33	0	6	54	21
"	34	1	7	55	22
#	35	2	8	56	23
\$	36	3	9	57	24
%	37	4	:	58	25
&	38	5	;	59	26
'	39	6	<	60	27
(40	7	=	61	28
)	41	8	>	62	29
*	42	9	?	63	30
+	43	10	@	64	31
,	44	11	A	65	32
-	45	12	B	66	33
.	46	13	C	67	34
/	47	14	D	68	35

0	48	15	E	69	36
1	49	16	F	70	37
2	50	17	G	71	38
3	51	18	H	72	39
4	52	19	I	73	40
5	53	20			

10.2.3 Quality control of RNA sequencing data

Table 34. Example FastQC input parameters

Input Parameter	Value
Input FASTQ file	Sample B, Merged Read 1s
Contaminant list	Nothing Selected
Adapter list	Illumina Adaptor Sequence File
Submodule and Limit specifying file	Nothing Selected
Disable grouping of bases for reads >50bp	No
Lower limit on the length of the sequence to be shown in the report	Nothing Selected
length of Kmer to look for	Test Disabled

Samples were inputted individually into FastQC using the input parameters specified (Table 34. Example FastQC input parameters). Using FastQC, samples were analysed for their Average Per Base Sequence Quality for every position in the read (total 75 bp) (Figure 103). Bases with a Q score of higher than 28 are good quality, with a very low probability of incorrect base calling. It is common in Illumina sequencing, for initial and final base readings to be of a poorer quality than the middle section of the fragment. At every position in the read, all samples had a Q score of >30 indicating high quality base identification. Samples were analysed to determine their overall per base sequence content (Figure 103 B). This module displays the percentage of each nucleotide base at every position in the read. Due to the high volume of fragments sequenced per sample, at each position, equal representation of each

base was expected at each position in the read. The first 10 bases of this sample display an uneven distribution of A/T/G/C. These first 10 bases are not sequenced incorrectly as their quality score was above 30. The uneven base distribution at the start of each read was likely due to the use of random hexamers in first strand synthesis. Cleaved RNA fragments were primed with random hexamers and reverse transcribed into first strand cDNA. Random hexamers are not that random and favour certain bases at the start of the sequence, resulting in enrichment of kmers at 5' end. Samples were analysed for their per base N content (Figure 103 C), all samples displayed a per base N content of 0%. Samples were analysed for per tile sequence quality (Figure 103 D), warm coloured tiles indicate a tile has a worse read quality than other tiles for that position in the read. A small number of samples displayed this issue which may have been the result of bubbles or debris in the flow cell lane. The issue appeared to occur for just one whole 75bp sequence in the affected samples so affected sequences were filtered out. The presence of many warm coloured tiles would have indicated that the flow cell had been overloaded but this was not an issue in any samples. Samples were analysed for adapter content (Figure 103). This module gives information on the percentage of adaptor sequence that is found in the sample. If the percentage of adapter was high in a sample, specific adapter sequences were filtered out. All samples analysed passed this module and did not present with a significant amount of adapter present. Samples were analysed for their per sequence quality scores (Figure 103). This module looks at the quality score distribution across all samples and gives an average quality per read. Entire sequences which are poor quality were filtered out. The average quality per read for all samples was >30. All samples were analysed for their sequence length distribution (Figure 103). This module gives information on the distribution of sequence lengths over all sequences. Sequence lengths that were too long were trimmed and sequence lengths that are too short were filtered out, this module raises a warning when all sequences are not of the same length. All fragments were sequenced to between 72 and 76 bp, with the majority of fragments at 75bp. Samples were analysed for their

levels of sequence duplication, (Figure 103) this module displays the percent of sequences that would remain if duplicated samples were removed. De-duplication of sequences can be used to remove technical duplication, but would also remove biological duplication, when working with RNA sequencing data, removing biological duplication would mean enriched genes would be missed. For this reason, samples were not de-duplicated. All samples were analysed for their per sequence GC content (Figure 103). In a normal random library, you expect to see roughly normal distribution of GC content, GC content was normally distributed in all samples with most samples having a mean GC content of 50%.

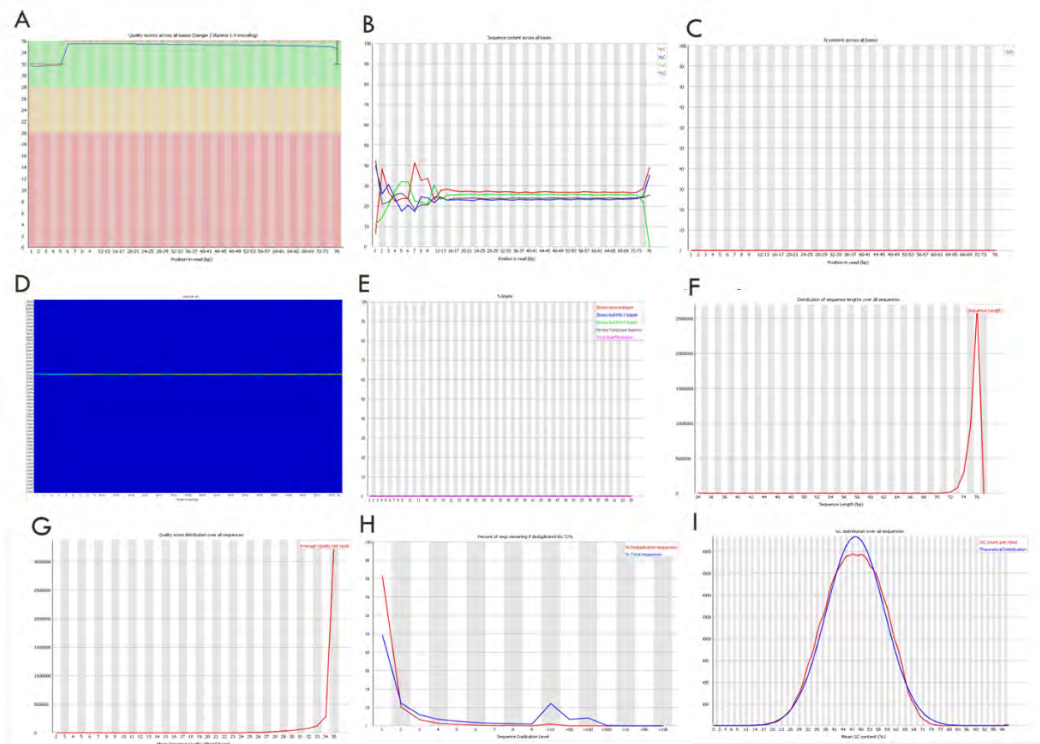


Figure 103. FastQC results for sequencing samples

A sample of results generated using tool FastQC. Results displayed have been selected to display any issues that were found to be present in sequencing samples. A.) Per Base Sequence Quality. The y-axis displays the Q score, bases with a Q score of higher than 28 are considered to be good quality. The x-axis displays the base position in the read (bp). The results display the average quality score given at each position in the read. All samples displayed very good average sequencing quality at every base position in the read. B.) Per Base Sequence content. This graph displays the

All samples were analysed for the presence of overrepresented sequences. A sequence is considered overrepresented if it accounts for >0.1% of reads. This module can be triggered when used to analyse small RNA libraries where sequences are not subjected to random fragmentation, and the same sequence may naturally be present in a significant proportion of the library. The majority of samples had no overrepresented sequences. The overrepresented sequences detected were derived from adaptors or were composed of a long sequence of G's. The G is generated when the sequencer detects no signal, so has run out of template. These bases were of low quality so were removed.

10.2.4 Trimming and filtering of sequencing data

Table 36. Example Trimmomatic settings for merged Fastq files.

Tool	Trimmomatic
Input Parameter	Value
Single-end or paired-end reads?	pair_of_files
Input FASTQ file (R1/first of pair)	B, Merged Read 1s
Input FASTQ file (R2/second of pair)	B, Merged Read 2s
Perform initial ILLUMINACLIP step?	Yes
Select standard adapter sequences or provide custom?	Custom
Custom adapter sequences in fasta format	AGATCGGAAGAGCACACGTCTGAACTCC AGTCA AGATCGGAAGAGCGTCGTGTAGGGAAA GAGTGT GATCGGAAGAGCACACGTCTGAACTCCA GTCACGGCTACATCTCGTATGC
Maximum mismatch count which will still allow a full match to be performed	2

Tool	Trimmomatic
Input Parameter	Value
How accurate the match between the two 'adapter ligated' reads must be for PE palindrome read alignment	30
How accurate the match between any adapter etc. sequence must be against a read	10
Minimum length of adapter that needs to be detected (PE specific/palindrome mode)	8
Always keep both reads (PE specific/palindrome mode)?	True
Select Trimmomatic operation to perform	SLIDINGWINDOW
Number of bases to average across	4
Average quality required	20
Select Trimmomatic operation to perform	MINLEN
Minimum length of reads to be kept	25
Output trimlog file?	False
Output trimmomatic log messages?	False
Job Resource Parameters	No

10.2.5 Determination of strandedness

Table 37. Infer experiment parameters

Tool	Infer Experiment
Input Parameter	Value
Select a reference genome	Human (Homo sapiens) (b38): hg38
Number of reads sampled from SAM/BAM file (default = 200000)	200000

Tool	Infer Experiment
Input Parameter	Value
Minimum mapping quality	30

Results from Infer Experiment tool:

This is PairEnd Data.

Fraction of reads failed to determine: 0.0122

Fraction of reads explained by "1++,1--,2+-,2--": 0.0060 <- the fraction of reads that assigned to forward strand

Fraction of reads explained by "1+-,1+,2++,2--": 0.9818 <- the fraction of reads that assigned to reverse strand. A greater fraction of reads assigned to the reverse strand, so the results indicate that the data is reverse stranded.

10.2.6 Alignment to reference genome

Table 38. Example parameters for alignment to reference genome using HISAT2

Tool	HISAT2
Input Parameter	Value
Source for the reference genome	indexed
Select a reference genome	hg38
Is this a single or paired library	Paired
FASTA/Q file #1	B Trimmed merged R1 samples
FASTA/Q file #2	B Trimmed merged R2 samples
Specify strand information	Reverse (RF)
Paired-end options	defaults

Tool	HISAT2
Input Parameter	Value
sum	
Output alignment summary in a more machine-friendly style.	True
Print alignment summary to a file.	True
adv	
Input options	defaults
Alignment options	defaults
Scoring options	defaults
Spliced alignment options	defaults
Reporting options	defaults
Output options	defaults
Other options	defaults
Job Resource Parameters	no

10.2.7 HISAT2 alignment scores

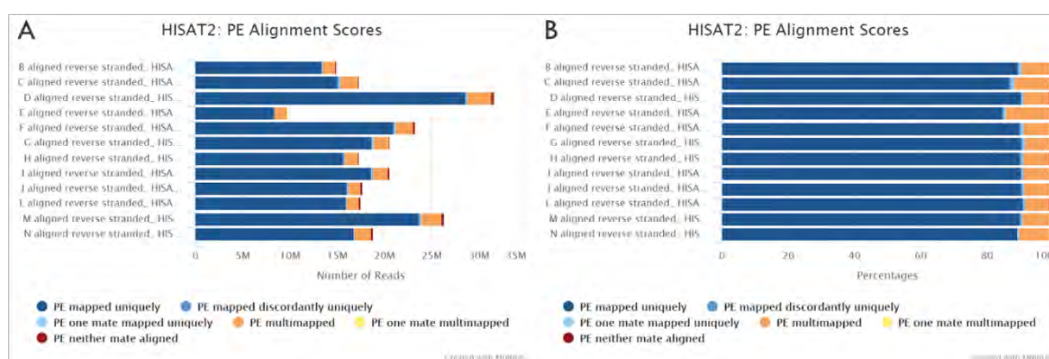


Figure 104. HISAT2 alignment scores

Alignment of samples to the reference genome (Hg38) using the tool HISAT2 resulted in >90% alignment rate for all samples which indicates successful alignment to the reference genome. A.) Displays the number of aligned reads per sample. B.) Displays the % of aligned reads per sample.

10.2.8 Filtering and QC of alignment

Alignment of sequences to the reference genome was analysed pre and post filtering. Filtering was carried out using the tool Filter BAM.

Table 39. Example filtering parameters post alignment with HISAT2

Tool	Filter
Input Parameter	Value
BAM dataset(s) to filter	Sample B Aligned to Hg38 using HISAT2
Select BAM property to filter on	mapQuality
Filter on read mapping quality (phred scale)	>=20
Select BAM property to filter on	isPaired
Select paired reads	True
Select BAM property to filter on	isProperPair
Select properly paired reads	True

Tool	Filter
Input Parameter	Value
Would you like to set rules?	False

10.2.8.1 Picard: MarkDuplicates

Pre filter:

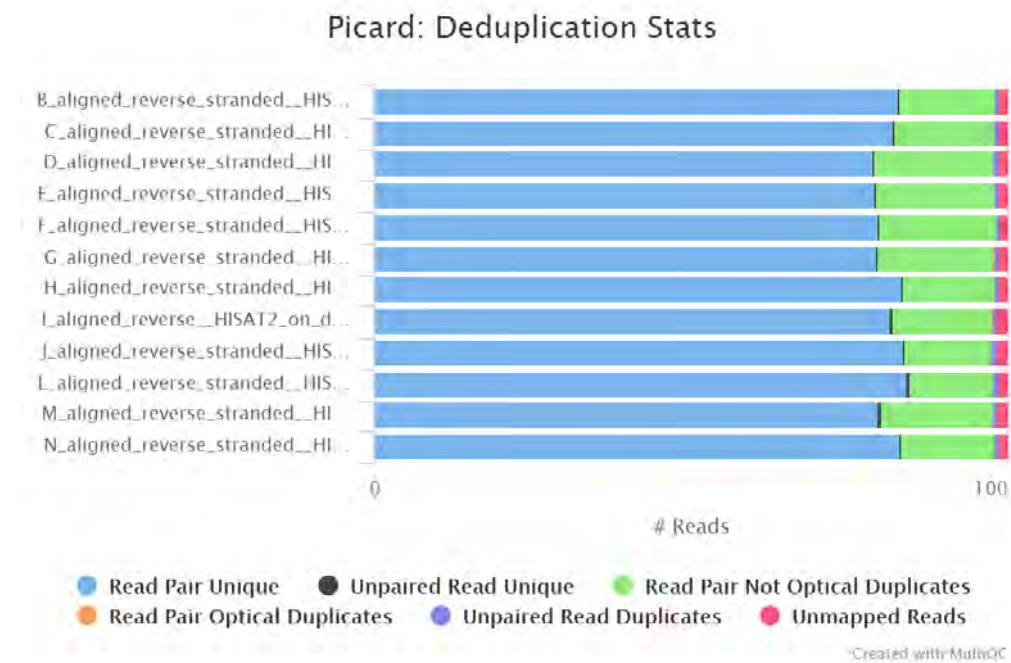


Figure 105. Deduplication Statistics

Percentage Duplication Data for all Samples Post-Alignment to Hg38. Less than or equal to 50% duplication can be considered normal to obtain. All samples displayed less than 50% duplication.

Table 40. Percentage duplication data for all samples post-alignment to Hg38

Sample Name	% Duplication
B Aligned BAM	15.6%
C Aligned BAM	16.3%

D Aligned BAM	19.5%
E Aligned BAM	19.3%
F Aligned BAM	19.0%
G Aligned BAM	19.1%
H Aligned BAM	15.1%
I Aligned BAM	16.4%
J Aligned BAM	14.4%
L Aligned BAM	14.0%
M Aligned BAM	18.4%
N Aligned BAM	15.3%

10.2.8.2 Samtools idxsats

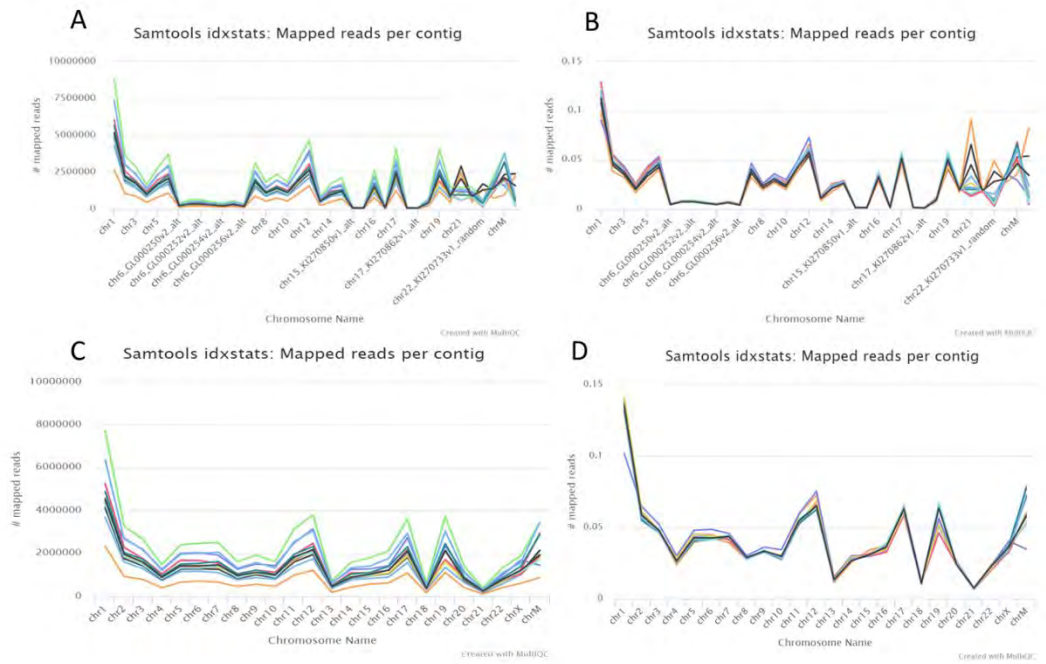


Figure 106. Number of mapped reads per contig

Results generated from the tool Samtools idxstats displaying Number of Mapped Reads per Contig. Results displayed are displayed for sequences aligned to Hg38. A.) Results displayed pre-filtering for mapping quality and pre-normalisation for read number per sample. B.) Pre-filtering, post-normalisation. C.) Post-filtering, pre-normalisation. D.) Post-filtering, post-normalisation.

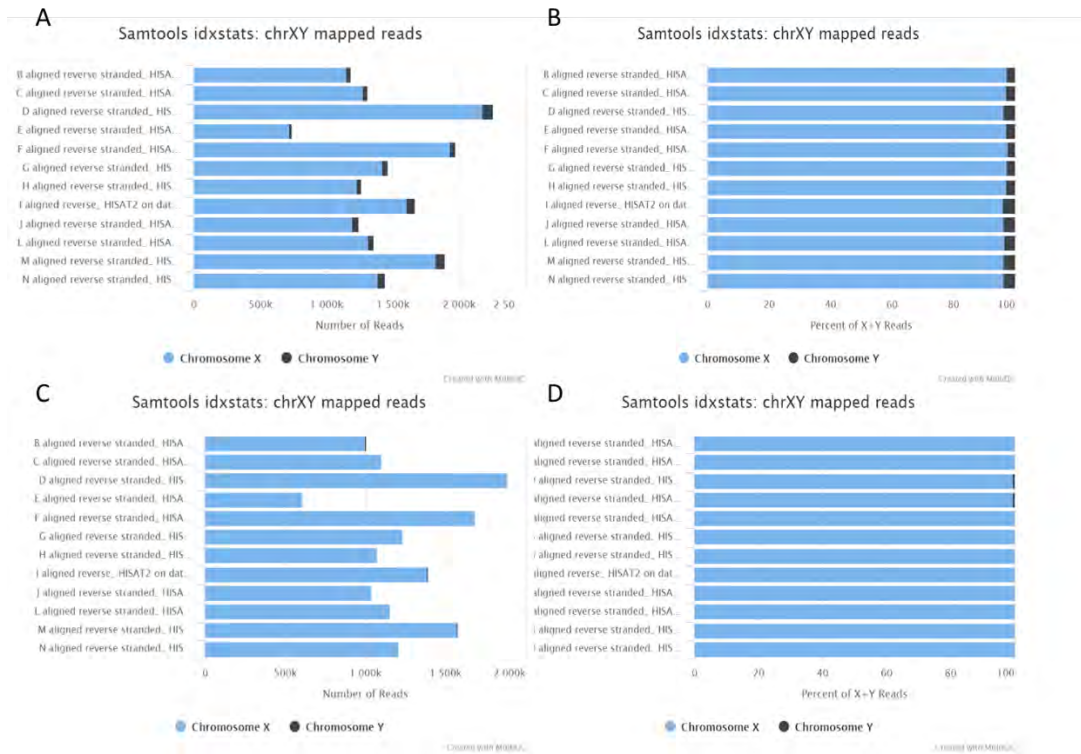


Figure 107. ChrXY mapped reads

ChrXY mapped reads for all samples A.)- B.) Pre-filter, C.)- D.) Post-filter

Samples are both female so reads aligning to the Y chromosome should not be seen. Quality based filtering removed reads that were specific to the Y chromosome indicating that their alignment was low quality.

10.2.8.3 RSeQC

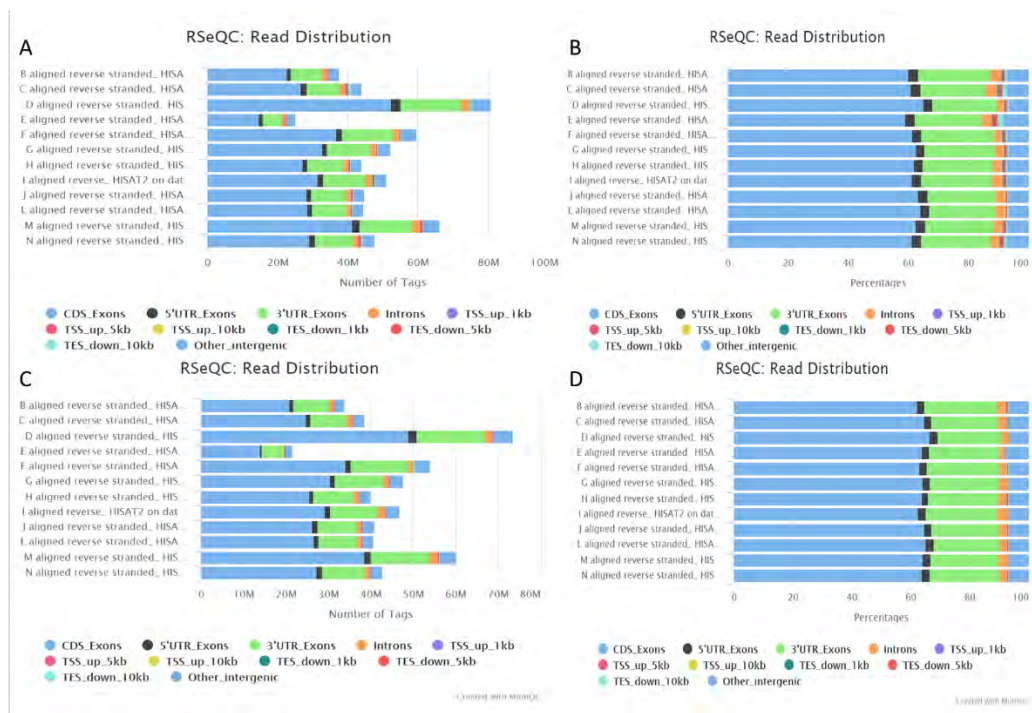


Figure 108. Read distributions before and after alignment-based filtering

A and B Read distribution pre-filter, C and D post filter

10.2.9 Feature counts

Table 41. Feature Counts Input Parameters

Tool	Feature Counts
Input Parameter	Value
Alignment file	Filtered BAM (sequences aligned to reference genome using HISAT2 and filtered based on alignment quality)
Specify strand information	Stranded (Reverse)
Gene annotation file	builtin
Select built-in genome	hg38

Tool	Feature Counts
Input Parameter	Value
Output format	Gene-ID "\t" read-count (MultiQC/DESeq2/edgeR/limma-voom compatible)
Create gene-length file	Yes
Count fragments instead of reads	fragments (or templates) will be counted instead of reads.
Check paired-end distance	No
Only allow fragments with both reads aligned	No
Exclude chimeric fragments	Yes
GFF feature type filter	Exon
GFF gene identifier	gene_id
On feature level	No
Allow reads to map to multiple features	disabled: reads that align to multiple features or overlapping features are excluded.
Minimum mapping quality per read	10
Long reads	False
Count reads by read group	False
Largest overlap	False
Minimum bases of overlap	1
Minimum fraction (of read) overlapping a feature	0
Minimum fraction (of feature) overlapping a read	0

Tool	Feature Counts
Input Parameter	Value
Read 5' extension	0
Read 3' extension	0
Reduce read to single position	Leave the read as it is
Only count primary alignments	False
Ignore reads marked as duplicate	False
Annotates the alignment file with 'XS:Z:'-tags to described per read or read-pair the corresponding assigned feature(s).	False
Ignore unspliced alignments	False
Job Resource Parameters	No

10.2.10 Percentage of reads assigned to the reference genome

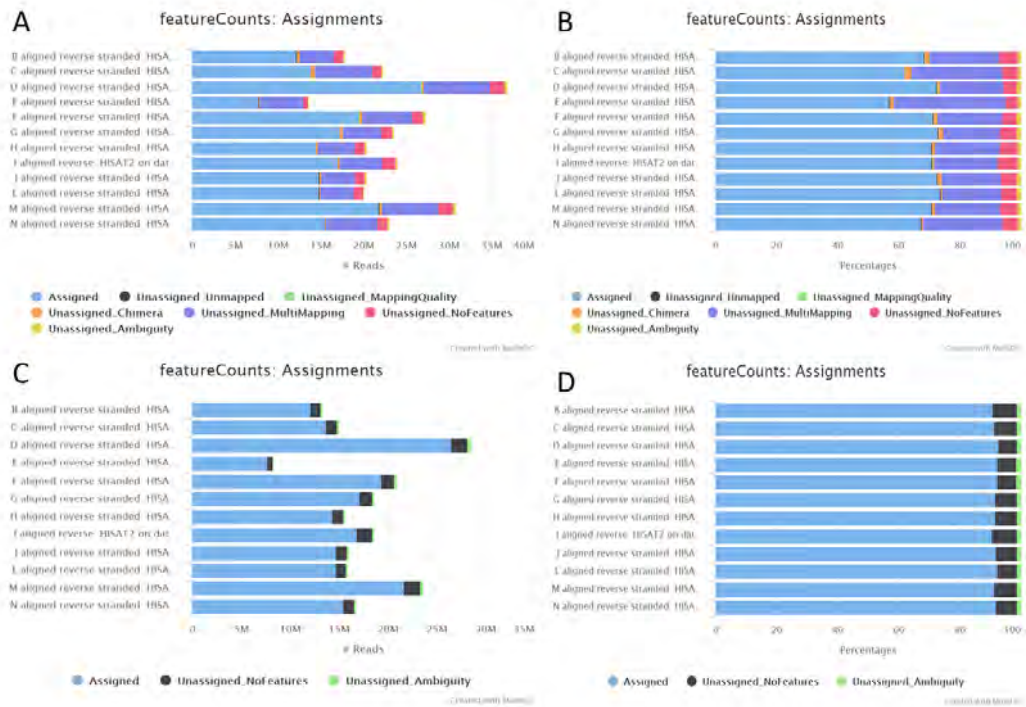


Figure 109. FeatureCounts: assignments before and after filtering

A and B are pre-filtering, C and D are post, Post filtering alignment: greater than 70% of reads assigned to genes so this is good quality

Table 42. Percentage of reads assigned pre- and post- filtering

Sample name	% Assigned Pre-filtering	M Assigned Pre- filtering	% Assigned Post-filtering	M Assigned Post- filtering
B Aligned BAM	68.40%	12.2	90.90%	12.1
C Aligned BAM	62.00%	13.9	91.40%	13.8
D Aligned BAM	72.50%	26.8	92.90%	26.6
E Aligned BAM	57.00%	7.8	92.50%	7.7

F Aligned BAM	71.40%	19.5	92.50%	19.4
G Aligned BAM	72.90%	17.3	91.80%	17.1
H Aligned BAM	70.80%	14.5	91.70%	14.4
I Aligned BAM	70.90%	17	90.70%	16.9
J Aligned BAM	72.70%	14.9	91.90%	14.7
L Aligned BAM	73.60%	14.9	92.50%	14.8
M Aligned BAM	70.90%	21.9	91.50%	21.7
N Aligned BAM	67.40%	15.6	92.00%	15.5

Filtering of reads aligned to Hg38 removed data such as reads mapping to the y-chromosome and improved quality of data, without greatly reducing number of reads. Therefore, all aligned BAM files were filtered for quality of alignment.

10.2.11 DeSeq2

DeSeq2 was used via the Galaxy wrapper to carry out differential gene expression analysis between all four groups.

Table 43. DESeq2 input parameters

Input Parameter	Value
	datasets_per_level
Specify a factor name, e.g. effects_drug_x or cancer_markers	Condition
Specify a factor level, typical values could be 'tumor', 'normal', 'treated' or 'control'	control P3

Input Parameter	Value
Counts file(s)	featureCounts on collection 1 :Counts
Specify a factor level, typical values could be 'tumor', 'normal', 'treated' or 'control'	control P2
Counts file(s)	featureCounts on collection 2: Counts
Specify a factor level, typical values could be 'tumor', 'normal', 'treated' or 'control'	PSEN1 P2
Counts file(s)	FeatureCounts on collection 3: Counts
Specify a factor level, typical values could be 'tumor', 'normal', 'treated' or 'control'	PSEN1 P3
Counts file(s)	FeatureCounts on collection 4: Counts
(Optional) provide a tabular file with additional batch factors to include in the model.	N/A
Files have header?	True
Choice of Input data	count
Visualising the analysis results	True
Output normalized counts table	True
Output rLog normalized table	True
Output VST normalized table	True
Output all levels vs all levels of primary factor (use when you have >2 levels for primary factor)	True

Input Parameter	Value
(Optional) Method for estimateSizeFactors	No Selection (use default)
Fit type	parametric
Turn off outliers replacement (only affects with >6 replicates)	False
Turn off outliers filtering (only affects with >2 replicates)	False
Turn off independent filtering	False
Job Resource Parameters	no

10.2.12 Volcano plot

The tool Volcano Plot was used (Galaxy Version 0.0.5) to create a volcano plot.

Table 44. Parameters for generation of volcano plot

Input Parameter	Value
Specify an input file	DESeq2 result file filtered for significance and fold change of 1.
FDR (adjusted P value)	12
P value (raw)	11
Log Fold Change	8
Labels	3
Significance threshold	0.05
LogFC threshold to colour	1.0
Points to label	signif
Only label top most significant	5

Input Parameter	Value
plot_options	
Label Boxes	True
Plot title	Empty.
Label for x axis	Empty.
Label for y axis	Empty.
Minimum value for x axis	Not available.
Maximum value for x axis	Not available.
Maximum value for y axis	Not available.
Label for Legend Title	Empty.
Labels for Legend	Down, Not Sig, Up

10.2.13 GeneOntology, Panther classification system

Table 45. Parameters for GO biological process

Analysis Type	PANTHER Overrepresentation Test (Released 20220202)
Analyzed List:	upload_1 (Homo sapiens)
Reference List:	Homo sapiens (all genes in database)
Annotation Data Set:	GO Biological Process Complete
Test Type	Fisher's Exact
Correction	Calculate False Discovery Rate

Table 46. Parameters for GO molecular function

Analysis Type	PANTHER Overrepresentation Test (Released 20220202)
Analyzed List:	upload_1 (Homo sapiens)

Reference List:	Homo sapiens (all genes in database)
Annotation Data Set:	GO Molecular Function Complete
Test Type	Fisher's Exact
Correction	Calculate False Discovery Rate

Table 47. Parameters for GO cellular component

Analysis Type	PANTHER Overrepresentation Test (Released 20220202)
Analyzed List:	upload_1 (Homo sapiens)
Reference List:	Homo sapiens (all genes in database)
Annotation Data Set:	GO Cellular Component Complete
Test Type	Fisher's Exact
Correction	Calculate False Discovery Rate